Development of equal and unequal filtered power splitter using substrate integrated waveguide

Amadu Dainkeh

A thesis submitted in partial fulfilment of the requirements of the University of East London for the degree of Doctor of Philosophy

July 2017

ABSTRACT

The objective of this thesis is to investigate and provide better solution to producing filtered power splitter with compact size and with use of no resistors for its isolation. The background investigation and utilisation of the established theories build up the design equations that are adapted to power dividers. These dividers contain filtering characteristics and are employed in microstrip and substrate integrated waveguide technology.

The work involves the design of a filtered power splitter with bandpass characteristics. It uses the conventional filter design synthesis to develop the design parameters that establish the coupling between the common resonator of the power splitter and the next resonator towards the output ports.

An equal and an unequal division using a 5-pole, 9-square resonators is used verify this concept; this is also implemented in microstrip using Square open loop resonators (SOLR) and in SIW. Furthermore, a 3-pole 5-square resonators is also implemented in SIW; all of these operating at 2 GHz.

For the equal split, the 5th order microstrip gives a bandwidth, minimum insertion loss, maximum return loss and isolation of 120MHz, 3.12dB, 15dB and 12.6dB respectively and the 3rd order SIW gives a bandwidth, minimum insertion loss, maximum return and isolation of 99Mhz, 3.57dB, 17.1dB and 6.79dB respectively; whilst the 5th order SIW gives a bandwidth, minimum insertion loss, maximum return and isolation of 140Mhz, 3.87dB, 18.3dB and 14.79dB respectively. However, it is recommended that this work can be extended to more than two output ports, to improve isolation, increase the Q factor and match the output ports.

ACKNOWLEDGEMENT

I would like to express my gratitude to Allah for making it possible in my academic pursuit this far. I would also want to give my particular thanks to my director of studies, Dr. Ken Yeo for his supervision, guidance and encouragement all throughout my studies, since my MSc. Thanks also go to Dr. W. Hosny for his advice and supports.

I would want to thank the staffs of the electronics lab at UEL, particularly Ben, for their assistance, especially during my lab work.

Special thanks go to everyone who have supported in diverse ways through financial, advice and encouragement. I really appreciate you all.

Finally, a very special appreciation to you my darling Sonia.

TABLE OF CONTENTS

LIST OF FIGURES

LIST OF TABLES

ACRONYMS

ADS	Advance Design system
BPF	Bandpass Filter
BW	Bandwidth
CBCPW	Conductor backed coplanar waveguide
CPW	Coplanar Waveguide
EBG	Electromagnetic Bang Gap
EMI	Electromagnetic Interference
EMPro	Electromagnetic Professional
FBW	Fractional Bandwidth
FEM	Finite Element Method
FPS	Filtered Power Splitter
FSIW	Folded Substrate Integrated Waveguides
HMSIW	Half-mode SIW
LTCC	Low temperature Co-fired Ceramic
MCM	Multichip Module
MMIC	Monolithic Microwave Integrated Circuit
MSL	Microstrip Line

NRN	Non-resonating node
PCB	Printed Circuit Board
PD	Power divider
PS	Power Splitter
Q_{ext}	External Quality Factor
RWG	Rectangular Waveguide
SIWs	Substrate Integrated Waveguides
SOLR	Square open loop resonators
TE	Transverse Electrical
TEM	Transverse Electromagnetic
TM	Transverse Magnetic
UPS	Unequal Power Splitter
VNA	Vector Network Analyser

CHAPTER 1

INTRODUCTION

Recent development in the telecommunications industry has led to the success and deployment of communications technologies including mobile and wireless communication. There is extensive demand for new microwave and millimeter-wave components to cater for the rapid growth in ultra-wide band system, broadband and wireless Internet, mobile and personal communications, remote sensing and satellite navigation that have the capabilities of meeting their stringent requirements. Filters, power dividers and diplexers are among the components used in frequency selectivity and they play a crucial role in achieving these systems realisations. There is a challenge in effective utilisation of the electromagnetic spectrum, which possess the need to design and implement these components. The microstrip antenna array feeding system needs a power divider with low loss, large bandwidth and high Q-factor in order to enable high power handling. Power splitters are passive microwave devices that are capable of splitting signal from the input port into at least two ports with the signal of lesser power. To achieve this unit with such features, it is desired to implement a component that is compact, lightweight and characteristics capable of usage in numerous microwave applications.

1.1 Thesis motivation

Conventionally, bandpass filters power dividers are cascaded to be used in several applications like image reject mixer and other circuits which produces two duplicated signals of a filtered input signal within a desired frequency range as given by Gunnarsson et al.

(2005) and Llorente-Romano et al. (2003). Two identical bandpass filters are cascaded to a power divider are shown in Figure 1.1 (Tang and Mouthaan, 2010). However, this configuration requires a considerable area to be implemented. This thesis addresses a novel network that can do the same functions of filtering and power splitting. Such networks are based on coupled resonator structures and when compared to conventional configurations, they may be miniaturized. The objective for the SIW power splitter design is to decrease the overall dimensions, to be able to integrate with other passive components.

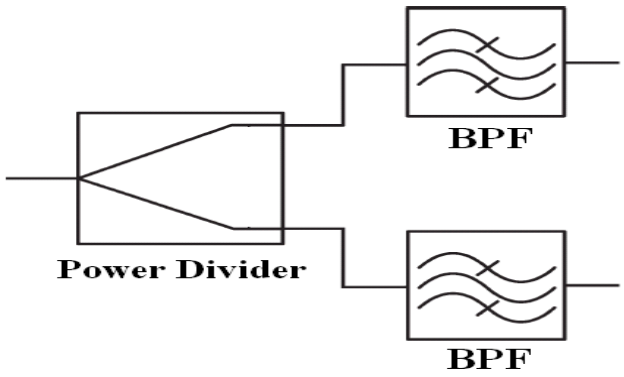

Figure 1.1 Divider cascaded with bandpass filter configuration (Tang and Mouthaan, 2010)

SIW-based components development symbolizes the revolutionary period in the design of all microwave and mm-wave circuits. The use of the SIW technology in high performance communication electronics is becoming very popular as integration density of electronics components increases. It has been reported by some researchers that due to the high Electromagnetic interference EMI isolation provided by the closed waveguide structures, the SIW can eliminate the unwanted signals in sensitive microwave and mm-wave circuits. Also some literatures including (Bozzi et al., 2008a) and (Kumari and Srivastava, 2013) have demonstrated that low conductor losses and higher power handling in the SIW circuits provide enhanced signaling performance when compared to other PCB based transmission lines. It is essential therefore to realize a component that will be capable of filtering whilst

splitting the power, and can have low loss and capable of handling high power. In order to route signals in SIW-based systems, compact SIW power dividers are required. The designs presented so far in literature follow the objectives of size reduction and achieving wide operational bandwidth. In this thesis, the developed compact filtered power splitters will provide a compact with even and uneven power splitting as well as filtering the signal as required in many microwave systems. Figure 1.2 (a) gives an example of a two-port coupled resonator filter topology. From the topology, the black dots depict resonators and the lines linking the resonators are the couplings. Coupled resonator filters Synthesis methods have been extensively presented in literatures. The work in this thesis implements the theory of two-port coupled resonator filters and multi-port coupled resonator circuits as given in Figure 1.2 (b) with its main focus to three-port components such as coupled resonator power splitter. The design approach allows the synthesis of filtering power dividers with arbitrary power division

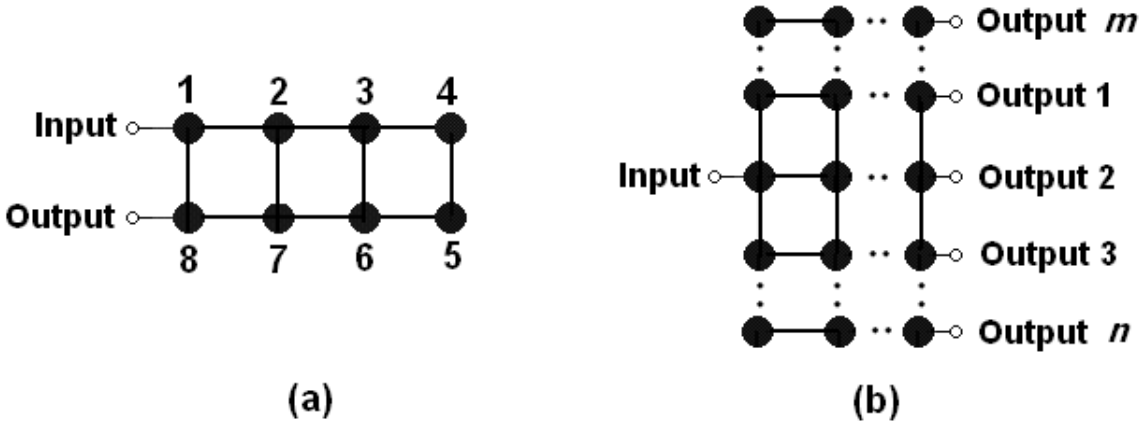

Figure 1.2 (a) two-port coupled resonator filter, (b) multi-port coupled resonator circuit (Skaik, 2011).

1.2 Research method

The most widely employed method when it comes to the design of RF and microwave filtered Power dividers is a planar type which is based on lumped element equivalent circuit of quarter-wave transformer (Jung-Hyun et al., 2002). This is having unique frequency, equal magnitude and phase and with a three-port impedance matching network. The combining network (i.e. the impedance matching network) is normally aimed at producing good transmission and exhibiting high impedance in the passband, in order to achieve the necessary output isolation (Wu et al., 2015).

The method of power divider design proposed in this thesis involves cascading two sections of a single band bandpass filter with power divider as shown in Figure 1.1. Each bandpass filter is designed with similar characteristics and frequency. The BPFs are connected in series of lumped elements whose equivalent resonators are designed in microstrip and SIW`. The main power division occur at the common resonator from the input port to the output channel. The division can be equally or unequally done. Generally, Filters should have small insertion loss, large return loss for good impedance matching with interconnecting components, and high frequency-selectivity to prevent the interference and high performance. The electrical performances of the filters are described in terms of insertion loss, return loss, and frequency-selectivity (i.e., attenuation at rejection band) (Davidson, 2010). The parameters to consider during this design include the operational bandwidth. This is the region of frequency at passband that can allow signal to pass through. This crucial in any filter design as bandpass mode is selected for a low interference environment (Cho and Rebeiz, 2014). Return loss, measured in decibels (dB), is the loss of power in the signal returned/reflected by a discontinuity in a transmission line. This discontinuity can be a mismatch with the

terminating load or with a device inserted in the line. The selected return loss used entirely for all designs in this thesis is 20dB. Insertion loss, also measured in dB, is the loss of signal power resulting from the transmission of these signals from the input ports to the output channels in a transmission line. The magnitude of this loss is determined by the Q of the filter circuit, usually supposed to be small (Dai et al., 2009); for example, in a 3dB power divider the insertion loss might be specified as 0.5dB. Another parameter of importance consideration in this design is Isolation. In an ideal power divider the output ports are mutually isolated. In other words, a signal entering output 2 does not leak out of output 3. Isolation is defined as the ratio of a signal entering output 1 that is measured at output 2, assuming all ports are impedance matched (usually 50Ω). Another parameter of importance is the bandwidth, which is the frequency region that allows the signal to pass through.

To verify these concepts, the design equations are used to generate the values of the parameters and its equivalent circuit model with lumped elements. A 5-pole microstrip equal split FPS using SOLR is designed and tested. Then the SIW was adapted to a 3-pole and 5-pole equal and unequal split. This proposed FPS promise to give a design with compact size while providing a low insertion loss and high return and isolation loss at 3GHz. The limit to this frequency designed for is due to the available VNA network analyser of maximum 3GHz, for the purpose of testing. The circuit model of the proposed FPS is simulated using the Keysight Advanced Design System (ADS) circuit simulator, while the microstrip layout simulation is achieved using the Keysight ADS momentum simulator. The electromagnetic (EM) simulation of the SIW layout of the proposed filtered power divider is based on the finite-element method (FEM) of the Keysight electromagnetic professional (EMPro) 3D simulator. It is important to note that any other professional circuit, EM or even FEM

simulators could be used to achieve results similar to those presented in this thesis. The microstrip filtered power divider's fabrication is based on the printed circuit board (PCB) milling process, while the SIW diplexer is fabricated using the PCB micro-milling process based on the Leiterplatten-Kopierfrasen (LKPF) Protomat C60.

1.3 Aims and objectives

The aim of this research work is to develop compact filtered power divider with Chebyshev's bandpass performance for wireless applications using conventional, microstrip and substrate integrated waveguide technologies.

The main objective is the design equations for even and uneven filtered power splitter and the secondary objective is to implement it using microstrip and SIW technology.

The first objective of the project is to develop the design parameters for equal power splitter. This achievement requires several approaches. The first approach is to develop filter design variables using standard filter synthesis procedures. This also involves developing a MATLAB code for determining the various parameters of the filter and the filter's bandpass response; determination of the coupling coefficients between resonators, and the external quality factor at the ports of the filter. The second objective here is to develop the splitter's design parameters, especially for the coupling coefficient constant between the common resonator and its next resonator; here the division ratio $\alpha = 0.5$ is the same for both output paths.

The second objective is to develop and design parameters for unequal power splitter. The initial objective here is to develop the filter prototype parameters as done in the first aim. The next objective is to develop filtered power splitter design parameters by implementing an equation for determining the coupling coefficient of the common resonator to the next

resonator along their respective output paths. The division ratio to be use here is $\alpha_1 = 1/3$ and $\alpha_2 = 2/3$, where α_1 and α_2 are division ratio towards port 2 and port 3 respectively.

The third objective is to verify the first aim by implementing it in Microstrip and SIW. For the microstrip, the first objective is to establish the relationships between parameters of the model and behaviour of the Square Open Loop Resonators, SOLR, which requires the development of a physical structure and employed in accordance with the design topology. Next, bandpass SOLR filters should be designed according to the design procedure in order to prove the viability of the presented model and procedure. The opportunities presented by the developed theoretical model should be considered for this purpose. For the SIW, The first objective is to determine the types of SIW resonators and potential coupling schemes, which can be implemented in conventional rectangular waveguide, taking into account the technological constraints. The second objective is to determine the type of microstrip-to-SIW transition. Then a suitable design procedure should be determined for realization of SIW bandpass filter. This should then be simulated and fabricated. The fabricated component should then be measured to establish its filter response.

The fourth aim is to verify by implementing the second aim in SIW. The objective here is to implement the unequal division power splitter in SIW technology. This should involve manufacturing and testing of both power splitters for a third order 5 resonator and fifth order 9 resonator power splitter. The main objective is to create new SIW splitter with improved performance using the approaches developed in this project from conventional rectangular waveguides. A further objective is to study the available SIW filter and power divider design and implementation techniques and find potential engineering solutions, which may improve their performance.

1.4 Thesis contribution

This thesis presents the readers with a comprehensive overview of the SIW research conducted over the past decade. Following an in-depth analysis of the previously published SIW research, an all-new 5 and 9 square resonator SIW-based components and systems are developed in this thesis.

- The most important novelty is the comprehensive set of design equations to achieve even and uneven filtered powered filter. This is developed in Chapter 4 and applied to the microstrip design in Chapter 5 and SIW design in Chapter 7.
- Another novelty is the design of microstrip filtered power splitter. A novel square open loop resonator (SOLR) power splitter is designed and reported in Chapter 5. This topology and structure are designed using microstrip technology and its novelty here is performance of filtering and splitting using this technology.
- Also, as a novel in this thesis is the implementation of the filter design and power splitter design concept of Chapter 4 and using the design parameters of the SIW in Chapter 6 to the realise a physical structure of equal and unequal division power split in SIW technology using square resonators; as reported in Chapter 7. The novelty is the structure (SIW) and performance of the performing splitting and filtering signal.

The contribution of this thesis can also be attributed from these journals and conference papers.

I. **Dainkeh, A.,** Nwajana, A. O. and Yeo, K. S. K. (2016) 'Filtered Power Splitter Using Square Open Loop Resonators', Progress In Electromagnetics Research C, 64, pp. 133–140.

II. Nwajana, A. O., Yeo, K. S. K. and **Dainkeh, A.** 'Low cost SIW Chebyshev bandpass filter with new input/output connection'. *2016 16th Mediterranean Microwave Symposium (MMS)*, 14-16 Nov. 2016, 1-4.

III. Nwajana, A. O., **Dainkeh, A.** and Yeo, K. S. K. (2017) 'Substrate Integrated Waveguide (SIW) Bandpass Filter with Novel Microstrip-CPW-SIW Input Coupling', Journal of Microwaves, Optoelectronics and Electromagnetic Applications, 16(2).

1.5 Thesis overview

Chapter 1 introduces the brief background of the importance, characteristics and application of power dividers in microwave technology. This chapter also explains the motivation to embark on this project, the research method involved in executing these tasks and it gives the aims and objectives, the contributions and overview of the thesis.

Chapter 2 gives the literature reviews of microwave power divider and substrate integrated waveguide and their applications. Also included are summary of the evolution, benefits and manufacturing techniques of these devices as given by numerous researchers. Some of the gaps that led to this research are also identified and reported.

Chapter 3 provides the reader with a comprehensive background of microwave power divider including its types and application found in literatures. The chapter also presents the theories and mathematical modeling associated with power dividers including Scattering matrix and polynomials of the different types of power dividers. The derived equations are used as a

basis to the synthesis of three-port components such as power splitters in chapter 5 and chapter 7.

Chapter 4 presents an introduction the theory coupled resonator circuits. This chapter develops various mathematical expressions, including generating expressions for the coupling coefficients between resonators and external quality factor for filter and PS design. Also, it provides the coupling expression between the common resonator to the output ports and the next resonator along that path for the PS. The evaluation of this chapter is vital for its adoption to Chapter 5, Chapter 6 and Chapter 7. Also included are the design expressions for the microstrip design.

Chapter 5 focuses on SOLR power splitter components in microstrip technology. The findings of chapter 3 and chapter 4 are used to realise this power splitter. A review of standard microstrip theory and technology is included; and adapted to the design of the SOLR microstrip line technology. This is followed by simulation and optimisation. This chapter also includes fabrication and measurement evaluations of the filtered SOLR power splitter.

Substrate integrated waveguide cavity resonators is presented in Chapter 5.

Firstly, it utilizes Maxwell's equation and conditions to formulate expressions relating to rectangular waveguides. Theories and mathematical modeling derived from the previous section will be analysed. This includes, SIW supported propagation mode and expressions to determine the resonator parameters. This will be adopted in chapter 6 and chapter 7.

In Chapter 6, the findings of chapter 3 and chapter 5 are adapted to designing an SIW bandpass filter. This chapter specifically deals with the novel coplanar to SIW transition at both input and output ports of an SIW bandpass filter. The coupling coefficient and Q factor are determined and it explains the SIW design process and simulations carried out in order to ascertain the correct dimensions. It also highlighted the SIW design process and the output frequency response curve after testing and the tuning process used to improve the result.

Chapter 7 presents coupled resonator power splitters that are designed and realised using SIW resonators to verify the new design methodology. The designed components are as follows: (1) Third-order equal division power splitter. (2) Third-order unequal division power splitter. (3) Fifth-order equal division power splitter and (4) Fifth-order unequal division power splitter.

Lastly, Chapter 8 provides summary and conclusions drawn from this thesis. Future work recommendations are provided to further improve the SIW components.

CHAPTER 2

LITERATURE REVIEW

2.0 Introduction

This chapter gives a review of many literatures as applied to power dividers and SIW and their applications. It includes the problem domain and what the existing research gaps are and how they have been addressed. It also discusses some of the limitations of the existing state of the art solution and lastly how this thesis intends to solve some these problems.

2.1 Review of Microwave power divider

A power splitter is a module that is frequently used in telecommunication and radar. The idea of power splitter dates back to 1940 when a variety of power dividers and couplers were invented at the MIT Radiation Laboratory (Fenn et al., 2000, Hong and Lancaster, 2001). Among them were the E & H plane waveguide T-junction, multi-hole coupler and different types of couplers using coaxial probes. Between 1950 & 1960 many of these Power dividers were re-invented with strip-line and microstrip technology. It was mainly due to increase in planar line usage and led to the development of Wilkinson Power divider and branch line couple (Pozar, 2011). The recent development of telecommunication equipment has shown a tendency to produce modules with unique splitting features.

In many microwave applications, power dividers/splitters have been used widely. Various examples include combiner network for solid-state power amplifier and applications in feeding network of the antenna-array system (Fenn et al., 2000). In the latter system,

considering a specific number of output ports, the signal is fed through a splitter with an equal division; alternatively, it can also be fed to a splitter arranged in a series of equal split power dividers. These divided signals are then transferred to a transmitting antenna through phase shifters. These antennas are used in beam steering applications that need direction change of the antenna beam with time.

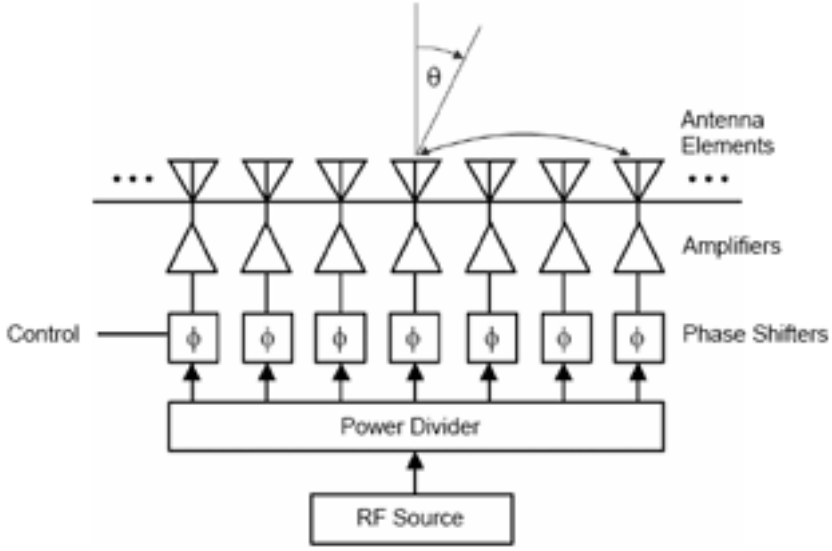

Figure 2.1 Phased array antenna system (Fenn et al., 2000)

Figure 2.1 shows a phase array antenna system that consists of phase shifters, amplifiers and antenna element (Ehmouda, 2009). These microwave devices use passive components for splitting or combining. In power splitting, an input signal is divided into two or more signals with lesser Power. The divider Power can be equal division or unequal division depending on the purpose for which it is designed. Three ports network are the simplest form of power dividers. To form a multi-stage structure, an extension of using N-way power splitters are used.

Commonly used power dividers in microwave system and circuits are the T-junction (Pozar, 2011) and the Wilkinson (Wilkinson, 1960) power dividers. Also, directional couplers and hybrids, which are four port devices are also used for power division. Between the output

ports, It contains a phase shift of either 180º (Magic-T) or 90º (branch-line hybrids) (Pozar, 2011).

Power divider or combiner network circuits are used when high power is required, as in case of distributed power amplifier system (Pengcheng et al., 2003) as shown in Figure 2.2. There is a combination of output power from a large number of power amplifiers. The power splitter first divides the power, which gives the power amplifiers a drive signal. The output of the amplifier then combines to form a single output with huge power by the use of the power combiner. Usually, the networks required for power division or combination needs to have a high port isolation and low loss in these systems. Tianyu and Wenquan (Zhang and Che, 2016) have designed a miniaturised network that promises to be use in this applications, however, the issue of a lossless network couldn't be achieved due to resistor component in the output isolation.

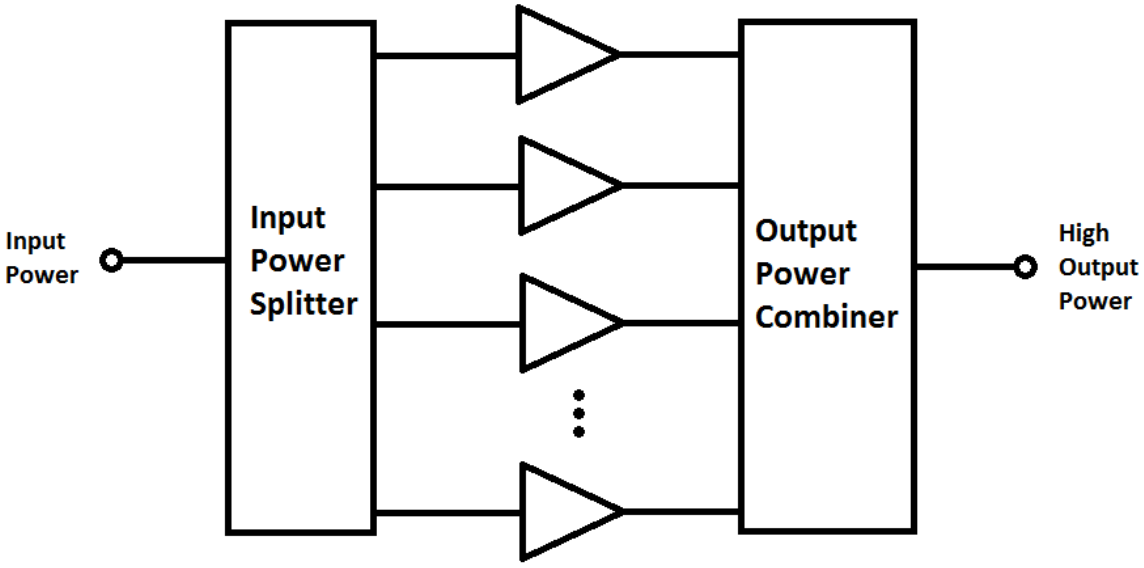

Figure 2.2 Amplifier system schematic

Power splitter is utilized in modern day's technology. One such application is implementing

1-by-64 multimode interference power splitter for optical communications (Rasmussen et al., 1995). Such filters have reflection and low losses performance characteristics, which is compatible with optical single mode fibers. It uniformly distributed the output power on the N-way waveguide. This proposed method avoided the sharp edges that are near to the branching point thus led to a process-tolerant design. Its structure is produced in fiber-compatible integrated devices due to it is inherent in the silica-on-silicon technology.

There have been many designs of power splitters. Recently, multi-layer microstrip technology has been used. This is used for the reduction of size of the microwave components. They are designed using different design methodologies and geometries, for example, a power splitter (PS) based on multilayer slot-line technique with bandpass filtering (Song and Xue, 2010), (Abbosh, 2007), (Abbosh and Bialkowski, 2007). Even though they are shown to give good insertion loss performance they are, however, complicated to fabricate due to exact positioning of the orthogonal isolation resistance (Song and Xue, 2010). In (Abbosh, 2007), a 3-way PS based on multilayer broadside coupled structure was presented. It shows a good power division and isolation but it's difficult to align and fabricate due to the two ground planes that the structure needs (Abbosh and Bialkowski, 2007).

In (Chen et al., 2013), miniaturized power divider with band-pass characteristics based on coupled-resonator topology was presented, the reduced circuit are due to shrinking of assembled resonator. A general unequal two way power splitter was designed by (Parad and Moynihan, 1965) and some design equations for a multi-way unequal power splitter and the design method for multi-way dual band, due to the development of dual band PS, is seen in (Hee-Ran et al., 2004) and (Wu et al., 2010) respectively. But they all failed to miniaturise the unequal power splitter (UPS). Recently there have been several methods proposed that is

focused on miniaturising the PS. The isolation impedance is placed within the quarter wavelength of the transmission line to be used for interconnection and impedance transformation to make the structure avoid extra line. However, the PS electrical length was not reduced (Wang et al., 2014), (Trantanella, 2010), (Choe and Jeong, 2014). There has been reduction of the electrical length and characteristics impedance for a four-way equal PS, but this cannot be used for UPS.

2.2 Review of substrate integrated waveguide

In the past few decades, there has been remarkable amount of research carried out to develop high-performance millimeter-wave and microwave waveguide components that are manufactured using low-cost technologies. Substrate integrated waveguides (SIWs) are among these. It was introduced initially as laminated waveguides (Hirokawa and Ando, 1998) and (Uchimura et al., 1998) that can be implemented easily using printed circuit board (PCB) technology of fabrication. Since SIWs and laminated waveguides are introduced, numerous SIW-based components, circuits and interconnects have been developed and their advantages are justified when compared to waveguide or equivalent transmission line based.

It has been discovered that Q factor and power handling achieved with SIW resonators are much higher than what's attained with traditional planar microstrip or stripline results, which made the SIW cavities the best entity for application in direct and cross-coupled filters (Bozzi et al., 2009b). However, the physical dimensions of SIW circuits may be too large for certain applications, especially those operating at low frequencies. Among the approaches to achieve reduced size of SIW resonators and filters there are ridged SIW (Shelkovnikov and Budimir, 2005) and EBG-substrate (Grigoropoulos et al., 2005) concepts. The use of advanced

multilayer technologies, such as LTCC inspired the development of newly folded SIW (FSIW) structures, which not only reduce the area occupied by waveguides or resonators on a chip but also offer new design solutions to realize advanced cross-coupled filters with and without non-resonating nodes (NRN). Hong (Hong, 2006) proposed and compared two types of compact FSIW resonant cavities. A quarter-wavelength FSIW cavity, obtained by the successive folding of a conventional $\lambda/2$ wavelength FSIW resonator, has been successfully developed, employed and implemented on a cross-coupled filter (Alotaibi and Hong, 2008); another miniaturisation method for FSIW resonators has been established in (Lin, 2007); a directional filter built upon a half-mode SIW (HMSIW) has been proposed in (Wang et al., 2007).

Substrate integrated waveguide (SIW) interconnects provide a broadband bandpass signaling medium with excellent electromagnetic interference (EMI) isolation (Suntives and Abhari, 2007), while planar conventional transmission lines are known as the performance tailback in ultra-wideband systems due to their high-frequency losses and limited bandwidth. The electric field in an SIW distribution fills the volume inside the waveguide interconnect and surface currents propagate on the larger total cross-sectional area of the waveguide walls, thereby reducing conductor losses (Patrovsky et al., 2007). Due to the open structure and increased susceptibility to EMI and unwanted signal transfer, closely spaced stripline and microstrip will no longer be a good option system module interconnection.

There has been continuously increasing demand for compact electronic systems and wideband interconnects. This brought about the necessity of using SIW technology in future UHF, broadband and highly integrated systems application.

SIW is a geometric structure for that has the capability of transmitting signals and integrating

with other planar circuits and other lines. However, this may be challenging and many researchers have developed different modes of impedance matching transition from stripline, microstrip, coplanar waveguide and conductor backed coplanar waveguide (CBCPW) to SIW (Deslandes and Wu, 2001), (Rayas-Sanchez, 2009). Just like the SIW, these transitions are all implemented using the same process of fabrication just like the rest of the system's layout.

2.3 Applications substrate integrated waveguide to power divider

Components such as filters, Power Dividers and resonator cavities have now been redeveloped to SIW based platform. One of the most criticised about SIW components is its large size, However, research that has been published by (Grigoropoulos et al., 2005) and other researchers like (Izqueirdo et al., 2006) and (Che et al., 2008) have particularly focused in trying to miniaturise these components.

Numerous types of SIW diplexers, couplers and power dividers have been implemented and optimised for operation at millimeter and microwave frequency bands using PCB substrates as explained by several researchers including (Zhen-Yu and Ke, 2008) and (Shen et al., 2009). Other SIW-based components like waveguide cavities have also been directly integrated into a PCB platform, thus, allowing significant cost decrease in the development and mass production of resonator-based microwave components including filters and oscillators. The waveguide cavities high quality factor provides excellent frequency selectivity for cavity coupled resonators (Hill et al., 2001).

There are many microwave filter topologies used in exploring SIW cavities. Some example

are reported in (Glubokov and Budimir, 2009), (Chen et al., 2007) and (Chen et al., 2009). Nowadays, it's possible to develop a fully integrated multichip module (MCM) systems incorporating high-gain antennas and SIW filters. SIW cavity-backed antennas and slot array SIW antennas enables microwave designers to incorporate low cost, high-performance antennas on the same substrate as monolithic microwave integrated circuits (MMIC)(Ocket et al., 2009)

There is huge interest in space exploration, including mission to Mars and SIW technology is one of the most attractive design platforms. Reducing payload is critical in maximising fuel efficiency as a result of the very long astronomical travel distances of such missions. Ultra-light SIW-based electronic communication systems development will reduce the overall spacecraft and satellite payloads when compared to the units deployed with milled metallic waveguides (Daneshmand and Mansour, 2005). Lightweight SIW antenna arrays are critical in the development of portable communication base stations for space exploration systems. Also, SIW components are excellent choice for Earth orbiting satellites, ground-to-air base stations and un-manned drone aircraft applications as well as high-speed data hubs and Internet.

In comparison to other popular planer guiding structures like microstrip and CPW, SIW offers lower losses (Khan et al., 2013) but occupies larger area. Therefore, miniaturisation of SIW based components is essential for a compact design. The width of a half-mode SIW (HMSIW) is almost half of that of a standard SIW (Jones and Daneshmand, 2016). So, components based on HMSIW occupy smaller area. Using the HMSIW technology, a compact four-way equal split power divider is reported in (Zou et al., 2011). In (Jin et al., 2013), size of the SIW based components is further reduced to obtain quarter mode SIW

(QMSIW). In (Zhang et al., 2015), further miniaturisation is obtained by one-eighth mode SIW resonator (EMSIW). EMSIW is utilised to design compact bandpass filter. In all the components, SIW-to-microstrip transitions are used for SMA connection. On the other hand, to reduce the circuit size and the loss introduced by SIW-microstrip transition, direct coaxial feed is used in SIW power dividers. In (Seo et al., 2009), a coaxial feed at the center of a rectangular SIW structure is used as the input and SIW-to-microstrip transitions are used for the output ports. Further, metallic posts are used to control the output power levels at the output ports. Whereas in (Song et al., 2008), equal split eight-way power divider using direct coaxial feed at all the ports is reported. Size reduction is achieved but suffer low bandwidths of the power dividers.

Studies on SIW based equal power dividers are described in (ZhargCheng et al., 2005), (Tiwari et al., 2015). In (Datta et al., 2013), (Karimabadi and Attari, 2012) , studies on broadband equal power divider using SIW technology are presented. Design of an equal and unequal power divider is described in (Yang and Fathy, 2007) but suffers mismatch between the predicted and measured insertion and also failed to include the output isolation.

In this thesis, a simple design approach is described to implement SIW based equal and unequal power divider while maintaining a broad operating bandwidth and capable of not transferring signals between the output ports. The manufactured component promises to be lightweight, compact and with high power handling.

2.4 Summary

This chapter has presented a brief literature review of some existing literatures relating to PD and SIW, it has highlighted some of the problems with these designs and what needed to be done in order to improve these gaps. Some of these gaps have been address and are also indicated. It has also shown the reasons that prompted this research through attempting to solving these problems. The next Chapter dwell deeply into power dividers.

CHAPTER 3

POWER DIVIDER

3.0 Introduction

In this chapter, emphasis will be made to theories relative to power dividers. It will outline the various examples of PD including some of their advantages and their respective applications and topologies as being used microstrip technology. The scattering (S) matrix is presented in which its phenomenon is used to express the insertion loss, return loss, isolation etc. of the PD. It provides the matrix from the theory of incident and reflected wave. The next section outlines the various types of PD that led to the development of the PD concept, including the Wilkinson PD. The following section focuses on the S-parameters of the Wilkinson PS owing to its unique PD characteristics. Then the reflection and insertion loss parameters are discussed using its mathematical expressions and lastly it outlines a brief on the PD polynomials.

3.1 Scattering matrix

The scattering matrix is used to express the characteristics of a power divider. It is also known as the S-matrix and it is used to give the relationship between voltage waves that are incident on a device port with respect to the voltages, which are reflected on the device port, considering both phase and magnitude. Equation 3.1 gives the S-matrix in terms of its incident V^+ voltage wave and the reflected voltage wave V^- (Pozar, 2011).

$$\begin{bmatrix} V_1^- \\ V_2^- \\ \vdots \\ V_N^- \end{bmatrix} = \begin{bmatrix} S_{11} & S_{12} & \cdots & S_{1N} \\ S_{21} & S_{22} & \cdots & S_{2N} \\ \vdots & \vdots & S_{33} & \vdots \\ S_{N1} & S_{N2} & \cdots & S_{NN} \end{bmatrix} \begin{bmatrix} V_1^+ \\ V_2^+ \\ \vdots \\ V_N^+ \end{bmatrix} \tag{3.1}$$

This equation can as well be written as:

$$[V^-] = [S][V^+] \tag{3.2}$$

From the above equations, the appropriate incident and reflected voltage wave can be used to deduce each S-matrix element. Therefore, the general equation for the S-matrix element can be defined as:

$$S_{ij} = \frac{V_i^-}{V_j^+}\Big|_{V_k^+ = 0 \; for \; k \neq j} \tag{3.3}$$

This equation implies that the ratio of the reflected wave of the voltage V_j^+ to the incident wave of the voltage V_i^- gives the element of the S-matrix S_{ij}; where the incident wave is the driving port j and port i exits the reflected wave. In addition, the incident waves on all ports are set to zero except the j^{th} port. This implies that to avoid reflections, all ports should be terminated in matched load. This can be used to explain that when looking at port i, S_{ii} is the reflection coefficient and S_{ij} is the transmission coefficient from port j to port i when all other ports have been terminted in matched loads (Pozar, 2011). To measure these parameters, a Vector Network Analyzer (VNA) is typically used. For power divider, which contains three ports, any port that is not measured is terminated with a matched load.

The input impedance as seen at each port is equivalent to the system's characteristics impedance when all the ports are matched. The reflection coefficient of the equivalent impedance is zero, which means that there is no insertion or reflection of the incident wave.

Therefore, the reflected wave voltage at that reference point is zero. Since the reflected wave is zero, from equation e.3 (the S-matrix element where $i = j$), it is obvious that the S-matrix element is also zero. This, therefore, shows that when a device is properly matched at each of its port, the S-matrix diagonal element will all be zero (Pozar, 2011, Grebennikov, 2011).

Power dividers, like other devices, possess a common characteristic, which is reciprocity. Reciprocity is a concept used to describe the power-transmitted devices or network ports similar irrespective of the propagation direction through the device or network. Hence for a reciprocal network;

$$S_{ij} = S_{ji} \tag{3.4}$$

For all values of i and j. This relationship shows that the reciprocal network has a symmetrical S- matrix (Pozar, 2011).

Another unique feature of the S-matrix is the amount of power which is lost that is attributed to it network. It would have been ideal for a power divider that is lossless to have been used, however, a completely lossless power divider is physically unrealisable. It has been highlighted on several occasions by (Pozar, 2011) that for a lossless network, the S-matrix must be unitary.

$$[S]^t[S]^* = [I] \tag{3.5}$$

Where the t represents the matrix transpose, the asterisk represents the matrix conjugate and I is the identity matrix. A unitary matrix means that the sum of squares of the column elements of that matrix is equivalent to one (Grebennikov, 2011, Chang, 2005).

Critical to the performance of output port of a power divider is the isolation. Isolation is a characteristic that possesses the ability to isolate signal between ports or for signals from one output port not to affect the other output port. For power divider, three port device, which has two outputs, 2 and 3. It is vital to reduce the unwanted signal transfer caused by the coupling between the ports. The element S_{23} and S_{32} are used to represent the isolation between the output ports 2 and 3. The S_{23} represents the signal leaving the port 2 and entering the port 3 and S_{32}, the reverse. A high isolation is achieved between port 2 and 3 when the magnitude of these elements are small (Pozar, 2011, Grebennikov, 2011, Chang, 2005)

An ideal power divider will be a very low loss or lossless, matched at each port and be reciprocal. However, this is impossible to achieve. To demonstrate that any three-port power divider network exhibits the ideal characteristics. Consider the S-matrix:

$$[S] = \begin{bmatrix} S_{11} & S_{12} & S_{13} \\ S_{21} & S_{22} & S_{23} \\ S_{31} & S_{32} & S_{33} \end{bmatrix} \tag{3.6}$$

Firstly, it is assumed that the device is reciprocal and matched to all the ports. Based on the relationship for the reciprocal and matched port cases, applying them to the S-matrix reduces the generic three-port S-matrix to (Collin, 2001):

$$[S] = \begin{bmatrix} 0 & S_{12} & S_{13} \\ S_{12} & 0 & S_{23} \\ S_{13} & S_{23} & 0 \end{bmatrix} \tag{3.7}$$

As stated above, for lossless condition, the sum of squares of column elements of the S-matrix in equation 3.7 must be unitary; that is equal to 1.

$$|S_{12}|^2 + |S_{13}|^2 = 1 \tag{3.8a}$$

$$|S_{12}|^2 + |S_{23}|^2 = 1 \quad (3.8b)$$

$$|S_{13}|^2 + |S_{23}|^2 = 1 \quad (3.8c)$$

$$S^*_{13}S_{23} = 0 \quad (3.8d)$$

$$S^*_{23}S_{12} = 0 \quad (3.8e)$$

$$S^*_{12}S_{13} = 0 \quad (3.8f)$$

This means that two of the three elements, S_{12}, S_{13}, and S_{23} must be zero in order to satisfy (equations (3.8a – 3.8f). For analysis purpose, S_{12} and S_{13} are set to zero. However, by setting these parameters zero equation 3.8a is not achieved as the sum gives zero. Consequently, when any two of the three S_{12}, S_{13}, and S_{23} are zero, then one of the equations 3.8a -3.8b will not be fulfilled. This therefore makes matched ports, lossless and reciprocal three-port network impossible to obtain (Pozar, 2011, Grebennikov, 2011, Chang, 2005).

3.2 Types of power divider

Although the ideal characteristics including reciprocal, matched and lossless of a power divider, are not physically realisable, there are some power dividers that exhibit at least two of the idle properties. The common power dividers with its unique features are T-Junction, resistive and the Wilkinson power divider. One of the various methods that is used to construct power divider is transmission lines method. This include, using a microstrip or waveguide or resistive network.

3.2.1 N-way Power divider

The N-way power splitter is used extensively in microwave applications, especially where it is required to split and then combine microwave power. Due to ease of manufacturing and low cost, microstrip line technology is mostly used in this N-way power divider and this can be easily integrated with amplifier system. There are several common N-way microstrip power divider; they include Fork power divider (Galani and Temple, 1977), radial power dividers (Fathy et al., 2006), tapered line power dividers (Yau et al., 1986) and sector-shaped power divider (Abouzahra and Gupta, 1988). Shown in Figure 3.2(a-d) are examples of the various power dividers discussed.

3.2.1.1 Fork power divider

The Fork power divider has low loss characteristics, a broad bandwidth and between its output ports, there is a good isolation performance (Galani and Temple, 1977). The divided part consists of N number of transmission lines as shown in Figure 3.1a. The adjacent output ports contain an N-1 number of isolation resistors and a quarter wavelength at the center frequency with input characteristics impedance Z_0.

3.2.1.2 Tapered Power Divider

The tapered microstrip power divider is advantageous as it provides a good amplitude, phase and wideband characteristics. As shown in Figure 3.1b, the output port of the special

microstrip line power divider are located in a straight line and the function of the holes the module is to ensure that there is equal transmission path length from input to the output port (Eccleston et al., 1997).

3.2.1.3 Radial Power divider

The radial Power divider is popular in its ability in achieving an N-way power division. It presents an excellent phase and amplitude performance balance and low noise, particularly for higher N (Fathy et al., 2006). There is two sections which the Radial Power splitter consists of: the radial line and the launcher. The radial line is used to divide the signal into the output ports that are positioned around the edge of the radial line. It's made of parallel plates transmission lines with low loss and has a circular shape. The launcher section is the coaxial line that serves as a feed to the radial line in the middle. An example of radial power divider is shown in Figure 3.1c.

3.2.1.4 Sector-shaped power divider

The sector-shaped power divider also contains a good balance performance of phase and amplitude and wide bandwidth. As seen in the example of Figure 3.1d (Abouzahra and Gupta, 1988), this power divider uses a sectoral transmission line to split the signal into the various N output ports. These ports are equally spaced and positioned on the sectorial side.

The radial power divider is a non-planar structure since it requires a probe (vertical) coaxial line feeding port, whilst the other three power dividers, which are Fork, tapered and sector-shaped power splitters are completely planar structures.

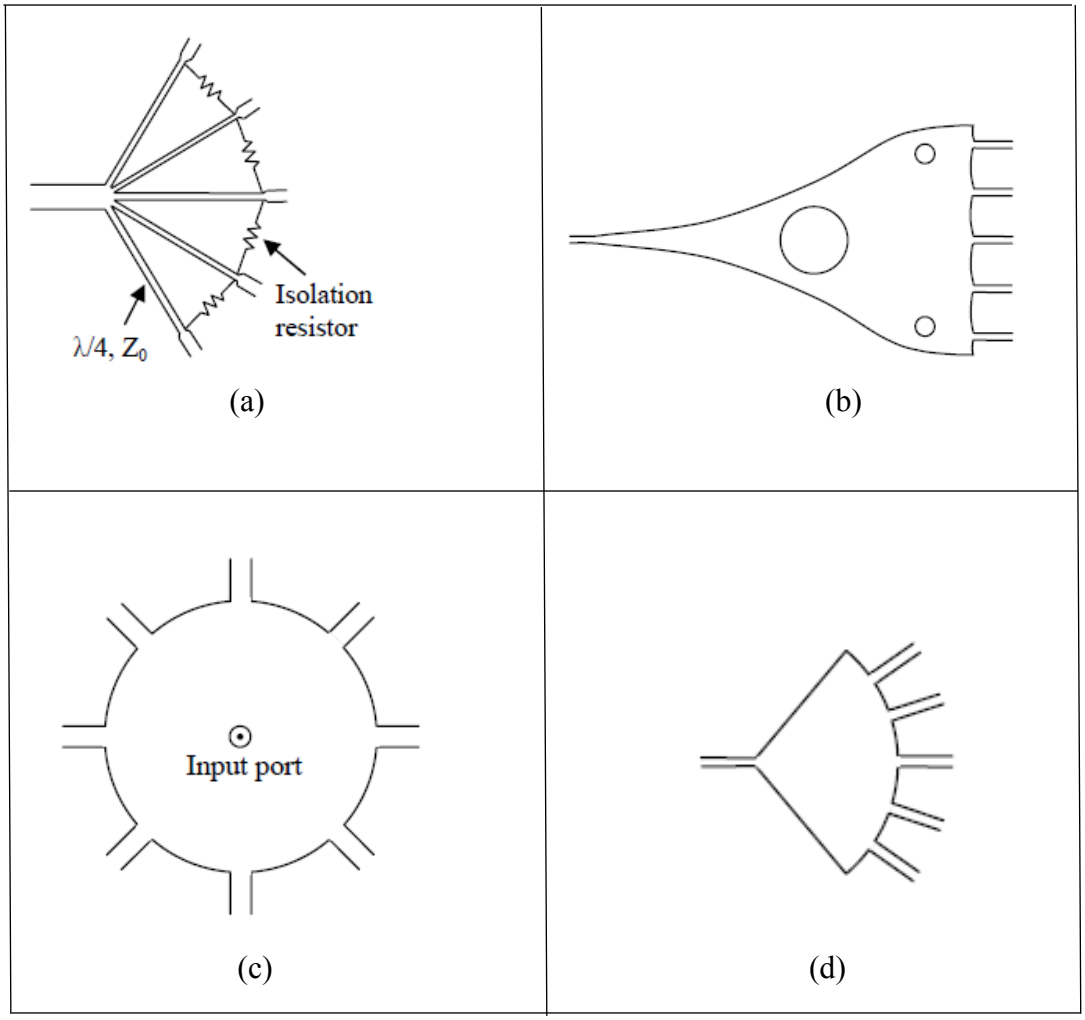

Figure 3.1a Fork Power divider (Galani and Temple, 1977)
Figure 3.1b Tapered Power divider (Eccleston et al., 1997)
Figure 3.1c Radial Power divider (Fathy et al., 2006)
Figure 3.1d sector-shaped Power Divider (Abouzahra and Gupta, 1988)

In summary, it is generally required that to achieve an improved isolation performance, the isolation resistors which are located between the output ports can be used and an N-way power divider requires a very good isolation over its bandwidth (Fathy et al., 2006, Abouzahra and Gupta, 1988)

When high power output is required in any power amplification system, power dividing/combining networks are essential (Zhang et al., 2010), (Yam and Cheung, 1997) and (Pengcheng et al., 2003). The input power divided firstly by the power divider to provide the signal that can be supplied to the power amplifiers. Using the power combiner, these amplified output signals can be combined into a single output with a higher power. Figure 2.2 shows an example of this system where there is a combination of output power from the many power amplifiers. There is structural identity between the N-way power divider and power combiner except that their inputs and output are placed in opposite order. When the power divider/combiner is symmetrical, the signals which are combined from the power amplifier should be the same in phase and magnitude to a maximum combining efficiency (Gupta, 1992).

3.2.2 Conventional T-Junction

The conventional T-Junction power divider is lossless which contains three transmission lines all connected at its common junction. There is a reactance linked to this junction. This is due to the effect of the fringing field and higher order mode. The T-Junction lossless transmission line model is shown in Figure 3.2, in accordance with (Pozar, 2011).

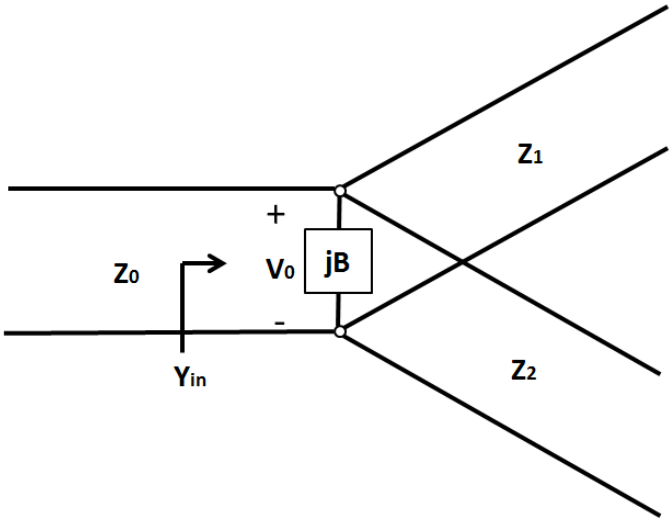

Figure 3.2 T-Junction lossless transmission line model

Even though this power divider is lossless, it suffers a drawback that not all the ports are matched and there is no isolation between its output ports. Lumped susceptance B can be used to represent the stored energy. To match the input characteristics Z_0, equation 3.9 must be satisfied:

$$Y_{in} = \frac{1}{Z_0} = jB + \frac{1}{Z_1} + \frac{1}{Z_2} \tag{3.9}$$

For a lossless or very low loss transmission lines, it means the characteristics impedances are real, that is the imaginary component is zero, and this makes $B = 0$. This equation 3.9 now becomes:

$$\frac{1}{Z_0} = \frac{1}{Z_1} + \frac{1}{Z_2} \tag{3.10}$$

Some reactive tuning elements can be utilized in the power divider configuration if B is not negligible.

Various power division ratios can be generated by calculating the output line impedance Z_1 and Z_2. For example, for an equal split (3dB) power divider, it can be designed by using two 100Ω for an input transmission line impedance of 50Ω. A quarter wavelength transformer could be utilised to realise the output lines impedance to its desired values. The input lines impedance are matched when the output lines are matched, however, the output ports will have no isolation.

If only two ports are matched, say port 1 and port 2, then a three-port network can be realized which is reciprocal and lossless. Hence, the scattered matrix is thus:

$$[S] = \begin{bmatrix} 0 & S_{12} & S_{13} \\ S_{12} & 0 & S_{23} \\ S_{13} & S_{23} & S_{33} \end{bmatrix} \tag{3.11}$$

Again, the following unitary conditions are achieved to make it lossless:

$$|S_{12}|^2 + |S_{13}|^2 = 1 \tag{3.12a}$$

$$|S_{12}|^2 + |S_{23}|^2 = 1 \tag{3.12b}$$

$$|S_{13}|^2 + |S_{23}|^2 + |S_{33}|^2 = 1 \tag{3.12c}$$

$$S^*{}_{13}S_{23} = 0 \tag{3.12d}$$

$$S^*{}_{12}S_{13} + S^*{}_{23}S_{33} = 0 \tag{3.12e}$$

$$S^*{}_{23}S_{12} + S^*{}_{33}S_{13} = 0 \tag{3.12f}$$

Equation 2.12a and equation 2.12f gives that $|S_{13}| = |S_{23}|$. This solves equation 3.12d to be $S_{13} = S_{23} = 0$ and $|S_{12}| = |S_{33}| = 1$. This network now consists of one matched two-port

lines and a mismatched one-port. The matrix and signal flow diagram for this arrangement is given below (Pozar, 2011).

$$[S] = \begin{bmatrix} 0 & e^{j\theta} & 0 \\ e^{j\theta} & 0 & 0 \\ 0 & 0 & e^{j\theta} \end{bmatrix} \tag{3.13}$$

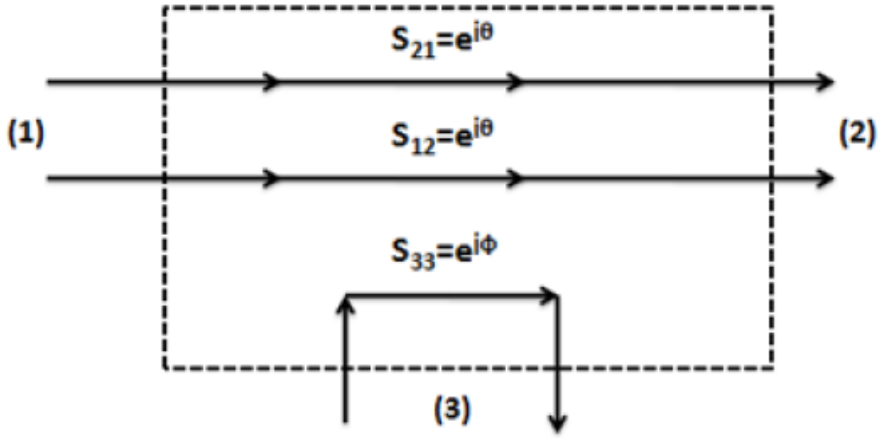

Figure 3.3 A Reciprocal, Lossless Three-Port Network Matched at Port 1 and 2 (Pozar, 2011)

3.2.3 Resistive Power Divider

For all the output ports to all be matched, a lossy component is introduced to the three-port network. However, there is no isolation between the output ports. This type of power divider contains lumped element resistors as illustrated in the Figure 3.4.

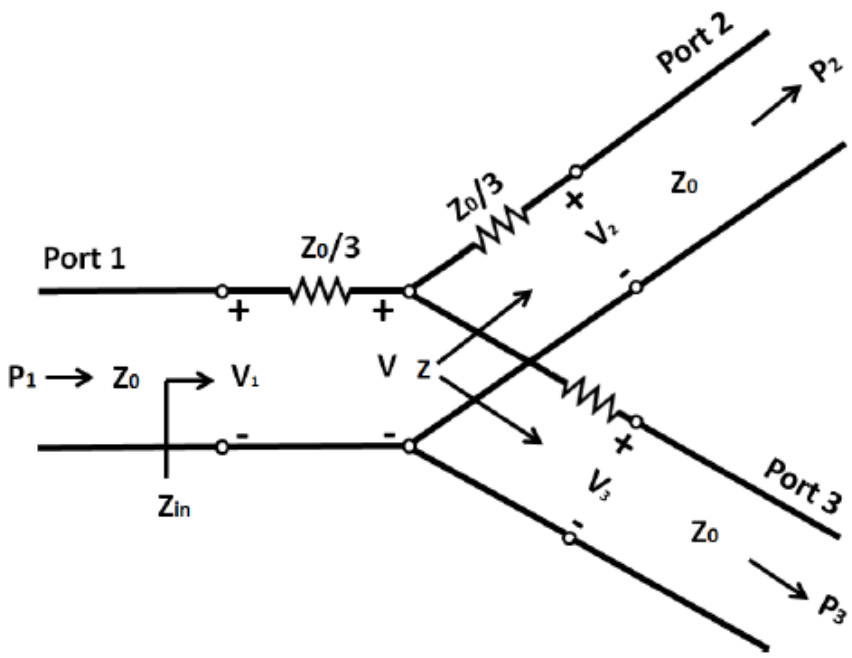

Figure 3.4 Equal-Split Three-Port Resistive Power Divider

Standard circuit theory can be used to analyze the resistive power divider. The characteristics impedance Z_o is used to terminate all the ports. Equation 3.14 gives the combination of the output lines and the impedance of $Z_0/3$ resistor.

$$Z = \frac{Z_0}{3} + Z_0 = \frac{4Z_0}{3} \tag{3.14}$$

The input impedance Z_{in} of the divider is given by:

$$Z_{in} = \frac{Z_0}{3} + \frac{2Z_0}{3} = Z_0 \tag{3.15}$$

All of the ports are matched since the resistive PD is symmetrical as demonstrated by equation 3.16.

$$S_{11} = S_{22} = S_{33} = 0 \tag{3.16}$$

Assuming that the voltage at the input port one is V_1, the voltage at the junction connecting all the ports is:

$$V = V_1 \frac{2Z_0/3}{Z_0/3+2Z_0/3} = \frac{2}{3}V_1 \tag{3.17}$$

The output voltages are then calculated as:

$$V_2 = V_3 = V \frac{Z_0}{Z_0+Z_0/3} = \frac{3}{4}V = \frac{1}{2}V_1 \tag{3.18}$$

This makes $S_{21} = S_{31} = S_{23} = 1/2$. Since the resistive power divider is reciprocal, then we have a symmetrical S-matrix.

$$S = \frac{1}{2}\begin{bmatrix} 0 & 1 & 1 \\ 1 & 0 & 1 \\ 1 & 1 & 0 \end{bmatrix} \tag{3.19}$$

The power that's delivered to the resistive power is:

$$P_m = \frac{1}{2}\frac{{V_1}^2}{Z_0} \tag{3.20}$$

Therefore, the power delivered to the output ports are:

$$P_2 = P_3 = \frac{1}{2}\frac{(1/2V_1)^2}{Z_0} = \frac{1}{8}\frac{{V_1}^2}{Z_0} = \frac{1}{4}P_m \tag{3.21}$$

The equation 3.21 shows that half of the power is dissipated in the resistors.

3.2.4 Wilkinson Power Divider

In 1960, Ernest Wilkinson proposed a Wilkinson power divider. This PD is capable of matching all the ports and can provide isolation between the output ports and is lossless when

all the output ports are matched (Wilkinson, 1960). Figure 3.5 and Figure 3.6 shows the microstrip and the equivalent transmission line circuit for the Wilkinson PD as taken from (Pozar, 2011) where there is equal power division to the two output ports.

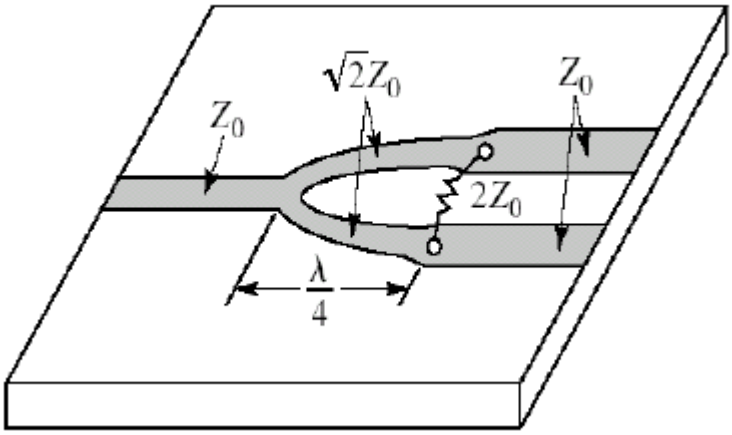

Figure 3.5 Equal-split Wilkinson power divider in microstrip form (Pozar, 2011)

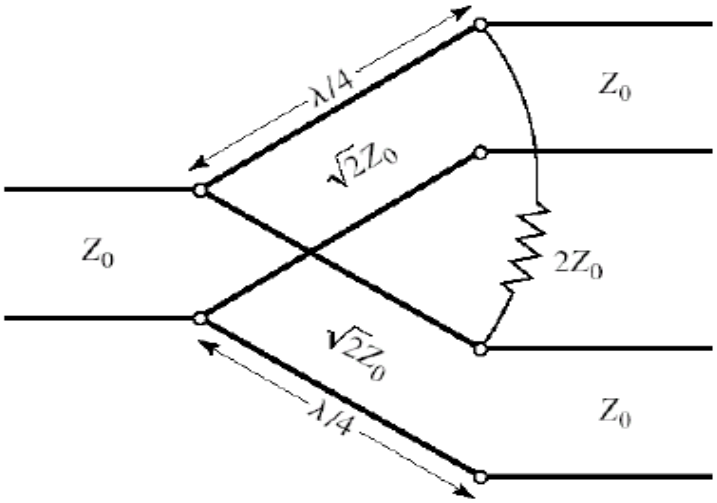

Figure 3.6 Equivalent transmission line circuit (Pozar, 2011)

Wilkinson PD design is made up of microstrip or stripline transmission line that has been divided into a number of transmission lines, each at the length of a quarter wavelength. In

his original proposal, each of the transmission lines is connected to the input through a shorting plate. There are resistors connected between the common junction and the each transmission line of the output. For an equal division Wilkinson PD, the voltages at the output of each transmission line contain equal magnitude and phase when all the output are connected to matched load. There will be no voltage drop across the connected resistors and therefore no power is dissipated (Wilkinson, 1960).

As seen in the Figure 3.5 and Figure 3.6, the characteristics impedance input transmission line is equal to the impedance of each quarter wave transmission line multiplied by a factor of $1/\sqrt{2}$. Additionally, the characteristics impedance input transmission line is equal to the internal resistor that connected the two-output ports multiplied by a factor of half. These impedances allow the input of the Wilkinson PD to be matched and also the output is matched and isolated (Wilkinson, 1960).

3.3 S-matrix derivation of Wilkinson power divider

The S-parameter matrix for the Wilkinson PD can be determined using even and odd mode analysis. It can be analyzed by using circuit symmetry and superposition. The circuit in Figure 3.6 is first redrawn by normalizing all impedance to the characteristics impedance Z_0 as shown in Figure 3.7 $Z = \sqrt{2}Z_0, r = 2Z_0$, where r is the introduced resistance that is connected between the two output ports.

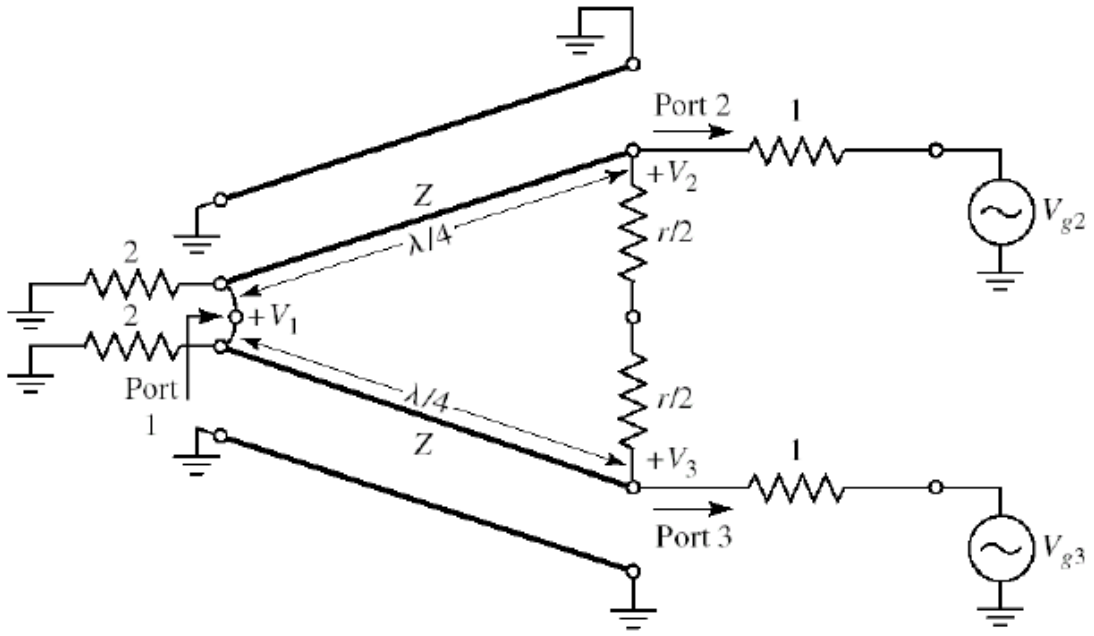

Figure 3.7 The Wilkinson power divider circuit in as normalized and symmetric form (Pozar, 2011)

Current is not flowing between the short circuit ends of the input of the two transmission lines, or between the $r/2$ resistors. Due to this, the circuit can, therefore, be bisected and separated into even and odd mode and each system can be analysed separately as given in Figure 3.8a and Figure 3.8b.

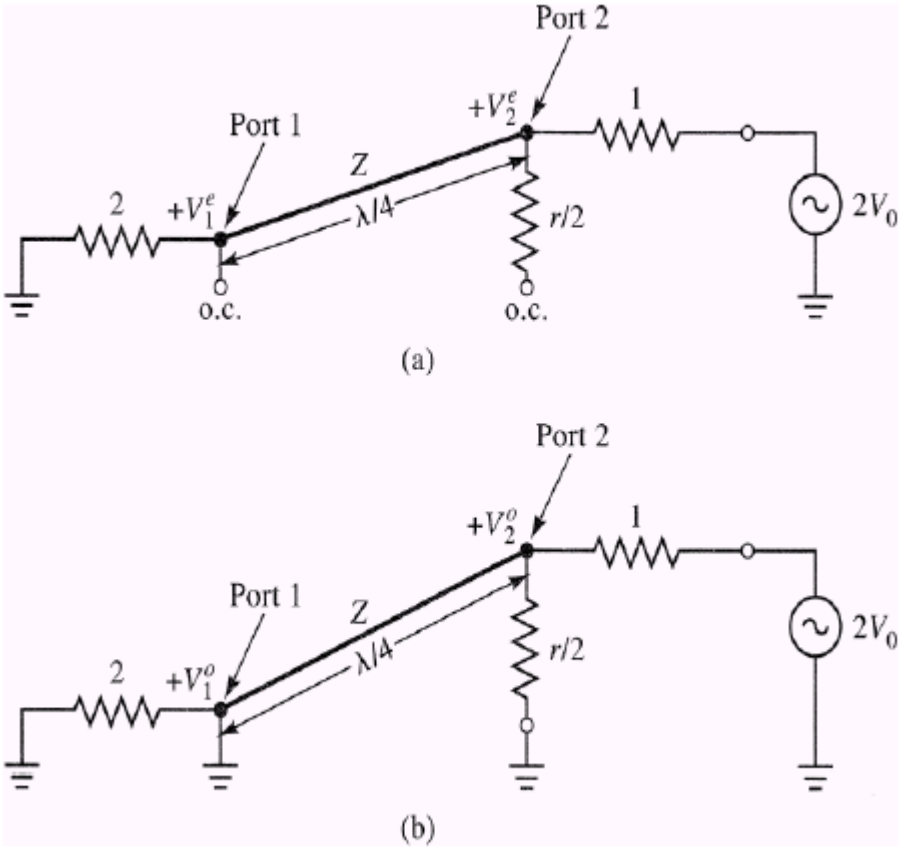

Figure 3.8 (a) Even-mode excitation. (b) Odd-mode excitation (Pozar, 2011)

3.3.1 Even mode analysis

In even mode excitation, $V_{g2} = V_{g2} = 2V$ and $V_2^e = V_3^e$. Since there is no current flow through the r/2 resistors, then the equivalent circuit in Figure 3.7 is then simplified into bisection with open circuit as shown in Figure 3.8 a-b. With reference to looking at port 2, the impedance is will be:

$$Z_{in}^{e} = \frac{Z^2}{2} \tag{3.21}$$

and

$$Z_{in}^{e} = \frac{(\sqrt{2}Z_0)^2}{2} = Z_0 \text{ (matched)} \tag{3.22}$$

The transmission line is a quarter-wave transformer. If $Z = \sqrt{2}Z_0$, for even mode excitation, the port 2 will be matched. Therefore, $V_2^e = V$ and $Z_{in}^e = Z$. The $r/2$ resistor is not necessary in this mode. Consider the voltage transmission line:

$$V(x) = V^+(e^{-j\beta x} + \Gamma e^{j\beta x}) \tag{3.23}$$

If x=0 at Port 1 and x=- λ/4 at Port 2, we've:

$$V_1^e = V(0) = V^+(1 + \Gamma) = jV\frac{\Gamma+1}{\Gamma-1} \tag{3.24}$$

$$V_2^e = V\left(-\lambda/4\right) = jV^+(1 - \Gamma) - V \tag{3.25}$$

The reflection coefficient Γ is that which is seen from looking at Port 1 towards the resistor of normalized value $2Z_0$. Therefore,

$$\Gamma = \frac{2-\sqrt{2}}{2+\sqrt{2}} \tag{3.26}$$

And

$$V_1^e = -jV\sqrt{2} \tag{3.27}$$

3.3.2 Odd mode excitation

In odd mode excitation,

$$V_{g2} = -V_{g2} = 2V \tag{3.28}$$

and

$$V_2^o = V_3^o \tag{3.29}$$

As in the even excitation mode, the voltage between the $r/2$ resistance of the equivalent circuit is negligible. Figure 3.11a and Figure 3.11b give an illustration of this mode that shows network being grounded at two points in the middle plane. There is an impedance of $r/2$ when looking into port 2 and the parallel transmission line is shorted at Port 1 and is $\lambda/4$ long whilst it's seem to be open circuited on Port 2. If $r = 2Z_0$, then port 2 will be matched in the odd excitation. Thus, $V_1^o = 0$ and $V_2^o = V$. This means there is no reflection of the signal at Port 1 and all of its power is transmitted to the r/2 resistor.

An equivalent circuit of a Wilkinson PD when terminally matched at Port 2 and 3 is shown in Figure 3.11a. Since $V_2 = V_3$, this circuit mode is similar to an even mode excitation. $2Z_0$ could be omitted since there is no current flow across that impedance. Figure 3.11b shows a simplified circuit to demonstrate the above assertions. The two-quarter wavelength parallel transformers are terminated in nominal loads; its impedance is given by:

$$Z_{in} = \frac{1}{2}\left(\sqrt{2Z_0}\right)^2 = Z_0 \tag{3.30}$$

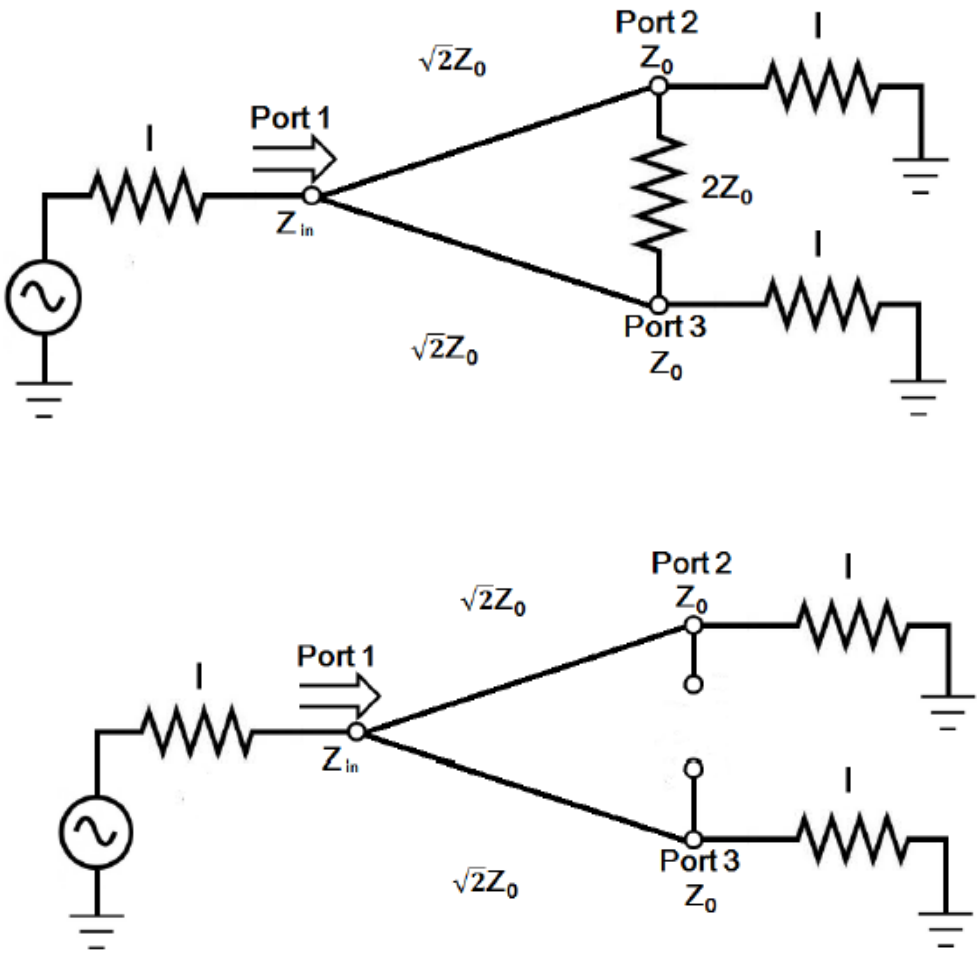

Figure 3.9 (a) Terminated Wilkinson Power Divider (b) Bisection Wilkinson Power Divider (Pozar, 2011)

In summary, the Wilkinson S-matrix can be concluded as follows:

$$S_{11}= 0\ (Z_{in} = Z_0, \text{ matched at Port 1}) \tag{3.31}$$

$$S_{22} = S_{33} = 0 \text{ (For the output port 2 and 3 are matched)} \tag{3.32}$$

$$S_{12} = S_{21} = \frac{V_1^e + V_1^o}{V_2^e + V_2^o} = -j/\sqrt{2} \text{ (They are symmetrical due to reciprocity)} \tag{3.33}$$

$$S_{13} = S_{31} = -j/\sqrt{2} \quad \text{(Symmetry of port 2 and 3)} \tag{3.34}$$

$$S_{23} = S_{32} = 0 \text{ (Due to short or open circuit at the bisection)} \quad (3.35)$$

It can be deduced from the above analysis that:

a. When the Wilkinson PD is terminated with matched loads, all the ports are matched.

b. No power is dissipated in the resistor when the divider network is driven by port 1 with the output ports matched.

c. When all the output is matched, the Wilkinson PD is lossless except that only the reflected power at port 2 and 3 are lost by the resistor.

d. There is high isolation between port 2 and 3 since $S_{23} = S_{32} = 0$.

Therefore, the Wilkinson PD S-matrix could be written as:

$$[S] = \frac{-1}{\sqrt{2}}\begin{bmatrix} 0 & j & j \\ j & 0 & 0 \\ j & 0 & 0 \end{bmatrix} \quad (3.36)$$

The following figures of merits are given by (Ludwig and Bogdanov, 2009), this evaluates the performance of the Wilkinson power divider.

$$RL_1\,[dB] = -20\log|S_{11}| \quad (3.37)$$

$$RL_2\,[dB] = -20\log|S_{22}| \quad (3.38)$$

$$CP_{12}\,[dB] = -20\log|S_{12}| \quad (3.39)$$

$$IL_{23}\,[dB] = -20\log|S_{23}| \quad (3.40)$$

where RL_1& RL_2 is the return loss at ports 1 and 2 respectively, CP_{12} is the coupling between ports 1 and 2; and IL_{23} is isolation between ports 2 and 3.

The Wilkinson S-matrix indicates that the power that enters port one can be equally divided into port 2 and port 3. This sets S_{11}, S_{22}, and S_{33} equal zero since the ports are matched. The Wilkinson PD is lossless and when a signal is applied at port 1, the sum of square of the column element of the matrix is unity (Pozar, 2011).

Also, if the signal is applied at port 2, only half of that applied signal is transmitted to port 1 and this implies that the other half of the signal has been lost through the resistor. However, reciprocity is achieved ($S_{21} = S_{12}$), Furthermore, no power can be observed at port 3 when it is applied to port 2 due to the isolation between those ports (S_{23} and S_{32} are equal to zero).

The Wilkinson PD has a good quality of effectively handling reflection in its network. The output port reflected signal is equivalent to applying the signal at the output port. The reflected signal travel through two routes; the first route is through initial input junction and the second route is through the resistor. The signal arrives at a specific phase through the resistor and since the transmission line is a quarter- wavelength, the signal through the two-quarter wave lines (the two 90^0 phase shift) reaches at 180^0 out of phase. When this out-of-phase signal is equal in magnitude, there is a complete cancellation of the signal resulting to an isolation of the output ports (Konishi, 1998).

The Table 3.1 gives merits and demerits of the 3 types of passive power dividers.

Table 3.1 Merits and Demerits of three passive power dividers

Power Divider	Merit	Demerit
T-Junction	➢ Lossless	➢ Not all ports are matched ➢ The output ports are not isolated
Resistive	➢ All ports can be matched	➢ The output ports are not isolated ➢ Lossy ➢ Very poor power handling capacity. Limitation due to resistor tolerance.
Wilkinson	➢ High Isolation ➢ Lossless (If all the ports are matched)	➢ If mismatched, there is reflected power dissipation through the isolated resistor

3.4 Reflection and Insertion loss parameters

The insertion and the loss equations (in dB) for a 3-port power splitter containing *N* numbers of coupled resonators are defined as follows:

$$L_{21} = -20\log|S_{21}| \tag{3.41}$$

$$L_{31} = -20\log|S_{31}| \tag{3.42}$$

$$R_L = -20\log|S_{11}| = -10\log|S_{11}|^2 \tag{3.43}$$

where L_{21}, L_{31} *and* R_L are the insertion loss between port 1 and 2, the insertion loss between port 1 and 3 and the reflection loss at port 1 respectively; all in dB. When the formula of conservation of energy is applied, we've.

$$|S_{11}|^2 + |S_{21}|^2 + |S_{31}|^2 = 1 \tag{3.44}$$

$$R_L = -10\log[1 - |S_{21}|^2 - |S_{31}|^2] \tag{3.45}$$

Consider, if the output powers are divided from the input power such that;

$$|S_{31}|^2 = \beta|S_{21}|^2 \tag{3.46}$$

where β is a positive integer factor.

By substituting the power of $|S_{21}|$ into the return loss equation and solving for $|S_{21}|^2$ and $|S_{31}|^2$, we've:

$$|S_{21}|^2 = \frac{1}{1+\beta}(1 - 10^{-0.1R_L}) \tag{3.47}$$

$$|S_{31}|^2 = \frac{\beta}{1+\beta}(1 - 10^{-0.1R_L}) \tag{3.48}$$

The power of $|S_{21}|$ and power of $|S_{31}|$ are then substituted into equation 3.44, L_{21} and L_{31} are now obtained as:

$$L_{21} = -10\log\left(\frac{1}{1+\beta}\right) - 10\log(1 - 10^{-0.1R_L}) \tag{3.49}$$

$$L_{31} = -10\log\left(\frac{\beta}{1+\beta}\right) - 10\log(1 - 10^{-0.1R_L}) \quad (3.50)$$

The term $10\log\left({}^{1}/_{1+\beta}\right)$ corresponds to the maximum value of $|S_{21}|$ and the term $10\log\left({}^{\beta}/_{1+\beta}\right)$ corresponds the maximum value of $|S_{31}|$ whilst the term $10\log(1 - 10^{.01R_L})$ is the ripple value in dB as shown in the Figure 3.10 (Skaik, 2011).

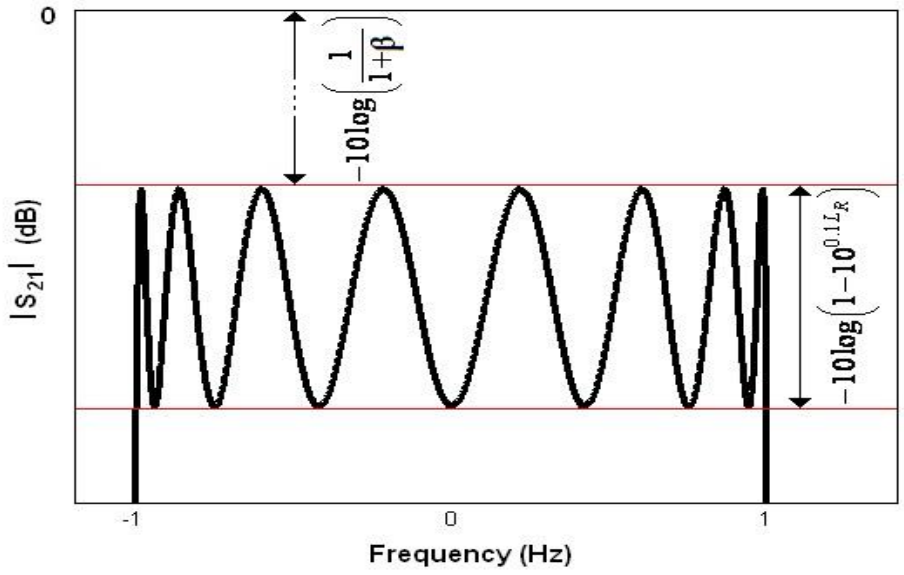

Figure 3.10 Insertion loss S_{21} (dB) (Skaik, 2011)

3.5 Polynomials of power divider

3.5.1 Two-port Power divider

According to Cameron et al. (2007), the reflection and transmission function for a two-port lossless network is defined in equation 3.51. This is a ratio of two N^{th} degree with reference to the network that composes of N inter-coupled resonator series filters.

$$S_{11}(s) = \frac{F_N(s)}{E_N(s)}, \qquad S_{21}(s) = \frac{P_N(s)}{\varepsilon E_N(s)} \tag{3.51}$$

where $s = j\omega$ is the imaginary of the complex frequency variable, and *E, F, P* are the characteristics polynomials. For a Chebyshev filtering function, at $\omega = \pm 1$ rad/s, the normalising constant for the transmission coefficient to the level of equal ripple is ε and is given by (Cameron et al., 2007).

$$\varepsilon = (10^{-0.1R_L} - 1)^{-0.5} . \left|\frac{P_N(s)}{F_N(s)}\right|_{s=\pm 1} \tag{3.52}$$

Here, the assumption is that $F_N(s)$, $P_N(s)$ and $E_N(s)$ are the normalized such that the coefficient of their highest degree is unitary; where R_L is the return loss (in dB).

3.5.2 Three-port Power divider polynomials

The reflection and transmission functions of a three-port power splitter that consists of N number of coupled resonators could be defined as a ratio of two polynomials as follows:

$$S_{11}(s) = \frac{F(s)}{E(s)}, \qquad S_{21}(s) = \frac{P(s)}{\varepsilon_1 E(s)}, \qquad S_{31}(s) = \frac{P(s)}{\varepsilon_2 E(s)} \tag{3.52}$$

where $s = j\omega$ is the imaginary of the complex frequency variable, and *E(s), F(s), P(s)* are the characteristics polynomials which are assumed to be normalized for the coefficient of their highest degree be unity. N is the filtering function order, $E(s)$ and $F(s)$ are the N^{th} order polynomial and the order of *P(s)* is the same as the prescribed number of transmission zero (Skaik, 2011).

A method of the recursive technique is used to find the roots of $F(s)$ which corresponds to the reflection zeros (Cameron, 1999). In a Chebyshev function, the constant ε_1 normalises $S_{21}(s)$ to a specified insertion loss level at $\omega = \pm 1$ whilst ε_2 normalise $S_{31}(s)$ under the same condition. If the constants ε_1 and ε_2 and the polynomials are known $F(s)$ and $P(s)$ are known, the polynomial $E(s)$ can be constructed. This polynomial has a complex root, which corresponds to the filter pole position. To derive the expression for ε_1, ε_2 and $E(s)$, the proceeding solutions are used.

From the conservation of energy of a three-port system which is defined as:

$$S_{11}(s)S_{11}(s)^* + S_{21}(s)S_{21}(s)^* + S_{31}(s)S_{31}(s)^* = 1 \tag{3.53}$$

Substituting equation 2.46 into equation 2.53, the next equation can be obtained, which is:

$$|S_{11}(s)|^2 + (1+\beta)|S_{21}(s)|^2 = 1 \tag{3.54}$$

The constant ε_1 is then obtained from equation 3.52 and equation 3.54 as:

$$\varepsilon_1 = \left|\frac{S_{11}(s)}{S_{21}(s)}\right| \cdot \left|\frac{P(s)}{F(s)}\right| = \frac{\sqrt{1+\beta}|S_{21}(s)|}{\sqrt{1-|S_{11}(s)|^2}} \cdot \left|\frac{P(s)}{F(s)}\right| \tag{3.55}$$

When $s = \pm j$, $|S_{11}|$ is equivalent to the maximum passband reflection coefficient, whose value is known from the given design specification. ε_1 can be expressed in terms of the polynomials $F(s)$ and $P(s)$, and the prescribed return loss level in dB, L_R, in the passband as follows:

$$\varepsilon_1 = \sqrt{\frac{1+\beta}{10^{-L_R/10}-1}} \cdot \left|\frac{P(s)}{F(s)}\right|_{s=\pm j} \tag{3.56}$$

Similarly, ε_2 can be obtained as:

$$\varepsilon_2 = \sqrt{\frac{1+\beta}{\beta(10^{-L_R/10}-1)}} \cdot \left|\frac{P(s)}{F(s)}\right|_{s=\pm j} \tag{3.57}$$

Once the polynomials $F(s)$ and $P(s)$, and the constants ε_1 and ε_2 are known, the denominator polynomial $E(s)$ can be derived by substitution of $F(s)$, $P(s)$ and $E(s)$, into the conservation of energy formula, as follows:

$$F(s)F(s)^* + \frac{P(s)P(s)^*}{{\varepsilon_1}^2} + \frac{P(s)P(s)^*}{{\varepsilon_2}^2} = E(s)E(s)^*$$

$E(s)E(s)^*$ is created by polynomials multiplications in the left-hand side of equation 2.57, which must be polynomial of the order 2*N* with real coefficients. The roots of $E(s)E(s)^*$ will be symmetric about the imaginary axis in the complex plane as shown in Figure 3.11, and they can be established using numerical analysis software such as MATLAB.

As $E(s)$ is strictly Hurwitz, then its roots are those in the left half plane, whereas the roots of $E(s)^*$ are those in the right half plane. The polynomial $E(s)$ is then constructed by choosing the *N* roots in the left half plane (Cameron et al., 2007).

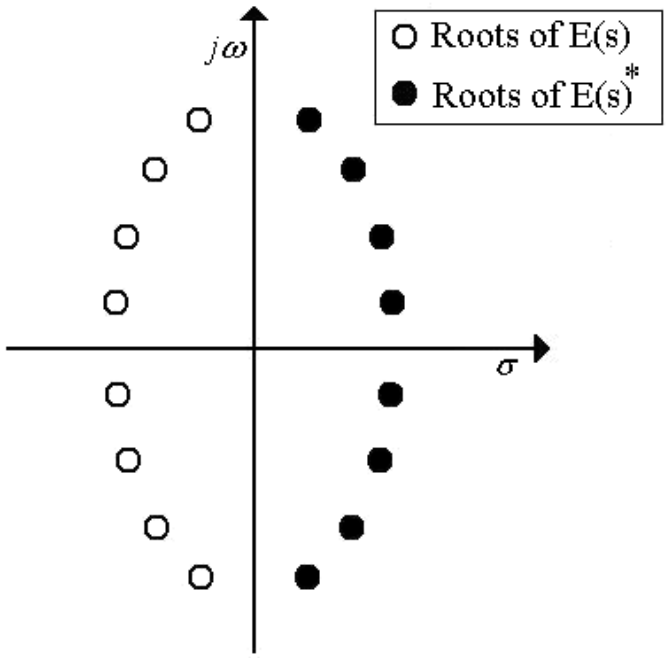

Figure 3.11 Pattern of the roots of $E(s)E(s)^*$

3.6 Summary

This chapter has outlined the theories that are related to PD including its applications. The scattering matrix associated with PD, including return and insersion loss have also been discussed. It also highlighted the matrix of the incident and reflected wave theory. The Wilkinson PD has been specifically dwelled into and its S-parameter has been shown which included mathematical expressions of its reflection and insertion loss parameters. Lastly, a brief outline has been made on the PD polynomial. The next chapter deals with the coupled resonator circuit.

CHAPTER 4

COUPLED RESONATOR CIRCUIT

4.0 Introduction

This chapter is focused on coupled resonator circuit. It concentrates on how the various filter design parameters are evaluated and derived. These include, the derivation of the coupling coefficient for synchronously tuned resonator circuit by considering electric and magnetic coupling. A single loaded resonator circuit is use to derive the external quality factor and its application to filter prototype circuit. Also, the common resonator coupling factor is formulated and the microstrip parameters are also evaluated and derived.

4.1 Coupling Overview

One of the most significant factors affecting a filter performance, in the design of an RF/Microwave filter, is the coupling of resonator circuit. Many literatures have extensively presented coupled resonator filter for many applications. Hong and Lancaster have given an approach for designing coupled resonator filters. This outlines a general technique which could be applied to any type of resonator used irrespective of its design or physical structure (Hong and Lancaster, 2001). They have included a technique that is based on a coupling matrix for coupled resonators, which has been aligned in a two-port, *n*-coupled resonator filter network. Some fundamental concept in coupled-resonator filter circuit theory will be introduced in relation to this work. Microwave filters using the fundamental concept of coupled resonators for its design purposes. In this thesis, the coupled resonator circuit design

technique is employed in the process of designing the filtered power splitter having a single input and two output circuit. Essentially, the derivation of the coupling matrix is important as it will serve as a foundation for the development of three port coupled resonator power splitter in Microstrip in Chapter 5 and in SIW in chapter 7.

Coupling coefficient of inter-coupled resonators and external Q factors of the input and output resonators are used as a general technique used to design coupled resonator filters. The coupling, k, of two coupled microwave resonators is defined based on the coupled to stored energy ratio. Mathematically, it could be given as:

$$k_{12} = \frac{\iiint \varepsilon \underline{E_1} \cdot \underline{E_2} dv}{\sqrt{\iiint \varepsilon \left|\underline{E_1}\right|^2 dv \times \iiint \varepsilon \left|\underline{E_2}\right|^2 dv}} + \frac{\iiint \mu \underline{H_1} \cdot \underline{H_2} dv}{\sqrt{\iiint \mu \left|\underline{H_1}\right|^2 dv \times \iiint \mu \left|\underline{H_2}\right|^2 dv}} \tag{4.1}$$

Where $\underline{E_1}$ and $\underline{E_2}$ & $\underline{H_1}$ and $\underline{H_2}$ are the respective electric and magnetic fields in resonator 1 & 2 respectively.

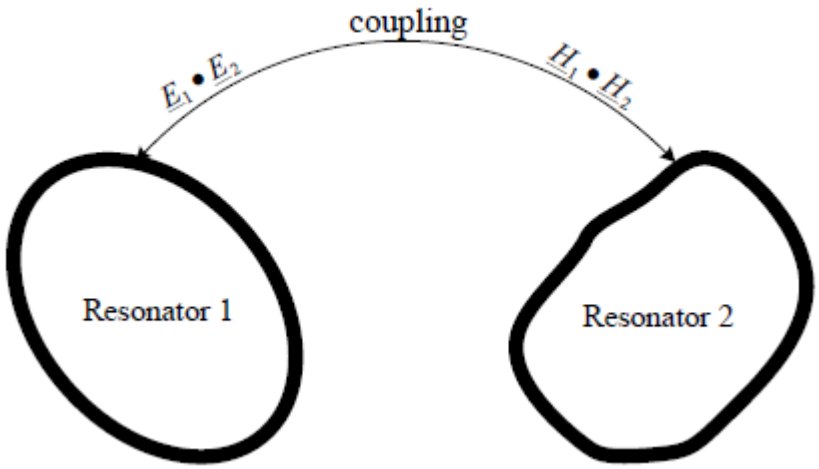

Figure 4.1 General coupled microwave resonators (Hong and Lancaster, 2001)

The dot operation of the space vector in equation 4.1 describes the interaction of the coupled resonator. The first term, on the right-hand side, indicated the electric coupling whilst the second term represents magnetic coupling. This then gives the allowance for either a positive or a negative coupling. The positive sign is used to describe when the coupling enhances the uncoupled resonators stored energy whilst the negative coupling sign implies that the uncoupled resonators stored energy is reduced. Therefore, the magnetic and electric coupling could have the same effect if the signs are the same or have the opposite effect if their signs are not the same (Hong and Lancaster, 2001).

It is quite an extensive and complex task to evaluate coupling coefficient since it requires field distribution and spatial integral performance. To overcome this, it may be much simpler by using full-wave EM simulation or an experiment is conducted to determine the characteristic frequencies that are linked to the coupled RF/microwave resonators coupling. However, for a narrow-band, a simplified lumped element circuit model is used to facilitate coupling coefficient analysis.

4.2 Synchronously Tuned Coupled-Resonator Circuits

4.2.1 Electric Coupling

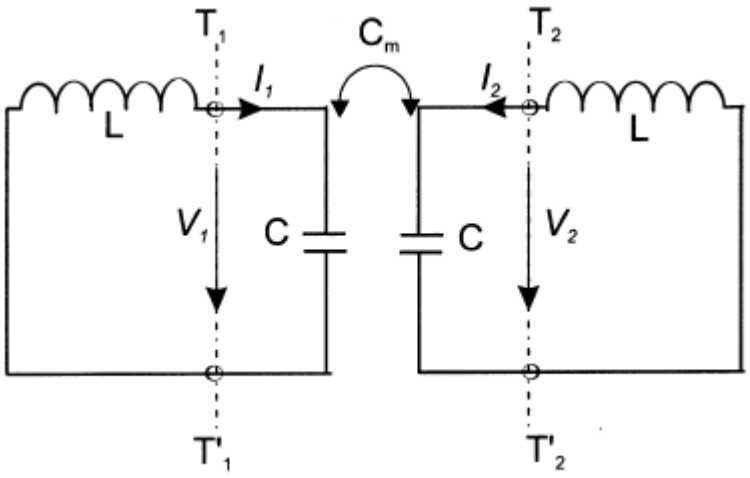

Figure 4.2 Synchronously tuned coupled resonator circuit with electric coupling (Hong and Lancaster, 2001)

Consider Figure 4.2 which gives an electrically coupled RF/microwave resonators equivalent lumped element circuit model; where L and C are the self-inductance and self-capacitance variables, C_m is the mutual capacitance and the angular resonant frequency $\omega_0 = 1/\sqrt{LC}$ of the uncoupled resonator. The mutual capacitance can be rearranged and included in the circuit to have a similar circuit representation according to Montgomery et al, (1948) (Montgomery et al., 1948), as seen in Figure 3.3.

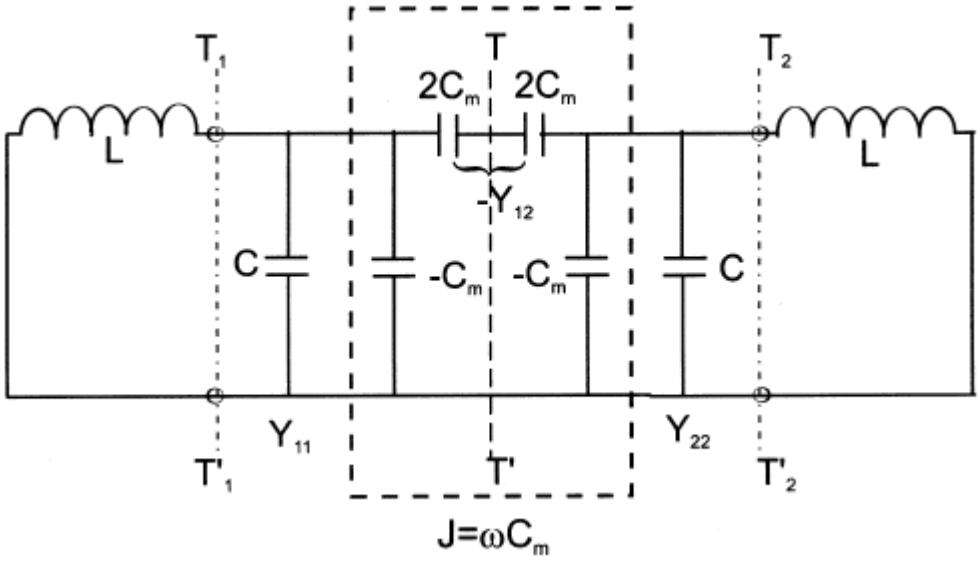

Figure 4.3 An alternative form of the equivalent circuit with an admittance inverter $j = \omega C_m$ to represent the coupling (Hong and Lancaster, 2001)

As seen in Figure 4.3, at the reference planes, T_1–T_1' and T_2–T_2', the two-port gives the following equations as:

$$I_1 = j\omega C V_1 - j\omega C_m V_2$$

$$I_2 = j\omega C V_2 - j\omega C_m V_1 \tag{4.2}$$

The admittance Y-parameters resulting from equation 4.2 are given as:

$$Y_{11} = Y_{22} = j\omega C$$

$$Y_{12} = Y_{21} = -j\omega C_m \tag{4.3}$$

If the symmetrical plan T-T' in Figure 4.3 is replaced by an electric wall or being short-circuited, the resonance frequency resulting from the resultant circuit is given by:

$$f_e = \frac{1}{2\pi\sqrt{L(C+C_m)}} \tag{4.4}$$

This concept is taken from $f_0 = 1/2\pi\sqrt{LC}$ for uncoupled resonance frequency by considering the two parallel mutual capacitors on one side of the symmetrical line.

It is worth noting that this electrical resonance frequency f_e is lower than the uncoupled single resonator f_0. This is because the coupling effect enhances the capability to store charge of the single resonator.

4.3.2 Magnetic Coupling

The magnetically coupled RF/microwave resonators equivalent lumped-element circuit model is given in figure 3.4

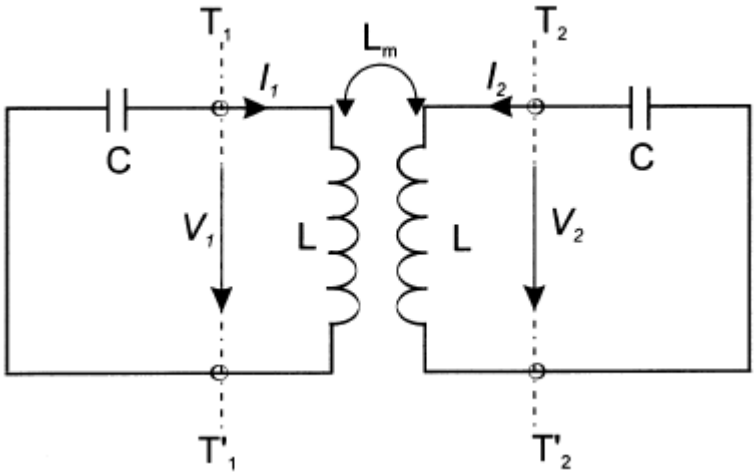

Figure 4.4 Synchronously tuned coupled resonator circuit with magnetic coupling (Hong and Lancaster, 2001)

where L and C are the self-inductance and self-capacitance variables, L_m is the mutual inductance. The mutual inductance can be rearranged and included in the circuit to have an alternative circuit as seen in figure 3.5.

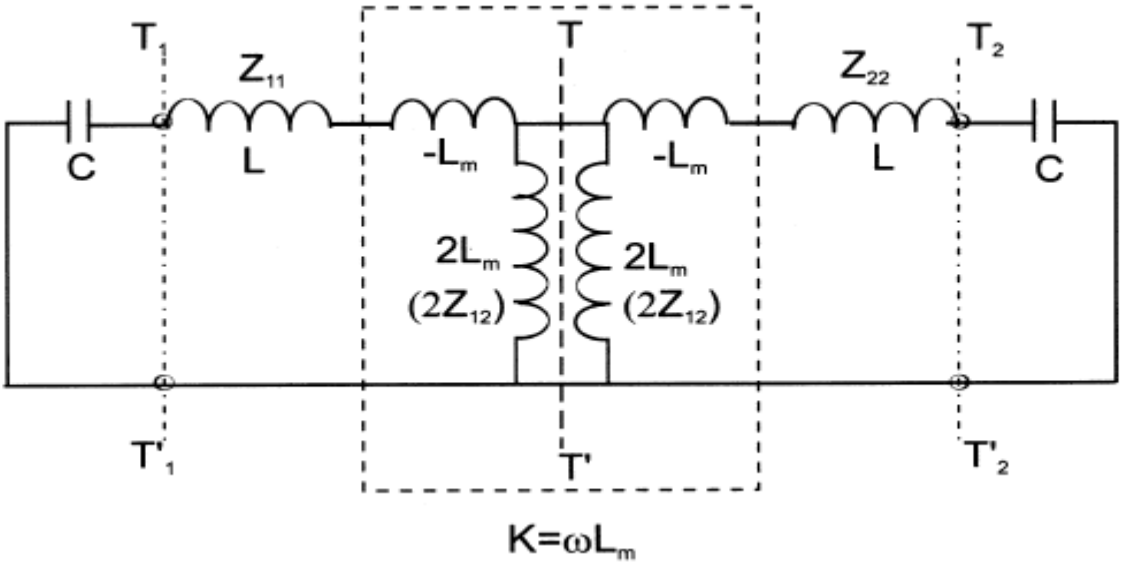

Figure 4.5 An alternative form of the equivalent circuit with an admittance inverter $K = \omega L_m$ to represent the coupling(Hong and Lancaster, 2001)

As seen in Figure 4.5, at the reference planes, T_1–T_1' and T_2–T_2', the two-port gives the following equations as:

$$V_1 = j\omega L I_1 - j\omega L_m I_2$$

$$V_2 = j\omega L I_2 - j\omega L_m I_1 \tag{4.5}$$

The admittance Y-parameters resulting from equation 4.5 is given as:

$$Z_{11} = Z_{22} = j\omega L$$

$$Z_{12} = Z_{21} = j\omega L_m \tag{4.6}$$

If the symmetrical plan *T*-*T*′ in Figure 4.3 is replaced by a magnetic wall or being open-circuited, the resonance frequency resulting from the resultant circuit is given by:

$$f_m = \frac{1}{2\pi\sqrt{L(C-C_m)}} \tag{4.7}$$

Also, it is important to state that this magnetic resonance frequency f_m is higher than the uncoupled single resonator f_0. This is because the coupling effect reduces the stored flux of the single resonator.

4.3.3 Determination of Coupling Coefficient

The electrical coupling coefficient is given by:

$$K_e = \frac{f_m^2 - f_e^2}{f_m^2 + f_e^2} \tag{4.8}$$

Considering equation 4.4 and equation 4.7, the electrical coupling now yields:

$$K_e = \frac{C_m}{C} \tag{4.9}$$

Similarly, the magnetic coupling coefficient is:

$$K_m = \frac{f_e^2 - f_m^2}{f_e^2 + f_m^2} = \frac{L_m}{L} \tag{4.10}$$

For synchronously tuned resonator, equation 4.10 generates to:

$$K = \frac{f_2^2 - f_1^2}{f_2^2 + f_1^2} \tag{4.11}$$

The mutual capacitance can also be written in terms of *J*-Inverters (Yeo, 2011). Given that $J = \omega C_m \rightarrow C_m = J/\omega$, the coupling coefficient is now:

$$K_e = \frac{C_m}{\sqrt{C_1 \cdot C_2}} = \frac{J}{\omega\sqrt{C_1 \cdot C_2}} \tag{4.12}$$

Where $\omega = \sqrt{\omega_1 \omega_2} = \frac{1}{\sqrt[4]{L_1 C_1 L_2 C_2}}$; L_1 and L_2 and C_1 and C_2 are inductance and capacitance of the first and second resonators respectively.

Therefore: $$K_e = J \cdot \sqrt[4]{\frac{L_1 L_2}{C_1 C_2}} \quad (4.13)$$

When all the inductors and capacitors are the same or $C = C_1 = C_2 = C_n$ and $L = L_1 = L_2 = L_n$, where n is the number of coupled resonators. The coupling coefficient now gives:

$$K_{k,k+1} = J''_{k,k+1} \sqrt{\frac{L_1}{C'_1}} = \frac{J_{k,k+1}\Delta}{\sqrt{g_k g_{k+1}}} \quad (4.14)$$

Where K represents the coefficient of the coupled resonators; $k = 1,2 \ldots n$ is the term used to represent the resonators; $J''_{k,k+1}$ is the J inverter value between the second, third and up to the last but one resonator; g are the normalised parameters and Δ is the fractional bandwidth.

4.4 Determination of external quality factor

Consider the two-input/output structure for the tapped line coupled microstrip SOLR. It is fed directly with a 50Ω feed line onto the input/output resonator. Changing the tapping position as indicated in Figure 3.6 alters the coupling or external quality factor. The smaller the value of t or closer the tapped line to the resonator's virtual ground, the weaker the coupling or larger the quality external factor (Hong and Lancaster, 2001).

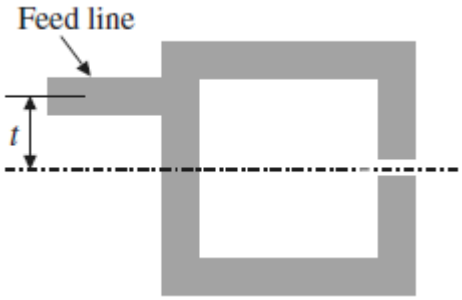

Figure 4.6 input/output structure for SOLR coupled resonator circuit (Hong and Lancaster, 2001)

4.4.1 Single loaded Resonator

The equivalent circuit of Figure 3.6 is given in Figure 3.7, where G is the external conductance affixed to the lossless LC resonator.

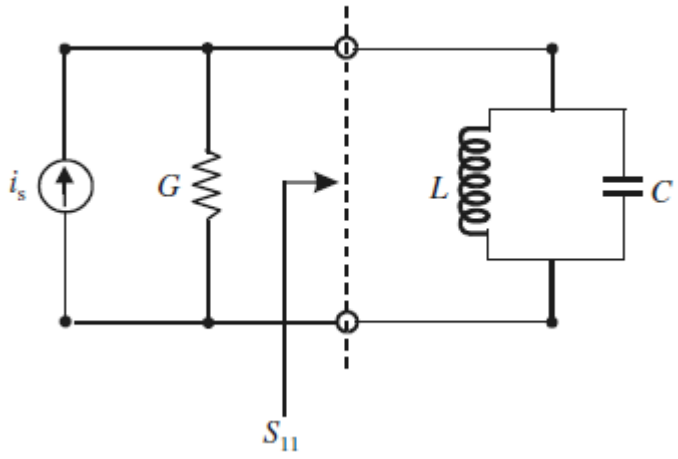

Figure 4.7 Input/output single loading equivalent circuit (Hong and Lancaster, 2001).

The reflection coefficient at the exciting port is:

$$S_{11} = \frac{G-Y_{in}}{G+Y_{in}} = \frac{1-Y_{in}/G}{1+Y_{in}/G} \tag{4.15}$$

where Y_{in}, the input resonator admittance is given by:

$$Y_{in} = j\omega C + \frac{1}{j\omega L} = j\omega_0 C\left(\frac{\omega}{\omega_0} - \frac{\omega_0}{\omega}\right) \tag{4.16}$$

In the resonance vicinity, $\omega = \omega_0 + \Delta\omega$, therefore we've:

$$Y_{in} = j\omega_0 C \cdot \frac{2\Delta\omega}{\omega_0} \tag{4.17}$$

The approximation $(\omega^2 - \omega_0^2)/\omega \approx 2\Delta\omega$ is used and substituting equation 4.17 into equation 4.15 and that $Q_{ext} = \omega_0 C/G$ yields:

$$S_{11} = \frac{1 - jQ_e \cdot (2\Delta\omega/\omega_0)}{1 + jQ_e \cdot (2\Delta\omega/\omega_0)} \tag{4.18}$$

The phase response of S_{11} varied with frequency and Figure 4.8 gives the curve of phase of S_{11} as a function of $\Delta\omega/\omega_0$.

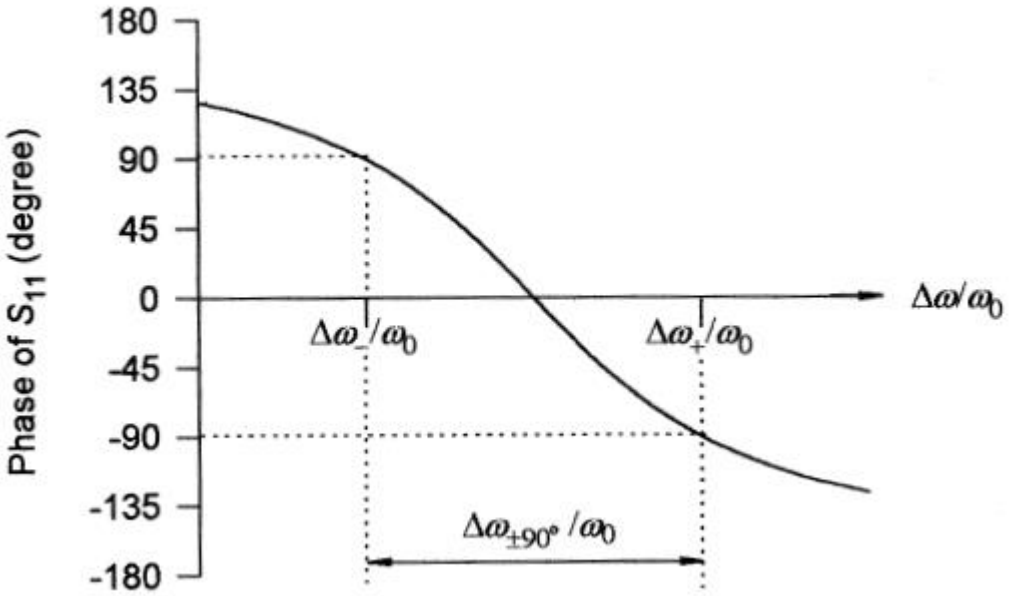

Figure 4.8 S_{11} phase response of figure 3.7(Hong and Lancaster, 2001)

When the phase is $\pm 90°$, the corresponding $\Delta\omega$ is:

$$2Q_{ext}\frac{\Delta\omega_{\mp}}{\omega_0} = \mp 1 \tag{4.19}$$

Therefore, the absolute bandwidth between the $\pm 90°$ points is:

$$\Delta\omega_{\pm 90°} = \Delta\omega_{+} - \Delta\omega_{-} = \frac{\omega_0}{Q_{ext}} \tag{4.20}$$

The external quality factor can now be extracted from equation 4.20 as:

$$Q_{ext} = \frac{\omega_0}{\Delta\omega_{\pm 90°}} \tag{4.21}$$

Similarly, J-inverter parameters can be used to determine Q_{ext}. Using $J = \omega C$ quality external factor gives4

$$Q_{ext} = \frac{\omega_0 C_1'}{J_{01}'} = \frac{g_0 g_1}{J_{01}\Delta} \tag{4.22}$$

Where C_1' is C_1/Δ and $J_{01}'$is the *J*-inverter value between the input and first resonator.

4.5 Determination of common resonators coupling coefficient factor

This concept was introduced by (Parad and Moynihan, 1965) and we modified to formulate/determine the factor or coefficient value, ψ between the common resonators and their respective next resonators. This is the value required to determine the coupling coefficient for both the equal and unequal split power splitter. To do this, consider the split T power splitter model in Figure 4.9. The split ratio is given by α:

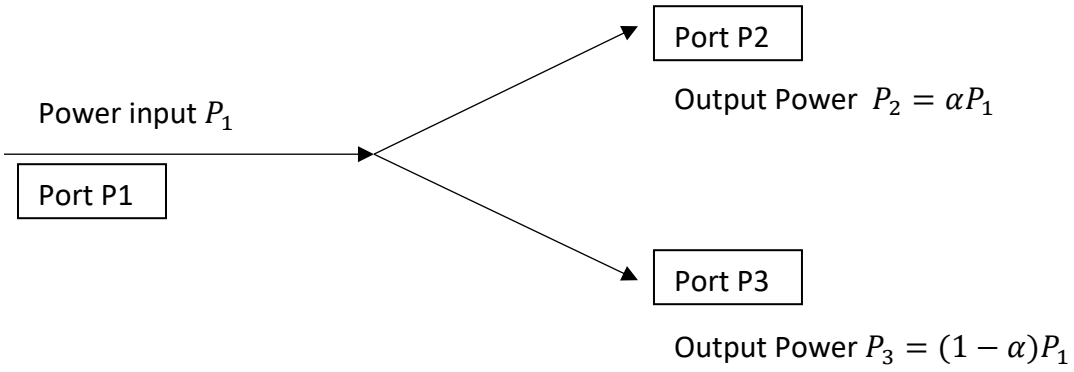

Figure 4.9 Split T power splitter model

$$P_2 = \alpha P_1$$

$$P_3 = (1-\alpha)P_1 \tag{4.23}$$

In (Mohammed and Wang, 2015), for the equal split between resonator 2 & 3; and 3 & 5, with $\alpha = 0.5$, the mutual coupling coefficient, *M* is given by:

$$M_{12} = M'_{12}/\sqrt{2};\ M_{35} = M'_{35}/\sqrt{2} \tag{4.24}$$

From equation 4.24, $\psi_{12} = \sqrt{2}$ or ${\psi_{12}}^2 = 2$ or ${\psi_{12}}^2 = 1/0.5$ and with $\alpha = 0.5$, we have;

$${\psi_{12}}^2 = 1/\alpha \tag{4.25}$$

Solving equations (4.23) and (4.25) gives:

$${\psi_{12}}^2 = \frac{P_1}{P_2} \tag{4.26}$$

This concept was similarly extended to unequal split power dividers with dissimilar split ratios owing to their different power at the output ports.

Therefore, we define the admittance coefficient factor for any path of the output, ψ_{1i}

$${\psi_{1i}}^2 = \frac{P_1}{P_i} \tag{4.27}$$

where $i = 2,3,4$ ... ...is the number of output ports

4.6 Summary

In this chapter, various filter design parameters have been evaluated and derived. Theory of synchronously tuned resonator circuit have been studied, taking into consideration both electric and magnetic coupling to formulate the coupling coefficient. A single loaded resonator circuit have also been utilised to give an expression of the external quality factor and its how it applied to filter prototype circuit. The common resonator coupling factor is formulated and will be deployed in the design of the power splitter and finally, the admittance coefficient factor for any path of the output have been evaluated and derived. The next chapter will implement these findings.

CHAPTER 5

FILTERED POWER SPLITTER USING SQUARE OPEN LOOP RESONATORS

5.0 Introduction

The theoretical evaluation and expressions derived in Chapter 5 is implemented in this Chapter. To achieve this, a brief overview of the filter types their features and the development of the filter formulas started with the general definition. This Chapter also introduces the Chebyshev's approximation and the lowpass network, which is an equivalent circuit that serves as an interface between the filtering function and filter's physical dimensions. Then lowpass and bandpass transformation and the impedance scaling followed by immittance inverters. The concept developed in these sections will now be developed in design a Bandpass filter and an even Filtering power.

5.1 Overview

To reduce circuit size and manufacturing cost, it is essential to integrate a power splitter and a bandpass filter into a single unit. This led to the proposition of filtering power dividers. To realise the filtered power divider, the design of a bandpass filter is critical. The bandpass filter circuit is divided at a common resonator, depending on the topology or resonators arrangement used. The design of a bandpass filter usually starts with the determination of a transfer function that approximates the required filter specification. There are several classic functions including Elliptic, Butterworth and Chebyshev. The design of a Chebyshev bandpass filter is carried out and the same idea is extended to the design of the filtered power

splitter with the same characteristics. The design of the filter and power divider is based on the theories as given in the subsequent sections.

5.2 General Definition

According to Hong and Lancaster, (2001), the transfer function for a two-port lossless passive filter network is defined as:

$$|S_{21}(j\omega)|^2 = \frac{1}{1+\varepsilon^2 {F_n}^2(\omega)} \tag{5.1}$$

Where ε is a ripple constant; ω is a frequency variable; $F_n(\omega)$ is the filtering or characteristic function. For a given transfer function of equation 4.1, the insertion loss response of the filter can be given as:

$$L_{AI}(\omega) = 10\log\frac{1}{|S_{21}(j\omega)|^2}\,dB \tag{5.2}$$

Considering the lossless, passive two port network; since it's given that $|S_{11}|^2 + |S_{21}|^2 = 1$, the filter return loss can be worked out as:

$$L_{AR}(\omega) = 10\log[1 - |S_{21}(j\omega)|^2]dB \tag{5.3}$$

5.3 Chebyshev Function Approximation

A Chebyshev approximation is defined as (Hunter, 2006):

$$K(\omega) = \varepsilon T_n(\omega) \tag{5.4}$$

where ε ripple constant is related to the maximum in band ripple L_{Ar} in (dB) by:

$$\varepsilon = \frac{1}{\sqrt{10^{L_{Ar}/10}-1}} \tag{5.5}$$

$Tn(\omega)$ is a Chebyshev function of the first order n, which can be expressed by $Tn(\omega) = cos(n * cos^{-1}\omega)$.

$$|S_{21}(\omega)|^2 = \frac{1}{1+\varepsilon^2 {T_n}^2(\omega)} \tag{5.6}$$

$$|S_{11}(\omega)|^2 = \frac{{T_n}^2(\omega)}{1+\varepsilon^2 {T_n}^2(\omega)} \tag{5.7}$$

Thus, the insertion loss can be given as:

$$L_A(\omega) = 10\log[1 + \varepsilon^2 {T_n}^2(\omega)] \tag{5.8}$$

The Chebyshev approximation has the capacity of providing sharper slope for a lower filter order (n) as compared to the Butterworth approximation, but with equal ripples introduced in the passband. A typical frequency response of the Chebyshev prototype filter is illustrated in Figure 5.1.

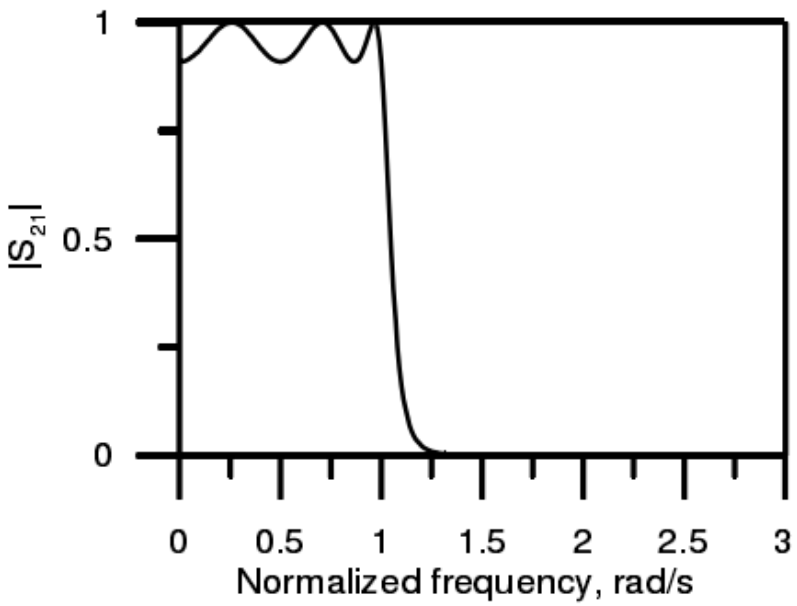

Figure 5.1 Chebyshev filter response (Hong and Lancaster, 2001)

5.4 Lowpass Prototype Networks

The next step of the filter design is the equivalent circuit synthesis to realising the transfer function characteristics derived from the approximation process.

The equivalent circuit model represents the electrical performance of the real construction that is used for filter implementation and acts as an interface between the filtering function and the practical filter structure, so that the filter's physical dimensions could be obtained from the element values of the prototypes.

In general, a normalized lowpass filter prototype is selected as an equivalent network, with the source resistance or conductance values equal to one (denoted by $g_0 = 1$) and the cutoff angular frequency is unity (given as by Ωc = 1 rad/s). This lowpass filter prototype can be further transformed to the desired highpass, bandpass and bandstop filter prototypes by

utilising frequency and element transformations (Matthaei et al., 1964), (Hong and Lancaster, 2001).

One of the most commonly used circuits for realising rational functions in filter design is the ladder network. This network is composed of alternating series and parallel impedances in ladder formation. Figure 4.2 presents two typical arrangements of the ladder network for realising an all-pole filter response. These two forms are dual from each other and hence either form can serve as a prototype for the design of filters with an all-pole response, such as the Butterworth and Chebyshev responses.

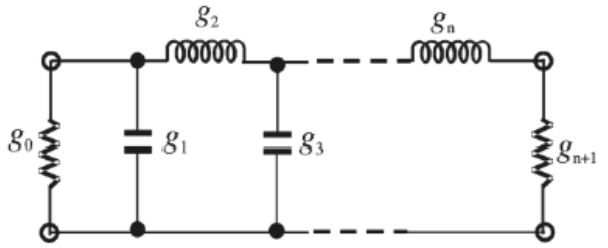

(a)

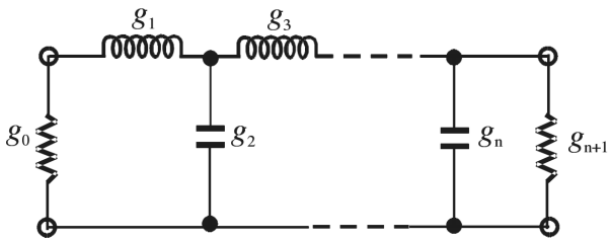

(b)

Figure 5.2 Lowpass prototype all-pole filters with: (a) a ladder network structure, and (b) its dual structure (Hong and Lancaster, 2001)

5.5 Chebyshev Lowpass Prototype

For a Chebyshev lowpass prototype filter with cutoff frequency $\Omega_c = 1$, and a passband ripple L_{Ar} element values shown in Figure 5.2 can be calculated by (Hong and Lancaster, 2001), (Hunter, 2006):

$$g_0 = 1 \tag{5.9}$$

$$g_1 = \frac{2}{\gamma}\sin\left(\frac{\pi}{2n}\right) \tag{5.10}$$

$$g_i = \frac{1}{g_{i-1}} \frac{4\sin\left[\frac{(2i-1)\pi}{2n}\right]\cdot\sin\left[\frac{(2i-3)\pi}{2n}\right]}{\gamma^2+\sin^2\left[\frac{(i-1)\pi}{n}\right]} \quad i = 1,2,3\ldots.n \tag{5.11}$$

$$g_{n+1} = \begin{cases} 1 & for\ n\ odd \\ \coth^2\left(\frac{\beta}{4}\right) & for\ n\ even \end{cases} \tag{5.12}$$

where $\beta = ln\left[\coth\left(\frac{L_{Ar}}{17.37}\right)\right]$, $\gamma = \sinh\left(\frac{\beta}{2n}\right)$,

The degree of the Chebyshev prototype, with the required passband ripple L_{Ar} and the minimum stopband attenuation L_{As} dB at $\Omega = \Omega_c$, is given by (Hong and Lancaster, 2001):

$$n \geq \frac{\cosh^{-1}\sqrt{\frac{10^{0.1L_{As}}-1}{10^{0.1L_{Ar}}-1}}}{\cosh^{-1}\Omega_c} \tag{5.13}$$

5.6 Frequency and Element Transformations

The lowpass prototype filters mentioned above has a cutoff frequency $\Omega_c = 1$ and a normalised source impedance $g_0 = 1$. Because of this, it makes them unsuitable for practical use. Therefore, it is necessary to apply the frequency and element transformations in order to

obtain the frequency responses and element values for practical filters. The frequency transformation has the ability of mapping a response in the lowpass prototype frequency domain Ω into the real angular frequency domain ω, where a practical filter's response is expressed (such as lowpass, highpass, bandpass and bandstop). It has an effect on all the reactive elements, but with no effect on the resistive elements.

5.6.1 Lowpass Transformation

Lowpass filter prototype is transformed into a practical lowpass filter with a cutoff frequency ω_c in the angular frequency axis ω, the following frequency transformation can be applied (Hong and Lancaster, 2001).

$$\Omega = \frac{\Omega_c}{\omega_c}\omega \tag{5.14}$$

The element transformation are described as:

$$L \rightarrow L\frac{\Omega_c}{\omega_c} \tag{5.15}$$

$$C \rightarrow C\frac{\Omega_c}{\omega_c} \tag{5.16}$$

Figure 5.3 shows the lowpass element transformation. It can be seen that the lowpass to lowpass transformation has a linear scaling and all the frequency dependent elements of the prototype have new values but retaining their configuration.

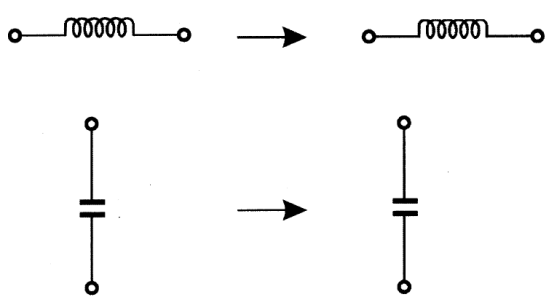

Figure 5.3 Lowpass element transformation (Hong and Lancaster, 2001)

5.6.2 Bandpass Transformation

Converting the lowpass prototype response to a bandpass response with a passband $\omega_2 - \omega_1$, where ω_1 and ω_2 denote the passband edge angular frequency, the required frequency transformation can be expressed as (Hong and Lancaster, 2001):

$$\Omega = \frac{\Omega_c}{\Delta}\left(\frac{\omega}{\omega_0} - \frac{\omega_0}{\omega}\right) \tag{5.7}$$

whereby the fractional bandwidth Δ is given by:

$$\Delta = \frac{\omega_2 - \omega_1}{\omega_0} \tag{5.18}$$

And the centre frequency ω_0 is stated as:

$$\omega_0 = \sqrt{\omega_1 \omega_2} \tag{5.19}$$

Figure 5.4 gives the bandpass transformation. When this frequency transformation is applied to a lowpass prototype reactive element, the inductors will be converted into a series *LC* resonant tank with the values given as:

$$L_s = \frac{\Omega_c L}{\Delta\omega_0} \tag{5.20}$$

$$C_s = \frac{\Delta}{\omega_0 \Omega_c L} \tag{5.21}$$

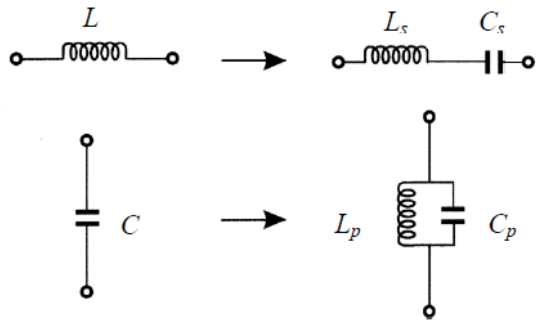

Figure 5.4 Bandpass element transformation (Hong and Lancaster, 2001)

Consequently, the capacitors are transformed into a parallel tank of *L&C* components, and the parameters of the *LC* resonant circuit can be gotten from:

$$C_p = \frac{\Omega_c C}{\Delta\omega_0} \tag{5.22}$$

$$L_p = \frac{\Delta}{\omega_0 \Omega_c C} \tag{5.23}$$

It should be emphasised, however, that the resonant frequency of the resonators coincides with the centre frequency of the filter, namely:

$$\omega_0 = \frac{1}{\sqrt{L_s C_s}} \tag{5.24}$$

$$\omega_0 = \frac{1}{\sqrt{L_p C_p}} \tag{5.25}$$

5.7 Impedance Scaling

The impedance scaling process requires to be carried out after the frequency and element transformations in order to fine-tune the normalized source impedance of the lowpass prototype filter to any required value Z_0. The impedance scaling factor *γ0* is defined as (Hong and Lancaster, 2001):

$$\gamma_0 = \begin{cases} Z_0/g_0 & for\ g_0\ being\ the\ resistance \\ g_0/Y_0 & for\ g_0\ being\ the\ conductance \end{cases} \quad (5.26)$$

where the source admittance, $Y_0 = 1/Z_0$

Apparently, the filter prototype elements values can be scaled with the following criteria:

$$L \rightarrow \gamma_0 L \ldots\ldots\ldots\ldots for\ inductance$$

$$C \rightarrow C/\gamma_0 \ldots\ldots\ldots for\ capacitance$$

$$R \rightarrow \gamma_0 R \ldots\ldots\ldots\ldots . for\ impedance$$

$$G \rightarrow G/\gamma_0 \ldots\ldots\ldots for\ admittance$$

5.8 Filter Prototypes with Immittance Inverters

From Figure 5.2, ladder network structure consists of series resonators alternating with shunt resonators. Such structure is practically impossible to implement in a practical microwave filter. As a result of this, it is more viable to convert the prototype to an equivalent form where all of the resonators are of similar type. Employing impedance inverters can do this. Furthermore, since lumped-circuit elements are difficult to realise at higher operating frequency example microwave and mm-wave, it is also necessary to convert the lumped-

circuit prototype into an equivalent distributed-circuit form in order to have a more convenient filter construction.

5.8.1 Impedance and Admittance Inverters

A conceptualised impedance inverter, also referred to as the *K*-inverter, operates like a quarter-wavelength line with a characteristic impedance *Z* at all frequencies. As seen in Figure 4.5(a), if the impedance inverter is terminated an impedance Z_2 from one end, the impedance Z_1 as seen from the other end is (Hong and Lancaster, 2001):

$$Z_1 = \frac{K^2}{Z_2} \tag{5.27}$$

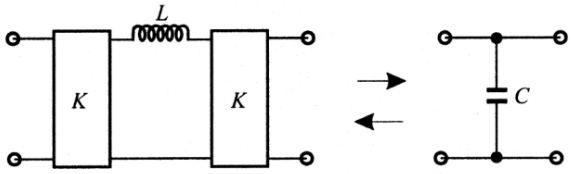

(a)

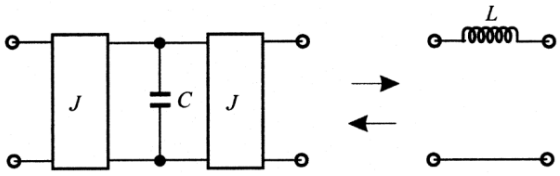

(b)

Figure 5.5(a) Immittance inverters used to convert a shunt capacitance into an equivalent circuit with series inductance. (b) Immittance inverters used to convert a series inductance into an equivalent circuit with shunt capacitance (Hong and Lancaster, 2001):

A conceptualised admittance inverter, also referred to as the *j*-inverter, operates like a quarter-wavelength line with a characteristic admittance Y at all frequencies. As seen in Figure 5.5(b), if the impedance inverter is terminated an impedance Y_2 from one end, the impedance Y_1 as seen from the other end is (Hong and Lancaster, 2001):

$$Y_1 = \frac{J^2}{Y_2} \tag{5.28}$$

It can be deduced that the loaded admittance *Y* can be transformed to an arbitrary admittance by selecting an appropriate *J* value. Likewise, the loaded impedance *Z* can be transformed to an arbitrary impedance by selecting an appropriate *K* value.

As shown by equation 5.27 equation 5.28, the quarter-wavelength line can be used to devise an impedance inverter with the inverter parameter $K = Z_c$, where Z_c is the characteristic impedance of the line. Also, serves as an admittance inverter with the admittance inverter parameter $J = Y_c$, where $Y_c = 1/Z_c$ denotes the transmission line characteristic admittance. However, it should be emphasised that this type of inverters is somewhat narrow-band, and hence it is best used in narrow-band filters design. The impedance K is represented using inductor or capacitor network, a T or Y network is used as shown in Figure 5.6a. The admittance J is also represented using inductor or capacitor network and a pi-network is utilised as given in figure 4.6b. The PI-network of capacitors is applied in the realization of the filter and power splitter circuit as would be seen in Figure 5.13 and throughout the circuit model design.

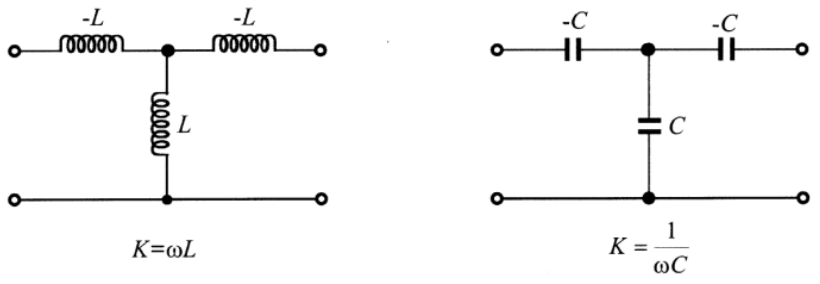

(a)

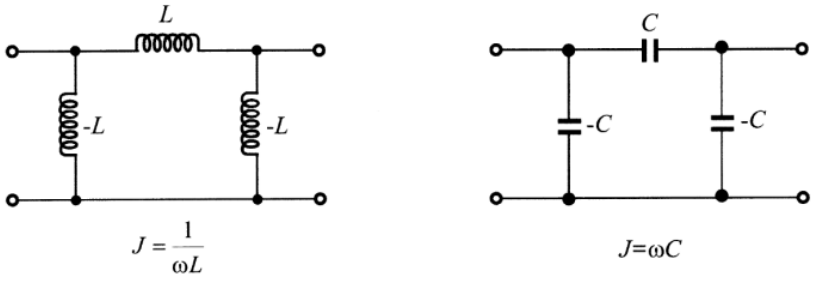

(b)

Figure 5.6 Circuits for the realisation of immittance inverters (Hong and Lancaster, 2001)

5.8.2 Filter Prototypes with Immittance Inverters

As described in the previous section, a shunt capacitance with an inverter on each side behaves like a series inductance, and similarly, a series inductance with an inverter on each side acts like a shunt capacitance from equation 5.27 equation 5.28. Utilising these properties enables to convert a filter circuit to an equivalent form of more convenience for implementation with microwave structures. Figure 5.7 illustrates an equivalent-circuit form of the lowpass filter prototypes shown in Figure 5.2.

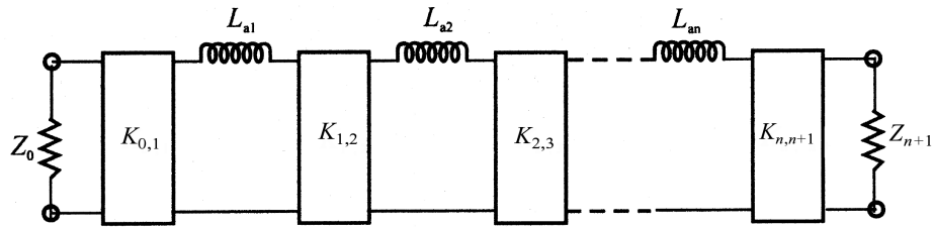

(a)

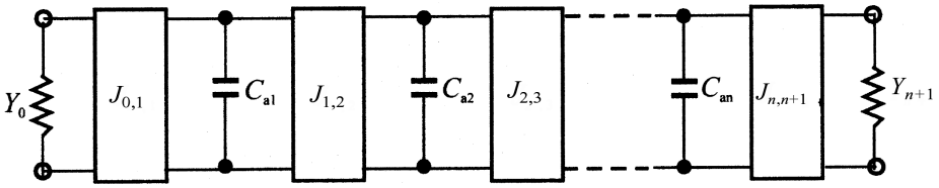

(b)

Figure 5.7 Lowpass networks of immittance inverters (Hong and Lancaster, 2001)

From the immittance inverters, it's observed that the new equivalent circuits are made up of lumped elements of similar type connected by *K* or *J* inverters. The new element values, such as first and last element impedance, Z_0 and Z_{n+1}, first and last element admittance Y_0, and Y_{n+1}, common inductance L_{ai}, and common capacitance C_{ai}, can be selected arbitrarily, and the filter responses will be identical to that of the original prototype if the immittance inverter parameters $K_{i,i+1}$or $J_{i,i+1}$meet the following requirements (Hong and Lancaster, 2001):

$$K_{0,1} = \sqrt{\frac{Z_0 L_{a1}}{g_0 g_1}} \tag{5.29}$$

$$K_{j,j+1} = \sqrt{\frac{L_{a1} L_{a(a+1)}}{g_1 g_{i+1}}}\Bigg|_{i=1\ to\ n-1} \tag{5.30}$$

$$K_{n,n+1} = \sqrt{\frac{L_{an} Z_{n+1}}{g_n g_{n+1}}} \tag{5.31}$$

$$J_{0,1} = \sqrt{\frac{Y_0 C_{a1}}{g_0 g_1}} \tag{5.32}$$

$$J_{i,i+1} = \sqrt{\frac{C_{a1} C_{a(a+1)}}{g_1 g_{i+1}}}\Bigg|_{i=1\ to\ n-1} \tag{5.33}$$

$$J_{n,n+1} = \sqrt{\frac{C_{an} Y_{n+1}}{g_n g_{n+1}}} \tag{5.34}$$

where g_i represents the original prototype element values defined earlier.

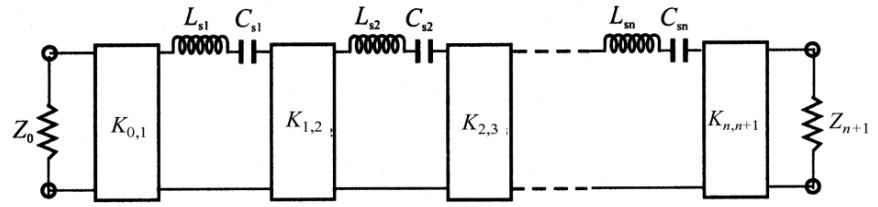

(a)

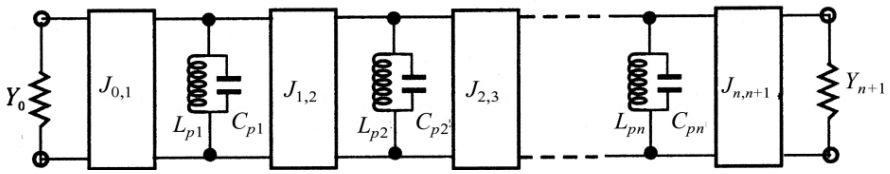

(b)

Figure 5.8 Bandpass networks using immittance inverters (Hong and Lancaster, 2001)

The lowpass prototype network seen in Figure 5.7 can be transformed into other types of filters by applying the frequency and element transformations discussed in section (check section). Figure 4.8 illustrates two typical bandpass filter circuits transformed from the lowpass network in Figure 4.8. It can be seen that the new bandpass network is composed of resonators that are of the same type and connected by *K* or *J* inverters. The parameters of the filter prototype in Figure 4.8(a) can be computed by:

$$L_{si} = \left(\frac{1}{\Delta\omega_0}\right) L_{a1}|_{i=1\ to\ n} \tag{5.35}$$

$$C_{si} = \frac{1}{{\omega_0}^2 L_{si}}\Big|_{i=1\ to\ n} \tag{5.36}$$

$$K_{0,1} = \sqrt{\frac{Z_0 \Delta\omega_0 L_{si}}{\Omega_c g_0 g_1}} \tag{5.37}$$

$$K_{j,j+1} = \frac{\Delta\omega_0}{\Omega_c}\sqrt{\frac{L_{a1} L_{a(a+1)}}{g_1 g_{i+1}}}\Big|_{i=1\ to\ n-1} \tag{5.38}$$

$$K_{n,n+1} = \sqrt{\frac{\Delta\omega_0 L_{sn} Z_{n+1}}{\Omega_c g_n g_{n+1}}} \tag{5.39}$$

where L_{ai} is the value of the lumped elements shown in Figure 5.7(a).

The bandpass filter circuits shown in Figure 5.8 are created on the circuit in the lumped-element form. However, lumped-circuit elements are usually difficult to create at microwave frequencies. Hence, it is more practical to change the ladder network in Figure 4.8 into an equivalent circuit formed by distributed elements.

Two types of generalized bandpass filter circuits are shown in Figure 5.9, where distributed circuits substitute the lumped LC resonators in Figure 5.8. The distributed circuits can be

microstrip resonators, microwave cavities or any other suitable resonant structures. Two quantities, referred to as the reactance slope parameter and susceptance slope parameter, are added to establish the resonators' resonance properties.

The reactance slope parameter for resonators with zero reactance at the centre frequency ω_0 is defined by:

$$x_i = \frac{\omega_0}{2}\frac{dX_i(\omega)}{d\omega}\Big|_{\omega=\omega_0} \tag{5.40}$$

where $X_i(\omega)$ is the reactance of the distributed resonator.

The susceptance slope parameter for resonators with zero susceptance at the centre frequency ω_0 is defined by:

$$b_i = \frac{\omega_0}{2}\frac{dB_i(\omega)}{d\omega}\Big|_{\omega=\omega_0} \tag{5.41}$$

where $B_i(\omega)$ is the susceptance of the distributed resonator.

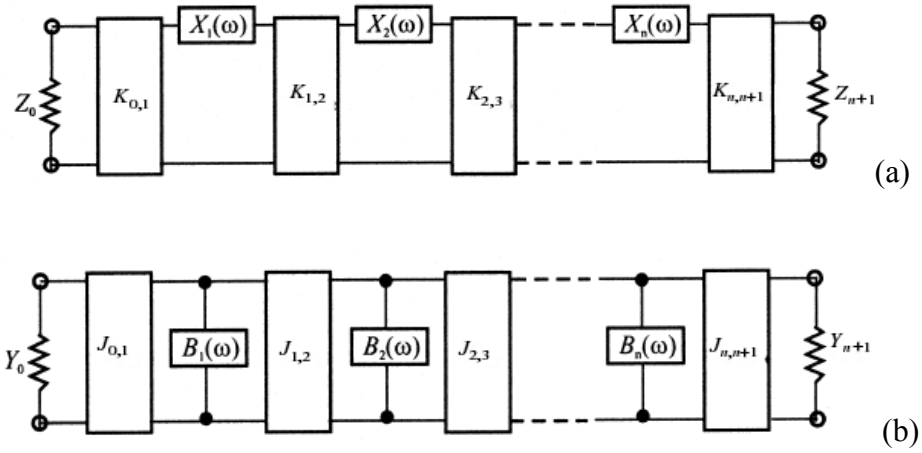

Figure 5.9 Generalized bandpass filter circuits using immittance inverters (Hong and Lancaster, 2001)

From equation 5.40 and equation 5.41, it is observed that the reactance slop parameter of a series *LC* resonator is $\omega_0 L$, and the susceptance slope parameters of a parallel *LC* resonator is $\omega_0 C$. Hence, replacing $\omega_0 L_{si}$ and $\omega_0 C_{pi}$ in equation 5.38 and equation 5.39 with x_i and b_i, respectively, results in the following equations for the calculation of the values of the *K*- and *J*- inverters in Figure 5.9:

$$K_{0,1} = \sqrt{\frac{Z_0 \Delta x_1}{\Omega_c g_0 g_1}} \tag{5.42}$$

$$K_{j,j+1} = \frac{\Delta}{\Omega_c} \sqrt{\frac{x_i x_{i+1}}{g_1 g_{i+1}}}\Bigg|_{i=1\ to\ n-1} \tag{5.43}$$

$$K_{n,n+1} = \sqrt{\frac{\Delta x_n Z_{n+1}}{\Omega_c g_n g_{n+1}}} \tag{5.44}$$

$$J_{0,1} = \sqrt{\frac{Y_0 \Delta b_1}{\Omega_c g_0 g_1}} \tag{5.45}$$

$$J_{i,i+1} = \frac{\Delta}{\Omega_c} \sqrt{\frac{b_1 b_{i+1}}{g_1 g_{i+1}}}\Bigg|_{i=1\ to\ n-1} \tag{5.46}$$

$$J_{n,n+1} = \sqrt{\frac{\Delta b_n Y_{n+1}}{\Omega_c g_n g_{n+1}}} \tag{5.47}$$

5.9 5-pole Chebyshev's bandpass filter circuit design

Table 5.1 Design specifications

Parameters	Values
Return Loss (R_L)	20dB
Characteristics impedance (Z_o)	50Ω
Centre frequency (f_o)	2 GHz
Fractional Bandwidth (Δ)	5%
Number of Poles (N)	5

Using the design procedure as given theoretically in the sections above, the fifth order Chebyshev function bandpass filter is design with the following steps.

1. Calculate the normalised low pass parameters using equation 5.9 – 5.12 and the calculated values are given as follows:

Table 5.2 Lumped element g values

g_0	g_1	g_2	g_3	g_4	g_5	g_6
1	0.9714	1.3721	1.8014	1.3721	0.9714	1

2. Transforming the normalised LP values to BP

A MATLAB program is developed (see appendix II) to generate all the solutions, the resulting return and insertion loss response is given in Figure 5.10

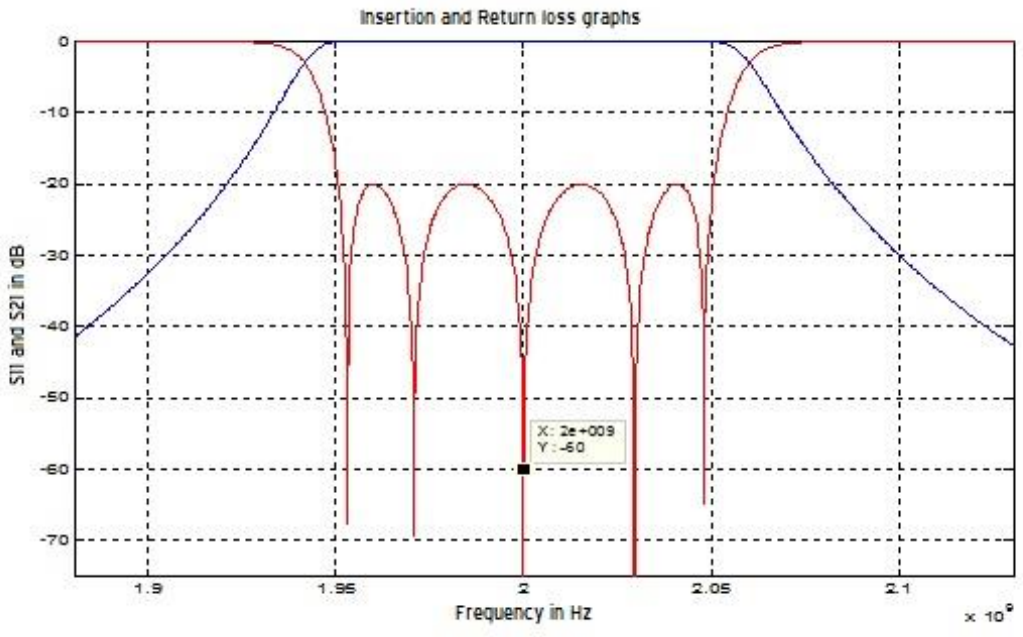

Figure 5.10 Bandpass Filter response (From MATLAB)

3. Transforming the Lowpass schematic diagram to shunt only lowpass

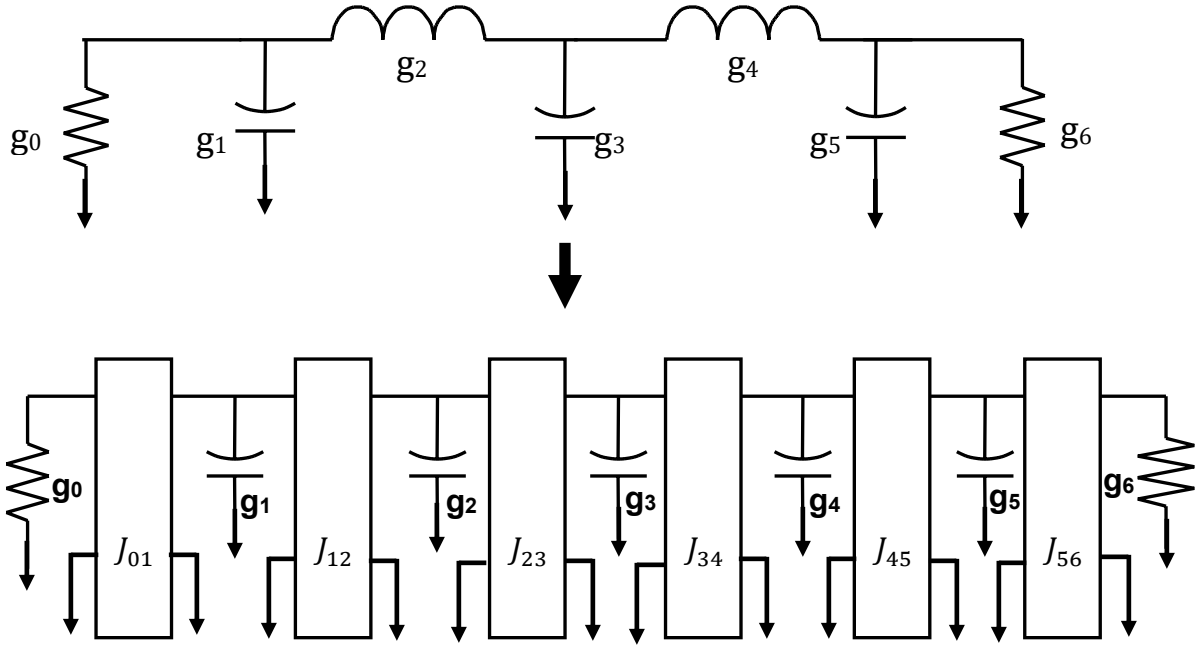

Figure 5.11 Transformation to shunt only lowpass (Yeo, 2011), (Yeo and Nwajana, 2013)

This is achieved by making all the J parameter equal 1, that is $J_{0,1} = J_{1,2} = J_{2,3} = J_{3,4} = J_{4,5} = J_{5,6} = 1$.

4. Making the Capacitors the same: making all the g values g_1 except g_0 and g_6. To do this, $J_{01} = J_{56} = 1$.

$$J'_{k,k+1} = \sqrt{\frac{g_1^2}{g_k g_{k+1}}} \qquad k = 1,2,3,4 \tag{5.48}$$

5. Frequency and impedance scaling: following the modification of the equations in section 5.7, the following equations are used for the frequency impedance and scaling (Yeo, 2011)

$$C_1 = \frac{g_1}{\omega_0 R_0} \tag{5.49}$$

$$J'_{0,1} = \frac{J_{0,1}}{R_0} \tag{5.50}$$

$$J''_{k,k+1} = \frac{J'_{k,k+1}}{R_0} \tag{5.51}$$

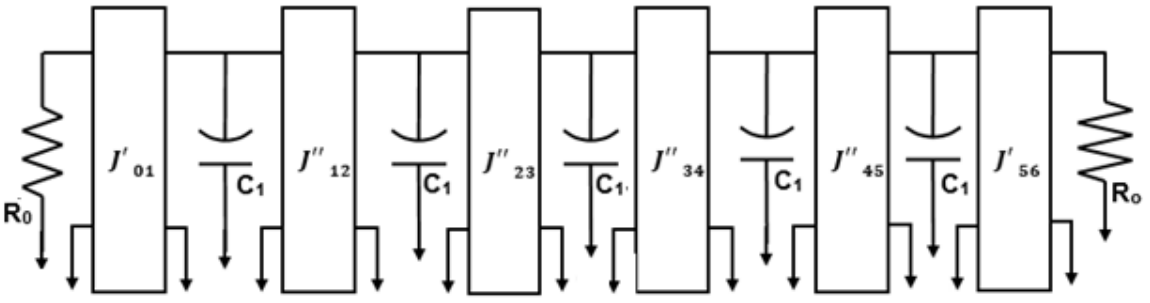

Figure 5.12 Making the Capacitors the same

6. Converting the shunt Lowpass circuit to Bandpass Filter: This is achieved by using the following relationship:

$$C'_1 = \frac{C_1}{\Delta} \text{ and } L_1 = \frac{1}{\omega^2{}_0 C'_1} \tag{5.52}$$

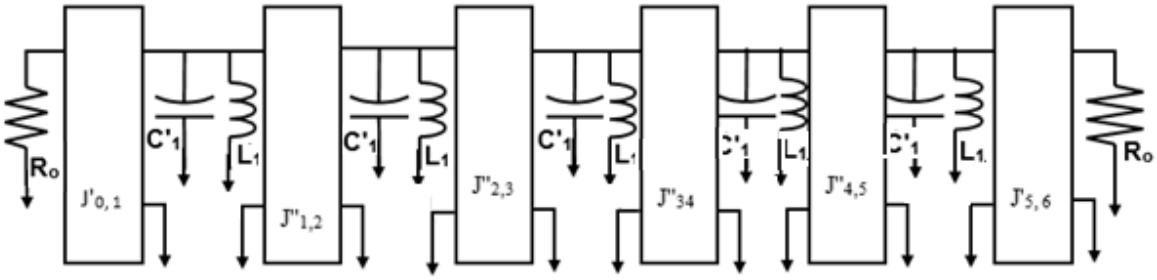

Figure 5.13 Conversion to Band Pass Filter parameters

The J parameters are also converted to it equivalent pi-network of capacitors as indicated in Figure 5.6b. The circuit is constructed in ADS EM software as shown Figure 5.14 and its filter response is given in Figure 5.15:

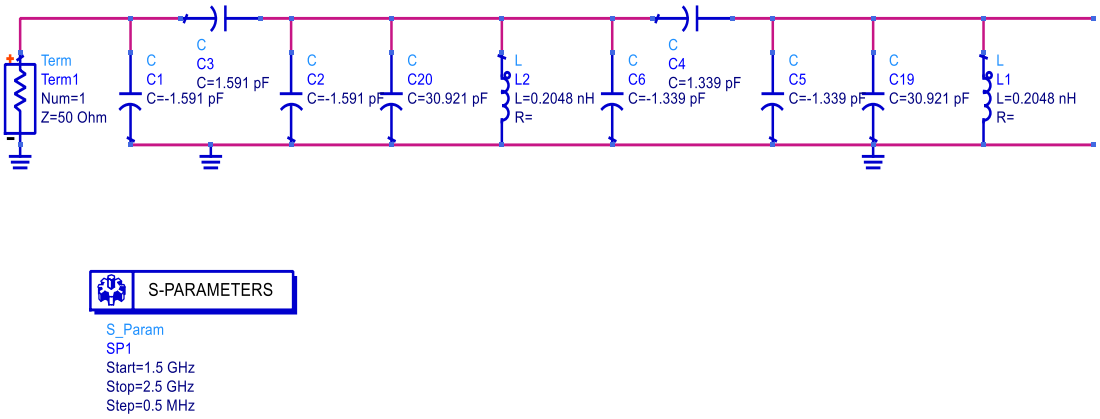

Figure 5.14 Circuit realization of the BPF

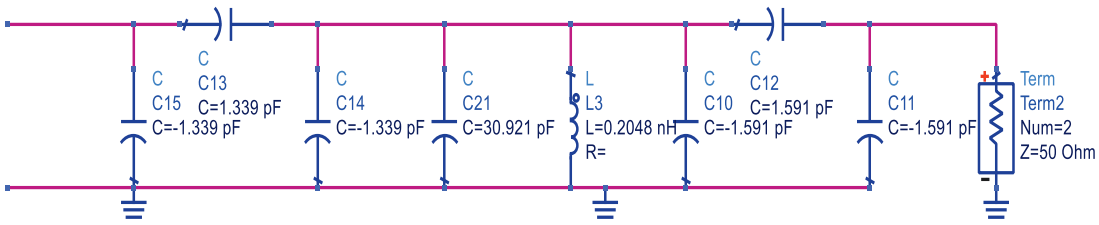

Figure 5.14 (Continued)

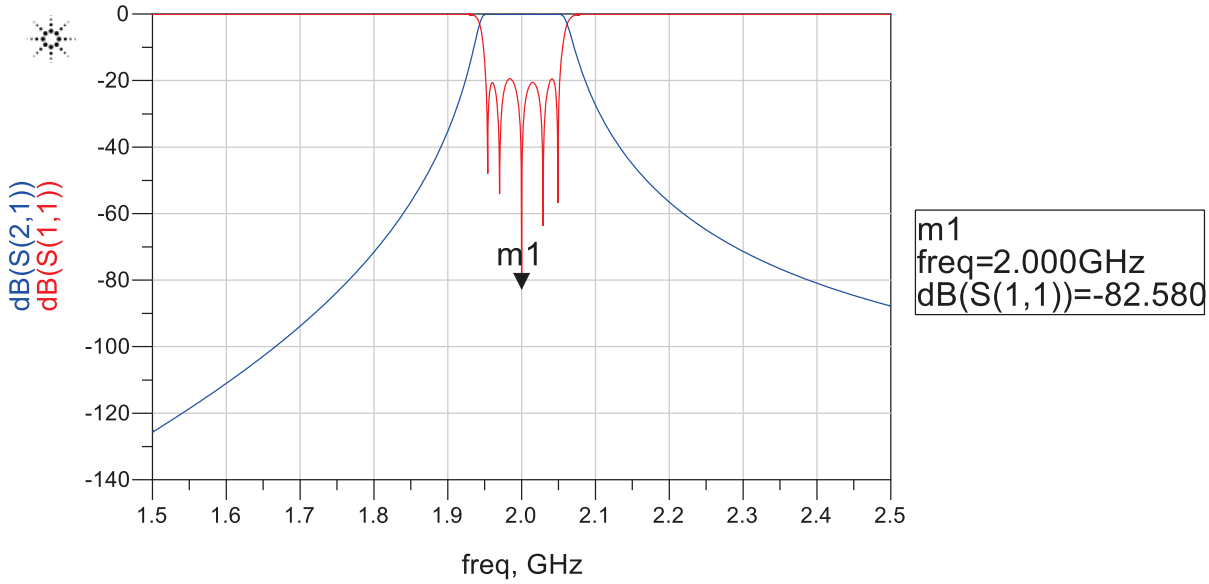

Figure 5.15 BPF frequency response of figure 4.14

The coupling coefficients K and the external quality factor Q_{ext} are also obtained as:

$$K_{k,k+1} = J''_{k,k+1}\sqrt{\frac{L_1}{C'_1}} \tag{5.53}$$

$$Q_{ext} = \frac{\omega_0 C'_1}{J'_{0,1}} \tag{5.54}$$

5.10 Power splitter circuit

The coupling topology of the filtered power splitter is shown in Figure 4.15. The solid lines represent the coupling path and each of the nodes represent a resonator. At resonance, there

is coupling of signal energy from port 1 to port 2 through resonators 1, 2, 3, 4 & 5; and port 1 to port 3 through resonator 1, B, C, and D & E. The circuit is similar to joining two identical 5 – pole bandpass Chebyshev filter at a common resonator 1.

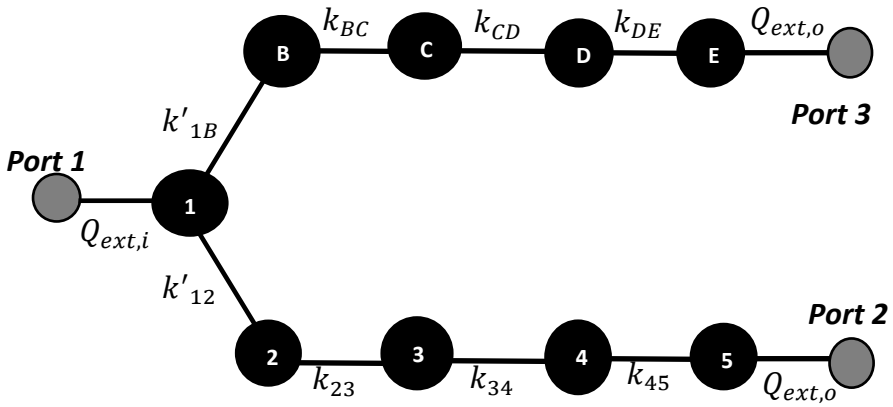

Figure 5.15 Coupling arrangement of a five-pole Chebyshev band-pass filtered splitter

The conventional theory based on coupled resonator bandpass filter knowledge is applicable here. The external quality factor, Q_{ext}, and the coupling coefficient, k_{nm} can be determined using the usual method used in band-pass filter design as described in the section 4.3 and 4.4. To ensure an equal power split in splitter (Mohammed and Wang, 2015), as explained in section 4.5 is:

$$\psi_{12}{}^2 = \psi_{1B}{}^2 = \frac{P_1}{P_2} = \frac{P_1}{P_3} = 1/\alpha \tag{5.55}$$

Where ψ_{12} and ψ_{1B} are the admittance coefficient factor of the common resonator and the next resonator towards port 2 and port 3 respectively.

The coupling coefficient then becomes,

$$K'_{12} = K_{12}/\psi_{12}$$

And

$$K'_{1B} = K_{1B}/\psi_{1B} \tag{5.56}$$

where K_{12} and K_{1B} are the coupling coefficients of a standard band-pass filter. Here the split ratio $\alpha = 0.5$, we have $\psi_{12} = \psi_{1B} = \sqrt{2}$. This is based on the theory of establishing equal power splitting with half power delivering to and have the same return loss performance for each branch (Pozar, 2011), (Lap Kun and Ke-Li, 2006).

Figure 5.16 gives the equivalent circuit of a 5-pole Bandpass filter. The admittance *J* - Inverter method is used to determine the coupling between resonators. g is the normalised low pass filter values. Z_o is the characteristics impedance and $k = 1$ to n where n is the order of the filter.

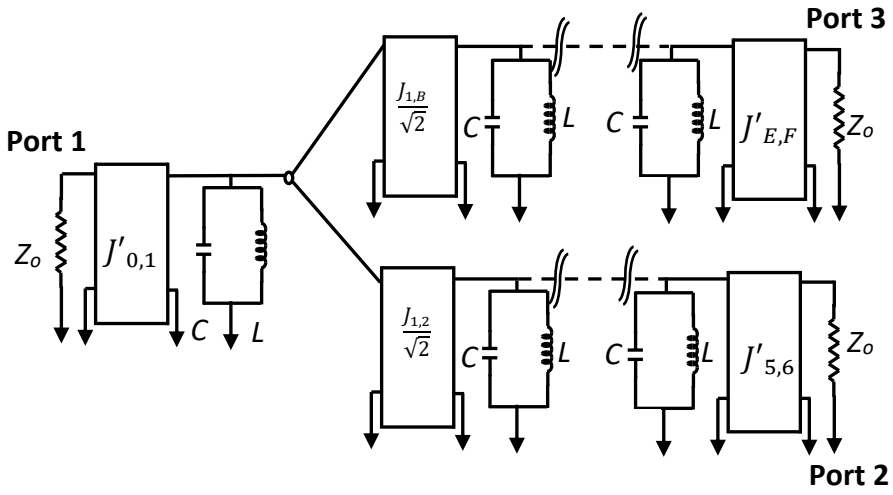

Figure 5.16 Equivalent circuit of a five - pole Chebyshev bandpass power splitter

Figure 5.17 gives the simulated result of the filtered splitter circuit. It shows that it has a centre frequency of 2 GHz, which is the specified centre frequency and a minimum return loss of 20dB. This is in conformity with the original design specification.

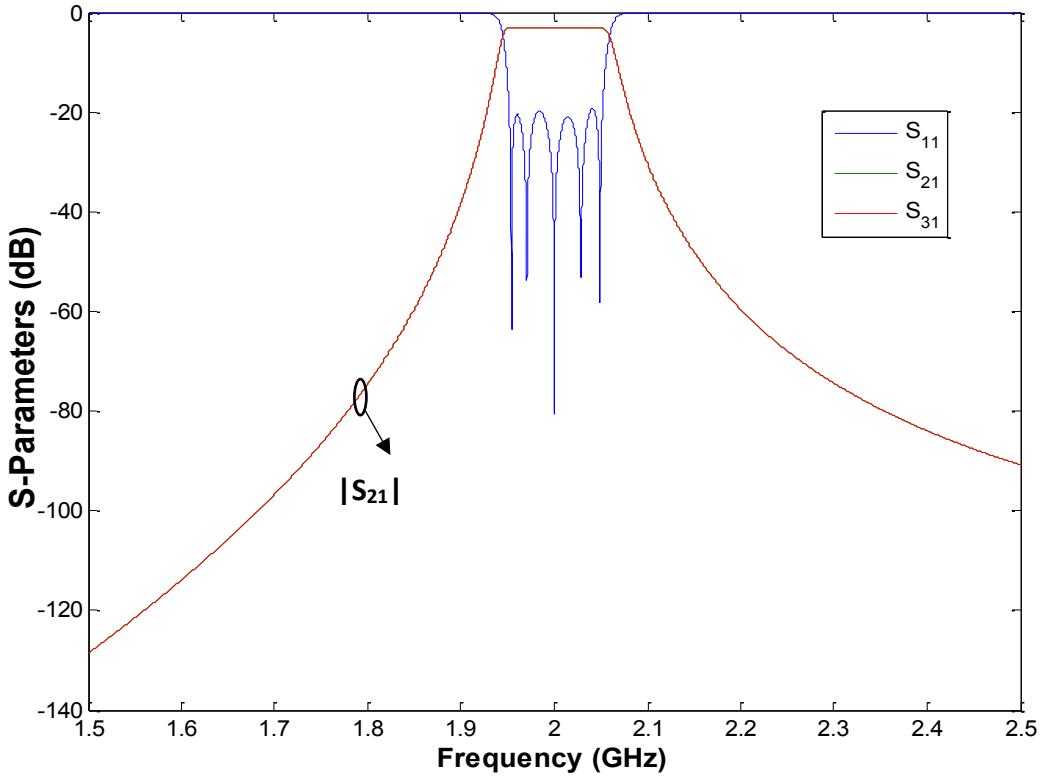

Figure 5.17 Ideal circuit model responses for proposed five-pole Chebyshev filtered power splitter

5.11 Microstrip design of bandpass power splitter

This includes several empirical formulas, which has been formulated by various authors for the realization of the Microstrip parameters like the width, thickness, the guided wavelength and the length of the Microstrip resonator. All of these have been included in the MATLAB program.

The proposed filtered Chebyshev power splitter is designed and implemented using the microstrip technology. The Square Open Loop Resonators (SOLR) topology is deployed. This topology is used since it has the advantage of size, weight and cost reduction; also, when compared to waveguide cavity cross-coupled filters, it is more flexible to construct a variety

of cross-coupled planar filters (Hong and Lancaster, 2001). The calculated circuit model is simulated using Keysight's Advance Design System (ADS) EM simulator software.

Table 5.3 Microstrip design specification

Substrate variable	Value
Dielectric Constant, ε_r	10.8
Characteristics Impedance, Z_o	50Ω
Thickness, h	1.27mm

According to (Pozar, 2011) and (Yeo, 2011) the equations derived and explained in section 3.6 are used to determine the microstrip design parameters for the specification given in Table 5.3.

The expression for Coupling Coefficient, $K_{k,k+1}$ and External Quality factor, Q_{ext} have been provided in equation 4.3 and equation 4.4. K'_{12} & K'_{1B} represents the coupling between the common resonator, 1 and the next resonator towards Port 2 & Port 3 respectively. This gives: $K_{12} = K'_{1B} = 0.0306,\ k_{23} = K_{34} = K_{BC} = K_{CD} = 0.032,\ k_{45} = K_{DE} = 0.043$ and $Q_{ext,i} = Q_{ext,o} = \omega_o Z_o C = 19.428$.

The coupling space between microstrip resonators is determined by considering two coupled microstrip resonators that is simulated and the two resonance mode frequencies are extracted as f_1 and f_2, where f_1 is lower resonance mode and f_2 is the higher resonance mode. The coupling coefficient can be calculated as: $K = ({f_2}^2 - {f_1}^2)/({f_2}^2 + {f_1}^2)$ as derived in Section 4.3.

Figure 5.18 shows the simulated curve of the coupling coefficients as a function of the coupling space between the microstrip resonators. The graph of Figure 5.18 is used to determine the physical dimensions of the power splitter. From the graphs, the following are obtained.

$s_{12} = s_{45} = s_{1B} = s_{DE} = 1.43mm;\ \ s_{23} = s_{34} = s_{BC} = s_{CD} = 1.77mm$ and $s'_{12} = s'_{1B} = 1.8mm$, where s is the spacing between resonators as shown in the inset of Figure 5.18.

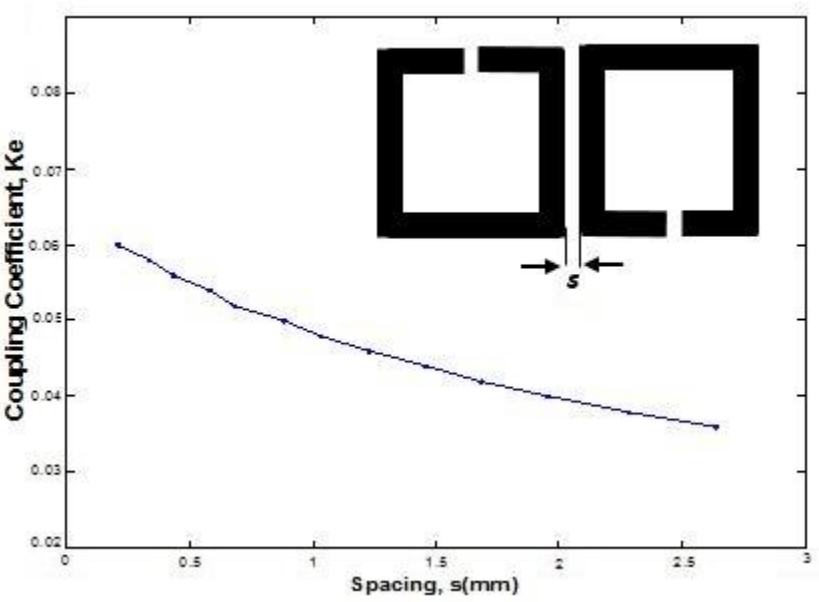

Figure 5.18 Coupling Coefficient against spacing

Similarly, to determine the tapping, *t* point from the input and output resonators, the arrangement as shown in Figure 4.19 (inset) is designed and simulated. The insertion loss curve is used to determine the external quality factor, Q_{ext}, using the relation $Q_{ext} = \frac{f_0}{\delta f@-3dB}$ as derived in Section 4.4.

Figure 5.19 shows the external quality factor as a function of the tapped location along the microstrip resonator, from which the initial value of t obtained for simulation as $t = 6.88mm$.

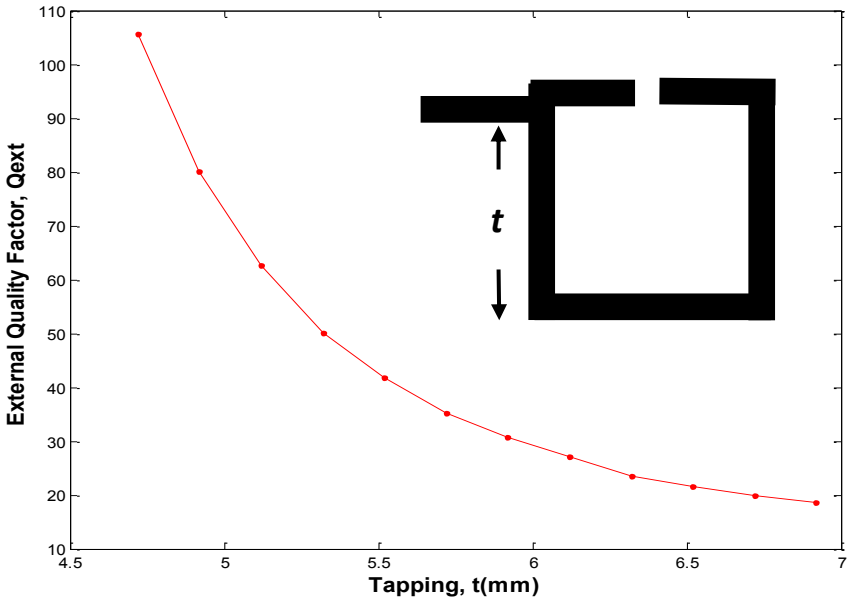

Figure 5.19 External quality factor against tapping

5.12 Final Circuit Layout

The microstrip power splitter is achieved by using 9 multi-coupled SOLR as shown in Figure 4.20. Using Rogers RO3210 substrate with a dielectric constant of 10.8, a loss tangent of 0.0023 and thickness of 1.27mm, the designed circuit is fabricated on this substrate. Copper conductor with conductivity of 5.8 x 10^7 S/m is used for the top and bottom of the microstrip. The figure also gives the final microstrip schematic layout including its physical dimensions. The effective area is measured as $0.97\lambda_g$ X $0.90\lambda_g$; where λ_g is the guided wavelength at 2 GHz. The physical dimensions are given in Table 5.4.

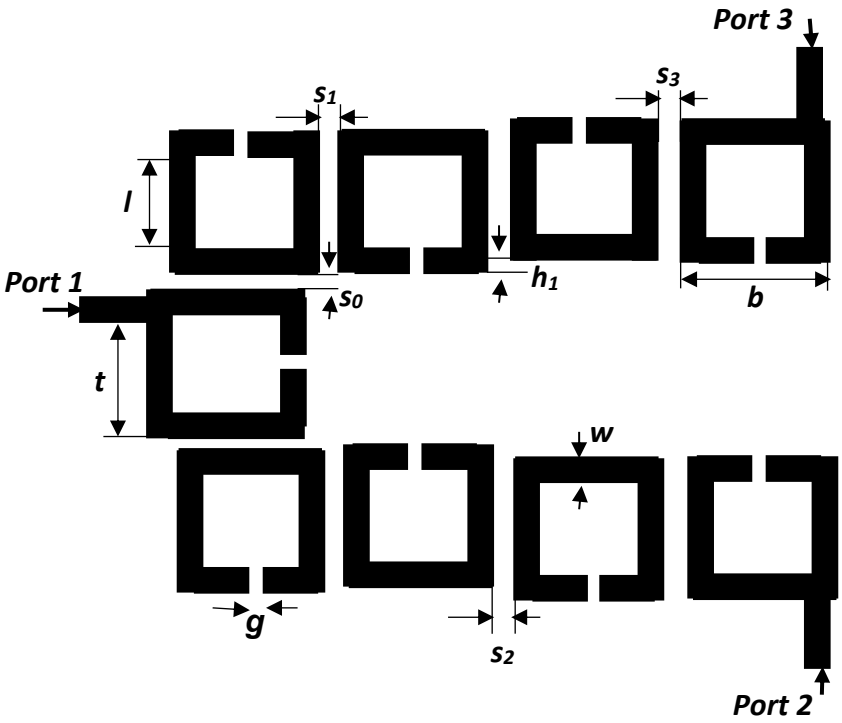

Figure 5.20 Microstrip Schematic Layout of the 9 resonators power splitter

Table 5.4. Physical dimensions of the filtering splitter (mm)

Dimension	Value	Dimension	Value
s_0	1.28	h_1	0.61
s_1	1.65	g	0.44
s_2	1.39	w	1.12
s_3	1.57	t	6.88
l	7.00	b	8.12

5.13 Simulation and measured results

The full wave simulation is carried out in Keysight's ADS EM simulation platform. Printed circuit board technology is used to construct the circuit and the proposed filtering power splitter is measured using Agilent Vector Network Analyser. The proposed splitter is

designed to operate at 2GHz. The values given in Table 4.4 are utilised in realising the power splitter given in Figure 4.20. The graph in Figure 5.21 depicts the EM lossy simulation insertion loss of the input to the output ports ($|S_{21}|$ and $|S_{31}|$); and the return loss at input port ($|S_{11}|$). The measured return loss is better than 15dB; the measured insertion loss of port 2 and port 3 path are 3.12dB and 3.05dB $\pm$18% of ripple respectively and a fractional bandwidth is about 6%. In the EM simulation, the minimum return loss is better than 13dB and the output ports insertion loss are at 3.1dB and 3.08dB for port 2 and 3 respectively, while the fractional bandwidth for this design is 5%. The minimum ideal return loss responses of the output port 2 and 3 ($|S_{22}|$ & $|S_{33}|$) are given in Figure 5.22 is 5.2dB, whilst the return loss on both ports of the simulated design are better than 5.40dB and the return loss on both ports of the measured design are better than 6dB. However, emphasises are not placed on better return loss at the output ports in this work. It is shown only as illustration of it outcome.

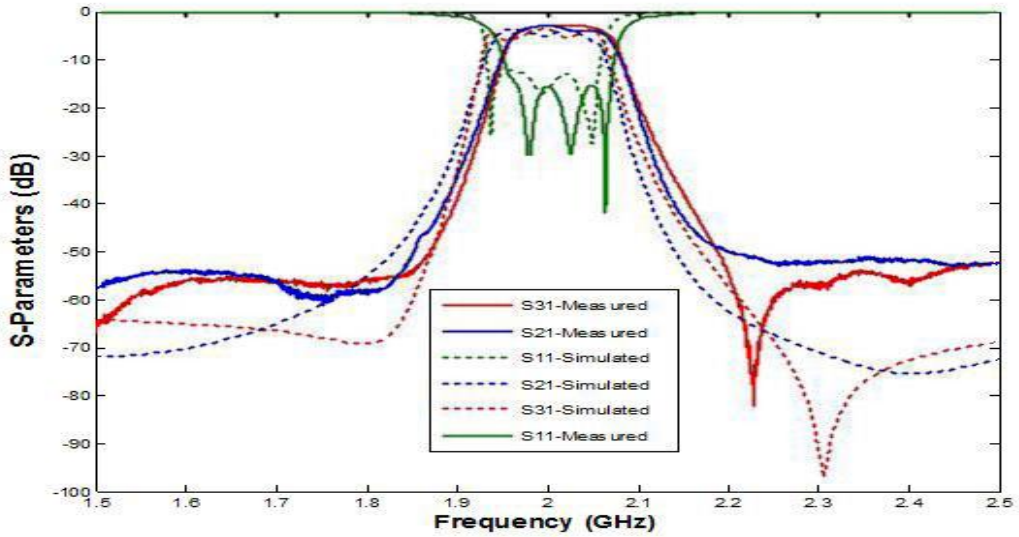

Figure 5.21 Simulated and measured responses of the fifth order filtering bandpass power filter.

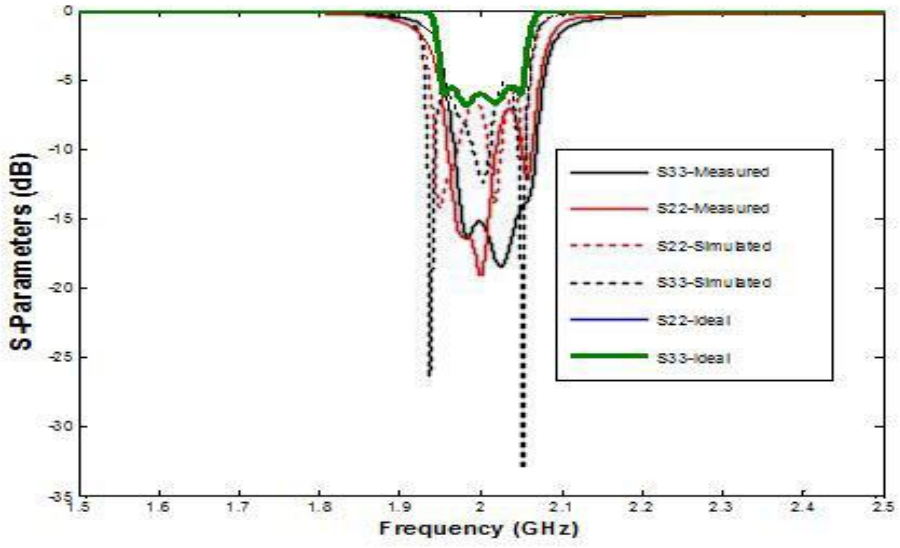

Figure 5.22 Output ports return loss curves

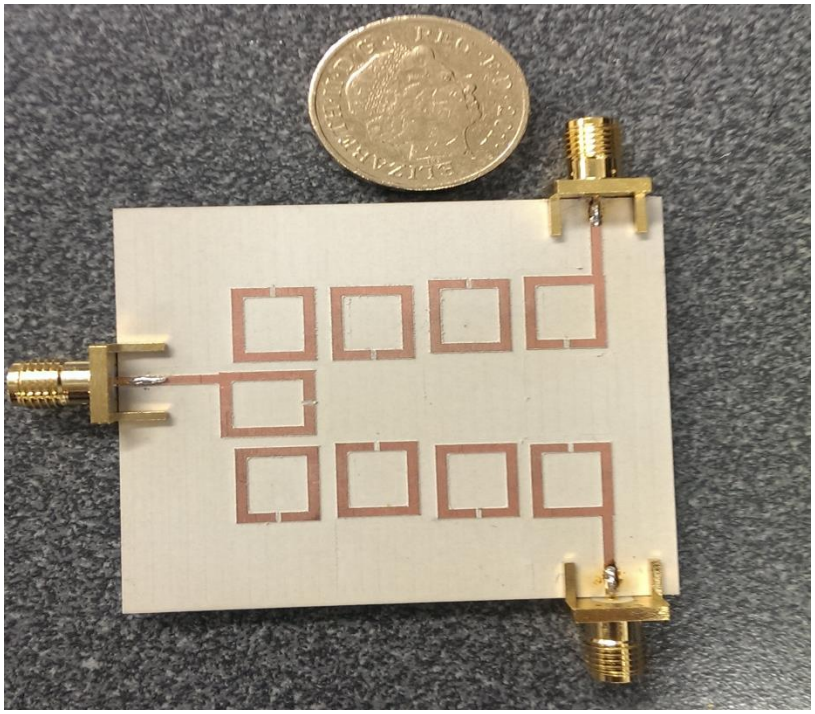

Figure 5.23 Pictorial view of the 5-pole filtered power splitter

5.14 Design analysis

A fifth order Chebyshev Bandpass filtered power splitter is designed. The proposed design has eliminated the need for an additional power splitter when a filtered power splitter is required. The design is simulated and constructed. Measurement is also carried out to verify the design topology; in which there is reasonably good agreement between the simulated and the measured results. This design topology validates the concept of proposed design procedure, i.e. the power splitting can be achieved by merely changing the coupling coefficient of the adjacent resonators at the splitting point. However, there is a limitation in this design, which is the isolation of the output ports and the poor matching of the output ports. A good return loss at ports 2 and 3 cannot be easily achieved in the current design. However, this proposed design is still useful for filtered power splitting applications where there is no matching of ports 2 and 3.

5.15 Summary

This chapter has implemented the design concept to fabricating a microstrip FPS. Firstly, several theories, including, lowpass prototype network, frequency transformation, impedance scaling and immittance inverters in filter design are explored and numerous formulas developed. Then the ideas developed in Chapter 4 are utilise to realise the filter design parameters, especially the common resonators coupling coefficients. Schematic diagrams are designed and simulated and its typical frequency responses are recorded. Later, the FPS was designed and fabricated in microstrip and its frequency responses are compared with the ideal schematic responses. The fabricated component is tuned to give a better result with fractional

bandwidth of 6%. Table 5.5 gives the comparisons of frequency responses for the ideal circuit model, simulated and fabricated for this splitter. The next Chapter will deal with rectangular waveguide and SIW

Table 5.5. 5-pole FPS equal split Ideal, simulated and fabricated frequency responses comparison

Parameters	Ideal Circuit	Simulated	Fabricated
S_{11} (dB)	20	13.2	15
S_{21} (dB)	3	3.1	3.12
S_{31} (dB)	3	3.08	3.05
S_{22} (dB)	5.2	5.4	6
S_{33} (dB)	5.2	5.4	6

CHAPTER 6

THEORY OF RECTANGULAR WAVEGUIDES AND SIW

6.0 Introduction

This chapter provides some theory as applied to RWG. The significance of these led to the development of the cutoff frequency expression and other parameters used in the design of the SIW PS. It deals with the SIW including its brief introduction to minimising losses in SIW and SIW transition. Also, a microstrip line theory is introduced which is needed to get the design parameters in its MSL to SIW transition. Lastly, these relationships will be adapted to making a SIW BPF with microstrip - CPW - SIW input coupling.

6.1 Overview

Substrate Integrated Waveguides (SIW) strikes the balance between, and has the properties, of both microstrip and waveguides. It has an integrated waveguide like structure. It is a synthesized non-planar waveguide that has been transformed into a planar one and it can easily be integrated. Its fabrication process includes embedding two or more parallel rows on metal vias holes that is sandwiched between dielectrics substrate, and is connected between the paralleled metal plates (Deslandes and Wu, 2001). These metal rows form the sidewalls. The manufacturing of SIW has a process similar to other printed planar architecture. Figure 6.1 gives a geometric structure of a typical SIW. The most important geometrical parameters of the SIW are the width (a_s), which separates of the vias in the

transverse direction, the pitch length (p) and the diameter (d) of the vias. Just like a rectangular waveguide, the dominant mode of operation is TE_{10}.

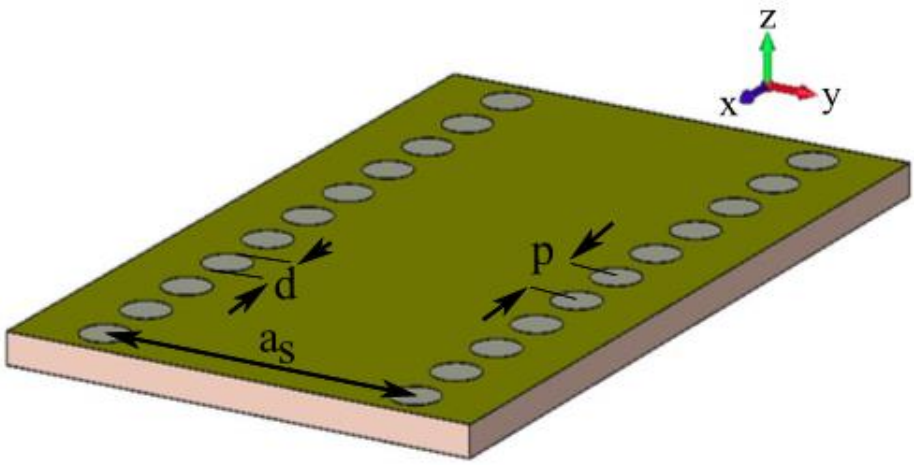

Figure 6.1. Substrate Integrated Waveguides (SIW) configuration (Deslandes and Wu, 2001)

6.2 Rectangular waveguides

A rectangular waveguide is a geometric structure that directs the electromagnetic wave propagation by confining the energy of the wave. It has a uniform cross section as seen in Figure 6.2 that is composed of a dielectric filled or hollow metallic pipe. The rectangular waveguide is still being used today, albeit being one of the earliest transmission lines that was used to transport microwave signal (Pozar, 2011). Standard waveguide band ranging from 1GHz to 220GHz are available for commercial adaptation on variety of microwave components such as couplers, isolators, filters etc. Stripline and microstrip planar transmission lines are used to fabricate most of microwave circuits because of the quest towards integration and miniaturization. However, many applications such as high- power systems, millimeter wave systems and satellite systems still require the need for a waveguide.

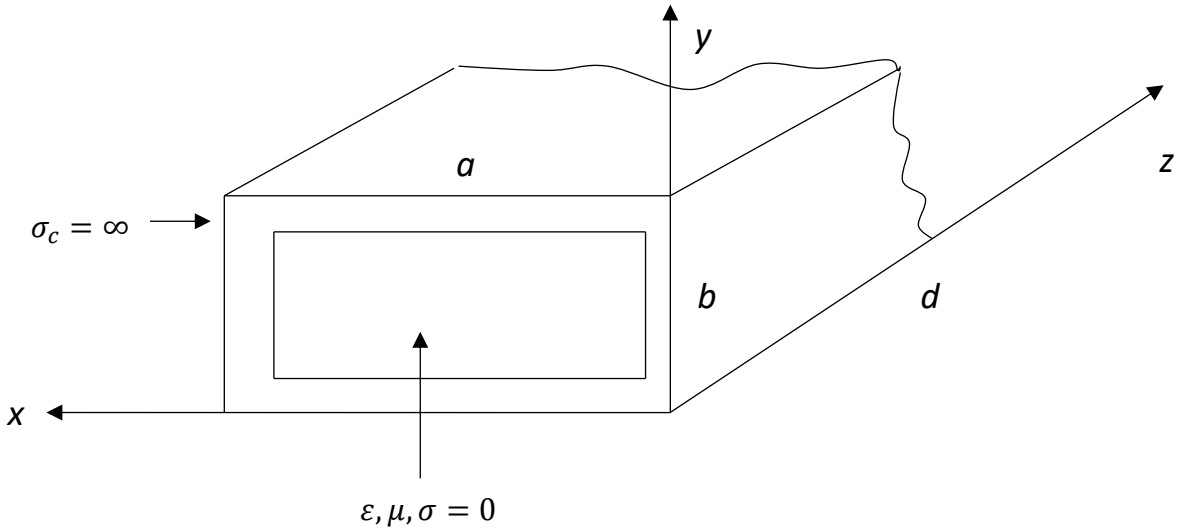

Figure 6.2 Rectangular waveguide configuration

Consider a section of a rectangular waveguide terminated at both sides with walls perfectly conducting, $\sigma_c = \infty$, and assuming a lossless dielectric material, $\sigma = 0$, as shown in Figure 6.2, the rectangular cavity width w, height h and length l, corresponding to the x, y and z axes.

From (Pozar, 2011), the transverse Electric fields (E_x, E_y) of the TE_{mn} and TM_{mn} mode of a rectangular waveguide can be described as:

$$\overline{E}_t(x, y, z) = \vec{e}(x, y)[A^+ e^{-j\beta_{mn}z} + A^- e^{j\beta_{mn}z}] \tag{6.1}$$

where the transverse variations in the *x* and *y* directions is represented by $\vec{e}(x, y)$, A^+ and A^- are the travelling waves amplitude in the positive and negative z directions. The mode propagation constant for the rectangular waveguide, β_{mn} can be expressed as:

$$\beta_{mn} = \sqrt{k^2 - \left(\frac{m\pi}{w}\right)^2 - \left(\frac{n\pi}{h}\right)^2} \tag{6.2}$$

where $k = 2\pi f_0\sqrt{\mu\varepsilon}$, μ and ε are respectively the waveguide dielectric filling material permeability and permittivity.

The waveguide cavity boundary conditions at $z = (0, l)$ requires that the transverse electric field $\overline{E}_t(x, y, z) = 0$. When the condition $\overline{E}_t = 0$ is applied at $z = 0$, from equation 6.1, it results that $A^+ = -A^-$. When the condition $\overline{E}_t = 0$ is applied at $z = l$, it produces $\beta_{mn} l = d\pi$, where d has positive integers, 1,2,3 etc. This indicated that the length of the cavity should be integer multiple of half guided wavelength at its resonance frequency. Therefore, the rectangular cavity cut-off wavenumber k is given by

$$k_{mnl} = \sqrt{\left(\frac{m\pi}{w}\right)^2 + \left(\frac{n\pi}{h}\right)^2 + \left(\frac{q\pi}{l}\right)^2} \tag{6.3}$$

where the indices m, n, q relates to the number of half wavelength variations in the x, y, z directions respectively. The resonant frequency for the TE_{mnl} or TM_{mnl} mode will now be:

$$f_{mnl} = \frac{ck_{mnq}}{2\pi\sqrt{\mu_r \varepsilon_r}} = \frac{c}{2\pi\sqrt{\mu_r \varepsilon_r}} \sqrt{\left(\frac{m\pi}{w}\right)^2 + \left(\frac{n\pi}{h}\right)^2 + \left(\frac{q\pi}{l}\right)^2} \tag{6.4}$$

where c is the speed of light.

When $l > w > h$, the mode with the lowest resonant frequency, known as the dominant mode, will be TE_{101} mode. Figure 6.3 shows the dominant TE_{101} mode field configuration. Here, the circles and solid lines represents the electric field whist the dashed lines represents the magnetic field (Bahl and Bhartia, 2003).

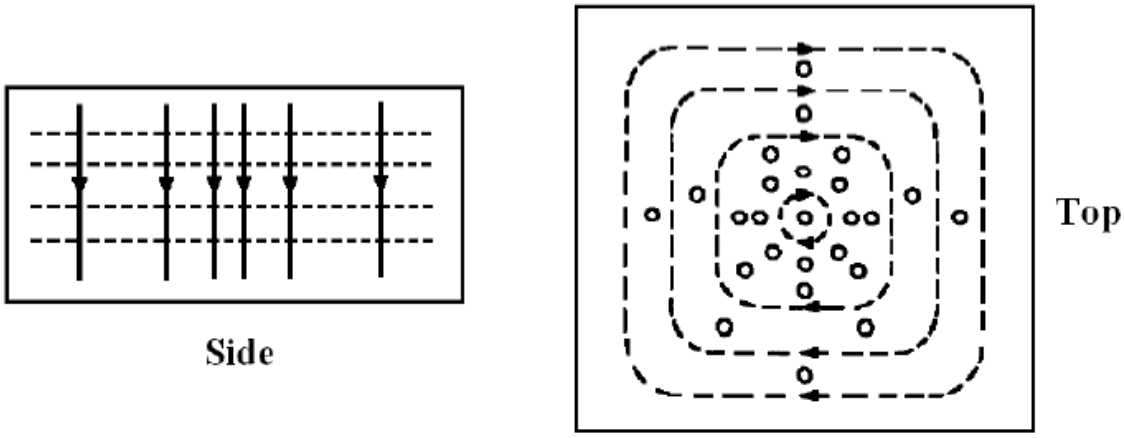

Figure 6.3 Dominant TE_{101} mode field configurations

6.3 Substrate Integrated Waveguide

As already stated in the chapter overview, SIW is an integrated geometric waveguide structure that into contains planar dielectric substrate with periodic row of metallic vias that connects the top and bottom planes (Deslandes and Wu, 2001). As seen in Figure 6.1, both the top and bottom planes of the SIW completely are engulfed with a metal ground. The rectangular wave-guide is made within a substrate that is sandwiched by rows of metallic vias on either side of the structure. High power handling capabilities, higher Q-factor, and low loss are some of the main advantages of a conventional rectangular waveguide, which are also preserved in the SIW. Other advantages of planar printed SIW circuits include compact size, ease to fabricate and integrate with other components/circuits and low cost.

It has been proven that the guided wave properties of a conventional rectangular waveguide with certain width equivalent have similarity with its corresponding SIW. Numerous researchers like (Xu and Wu, 2005), (Deslandes and Wu, 2006) and (Cassivi et al., 2002) have delivered some findings on the electromagnetics properties of SIW. Therefore, with an

equivalent width of SIW given, the design and analysis of SIW structure can be possible by adapting the well-developed theories of waveguides. However, there are noticeable differences of wave propagation between a conventional rectangular waveguide and the SIW due to the existence of certain type of leakage of the latter. This is because the SIW is kind of discrete or periodic guided- wave structure and due to these periodic gaps (Xu and Wu, 2005).

6.4 SIW Cavity Parameters

Consider the top view of the SIW cavity in Figure 6.4, the effective width w_{eff} and the effective length L_{eff} of the SIW structure corresponds to w and l of the rectangular waveguide as seen in equation 6.4.

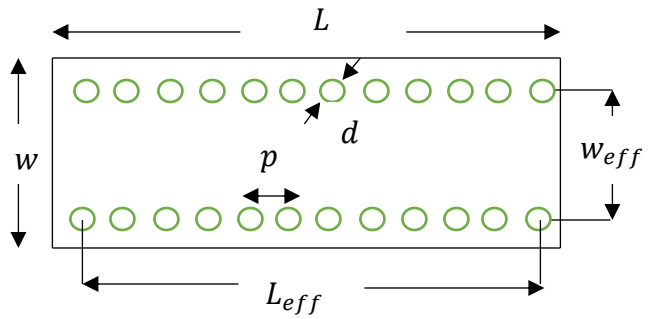

Figure 6.4 SIW rectangular waveguide resonance cavity

The resonant frequency for a SIW waveguide cavity is operating at resonant mode 101, which is, the variables m, n & q that corresponds to 1,0,1 respectively. This solves the resonant frequency as:

$$f_{101} = \frac{c_0}{2\sqrt{\mu_r \varepsilon_r}} \sqrt{\left(\frac{1}{a_{eff}}\right)^2 + \left(\frac{1}{L_{eff}}\right)^2} \tag{6.5}$$

The dominant mode in a hollow metallic rectangular waveguide is $TE_{10.}$ The resonance frequency according to (Hong and Lancaster, 2001), is f_{mn}, which is given by:

$$f_{mn} = \frac{\omega_c}{2\pi} = \frac{1}{2\pi\sqrt{\mu_r \varepsilon_r}} \sqrt{\left(\frac{m\pi}{w}\right)^2 + \left(\frac{n\pi}{h}\right)^2} \tag{6.6}$$

For the TE_{10} dominant mode, the resonance frequency now becomes:

$$f_{10} = \frac{1}{2w\sqrt{\mu_r \varepsilon_r}} \tag{6.7}$$

where w corresponds to the width of the SIW cavity.

For simplicity, the relationship between the resonant frequency for TE_{10} of the rectangular waveguide cavity and TE_{101} for the SIW waveguide cavity is utilised which is given as:

$$f_{101} = 2f_{10} \tag{6.8}$$

All the SIW cavity parameters are related in accordance with the following relationship as given by (Zakaria et al., 2013):

$$w_{eff} = w_{SIW} - \frac{d^2}{0.95p} \tag{6.9}$$

$$L_{eff} = L_{SIW} - \frac{d^2}{0.95p} \tag{6.10}$$

$$p \leq 2d \tag{6.11}$$

where, L_{SIW} and a_{SIW} are the length and width of the resonant SIW cavity, d and p are the diameter and the distance between adjacent vias respectively. μ_r and ε_r are the relative permeability and the dielectric constant of the substrate respectively.

6.5 SIW Effective width

The SIW cutoff frequency has been studied in (Cassivi et al., 2002). It indicates that the cutoff frequencies of the TE_{10} and TE_{20} modes in the SIW with respect to the metallized vias diameter and the spacing between them can be expressed as follows:

$$f_{c(TE_{20})} = \frac{c_0}{2\sqrt{\varepsilon_r}}\left(w - \frac{d^2}{0.95 \cdot p}\right)^{-1} \tag{6.12}$$

$$f_{c(TE_{20})} = \frac{c_0}{2\sqrt{\varepsilon_r}}\left(w - \frac{d^2}{1.1 \cdot p} - \frac{d^3}{6.6 \cdot p}\right)^{-1} \tag{6.13}$$

where c_0 is the speed of light in free space; w is the width of the SIW, d is the via diameter and p is the via spacing as seen in Figure 6.1. This equation is useable for $d < \lambda_0\sqrt{\varepsilon_r}/2$ and $p < 4 \cdot d$.

The cutoff frequency of TE_{m0} modes in a conventional rectangular waveguide using the waveguide width w and height h can be expressed as:

$$f_c = \frac{c_0}{2\sqrt{\varepsilon_r}}\left(\frac{m}{w}\right) \tag{6.14}$$

From equations 6.12, 6.13 and 6.14; it is observed that the SIW is comparable to the conventional rectangular waveguide. Furthermore, in terms of the fundamental propagating (TE_{m0}) mode, the SIW can be analysed as a rectangular waveguide by using an effective width (w_{eff}) as described in equation 6.9 (Cassivi et al., 2002)

Equation 6.9 gives a good approximation between a SIW and its equivalent rectangular waveguide. However, this approximation failed to include the effect of d/w, which may cause small errors when d rises (Xu and Wu, 2005). To reach at a better approximation, a

more accurate empirical equation that calculates the effective SIW width was reported in (Xu and Wu, 2005) which can be described as:

$$w_{eff} = w - 1.08\frac{d^2}{0.95 \cdot p} + 0.1\frac{d^2}{w} \quad (6.15)$$

Equation 6.15 is accurate when the requirement $l/d < 3$ and $d/w < 0.2$ are met.

6.6 Determination of the Microstrip parameters

Figure 6.6 represents a microstrip line of width w and substrate height h. The strip conductor provides path for signal flow. Microstrip is essentially a non-homogeneous line of two dielectrics, typically the substrate and air. The height, width, permittivity and permeability of the microstrip are all function of the characteristic impedance. That is $Z_0 \propto h, w, \varepsilon_r, \mu_r$ and $\mu_r = 1$ for non-magnetic material.

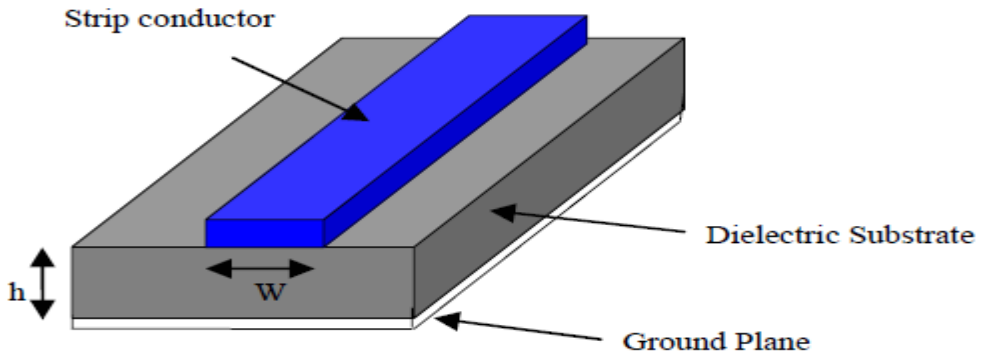

Figure 6.6 Microstrip Line (Mutiara et al, 2011)

Most of the electric field lines reside in the substrate and some parts lines in air as seen in Figure 6.7, As a result, this transmission line cannot support pure transverse electric-magnetic (TEM) mode of transmission, since the phase velocities would be different in the air and the substrate.

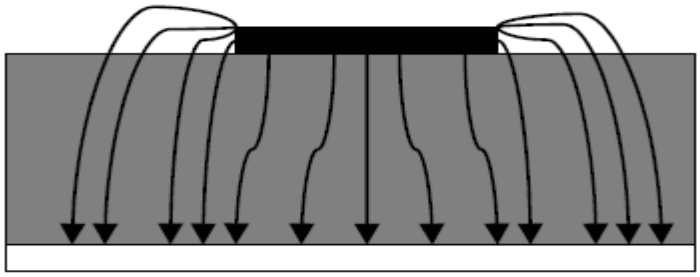

Figure 6.7 Electric Field Lines

Instead, the dominant mode of propagation would be the quasi-TEM mode. Hence, an effective dielectric constant (ε_{reff}) must be obtained in order to account for the fringing and the wave propagation in the line. The value of ε_{reff} is slightly less then ε_r because the fringing fields around the periphery of the patch are not confined in the dielectric substrate but are also spread in the air as shown.

Hence, as seen from Figure 6.7, most of the electric field lines reside in the substrate and parts of some lines in air. As a result, this transmission line cannot support pure transverse electric- magnetic (TEM) mode of transmission, since the phase velocities would be different in the air and the substrate. Instead, the dominant mode of propagation would be the quasi-TEM mode. Hence, an effective dielectric constant (ε_{reff}) must be obtained in order to account for the fringing and the wave propagation in the line. The value of ε_{reff} is slightly less then ε_r because the fringing fields around the periphery of the microstrip. The expression for ε_{reff} is given by (Balanis, 2005), as:

$$\varepsilon_{eff} = \frac{\varepsilon_r+1}{2} + \frac{\varepsilon_r-1}{2} \cdot \frac{1}{\sqrt{1+12\frac{h}{w}}} \tag{6.16}$$

where ε_{eff} = Effective dielectric constant of the substrate

ε_r = Dielectric constant of substrate

h = Height of dielectric substrate

w = Width of the patch

6.7 Synthesis of w/h

To determine *w/h* ratio, Hammerstad (Hammerstad, 1975) and Wheeler (Wheeler, 1965) derived the following expressions:

For $^{w}/_{h} \leq 2$,

$$^{w}/_{h} = \frac{8e^{A}}{e^{2A}-2} \tag{6.17}$$

$$A = \frac{Z_o}{60}\sqrt{\frac{\varepsilon_r+1}{2}} + \frac{\varepsilon_r-1}{\varepsilon_r+1}(0.23 + \frac{0.11}{\varepsilon_r}) \tag{6.18}$$

For $^{w}/_{h} > 2$,

$$^{w}/_{h} = \frac{2}{h}[B - 1 - \ln(2B-1) + \frac{\varepsilon_r+1}{2\varepsilon_r}(\ln(B-1) + 0.39 - \frac{0.11}{\varepsilon_r}] \tag{6.19}$$

$$B = \frac{377\Pi}{2Z_o\sqrt{\varepsilon_r}} \tag{6.20}$$

The wavelength (or guided wavelength) is determined using the relation:

$$\lambda_g = \frac{C_o}{\sqrt{\varepsilon_{eff}}.f} \tag{6.21}$$

6.8 SIW losses minimisation

One major concern in the design of SIW components is the challenge of minimizing losses. There are three main mechanisms of SIW losses. Due to the finite metallic walls conductivity and the dielectric substrate, the SIW displays conductor losses and likewise dielectric losses as in the conventional metallic waveguide. Additionally, the presence of gaps along the SIW

sidewalls can lead to radiation losses due to possible leakages through those gaps (Bozzi et al., 2008) and (Bozzi et al., 2007).

Modifying its geometrical parameters; namely, substrate thickness h, the vias diameter d and their longitudinal spacing p can minimize SIW losses. The dielectric substrate thickness h plays a vital role in the conductor loss in the SIW. Increasing thickness h can lead to a substantial reduction of the conductor losses. This is as a result of the lower electric current density flowing on the metal surface with the increasing substrate thickness. The metallic vias diameter D and their spacing p have great influence on the radiation losses. It is proven that radiation leakages will become important when the condition $p / d < 2.5$ is not met (Xu and Wu, 2005). In general, the following two design rules can be used to ensure the radiation losses kept at an insignificant level (Deslandes and Wu, 2002).

$$d < \lambda_g/5 \tag{6.22}$$

$$p < 2 \cdot d \tag{6.23}$$

where λ_g is the guided wavelength in the SIW. In this instance, the SIW can be modelled as a conventional rectangular waveguide.

Literatures such as (Xu and Wu, 2005), (Deslandes and Ke, 2006) and (Deslandes and Wu, 2002) contains more details about the transformation from the SIW to an equivalent rectangular waveguide.

Lastly, it's vital to notice that the dielectric losses of SIW structures depend greatly on their operating frequencies (Bozzi et al., 2009), Dielectric loss is typically very significant contribution to losses especially when it operates in mm-wave frequencies. It is therefore

important that a proper selection of the dielectric material is made in order to get minimum losses for the SIWs that operate in a relatively high frequency.

6.9 Substrate Integrated Waveguide Transition

SIW transitions play a vital role in integrating other electronic devices with SIW components. The design and implementation of transition structures between planar circuits and traditional rectangular waveguides have widely been studied as reported in (Lou et al., 2008), (Grabherr et al., 1994) and (Villegas et al., 1999). Many of these structures are used for the transition between SIW structures and planar circuits directly, and/or with little modification. Additionally, since the SIW can be integrated with planar circuits on the same substrate, the whole circuit, including the planar circuit, transition and SIW structures, can be constructed in a dielectric substrate conveniently by just using a standard PCB processing technique (Huang et al., 2009).

6.10 Tapered microstrip transition

One of the most commonly used structure for the transition between the microstrip line (MSL) and SIW is the tapered microstrip transition (Deslandes and Wu, 2001a). A microstrip line contains a tapered section, which is directly connected to the top wall of the SIW as illustrated in Figure 6.8. The transition is easily achieved by matching the vertical components of the electric field in both microstrip line and SIW regions. The tapered

microstrip transition is a wideband structure that covers the complete useful bandwidth of the SIW. Nevertheless, if a thicker substrate is used in SIWs in order to achieve a reduced conductor loss, the radiation loss will increase in the microstrip line as the substrate thickness is increased. Therefore, the tapered microstrip transition is not appropriate for active component integration, especially for those at millimeter-wave frequencies (Wu et al., 2003)

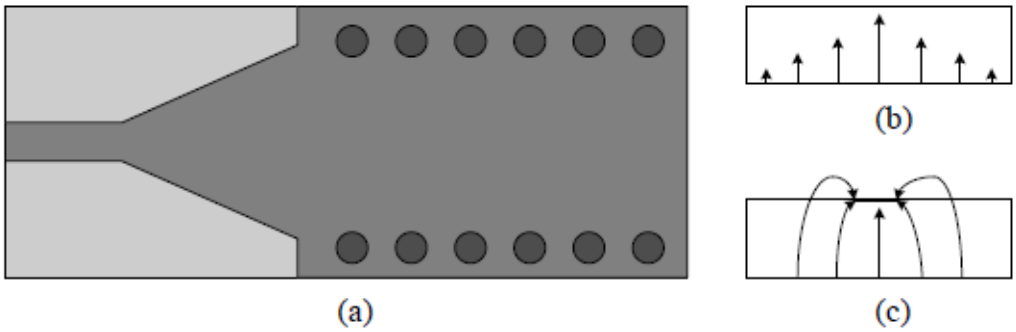

Figure 6.8 MSL to SIW transition with tapered microstrip feeding: (a) transition structure; (b) electric field distribution in SIW cross section, and (c) electric field distribution in MSL cross section (Deslandes and Wu, 2001a), (Wu et al., 2003)

6.10.1 Coplanar waveguide (CPW)-to-SIW transition

Coplanar waveguide (CPW) is an alternative structure for the transition between planar circuits and SIWs as shown in Figure 6.8. The CPW-SIW transition (Deslandes and Ke, 2001) utilises a coplanar waveguide section to send signal to the SIW, with an inset conducting stub employed to better match the CPW and SIW. Since increasing the height of the dielectric substrate does not influence on the inherent characteristics of CPW, this transition is less sensitive to substrate thickness and hence exhibits a better performance than the microstrip transition in relatively high frequencies, especially in mm-wave frequencies.

However, it should be noted that the CPW-SIW transition has a narrower bandwidth in comparison to the microstrip counterpart. Several modified structures, such as the elevated CPW-SIW transition (Lee et al., 2008), have been proposed to enhance the bandwidth performance.

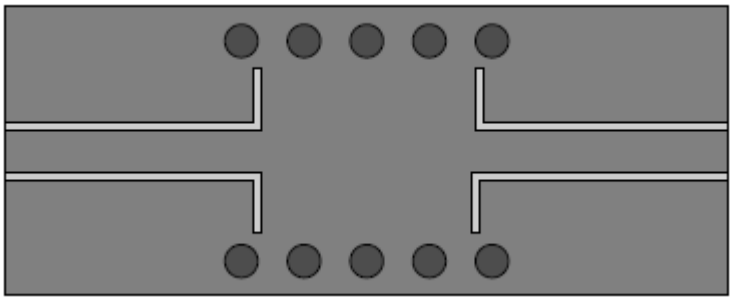

Figure 6.9 Configuration of the CPW-SIW transition (Deslandes and Ke, 2001)

6.11 SIW bandpass filter Design

This section is a joint work as given in (Nwajana et al, 2017) to further illustrate the SIW concept. In order to design the SIW transmission line to be able to operate at a certain frequency, consideration is made to the three main design parameter. These parameters are (1) the diameter of the via, d; (2) the pitch or separation between the metallic posts, p. and (3) the width of the SIW. The test filter is a 3-pole Chebyshev bandpass filter that is designed to meet the following specifications as shown in Table 6.1. For the given fundamental mode, i.e. TE_{101}, the size of the SIW cavity is determined using its corresponding resonance frequency mode f_{101} (Xiaoping et al., 2005) as given in equation 6.5.

Table 6.1 Test Bandpass design specifications:

Parameters	Values
Centre Frequency, f_0	1.684 GHz
Fractional Bandwidth, FBW	4%
Passband Return Loss R_L	20dB

The numerical design parameters for the bandpass filter is shown in Table 6.2.

Table 6.2 3-pole Chebyshev bandpass filter design parameters:

Filter	f_0 [GHz]	L [nH]	C [pF]	J_{01}	J_{12}
BPF	1.684	0.222	40.2424	0.02	0.0176

The bandpass is designed in accordance with the technique detailed in (Hong and Lancaster, 2001) and which is applied in (Dainkeh et al., 2016); where *L* is the inductance, *C* is the capacitance and *J* is the *J*-inverter values.

The 3-pole Chebyshev bandpass filter is then simulated using the ADS circuit simulator software. The couplings between resonators are modelled using the method described in Section 4.3.

The simulation S-parameter frequency responses of the test bandpass filter circuit model are shown in Figure 6.10.

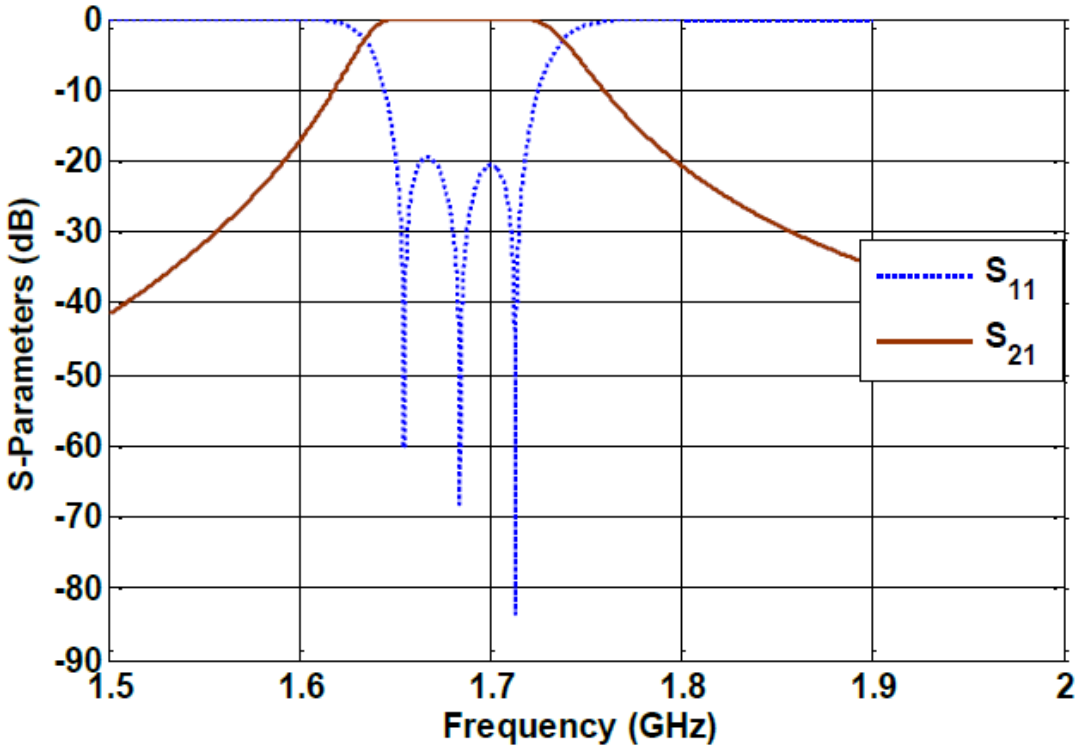

Figure 6.4 Simulation S-parameter responses.

6.12 SIW simulation

The test BPF is designed to resonate at the TE_{101} resonance mode with a resonance frequency f_0. The material used to design the substrate is Rogers RT/Duroid 6010LM substrate whose substrate thickness, h, dielectric constant, ε_r, and relative permeability, μ_r, is given in Table 6.3. Also included in Table 6.3 are the SIW chosen design parameters, which is the diameter, pitch, width and length of the cavity.

Table 6.3 SIW design parameters

f_0 (GHz)	ε_r	h(mm)	μ_r	d(mm)	p(mm)	w(mm)	l(mm)
1.684	10.8	1.27	1	2	3.725	37.25	37.25

The finite-element method (FEM) of the Keysight's 3-D Electromagnetic Professional (EMPro) simulator is used to carry out all the electromagnetic (EM) simulations. All the copper metal used was designated to have thickness of 17 μm and a conductivity σ of 5.8 x 107 S/m whilst the substrate was assumed to have a loss tangent, tan δ of 0.0023.

Figure 6.10 (inset) gives the arrangement that is used to determine the simulated value of the coupling coefficient, *k*, between each pair of SIW cavities. The curve in Figure 6.10 gives the correlation between the coupling coefficient, *K*, and the spacing between the center metallic posts shown in the inset figure.

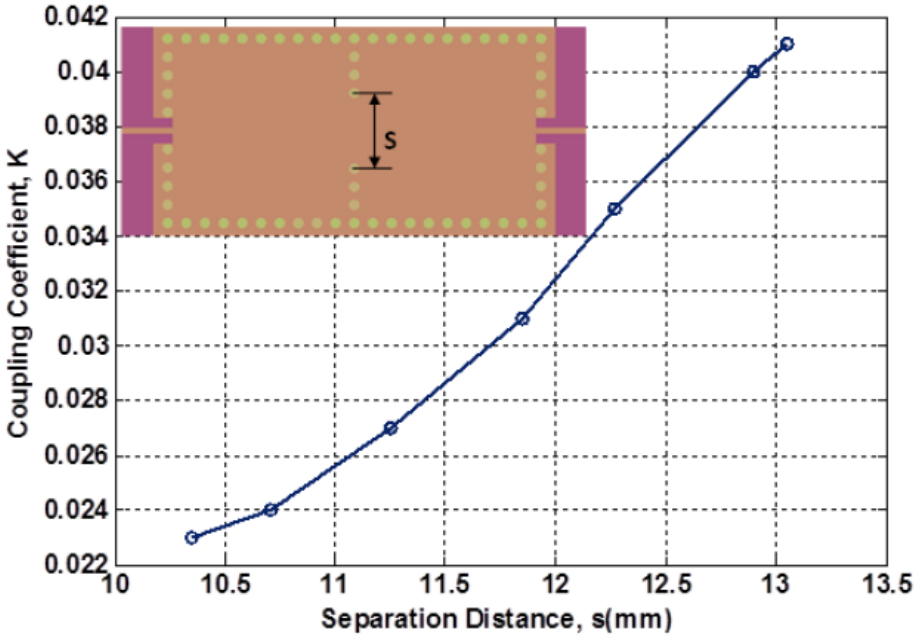

Figure 6.10 Coupling coefficient of a pair of SIW cavities

From Figure 6.10, the value of *K* that was used to achieve the test filter is 0.041 and it correspond to 13.05 mm.

The expression $Q_{ext} = \frac{2\pi f_0 C}{J_{01}}$ is used to establish the filter theoretical value of the external quality factor Q_{ext}; where f_0, J_{01}, and C correspond to the values given in table 6.3. The filter theoretical value of Q_{ext} is 21.21. Q_{ext} is also established through simulation. Figure 6.6 depicts the setup for determining it. The widely known expressions reported in (Yong and Ke-Li, 2003) are used to determine the length corresponding to the 50Ω impedance, Z_o, of the microstrip transmission line.

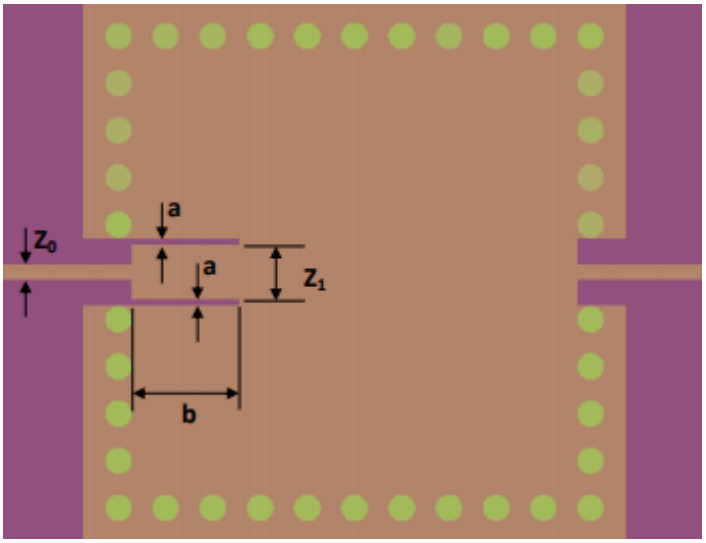

Figure 6.11 Microstrip CPW to SIW input coupling structure for extracting Q_{ext}

To achieve the impedance at the SIW end of the transition, the impedance Z_1 was adjusted by altering the dimensions of a and b until the required Q_{ext} is obtained.

Case 1. b is kept constant at 8.13mm whilst a is varied to ascertain the value of Q_{ext}. The corresponding Q_{ext} values were obtained and the correlation with length a is given shown in Figure 6.12a.

Case 2. a is kept at 0.7mm whilst b is varied to ascertain the value of Q_{ext}. The corresponding Q_{ext} values were obtained and the correlation with length a is given shown in Figure 6.12b.

The value of Z_1 that corresponds to the Q_{ext} required value of 21.21 is 24 Ohms. The length y_1 in Figure 6.13 is used to find the characteristics impedance values by using the expression as given by (Hong and Lancaster, 2001). It is important to note that there would be an increase in the characteristic impedance, Z_1 when there is an increment of the length a.

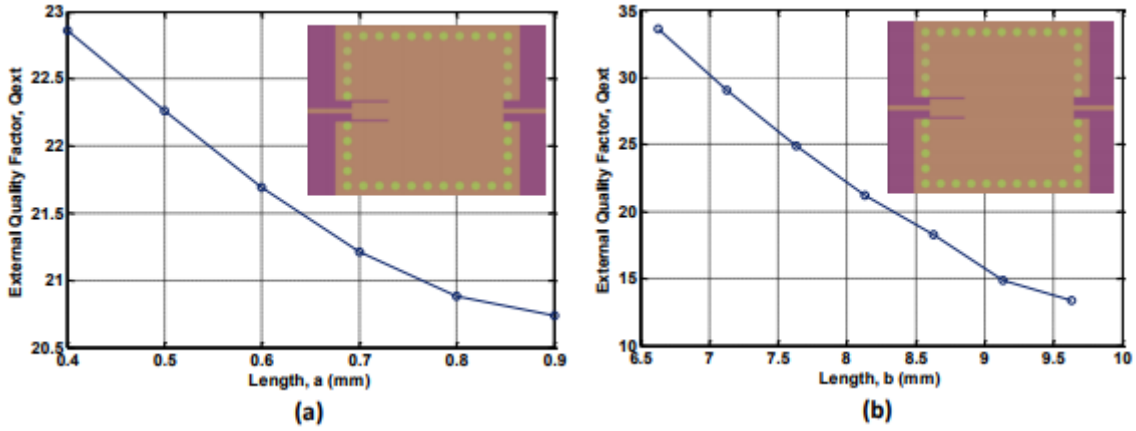

Figure 6.12 Graphs for extracting the external Q-factor, Q_{ext} (a) Variation of Q_{ext}, with length, a, at constant length, b = 8.13 mm. (b) Variation of Q_{ext}, with length, b, at constant length, a = 0.7 mm

The completed layout of the SIW BPF that is simulated using the FEM setting of the Keysight's EMPro 3D simulator is shown in Figure 6.13 with all its physical dimensions. These physical quantities are collated and presented in Table 6.4.

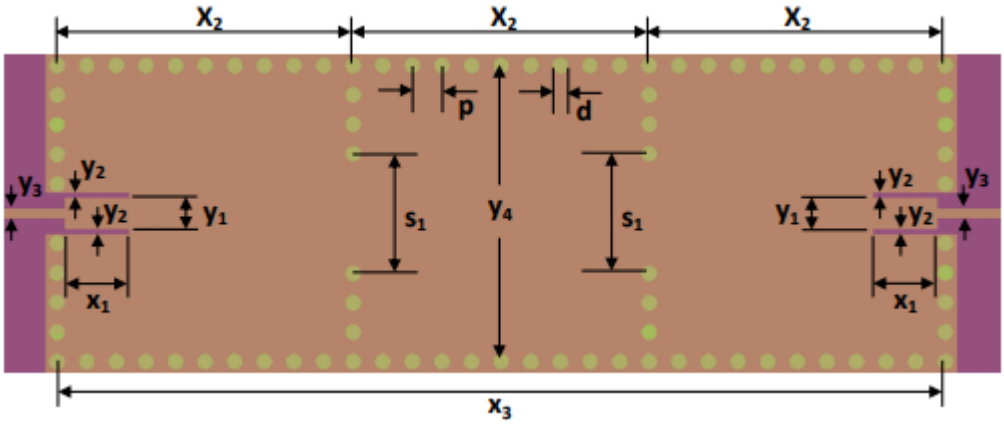

Figure 6.13 Substrate integrated waveguide bandpass filter layout with dimensions.

Table 6.4 SIW Bandpass filter physical dimensions

Dimension	Value (mm)	Dimension	Value (mm)
X_1	8.125	Y_1	3.9
X_2	37.25	Y_2	0.7
X_3	111.75	Y_3	1.1
d	2.0	Y_4	37.25
p	3.725	S_1	13.05

The simulated S-parameters response of the completed SIW BPF is shown in Figure 6.14 below as.

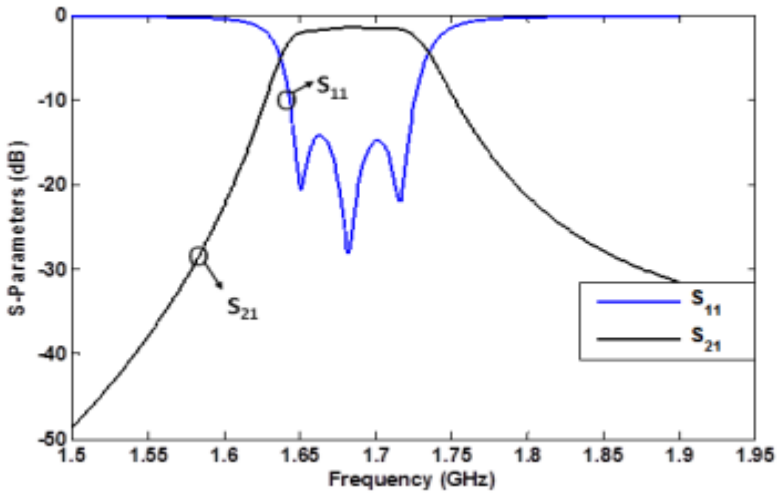

Figure 6.14 Simulation S-Parameter responses of the substrate integrated waveguide bandpass filter

It is seen from Figure 6.14 that the SIW BPF centre frequency was realised to be 1.68 GHz, which is in conformity with the desired design. A simulated minimum insertion loss, S_{21}, at the passband of 1.3 dB is realised. Also noticed is that the simulated return loss is better than 14.6 dB across the passband. The input/output coupling and the couplings between each pair of SIW cavities can be used to control the filter passband which can as well be based on the fractional bandwidth specification; in this case a FBW of 4%.

6.13 SIW Fabrication and measurement

The material specified and used in the FEM simulation in the EMPRo software is also employed in the SIW Bandpass fabrication. Using "Leiterplatten-Kopierfräsen" (LKPF) Protomat C60, the fabrication was done based on the printed circuit board (PCB) micro-milling process. The finished production is shown in the photograph of Figure 6.15. As seen in the picture, two SMA (Sub-Miniature version A) connectors were fitted onto the input and output ports in order to facilitate filter measurement. An Agilent Vector Network Analyser is used to measure the fabricated SIW filter.

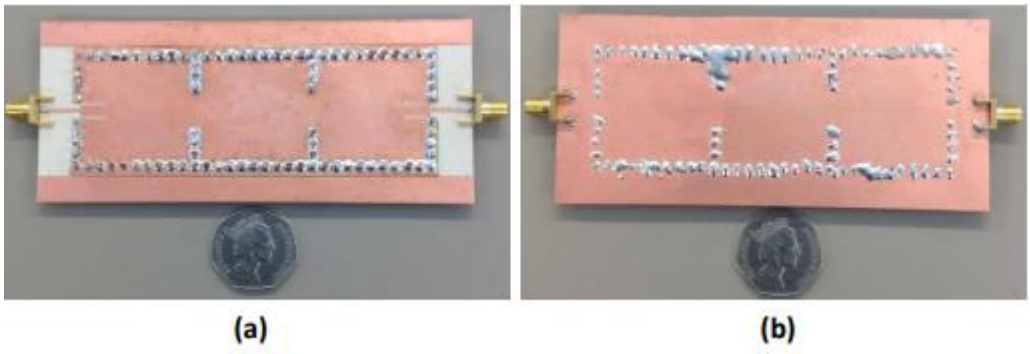

Figure 6.15 Fabricated SIW bandpass filter pictures. (a) Top view. (b) Bottom view

The measurements are done and Figure 6.16 gives the measured results that indicates that minimum insertion loss (S_{21}) of 1.3 dB is achieved at the passband. The minimum simulated return loss (S_{11}) is about 15dB whilst the measured return loss is about 16dB are achieved across the passband. Some tuning adjustments are made at the input and output coupling. This produce a much-improved measured return loss of better than 22dB at the passband. This improved return loss is given in Figure 6.16b.

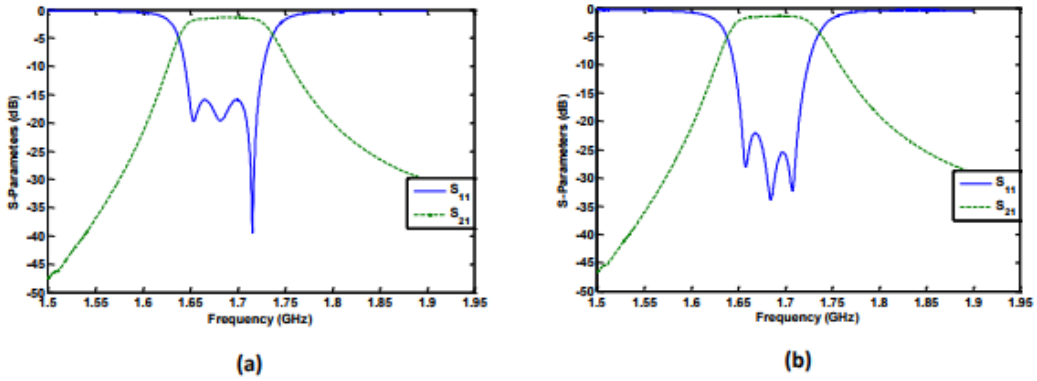

Figure 6.16 SIW bandpass filter measurement results. (a) Before tuning. (b) After tuning.

For ease of comparison, all the results included the tuned results are jointly presented in Figure 6.17.

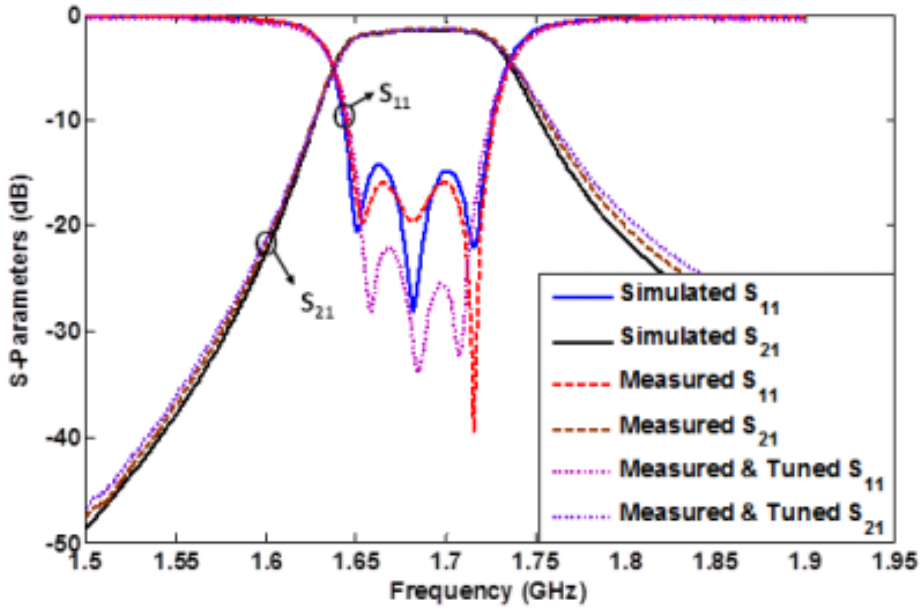

Figure 6.17 Comparison of the simulated and measured results of the SIW Bandpass filter

It can be clearly seen from Figure 6.17 that there is a good agreement between the simulated and the result of the initial measurement. By tuning the input and the output coupling, there is an achievement of an improved measurement result of better than 22 dB as viewed on the network analyser. When compared to the waveguide filter reported by (Mohottige et al., 2016), the fabricated SIW PBF electrical size is more compact of about $0.21\lambda_g$ X $0.63\lambda_g$ but less compact when compared to the microstrip filter as given in (Chen et al., 2016). The return loss of about 16 dB, when compared, is better here than that reported return loss of about 11 dB achieved and also, the band-rejection and roll-off in this simulated and measured results are steeper and in good agreement when compared the filter presented in (Mohottige et al., 2016).

6.14 Discussion

A novel Microstrip Coplanar Waveguide input coupling of a Substrate Integrated Waveguide Bandpass filter is presented. This SIW filter is designed, simulated, fabricated and measured. To control the Q-factor, the Microstrip Coplanar Waveguide to SIW transition utilised as the input coupling in the design allows two degrees of freedom. At the SIW end of the transition, stepping the 50Ω impedance feedline to a lower impedance makes it easier to accomplish the required filter external quality factor Q_{ext}. The Q_{ext} changes when the impedance at the SIW end of the transition is altered. The practically measured result shows that there is a minimum insertion loss of about 1.3 dB achieved across the passband. Initially, the measured minimum return loss of 16 dB is achieved but when tuning between input and output couplings of the filter is performed, there is an improvement of an achieved return loss with measured minimum of about 22dB. These results also show that there is a good agreement between the simulated and measured results of the filter responses.

6.15 Summary

This chapter has discussed extensively the theory of the rectangular waveguide and SIW. It uses the equations developed from RWG and its dominant mode to build up the formulas for its SIW counterpart such as resonance frequency and various dimensions. Furthermore, discussions were done on how to minimize losses and the transition from MSL to SIW. To prove this concept, a test bandpass filter was co-designed using two degree of freedom to ascertain the required filter's Q factor. The test filter achieved an improved return loss after

tuning at its ports. This was done as benchmark for its implementation to the SIW equal and unequal FPS as seen in the next Chapter.

CHAPTER 7

EQUAL AND UNEQUAL POWER SPLITTER IN SIW

7.1 Introduction

This chapter presents the designs, realisation and measurement of the design components with bandpass Chebyshev's filtering response. These include; 5-resonators 3-dB equal power splitter, 5-resonators unequal power splitter, 9-resonators 3-dB equal power splitter and 9-resonators unequal power splitter. These devices implementation is done using substrate integrated waveguide that are suitable for low cost mass fabrication. As already mentioned previously in Chapter 2, they have advantage in microwave frequencies application due to their high power handling capabilities and their high unloaded quality factor.

Rectangular waveguide cavities' importance to the design process of the SIW cavities is first discussed in this chapter. Coupling coefficient and external quality factor extracted from the physical structure are also included. The design, fabrication and measurement of the proposed devices will be discussed all the way through this Chapter.

7.2 Determination of actual SIW resonator size

The actual size of the SIW synchronous resonator size is determined by simulating the physical dimensions as derived by equations 6.9 and 6.10. Each SIW resonator is naturally

rectangular in shape with $L_{siw} > w_{siw}$ as seen in Figure 6.4. But due to the desired resonant frequency of 2GHz; it is observed that, in this instance $w_{siw} > L_{siw}$ as seen in Figure 7.1.

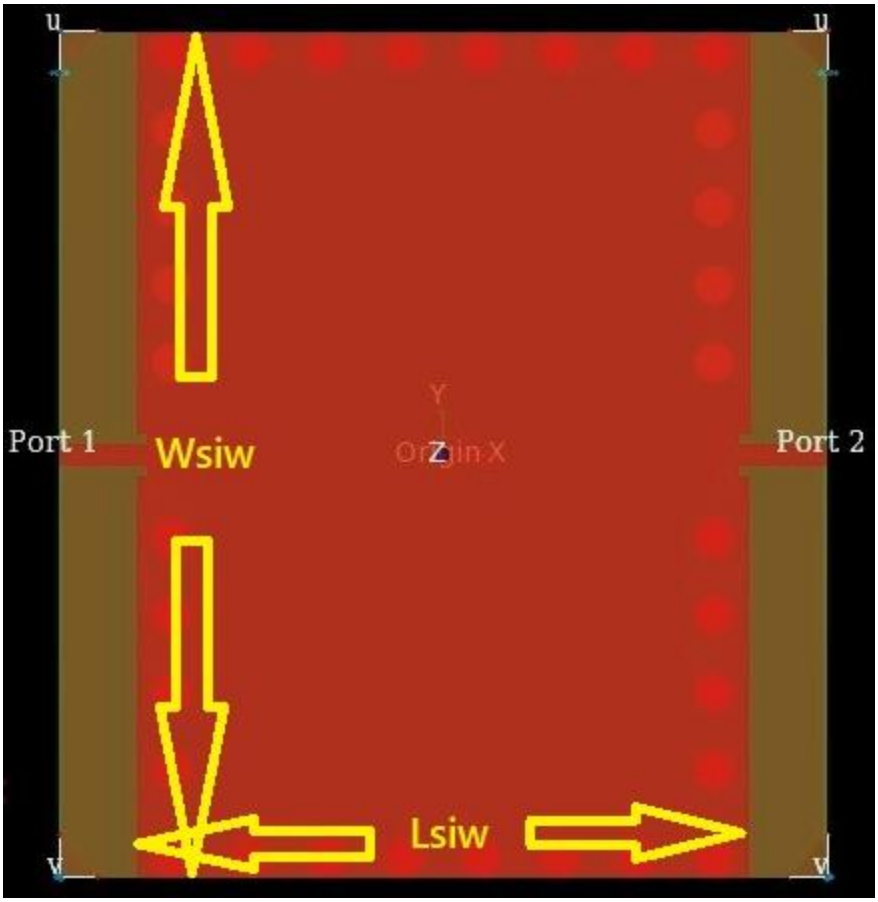

Figure 7.1 Original rectangular shaped SIW resonator as captured from EmPro simulator

However, the proposed SIW resonator is made a square resonator by maintaining the structure's perimeter whilst ensuring it resonates at its resonant frequency as shown in Figure 7.2 a and b.

$$2(w_{siw} + L_{siw}) = 4\mathrm{A}_{siw} \tag{7.1}$$

where A_{siw} is the size of one length of the square resonator

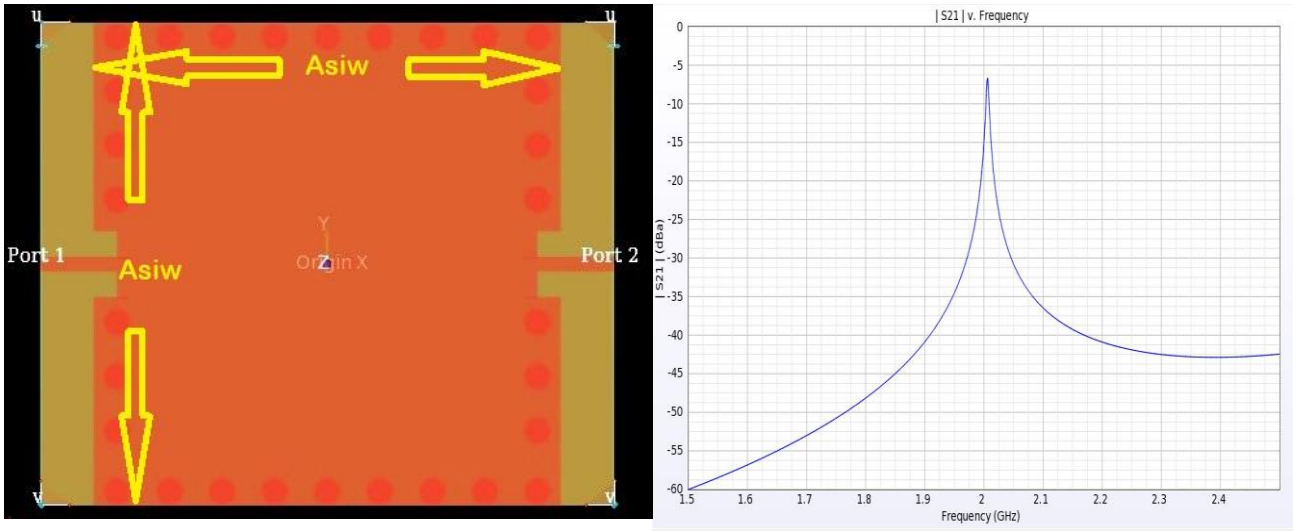

(a) (b)

Figure 7.2 (a) Square shaped SIW resonator and (b) Simulated resonance frequency response

7.3 Coupling Coefficient extraction from SIW structure

Keysight's EMPro 3D EM simulation software is used to obtain the coupling coefficient for a selected resonator pair in any resonator coupling circuit. To realise the coupling coefficient of two synchronously coupled resonators, equations 4.11 is applied as derived in section 4.3. (Hong, 2000). The characteristic parameters f_1 and f_2 can be determined using full wave EM simulation. Figure 7.3 shows an arrangement of two SIW cavity resonator structures that is weakly coupled to the ports. Ultimately, the frequency response is shown in Figure 7.4 which depicts the simulated $|S_{21}|$ response showing the frequency peaks f_1 and f_2.

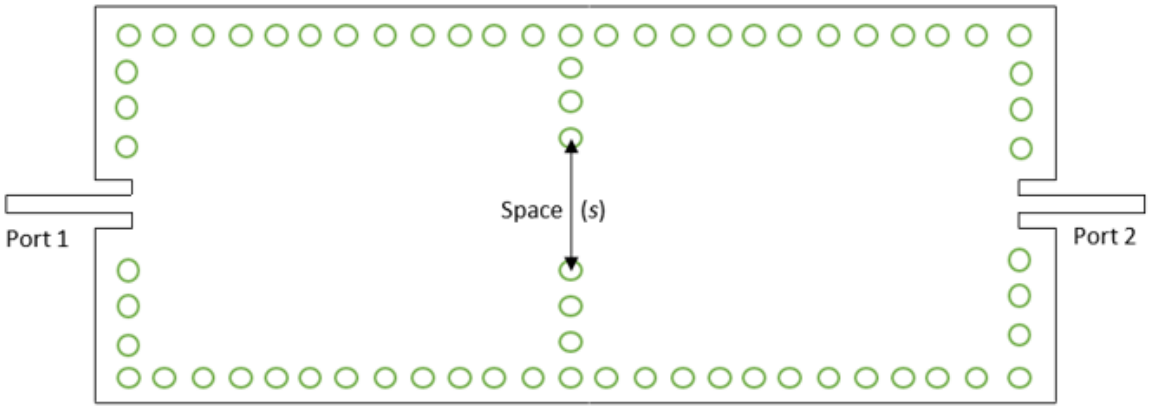

Figure 7.3 Two coupled SIW waveguide cavity resonators

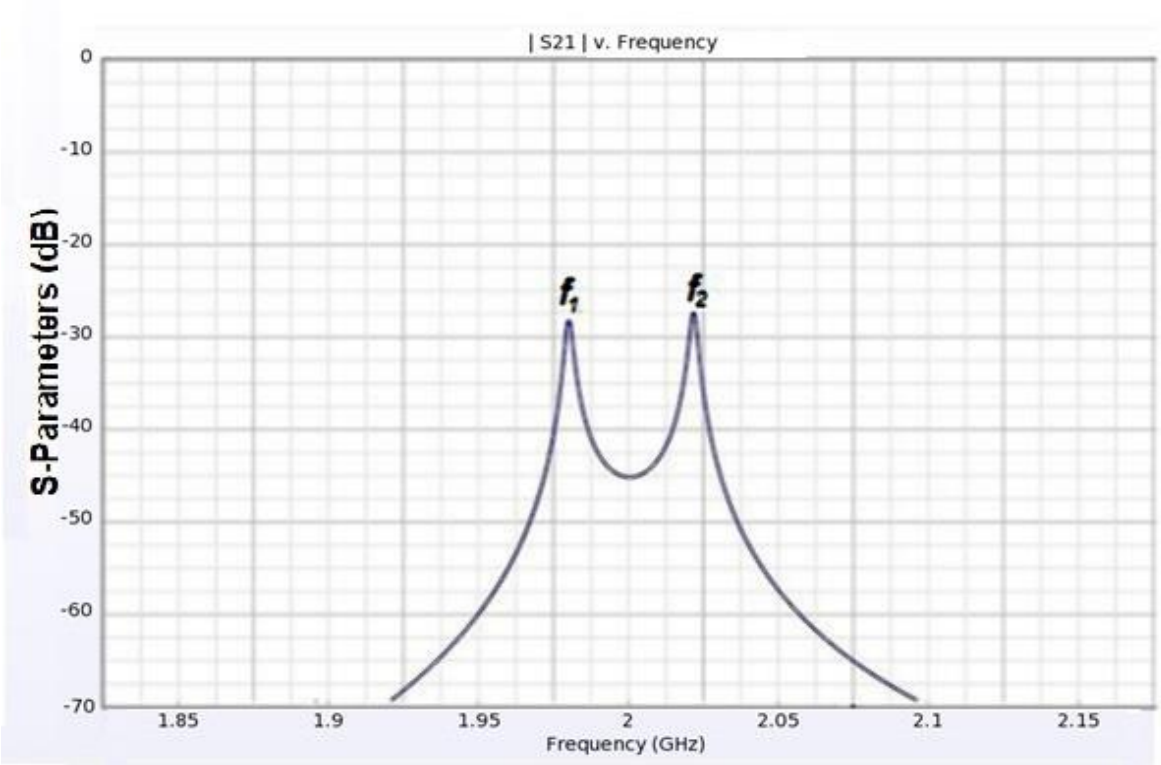

Figure 7.4 $|S_{21}|$ of two coupled resonators showing two frequency peaks at 2GHz resonant frequency

7.4 External quality extraction from SIW structure

The External quality factor of a resonator is found by physical structure such that one port is made weakly coupled and the other port made strong. The $|S_{21}|$ response is used to determine the value of the external quality factor. Figure 7.5 shows the arrangement of a waveguide cavity that is externally coupled to the input port through the microstrip transition, and weakly coupled to the output port. The expression derived in section 3.4 $Q_e = \frac{f_o}{\Delta f_{\pm 3dB}}$ is used to calculate the Q_e from the simulated $|S_{21}|$ response (Hong and Lancaster, 2001); where f_o is the resonant frequency of the loaded resonator and $\Delta f_{\pm 3dB}$ is the 3 dB bandwidth, as depicted in Figure 7.6

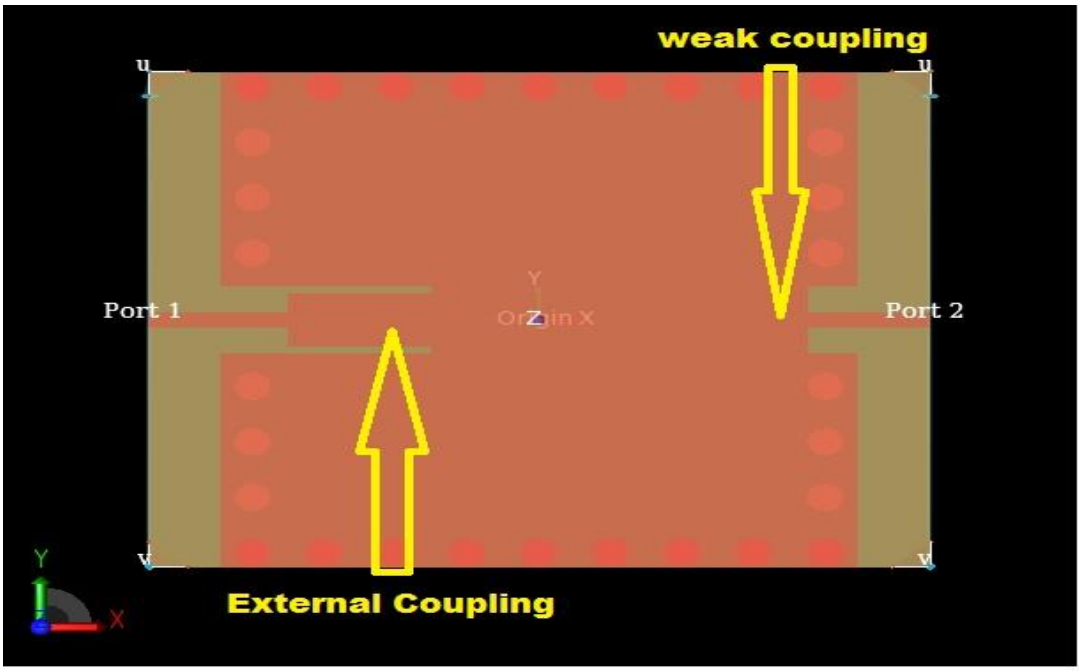

Figure 7.5: Externally coupled SIW waveguide cavity resonator

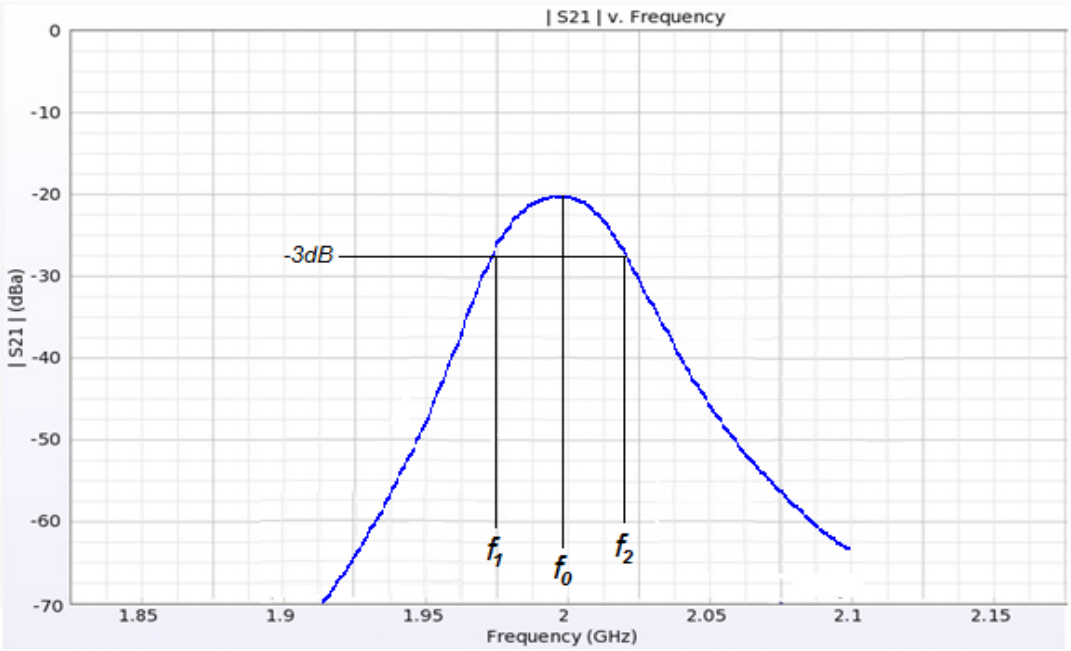

Figure 7.6 $|S_{21}|$ response curve depicting external coupling

7.5 SIW power splitter implementation

Coupled resonator power dividers have been implemented using Substrate integrated Waveguide cavity. The first step in the design of these components is to synthesise a lowpass prototype by determining appropriate lowpass parameters as explained in section 4.5. The next step is to construct a structure of cavity resonators coupled together depending on the required response. The cavities used in all the devices presented in this work operate in the fundamental mode, the TE_{101} mode, in which its resonant frequency can be calculated from equation 6.5. The desired coupling of the respective resonators is determined by altering the gap between the vias as shown in Figure 7.10. Half wavelength cavities that resonate at the fundamental TE_{101} mode are commonly used in rectangular waveguide filters. The following equations satisfies this statement according to the derivations from equation 6.7 and 6.8:

Microsoft Excel application is used to generate the coupling coefficient for the arrangement in Figure 7.3. Three vias are used vertically at the middle of the two resonators and with spacing (*s*) between them. Making wide or narrow through altering vertical pitch between the vias alters the spacing. Initially the pitch is 4mm and using equation 6.11, the corresponding Coupling coefficient is determined. It can be observed here that the narrower the pitch, that is, wider the spacing; the larger the coupling value. The spacing that corresponds to the various required coupling coefficients, as seen in Figure 7.7 and created through MATLAB, are determined from the graph. Further simulations of this structure give rise to further adjustment to ensure the desired response are attained.

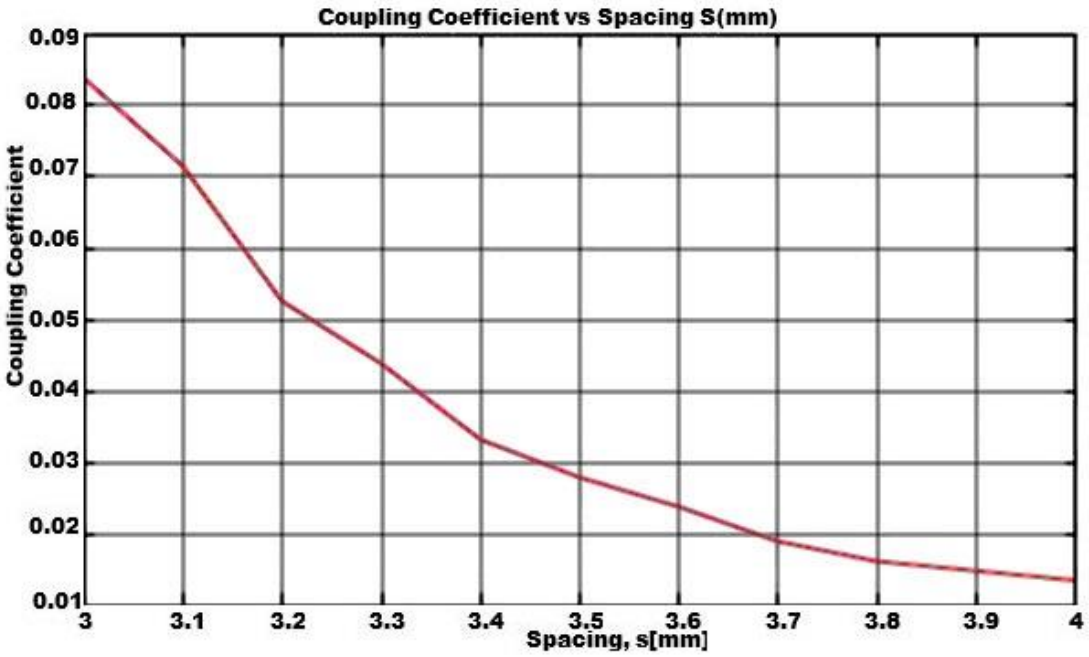

Figure 7.7 Coupling Coefficients vs Spacing

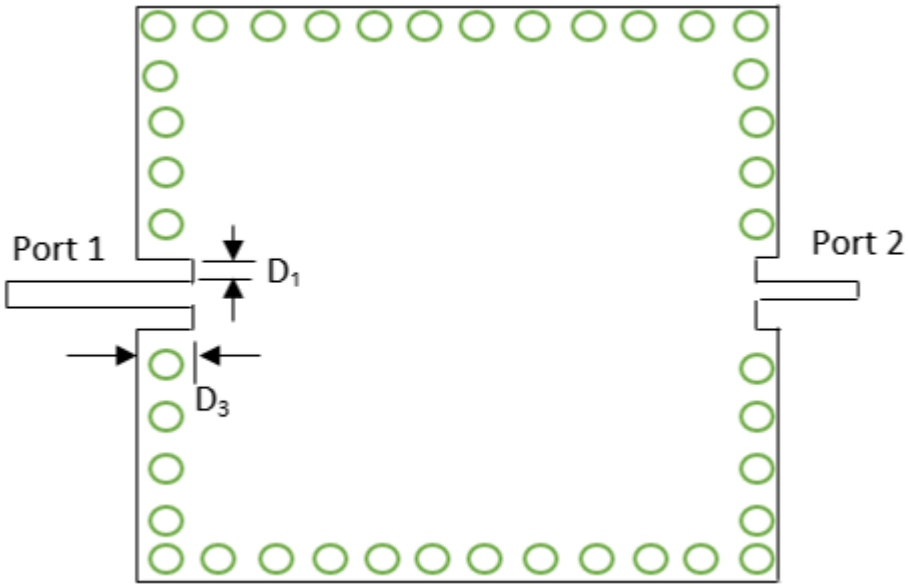

Figure 7.8 Desired external quality factor determination

The procedure for determining the respective dimensions that corresponds to the entire input and output port external quality factor has been extensively explained in section 6.12. Using the same process, it has been adapted in this design. Here, the dimension D_1 is kept constant at 0.5mm and D_3 is varied. The graph in Figure 7.9 gives the variation of the Q_e values and the corresponding values of D_3. The desired Q_e is drawn on the graph to determine the matching D_3 value and again along the span of simulation, there are continuous adjustments made.

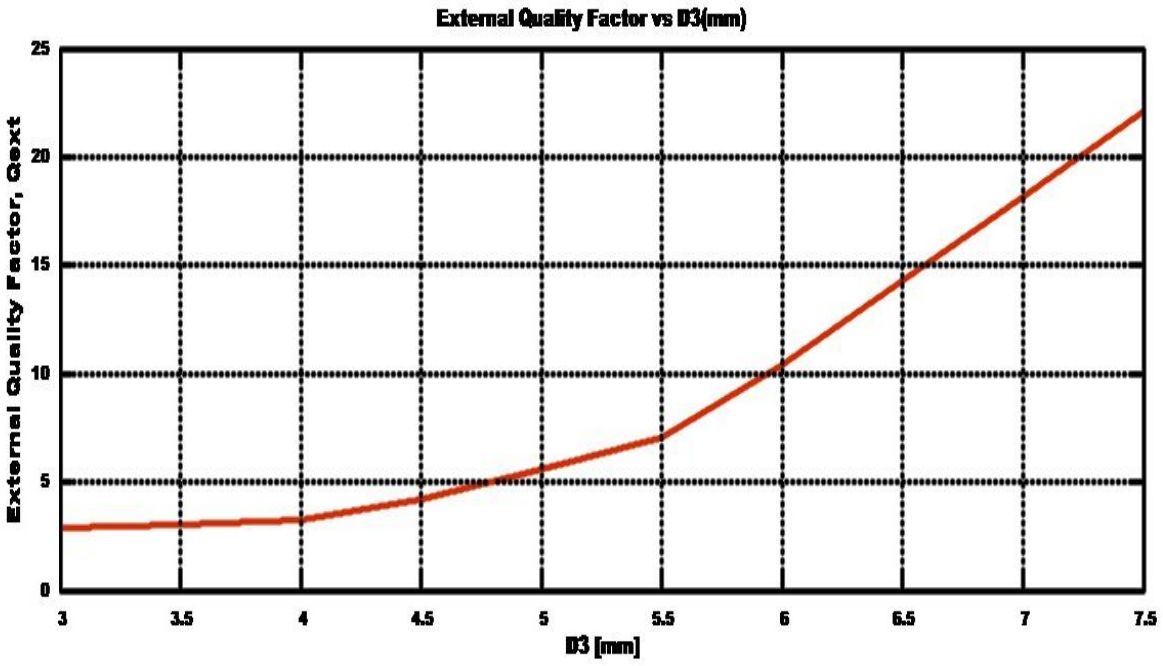

Figure 7.9 External Quality factor, Q_e vs D_3 spacing

The resonating cut off wavelength is given by:

$$\lambda_{mn} = \frac{2}{\sqrt{\left(\frac{m}{w_{siw}}\right)^2 + \left(\frac{n}{L_{siw}}\right)^2}} \tag{7.2}$$

$$w_{siw} = \frac{1}{2}\lambda_{10} \tag{7.3}$$

where w_{siw} is the width of the SIW resonator cavity at TE_{10} mode.

The resonating wavelength and the frequency for a rectangular waveguide are related as:

$$\lambda_{mn} = \frac{c_0}{f_{mn}\sqrt{\mu_r \varepsilon_r}} \tag{7.4}$$

where c_0 is the speed of light in free space.

Combining the equation 7.2 and 7.3 gives an expression of the rectangular waveguide parameters at TE_{10} mode in terms of its width and resonating frequency of the SIW resonator at TE_{101} mode:

$$w_{siw} = \frac{c_0}{f_{101}\sqrt{\mu_r \varepsilon_r}} \tag{7.5}$$

The utilisation of equations 6.5, 6.9, 6.10 and 7.3 gives the following SIW parameters and their respective dimensions for the following design specifications: $f_{101} = 2GHz$, $\mu_r = 1$, $\varepsilon_r = 10.8$, $d = 2mm$ and $p = 4mm$ (satisfying equation 6.11).

Table 7.1. 2 GHz SIW resonator Parameters

SIW Parameters	Dimensions (mm)
w_{siw}	45.64
w_{eff}	44.59
L_{siw}	27.62
L_{eff}	26.56
A_{siw}	142.48

The topologies of the resonators coupling arrangements are shown in Figure 7.10 and 7.11. This topology shows the arrangements of the resonators. As seen, along Port 1 to Port 2, labeled resonators 1, B, C etc. has coupling between resonators 1 and B, and resonators B and C. Along Port 1 to port 3, labeled resonators 1, 2, 3 etc. has coupling between resonator 1 and 2, and between resonators 2 and 3. It can be seen that there is a mutual resonator 1 which is coupled to both output paths. The value for this mutual coupling will be discussed in details in subsequent sections.

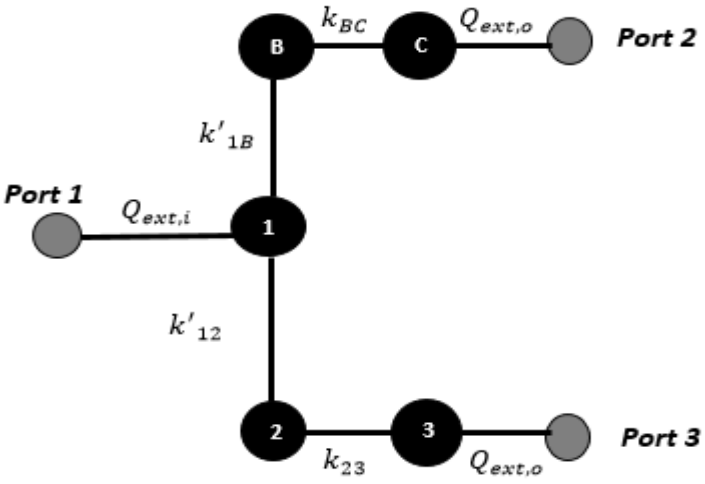

Figure 7.10 3-pole 5 resonators filtered power splitter topology

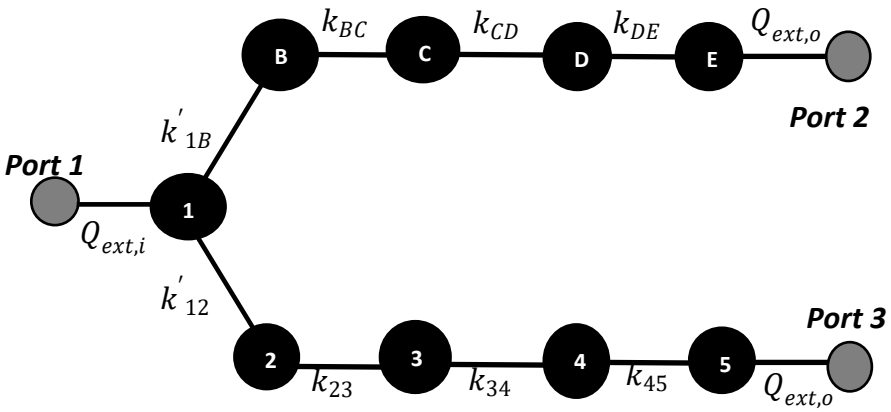

Figure 7.11 5-pole 9 resonators filtered power splitter topology

Particular emphasis and numerous works were done to determine the right design microstrip to SIW transition to ensure a 50Ω microstrip line is matched to the SIW input and output ports. This is so needed so that there will be equivalent of the external quality factor at the ports. Section 6.4 of this thesis has explained in details how this was obtained.

Once the initial geometries of the structure are known, a program is written in MATLAB as seen in appendix B that could depict the expected theoretical responses and specified designed values, and, the full-wave EM simulator such as Keysight's EMPro (Keysight, 2015) and Keysight's ADS are then used to obtain the optimum dimensions through adjustments of the structure to meet the target response.

Filtered power splitters with Chebyshev's bandpass filter responses have been implemented at a microwave frequency of 2GHz to verify the proposed design filter and power splitter. The SIW device is made up of parallel metal plates, specially designed as discussed above, sandwiching a dielectric material substrate and holes drilled through it to connect the top and bottom plates through soldering. To compensate for the degradation and unexpected performance resulted from manufacturing errors, the gaps at the SIW ports are altered and varied to ensure the final dimensions are obtained. This has helped to compensate for the degradation of performance resulted from manufacturing errors. The red regions shown in figure 7.12 is the region of high maximum electric field and that is the area where tuning is done.

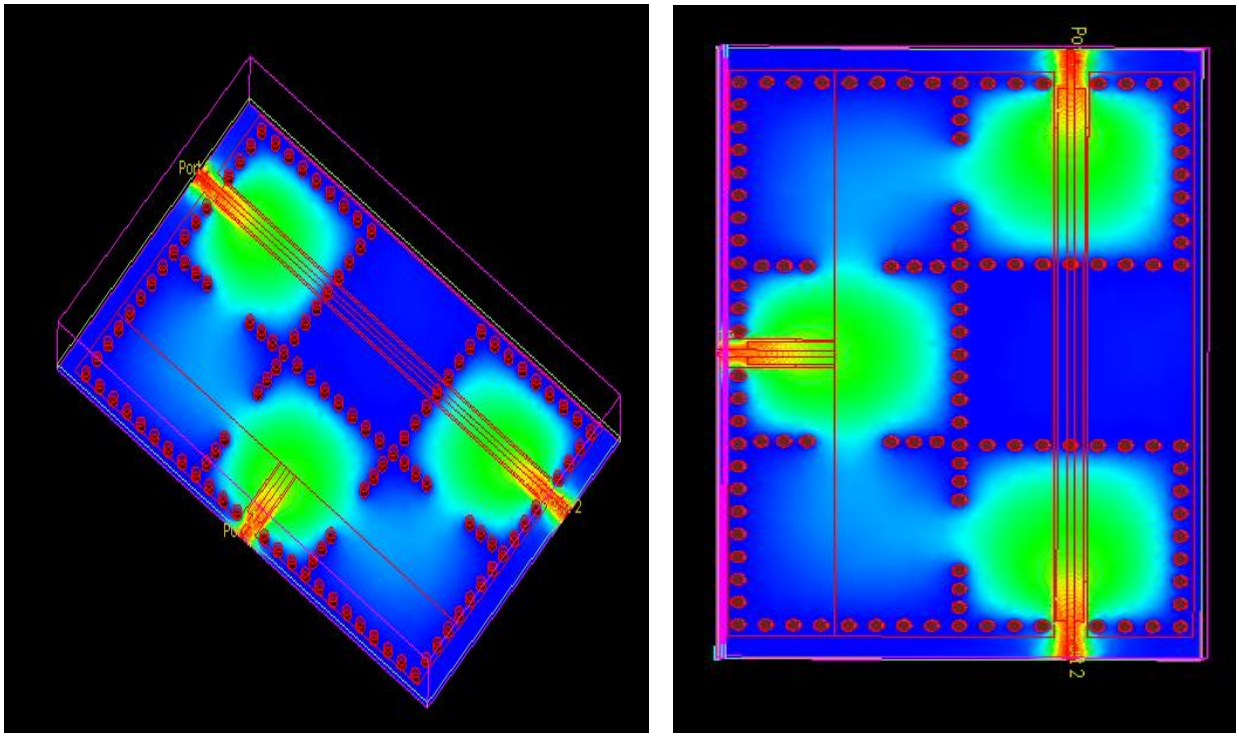

(a) (b)

Figure 7.12 Simulation animation showing region of maximum electric field (in red) (a) 3-D view (b) Top view.

7.6 Coplanar waveguide to SIW transition

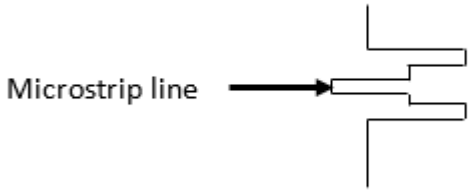

Figure 7.13 Microstrip line transition

Considering one of the ports of the Figure 7.8 as shown in Figure 7.13. The most important parameter is to determine the width of the microstrip line that is matched to a 50Ω input impedance. The expression in Section 6.6 is used to synthesize the microstrip line. Here, the width $w = 1.126mm$, $h = 1.27mm$, $\varepsilon_{eff} = 7.185$

7.7 Measurement Process

The measurement is done using E5062 300 KHz – 3GHz ENA series Network analyser, made by Agilent Technologies. This is first calibrated using the calibrator to ensure that is the horizontal line of the display scope is exactly on the 0dB mark as seen in Figure 7.14. This process involved connecting the two ports to the calibrator and wait for some time while it is calibration. When calibrated, the horizontal line along the 0dB is straight enough. The fabricated devices are connected via the respective ports and various measurements can be made through adjusting the various section of the VNA. Tuning and adjustment of the ports of the device are done to determine the required filter characteristics responses. The captured responses are saved and transferred using USB port to be synthesized using specific MATLAB code. The photograph shown in Figure 7.14 also shows the arrangement to obtain the VNA output calibration setup including the calibrator and the display scope.

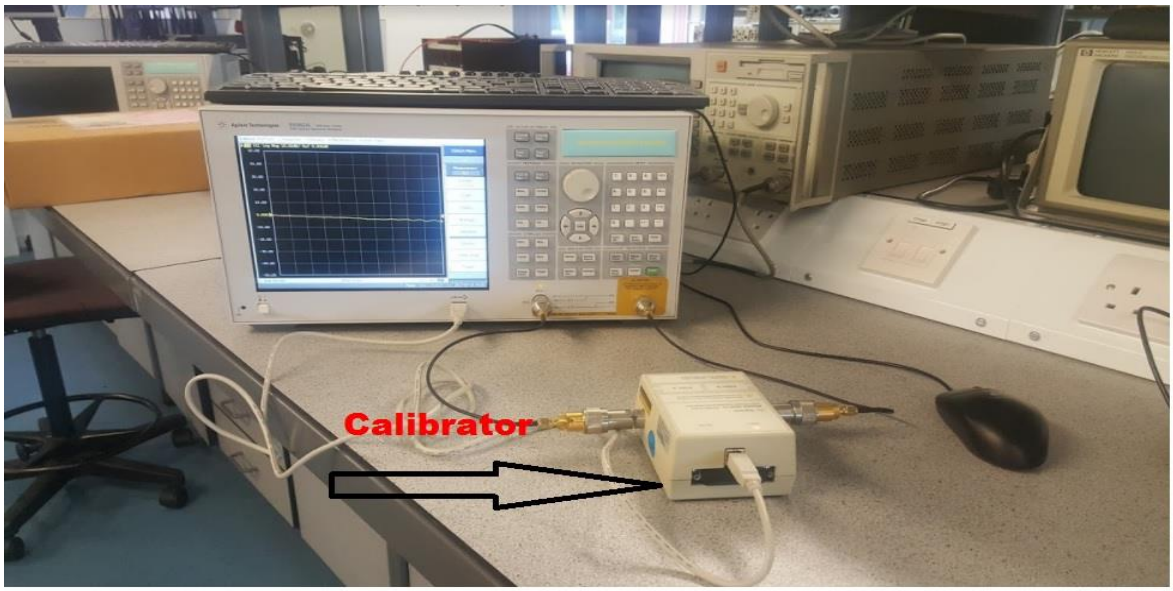

Figure 7.14 Fabricated devices measurement set-up

7.8 3-dB Equal power splitter

A 3-pole, 5 resonator $3-dB$ power splitter has been designed, fabricated and tested. The power splitter has been designed according to the coupled-resonator design process similar to that reported and used in Section 5.10. It is designed at a centre frequency of 2GHz, a fractional bandwidth of 5%, and return loss of $20\ dB$ at the passband. The divider topology is shown in Figure 7.10 and the ideal circuit and prototype response of the power splitter, as extracted from ADS, is shown in Figure 7.15 and 7.16 respectively.

The coupling coefficient for FBW of 5% for K_{BC} and K_{23} are extracted directly from the MATLAB computation, whilst the mutual coupling values for K'_{1B} and K'_{12} are derived from the equation 5.55 and 5.56 for $\alpha = 0.5$. The values obtained are $K'_{1B} = 0.0365, K'_{12} = 0.0365, k_{BC} = 0.0516, k_{23} = 0.0516$.

The input and output external quality factors are computed and found to be $Q_{ext} = 17.031$.

The divider has been implemented using SIW waveguide cavity resonators, and its

3D and structure and top view are shown in Figure 7.17.

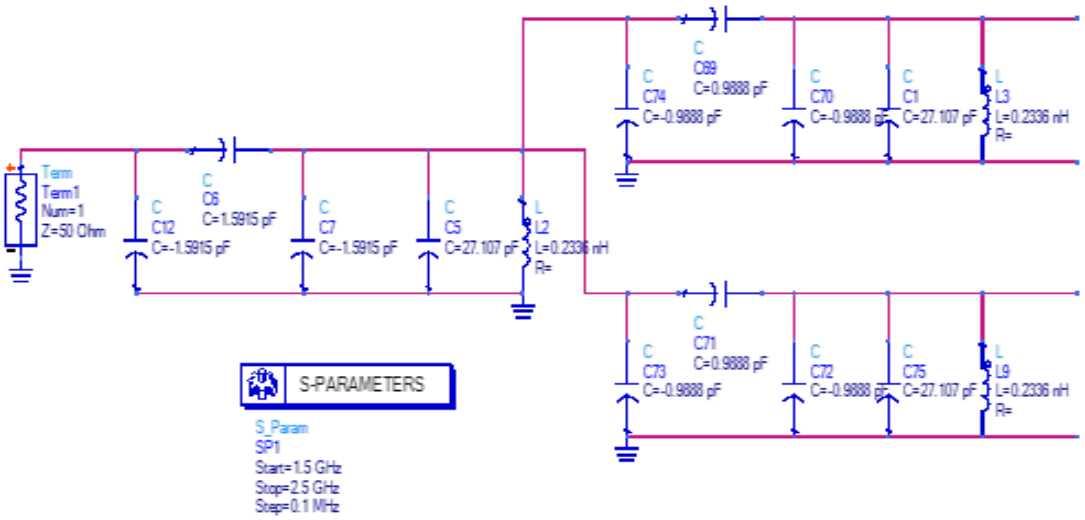

Figure 7.15 Circuit schematic of the 3-pole Equal split filtered power splitter (ADS design)

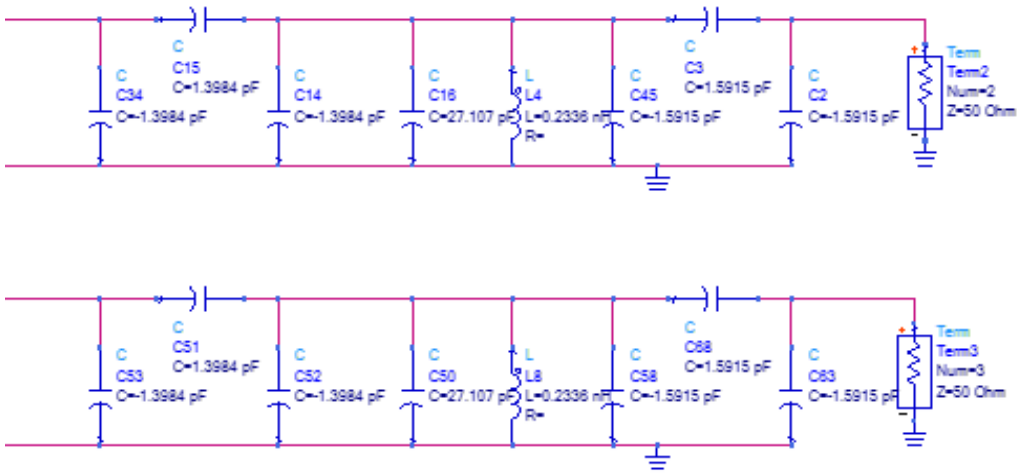

Figure 7.15 (Continued)

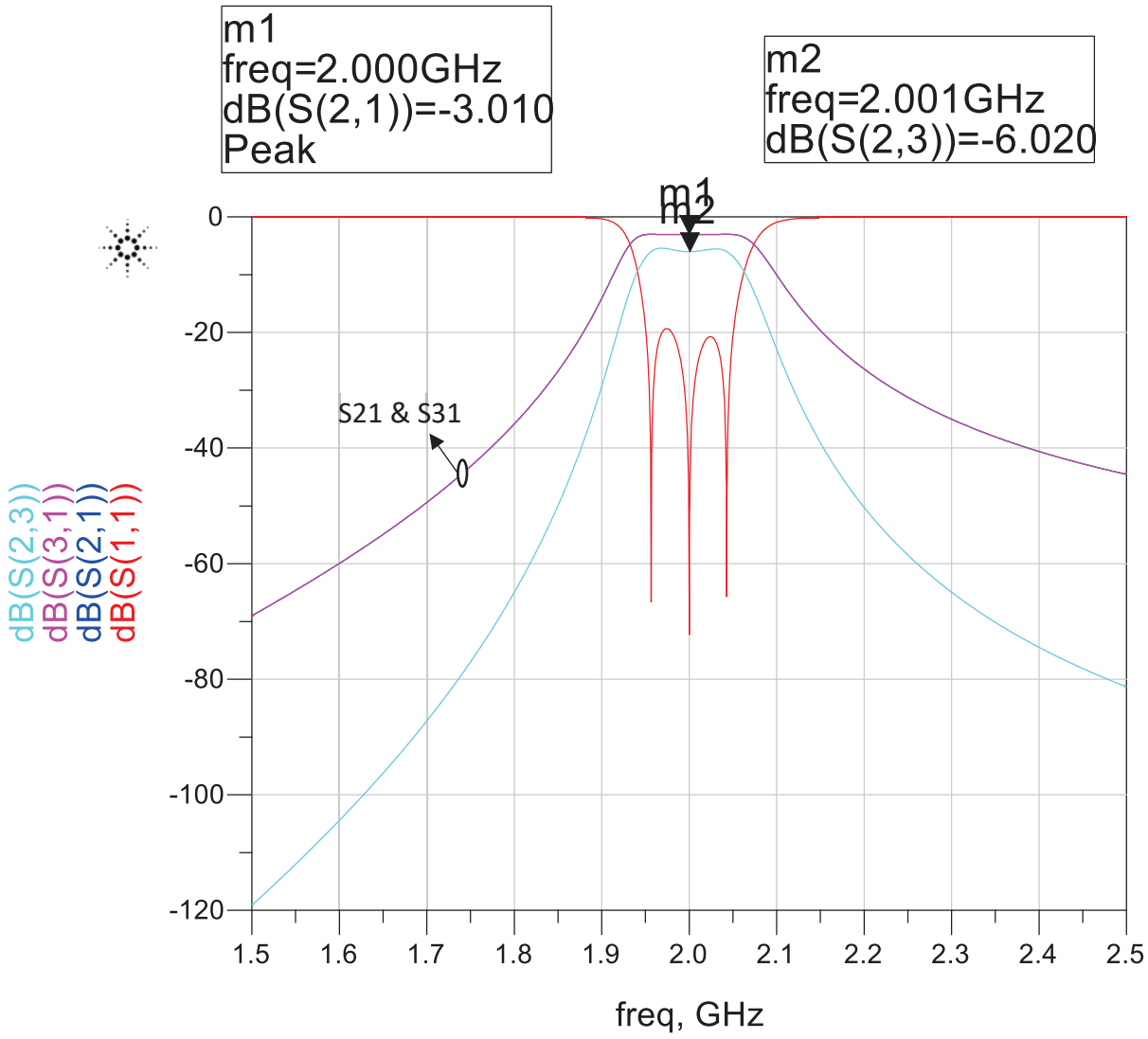

Figure 7.16 Equal Power Splitter ideal circuit prototype response

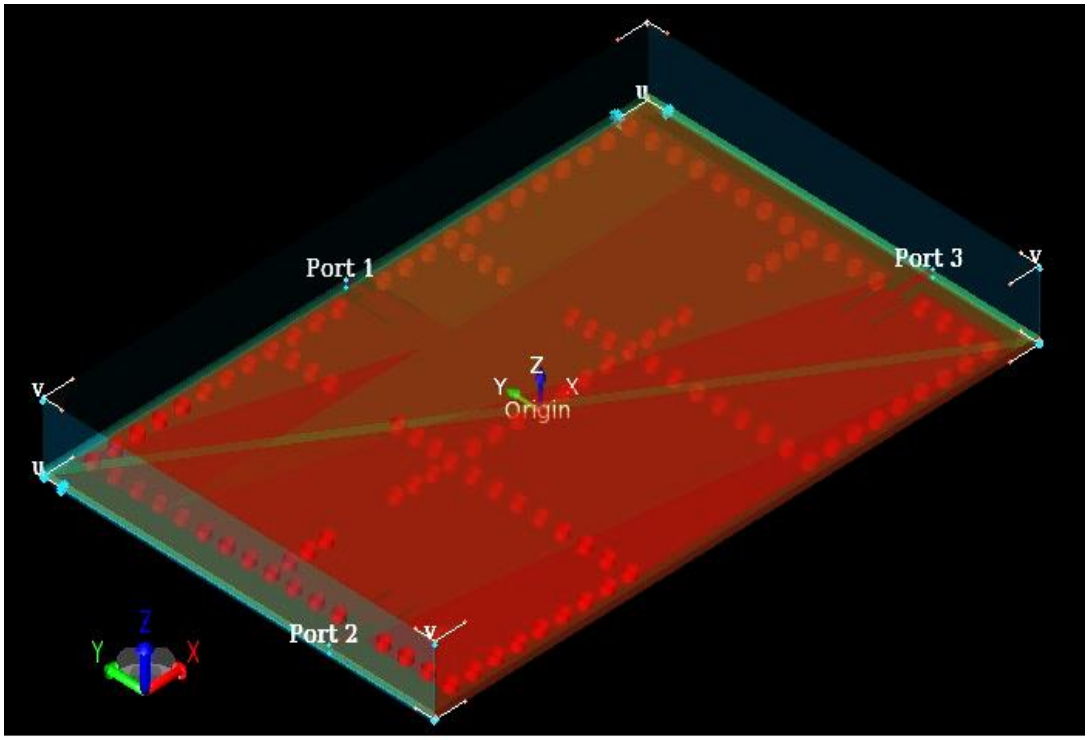

(a)

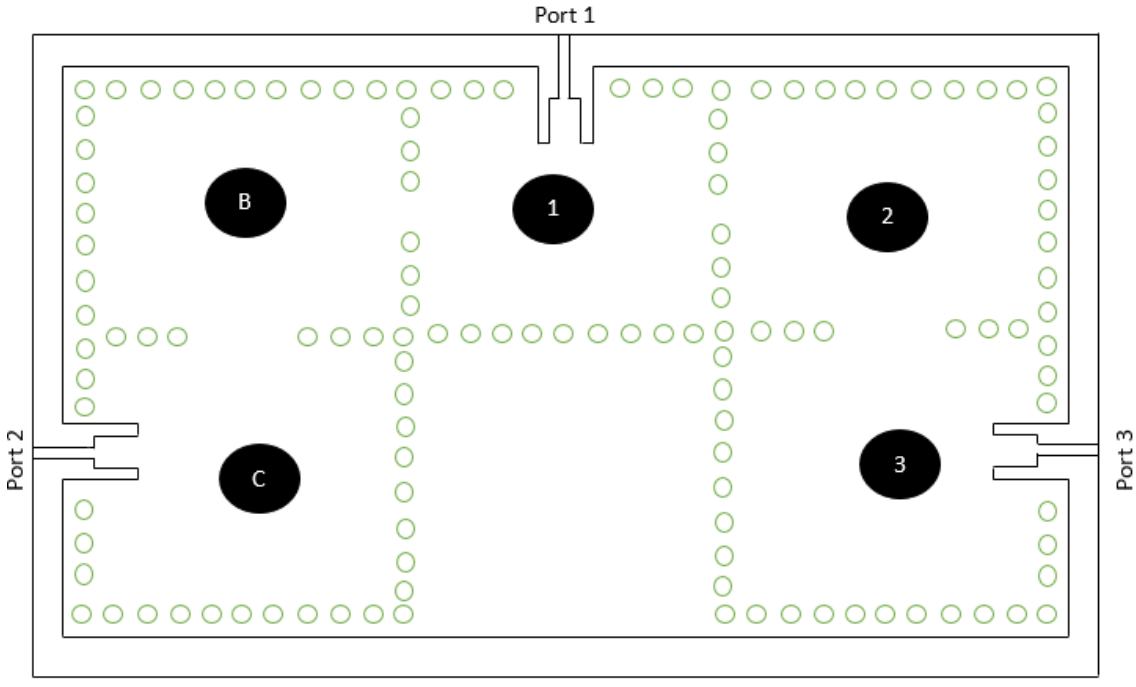

(b)

Figure 7.17 (a) 3D structure (EMPro), (b) Top View of 3-dB equal split power divider

EMPro has been utilised to find the initial rectangular dimensions of the waveguide cavities. This is then redesigned into its equivalent square shaped resonator cavity whilst maintaining its resonance frequency as given in Section 7.1; and waveguide cavities corresponding to the required coupling coefficient by following the procedure in Section 7.2. The dimensions of coupled resonators corresponding to external quality factors have been found from the full wave EM simulation by following the procedure in Section 7.3. The whole SIW structure of the power splitter is initially designed with the obtained initial values, and the EMPro simulation response of the initial structure as well as the isolation response between the output ports is depicted in Figure 7.18.

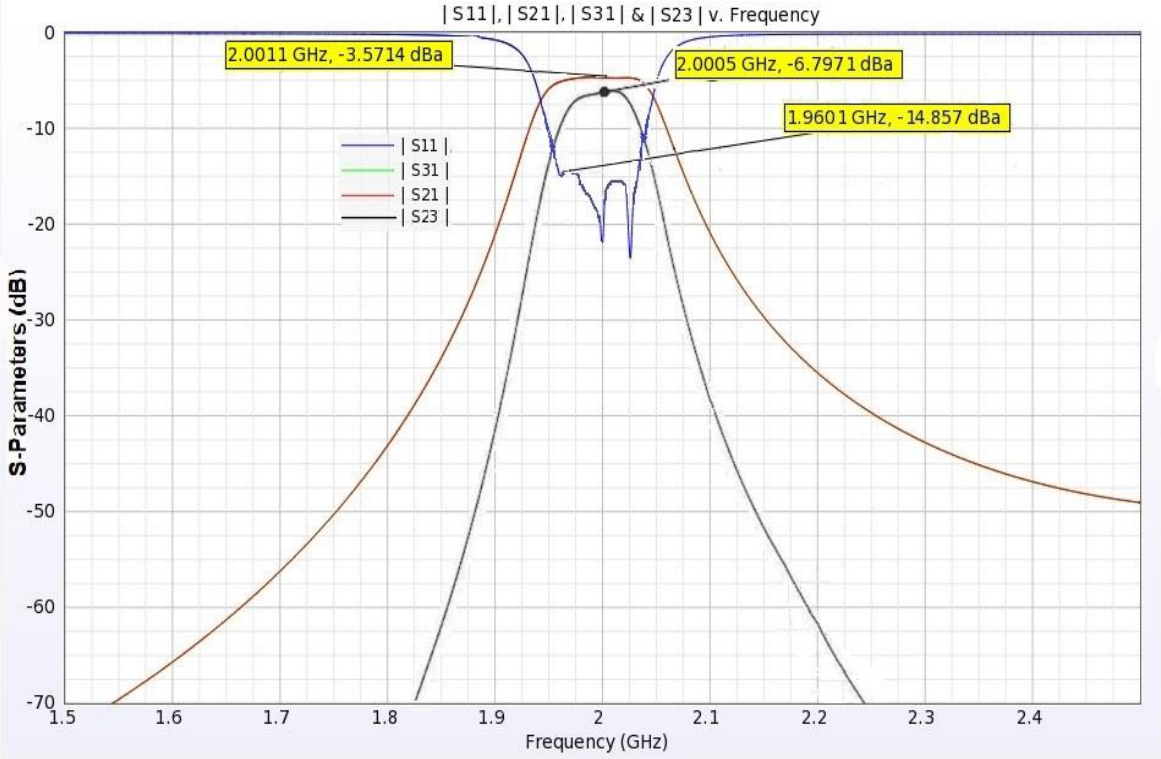

Figure 7.18 $|S_{11}|$, $|S_{21}|$, $|S_{31}|$ and $|S_{23}|$ EMPro simulation response of 3-pole equal split

7.9 Fabrication and Measurement

The power splitter has been implemented using SIW waveguide cavity resonators coupled together with the arrangement as shown in Figure 7.10 and 7.11. A photograph of the SIW power splitter is shown in Figure 7.19. The fabrication process involves using the Printed Circuit Board technology where a 2 mm drill is made to create the required vias that connects the top and bottom later of the power splitter. A conductor of the same thickness is inserted into the holes and is soldered on both ends. The thickness of the copper top and bottom conducting plates is 17 μm. The thickness of the substrate is 1.27 mm. The ports are all connected to 50 Ω SMA connectors.

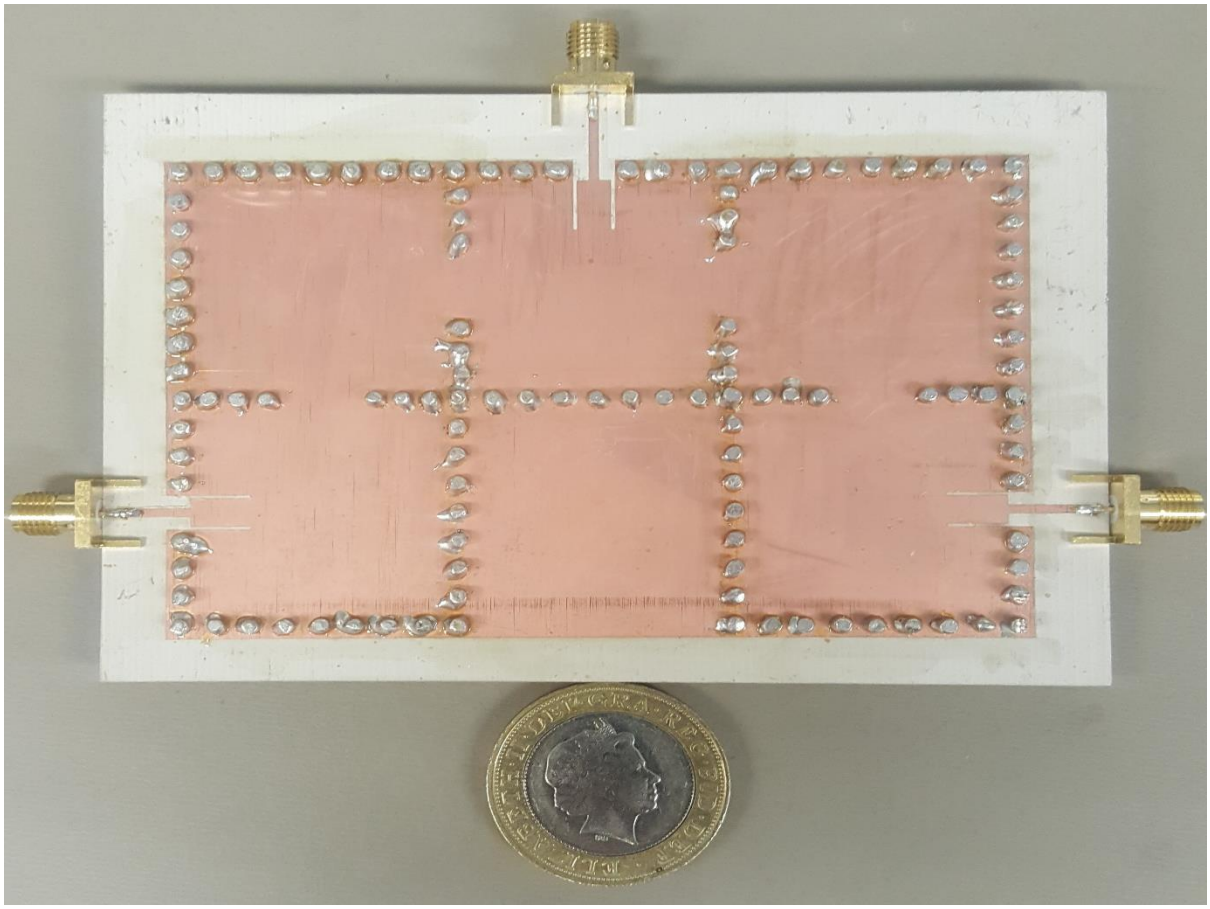

Figure 7.19 Photograph of the 3-pole SIW equal division power splitter

A cross sectional view of the equal split SIW power splitter, with parameters for the dimensions of resonator cavities is shown in Figure 7.22. The dimensions of resonator cavities forming the device have been measured using a standard mm ruler, and they are shown in Table 7.2 along with design values. The initial measured dimensions show that there is some fabrication error probably due to the soldering effect or signal leakages. However, during measurement when the ports are tuned the return loss exhibits a response of about 17.1dB whilst the simulated return loss is about 15dB. The simulated and measured results of the SIW filtered power splitter are depicted in Figure 7.20 for $|S_{11}|$, $|S_{21}|$ and $|S_{31}|$ and in Figure 7.21 for the isolation $|S_{23}|$. The measured response is in good agreement with the simulated response for the insertion loss between the input port and the two outputs; whilst the measured return loss gives a better response than the simulated return loss. The experimental results show that the maximum return loss within the passband is about 17.1dB and the minimum insertion loss is about 3.57dB. Figure 7.20 also shows that bandwidth of the measured response is wider than the simulated response. It shows that the fractional bandwidth of the measure response is about 4.95% whilst the fractional bandwidth for the simulated response is about 4.74%. Finally, Figure 7.21 shows that the isolation between the output ports is measured to be about 6.81dB whilst the simulated and the theoretical isolation are 6.79dB and 6.02dB respectively.

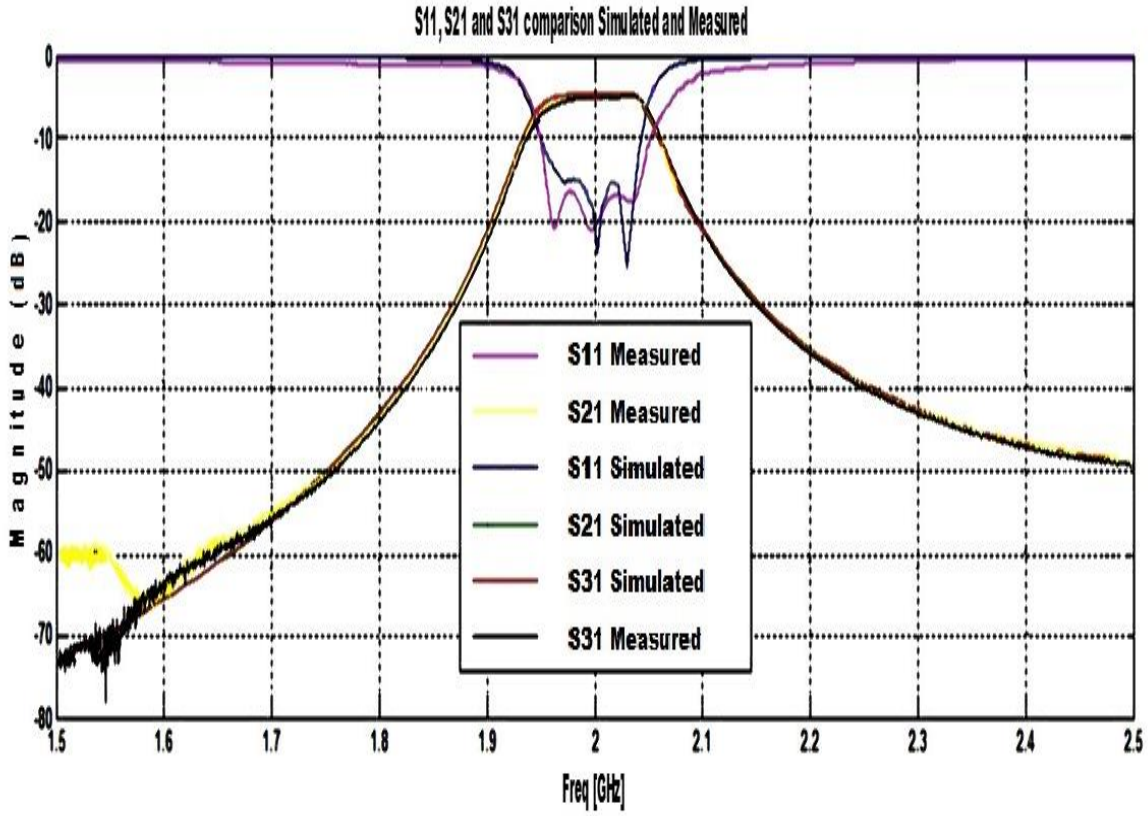

Figure 7.20 Comparison of $S_{11,}$ S_{21} and S_{31} for Simulated and fabricated SIW power splitter

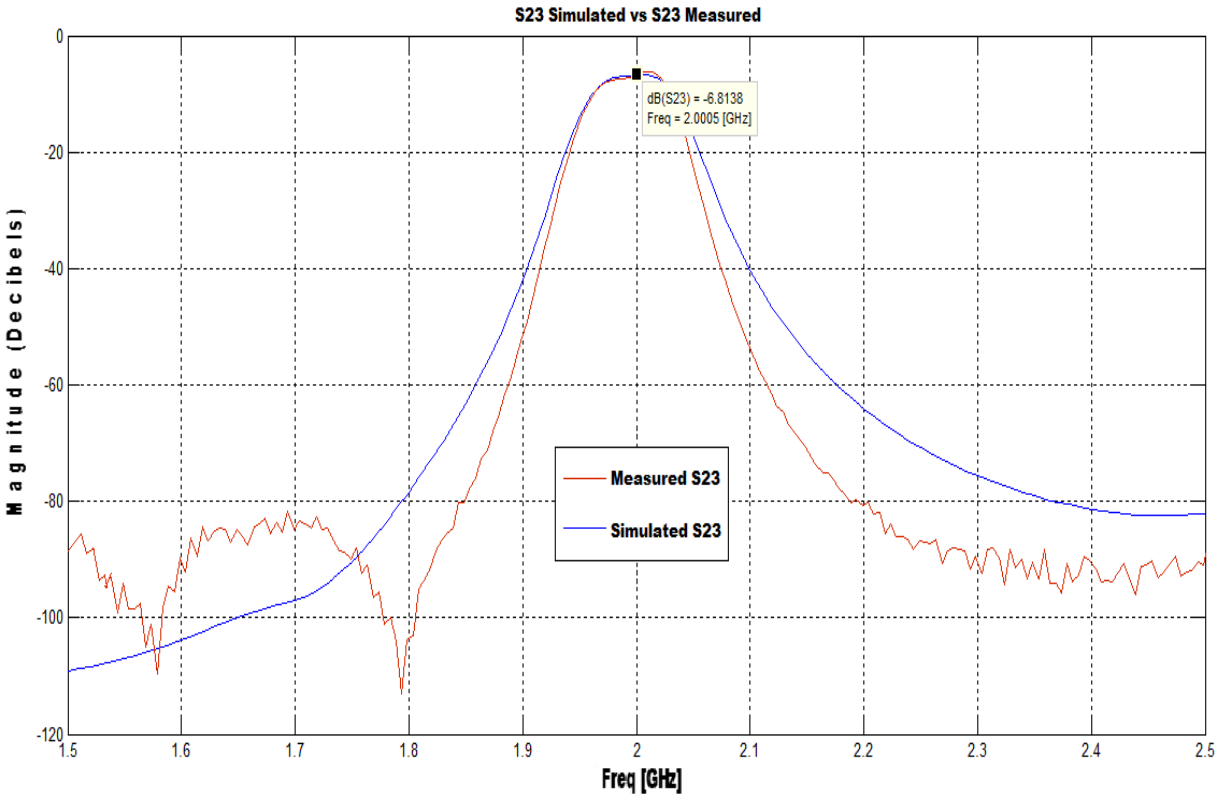

Figure 7.21 Equal split Simulated and measured S23

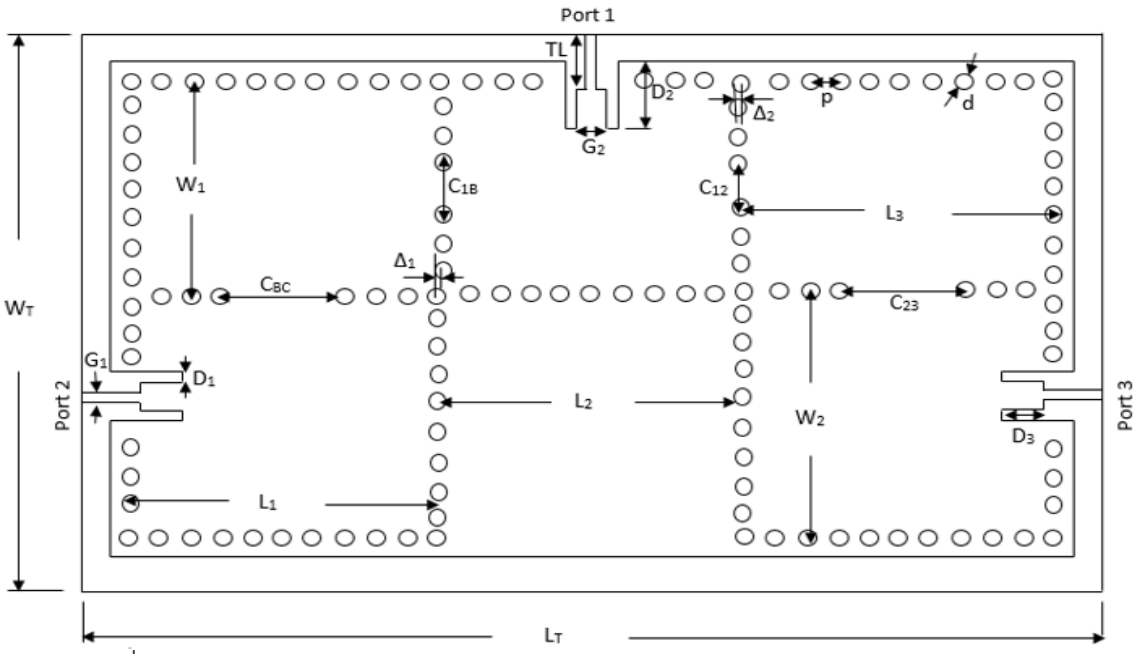

Figure 7.22 Cross sectional top view of the power splitter

Table 7.2 Power divider dimensions corresponding to the parameters in Figure 7.22

Parameters	Dimensions (mm)	Parameters	Dimensions (mm)	Parameters	Dimensions (mm)
TL	4.22	d	2.00	C_{12}	12.21
W_1	32.00	L_3	32.00	p	4.00
C_{1B}	12.21	C_{23}	12.53	L_T	108.00
Δ_1	0.50	W_2	32.00	G_1	1.12
C_{BC}	12.53	D_3	6.98	W_T	35.00
G_2	3.92	L_2	32.00		
D_2	9.82	L_1	32.00		
Δ_2	0.50	D_1	0.50		

7.10 3-pole unequal power splitter design

A 5-resonator unequal power divider has been designed, fabricated and tested. The divider has been designed according to the coupled-resonator design procedure presented in Section 4.5 and used in Section 5.9. It is designed at a centre frequency of 2 GHz, a fractional bandwidth of 5%, a reflection loss of 20 dB at the passband, and split ratio $\alpha = 1/3$. The unequal splitter topology is similar to that of the equal splitter as given in Figure 7.10 and the ideal prototype and response of the splitter, as extracted from ADS, is shown in Figure 7.23 and 7.24; and the EMPro designed (top view) structure of the unequal SIW power splitter is shown in Figure 7.25.

Special emphasis is made to the unequal splitter because of the non-uniform split ratio unlike the equal split. Here, one of the outputs, Port 2 is having 1/3 of the power from the input whilst the other output Port 3 is having 2/3 of the input power. Hence, as derived in section 3.5, the coupling coefficient factor between the common resonator 1 and B towards Port 2, ${\psi_{1B}}^2 = \frac{P_1}{P_2}$ or $\psi_{1B} = \sqrt{3}$; And between the common resonator 1 and 3 towards Port 3 are ${\psi_{12}}^2 = \frac{P_1}{P_3}$ or $\psi_{12} = \sqrt{3/2}$. These factors are used as multiples of the original coupling coefficients between those resonators. The coupling values are therefore:

$K'_{1B} = 0.0298$, $K'_{12} = 0.0421$, $K_{23} = 0.0516$ and $K_{BC} = 0.0516$.

It is worth noting here that the minimum insertion loss along its output path should conform to the expression

$$IL_{Si1} = 20 \log \psi_{1i}(dB) \tag{7.6}$$

Therefore, $IL_{S21} = 4.771dB$ and $IL_{S31} = 1.761dB$ is the same as seen in Figure 7.24.

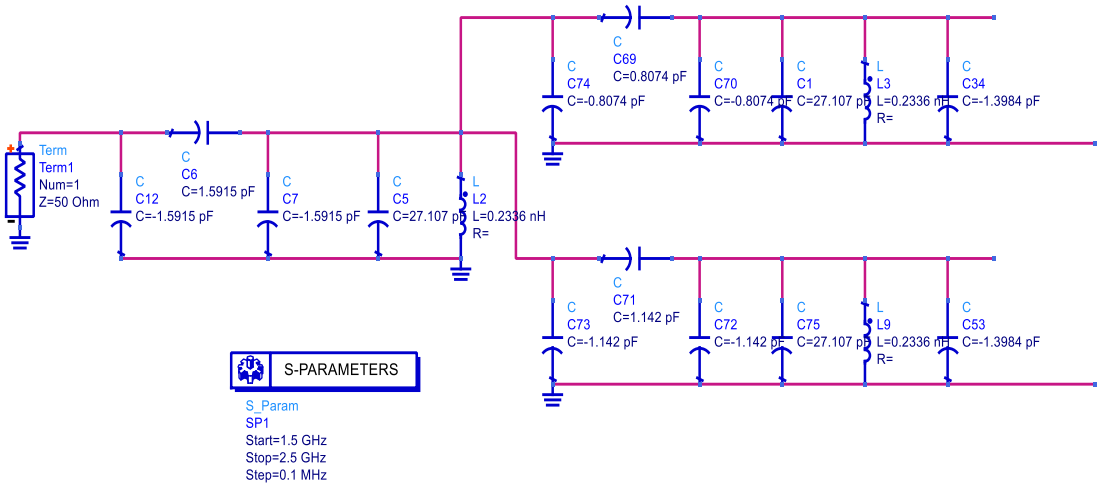

Figure 7.23 Circuit schematic of the unequal split filtered power splitter showing the lump elements L and C

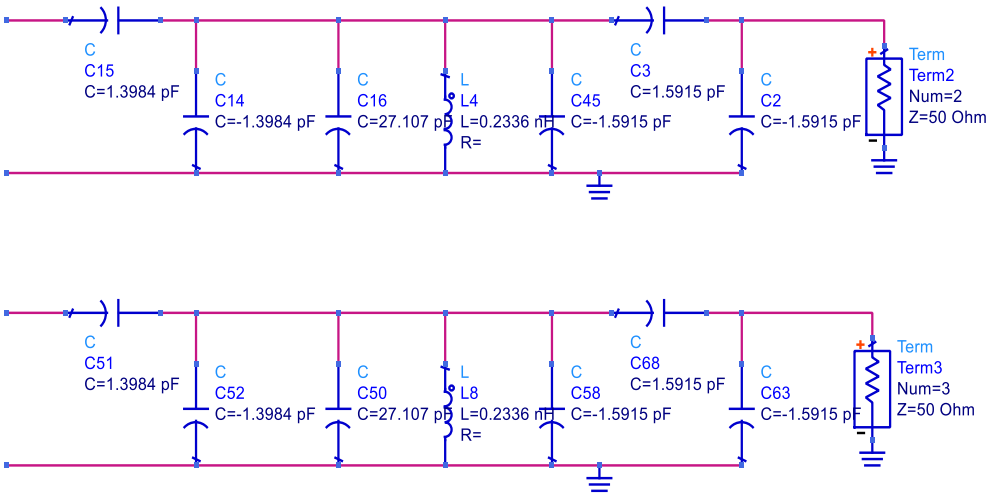

Figure 7.23 (continued)

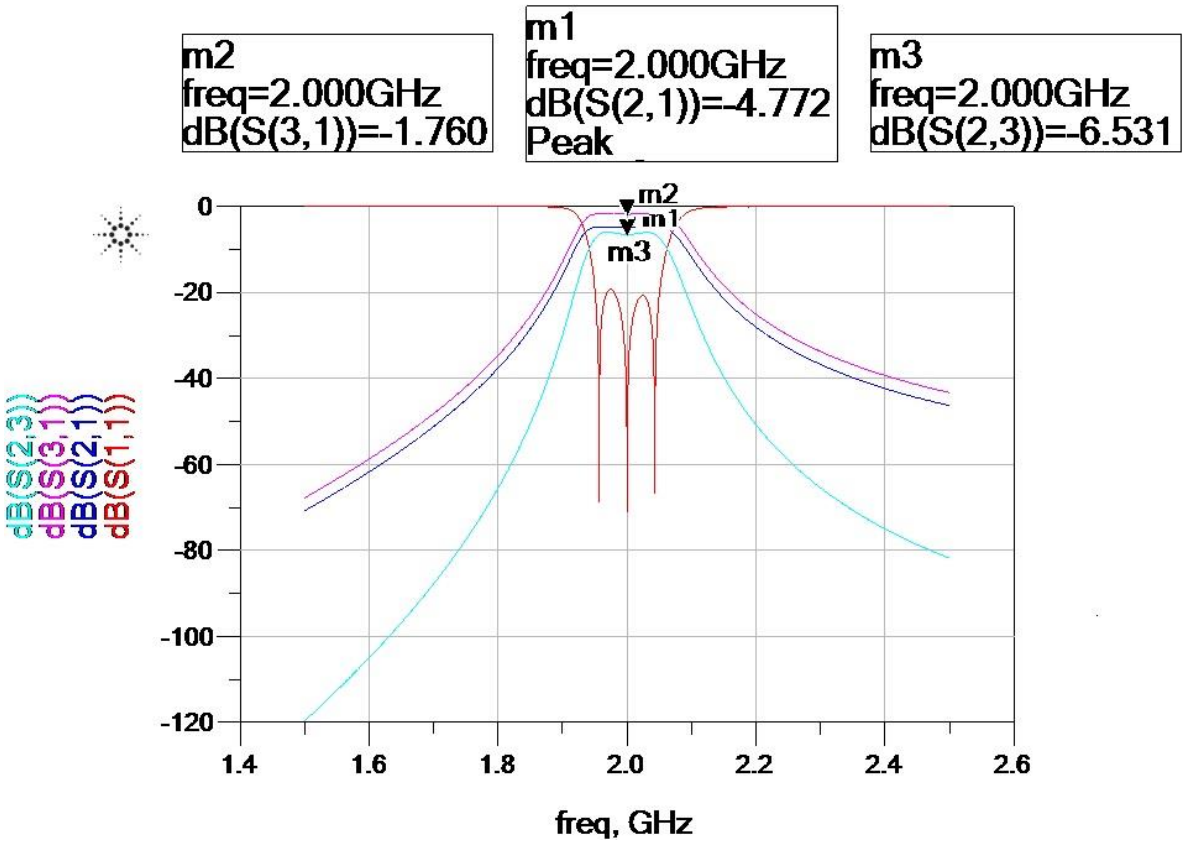

Figure 7.24 3-pole unequal power splitter ideal circuit prototype response

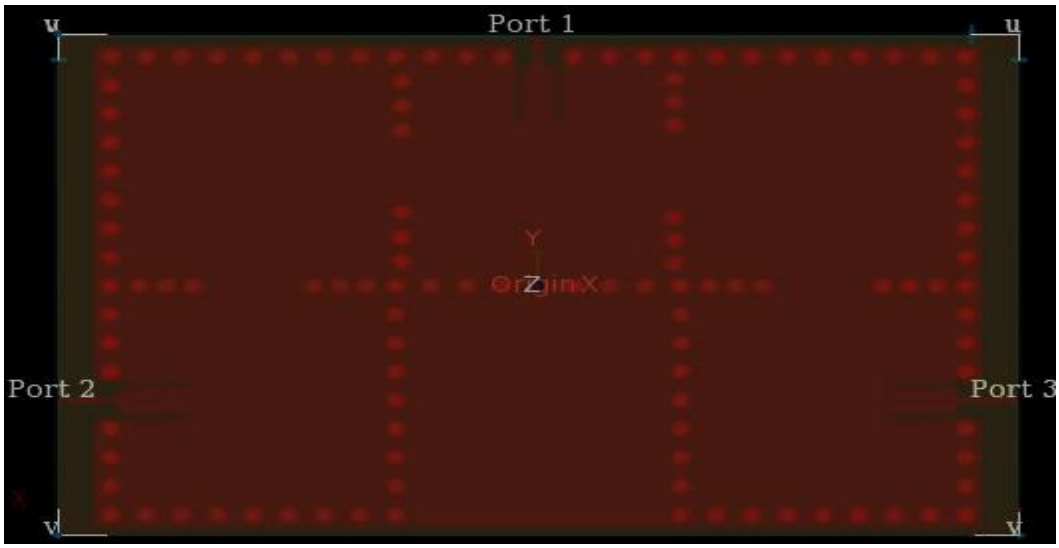

Figure 7.25 Screen capture of 3-pole unequal SIW power splitter

7.11 Fabrication and Measurement

The unequal split power splitter has been implemented using SIW waveguide cavity resonators coupled together. A photograph of this fabricated power splitter is given in Figure 7.26. This component has similarity with the designed equal power splitter in Section 7.10. The only difference is the C_{1B} and C_{12} values of Figure 7.22. Table 7.3 gives a comparison between the equal and the unequal 3-pole splitter.

Table 7.3 Common resonator coupling comparison (3-pole)

Dimension (mm)	Equal Split	Unequal split
C_{1B}	12.21	11.20
C_{12}	12.21	13.04

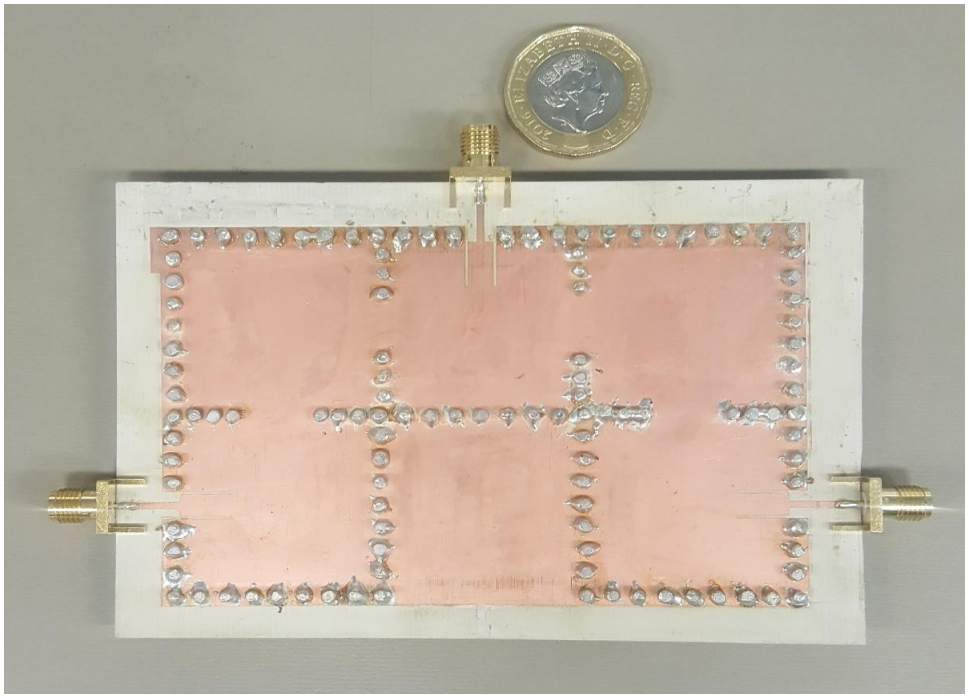

Figure 7.26 Photograph of the 3-pole SIW unequal division power splitter

The simulated and measured results of the unequal power divider are shown in Figure 7.27. The measured response is in good agreement with the simulated response. The experimental results show that the maximum return loss within the passband is about 20dB for the simulated and about 22dB for the fabricated component. The minimum insertion loss for $|S_{21}|$ is 5dB (about 4.8% error) and the minimum insertion loss for $|S_{31}|$ is 1.85dB (about 5.1% error). The percentage errors occur when compared the fabricated component response with the ideal responses. The measured isolation between the output ports is more than 9dB in the passband; whilst the simulated isolation is about 8.7dB and the ideal circuit isolation is 6.531dB as seen in Figure 7.24. A reduced bandwidth is observed in Figure 7.27 with the measured $|S_{11}|$ showing better performance with wide bandwidth.

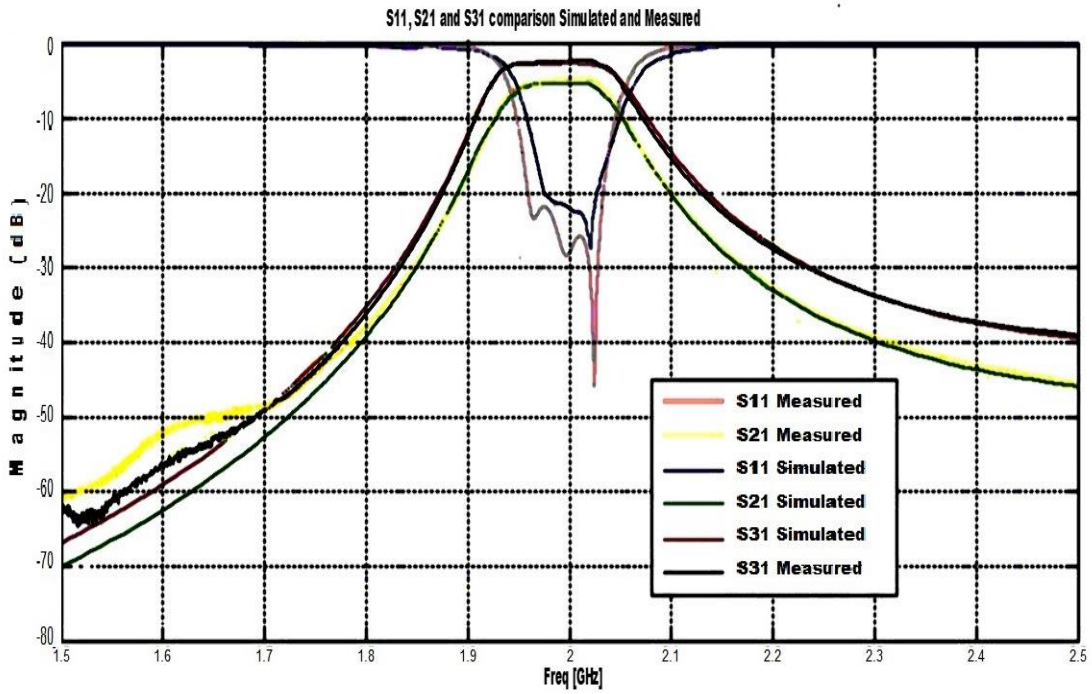

Figure 7.27 Comparison of S_{11}, S_{21} and S_{31} for simulated and fabricated 3-pole unequal division SIW power splitter

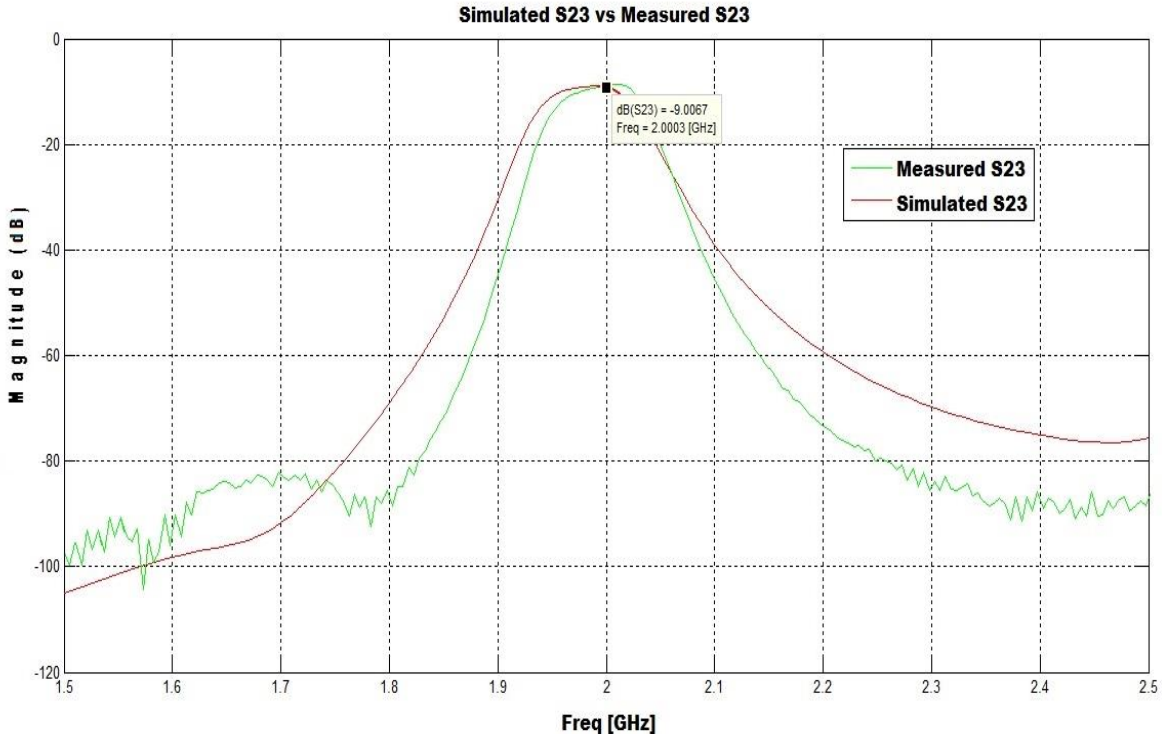

Figure 7.28 3-Pole unequal split simulated and measured S23

7.12 3-dB 9-resonators equal power splitter

A 5-pole, 9 resonators $3-dB$ power splitter has been designed, fabricated and tested. The power splitter has been designed according to the coupled-resonator design process presented in Section 4.9 and explained in Section 7.10. It is designed at a centre frequency of 2 GHz, a fractional bandwidth of 5%, and return loss of 20dB at the passband. The divider topology is shown in Figure 7.11 and the ideal circuit prototype and the corresponding response of the power splitter, as extracted from ADS, is shown in Figure 7.30 and figure 7.31 respectively. The coupling coefficient for FBW of 5% for K_{BC}, k_{23}, K_{32}, K_{CB}, K_{CD}, K_{34}, K_{DC}, K_{43}, K_{DE}, k_{45}, K_{ED}, K_{54} are extracted directly from the Matlab computation, whilst the mutual coupling values for K_{1B}, K_{12}, K_{B1} and K_{21} are derived from the equation 5.55 and 5.6 for

$\alpha = 0.5;\ K'_{1B} = 0.031,\ K'_{12} = 0.031,\ K_{23} = 0.032,\ K_{\boldsymbol{BC}} = 0.032,\ K_{34} = 0.032,\ K_{CD} = 0.032, K_{45} = 0.043$ and $K_{DE} = 0.043$.

The input and output external quality factors are computed and found to be $Q_{ext} = 19.428$. The divider has been implemented using SIW waveguide cavity resonators, and its 3D structure is shown in Figure 7.29.

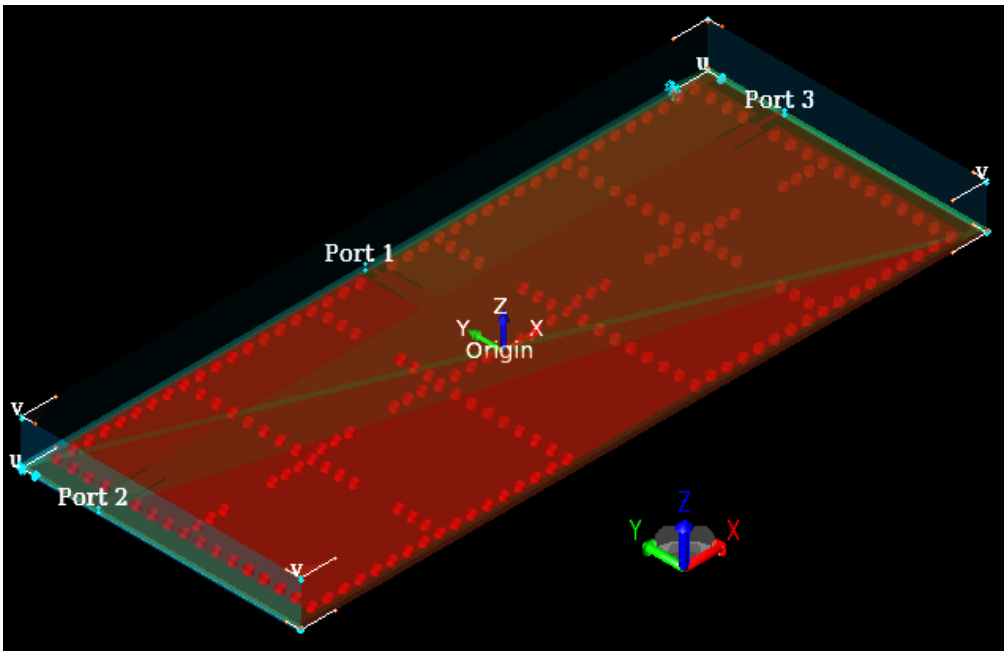

Figure 7.29 EMPro 3D screen capture of the 5-pole SIW power splitter structure.

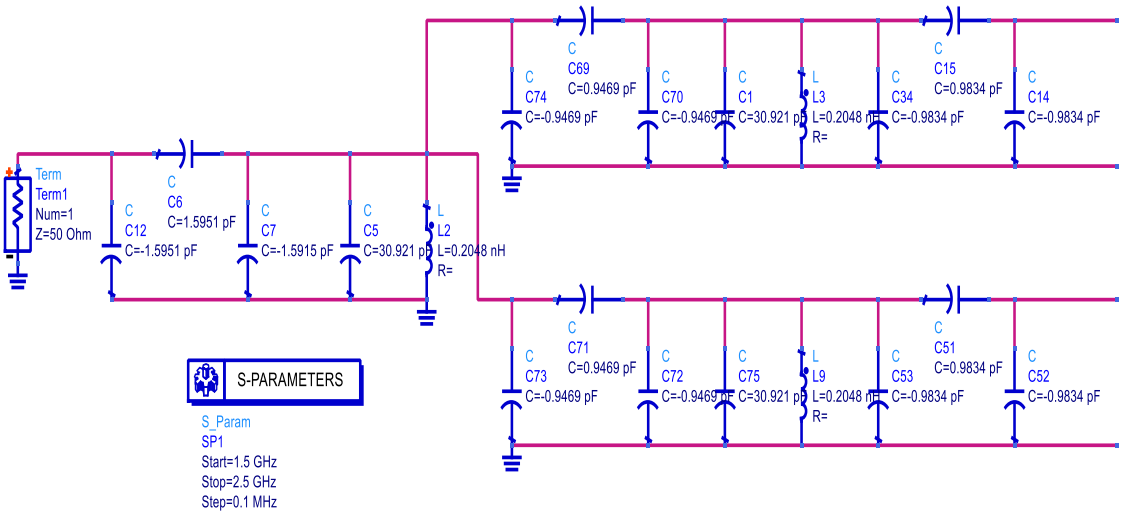

Figure 7.30 Circuit schematic of the 5-pole Equal split filtered power splitter

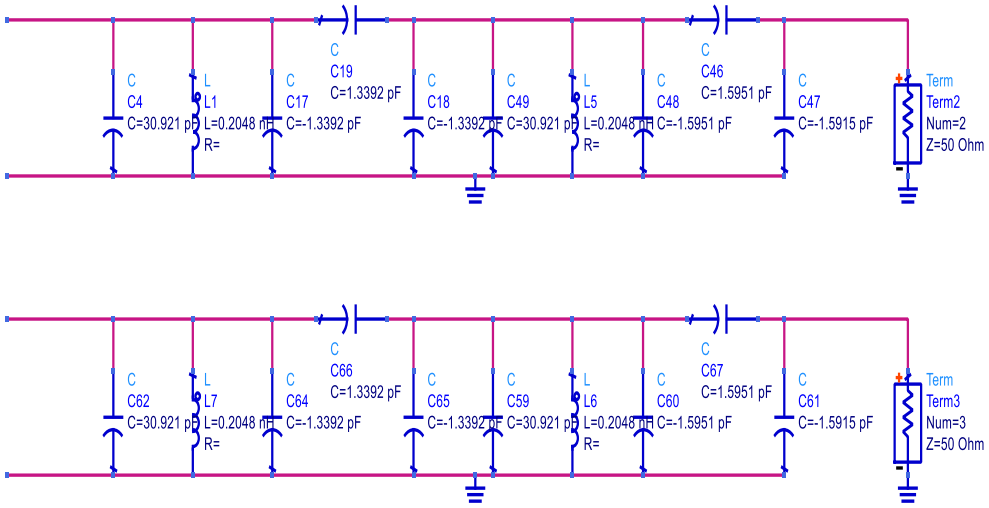

Figure 7.30 (Continued)

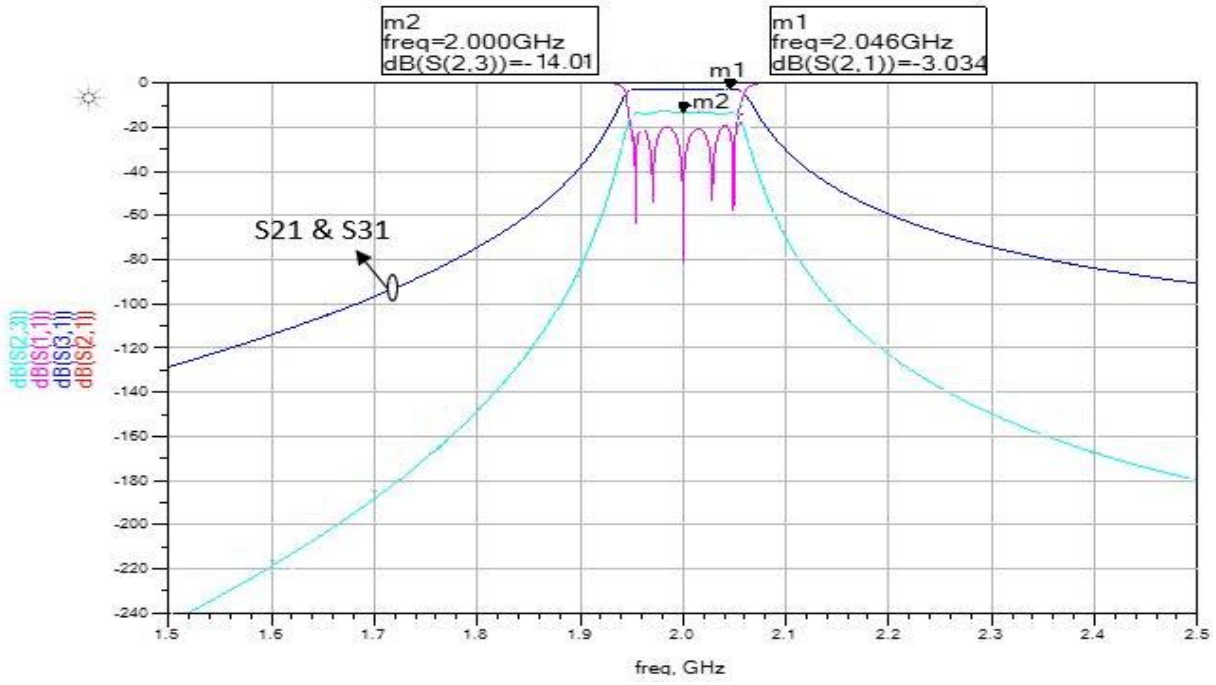

Figure 7.31 Equal Power Splitter ideal circuit prototype response

The EMPro simulation response of the structure is given in Figure 7.32 as:

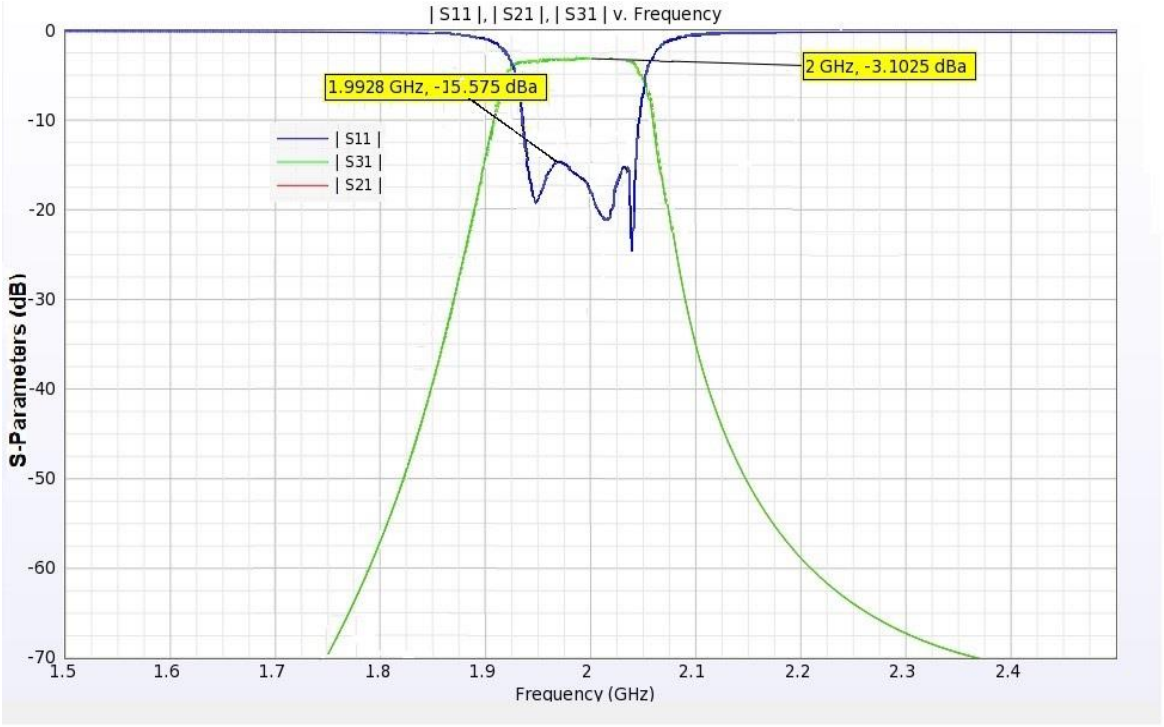

Figure 7.32 $|S_{11}|$, $|S_{21}|$ & $|S_{31}|$ EMPro simulation response of 5-pole equal split

7.13 Fabrication and Measurement

The 5-pole power splitter has been implemented using SIW waveguide cavity resonators coupled together with the arrangement as shown in Figure 7.11. A photograph of the SIW power splitter is shown in Figure 7.33. The fabrication process involves using the Printed Circuit Board technology where a 2 mm drill is made to create the required vias, which connects the top and bottom later of the power splitter. A conductor of the same thickness is inserted into the holes and is soldered on both ends. The thickness of the copper top and bottom conducting plates is 17 μm. The thickness of the substrate is 1.27 mm. The ports are all connected to 50 Ω SMA connectors.

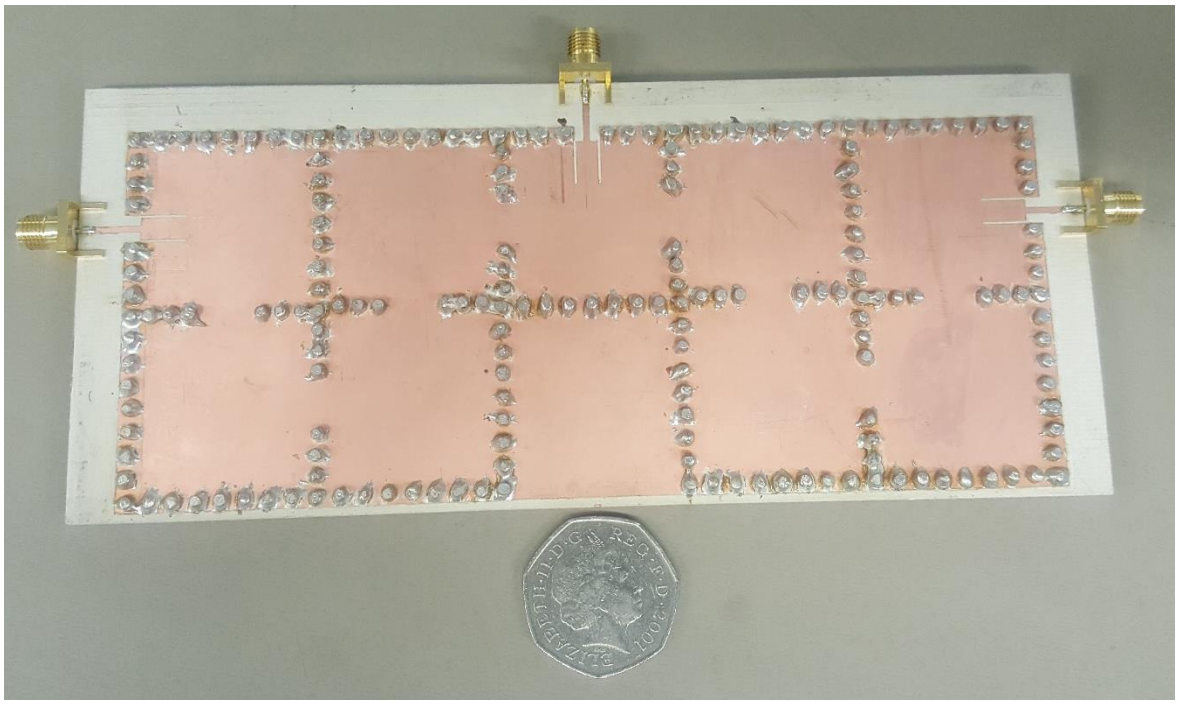

Figure 7.33 Photograph of the 5-pole SIW equal division power splitter

A cross sectional view of the equal split SIW power splitter with dimensions of resonator cavities shown in Figure 7.36. The dimensions of resonator cavities forming the device have

been measured using a standard mm ruler and they are shown in Table 7.4 along with design values. The initial measured dimensions show that there is some fabrication error of about 8% when compared with the designed values. This is probably due to the soldering effect or signal leakages. However, during measurement when the ports are tuned the return loss exhibits a response of about 18.3dB whilst the simulated return loss is about 15dB. The simulated and measured results of the 5-pole SIW filtered power splitter are depicted in Figure 7.35 for $|S_{11}|$, $|S_{21}|$ and $|S_{31}|$ and in Figure 7.36 for the isolation $|S_{23}|$. The measured response is in good agreement with the simulated response for the insertion loss between the input port and the two outputs; whilst the measured return loss gives a better response than the simulated return loss. The experimental results show that the maximum return loss within the passband is about 18.3dB and the minimum insertion loss is about 3.87dB. Figure 7.39 also shows that bandwidth of the measured response is wider than the simulated response. It shows that the fractional bandwidth of the measure response is about 7 % whilst the fractional bandwidth for the simulated response is about 5.5%. Figure 7.35 shows that the isolation between the output ports is measured to be about 14.79dB whilst the simulated and the theoretical isolation are 14.63dB and 14.01dB respectively.

Table 7.4 Dimension comparison between designed and measured parameters

Parameters	Dimensions (mm)		Parameters	Dimensions (mm)	
	Designed	Measured		Designed	Measured
TL	4.22	4.22	D_2	9.82	9.82
W_1	32.00	32.00	Δ_3	0.00	0.3
C_{1B}	12.75	12.72	C_{12}	12.75	12.72
Δ_1	0.00	0.50	p	4.00	4.00
C_{BC}	12.18	12.24	L_T	172.00	172.00
G_2	3.92	3.92	C_{CD}	12.49	12.58
Δ_2	0.00	0.50	C_{DE}	11.50	11.83

Table 7.4 (continued)

Parameters	Dimensions (mm)		Parameters	Dimensions (mm)	
	Designed	Measured		Designed	Measured
d	2.00	2.00	D_1	0.50	0.50
L_3	32.00	32.00	G_1	1.12	1.12
C_{23}	12.18	12.24	W_T	35.00	35.00
W_2	32.00	32.00	Δ_4	0.00	0.3
D_3	6.98	6.98	C_{34}	12.49	12.58
L_2	32.00	32.00	C_{45}	11.50	11.83
L_1	32.00	32.00			

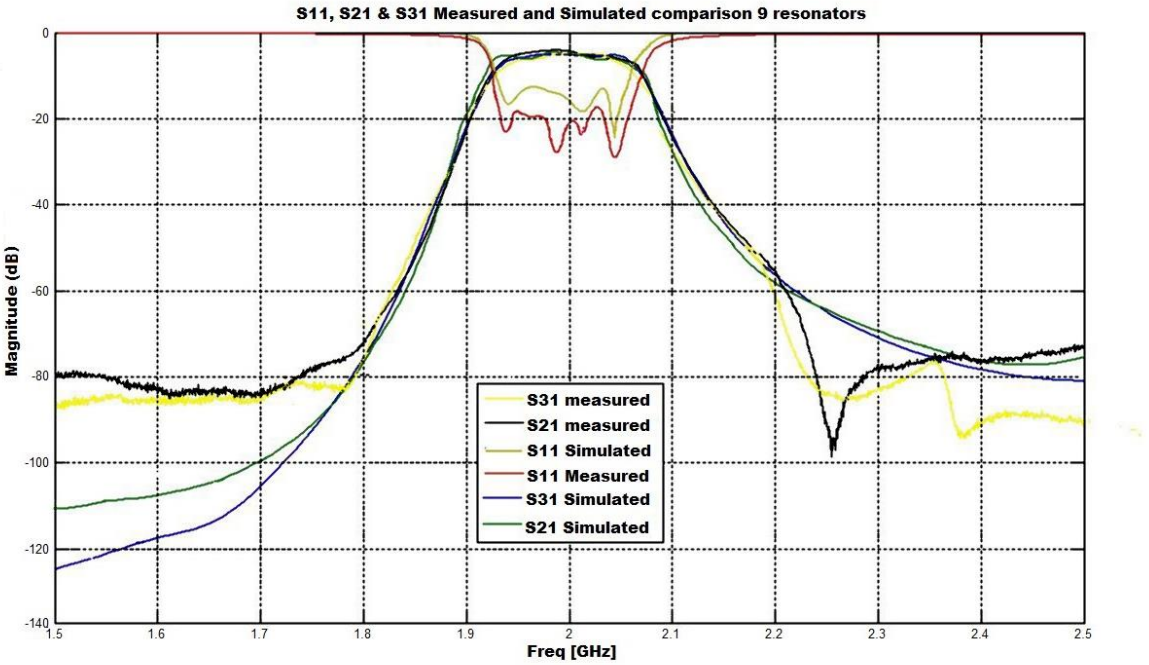

Figure 7.34 Comparison of $S_{11,}$ S_{21} and S_{31} for Simulated and fabricated 5-pole SIW power splitter

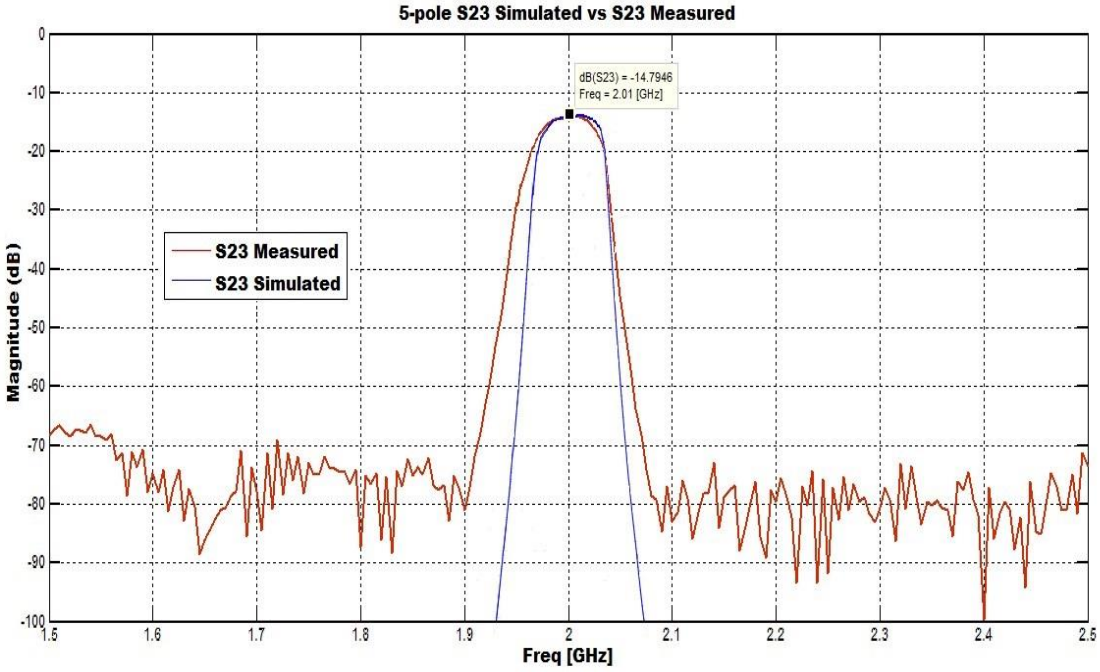

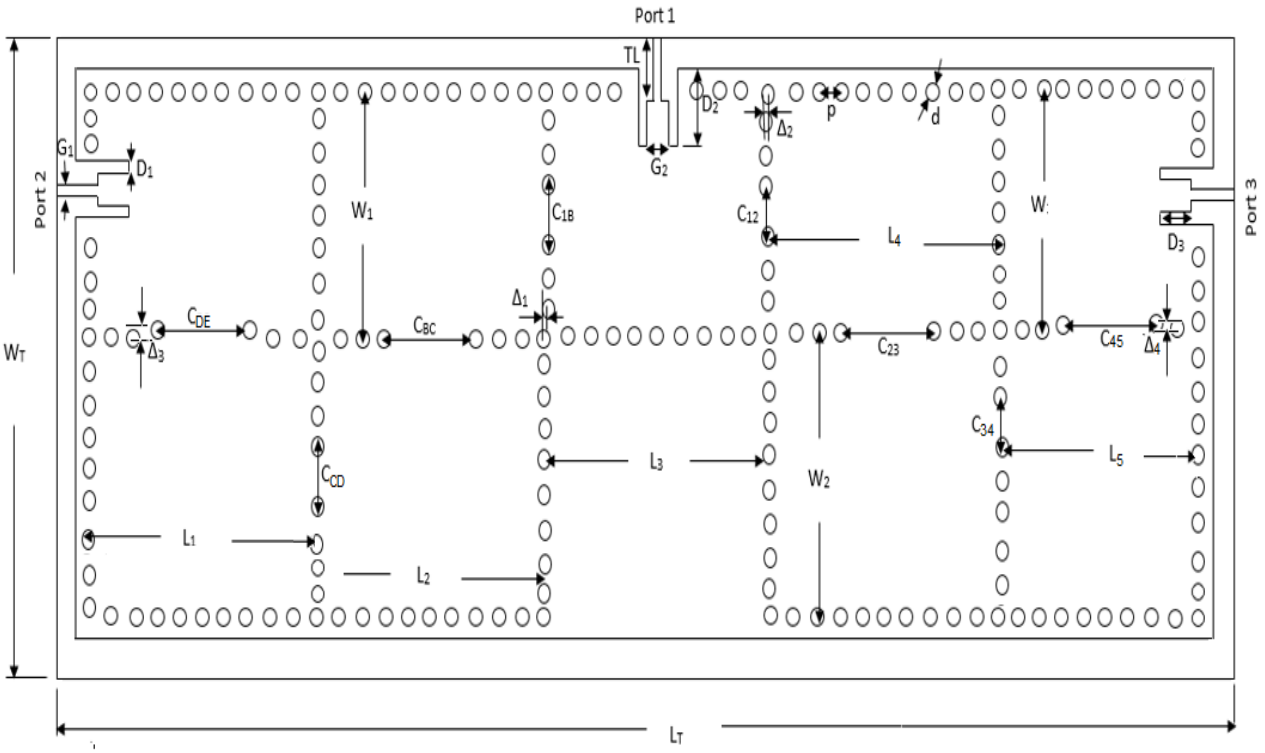

Figure 7.35 5-pole equal split simulated and measured S23
Figure 7.36 Cross sectional top view of the 5-pole power splitter

Table 7.5. Power divider dimensions corresponding to the parameters in Figure 7.36

Parameters	Dimensions (mm)	Parameters	Dimensions (mm)	Parameters	Dimensions (mm)	Parameters	Dimensions (mm)
TL	4.22	D_2	9.82	d	2.00	D_1	0.50
W_1	32.00	Δ_3	0.3	L_3	32.00	G_1	1.12
C_{1B}	12.72	C_{12}	12.72	C_{23}	12.24	W_T	35.00
Δ_1	0.50	p	4.00	W_2	32.00	Δ_4	0.3
C_{BC}	12.24	L_T	172.00	D_3	6.98	C_{34}	12.58
G_2	3.92	C_{CD}	12.58	L_2	32.00	C_{45}	11.83
Δ_2	0.50	C_{DE}	11.83	L_1	32.00		

7.14 9-resonators unequal power splitter

A 9-resonator unequal power divider has been designed, fabricated and tested. The splitter has been designed according to the coupled-resonator design procedure presented in Section 4.5 used in Section 5.9. It is designed at a centre frequency of 2 GHz, a fractional bandwidth of 5%, a reflection loss of 20 dB at the passband, and split ratio $\alpha = 1/3$. The unequal splitter topology is similar to that of the equal splitter as given in Figure 7.11. The prototype circuit and the ideal prototype response, as extracted from ADS, of the splitter is shown in figure 7.37 and 7.38; and the EMPro designed (top view) structure of the unequal SIW power splitter is shown in Figure 7.39.

Special emphasis is made to the unequal splitter because of the non-uniform split ratio unlike the equal split. Here, one of the outputs, Port 2 is having 1/3 of the power from the input whilst the other output Port 3 is having 2/3 of the input power. Hence, from equation 5.5 and 5.56 for $\alpha_2 = 1/3$, and $\alpha_2 = 2/3$, we've $K'_{1B} = 0.025$, $K'_{12} = 0.0125$, $K = 0.032$, $K_{\boldsymbol{BC}} = 0.032$, $K_{34} = 0.032$, $K_{CD} = 0.032$, $K_{45} = 0.043$ and $K_{DE} = 0.043$.

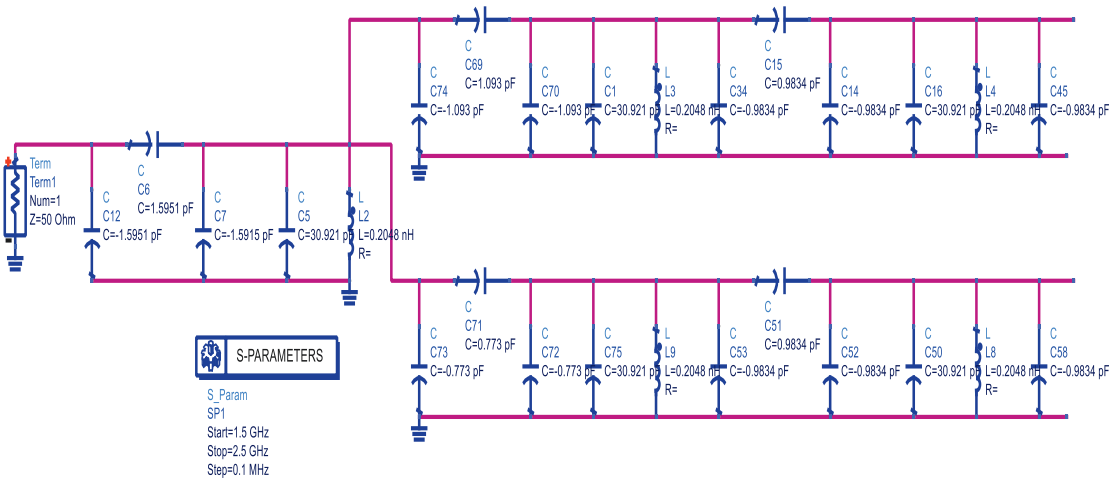

Figure 7.37 Circuit realization of the Equal split filtered power splitter

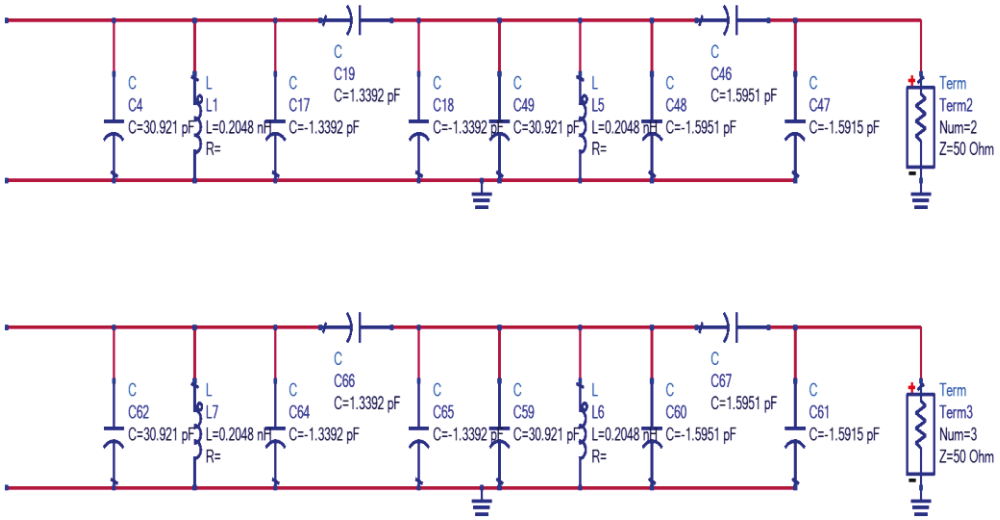

Figure 7.37 (Continued)

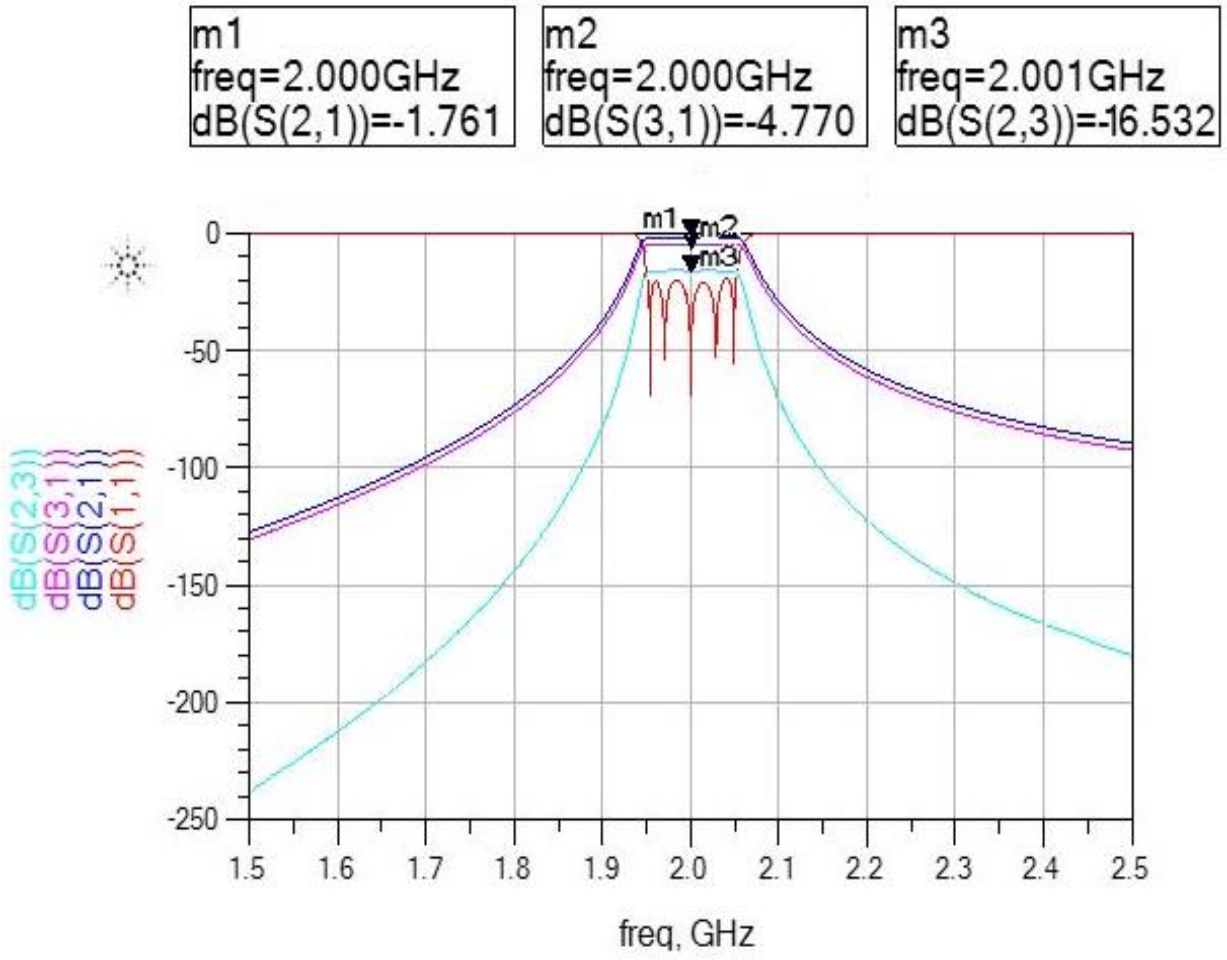

Figure 7.38 5-pole Unequal Power Splitter ideal circuit prototype response

7.15 Fabrication and Measurement

The unequal split power splitter has been implemented using SIW waveguide cavity resonators coupled together. A photograph of this fabricated power splitter is given in Figure 7.39. This component has similarity with the designed equal power splitter in Section 7.12. The difference, when compared to Figure 7.33 is given in Table 7.6 gives a comparison between the equal and the unequal splitter for the 5-pole PS.

Table 7.6 Common resonator coupling comparison 5-pole

Dimension (mm)	Equal Split	Unequal split
C_{1B}	12.72	11.71
C_{12}	12.72	13.24
Δ_1	0.5	0.55
Δ_2	0.5	0.35
Δ_3	0.3	0.25
Δ_4	0.3	0.35

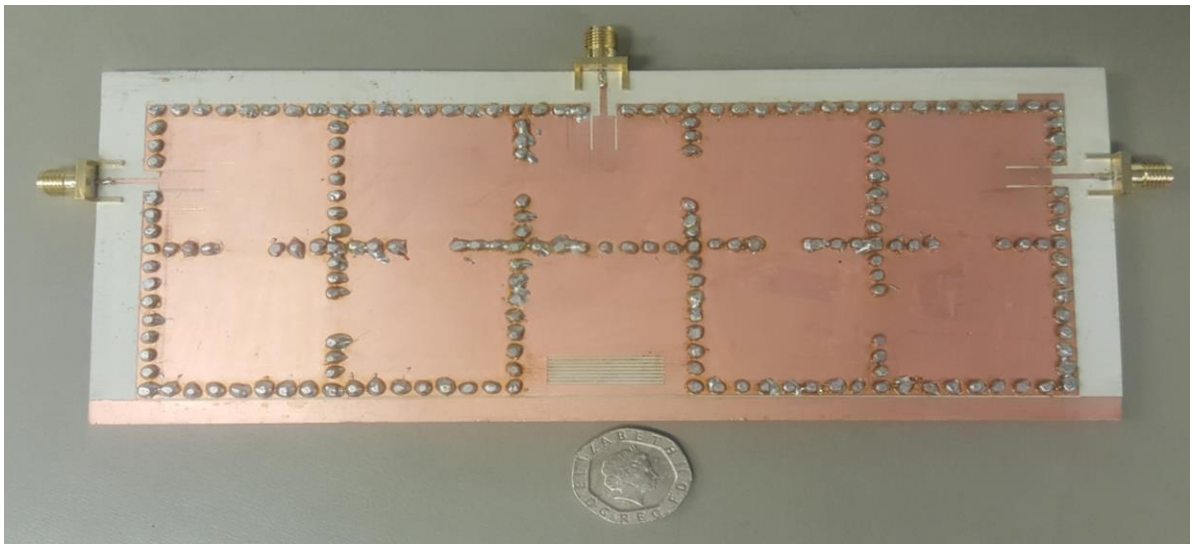

Figure 7.39 Photograph of the 5-pole SIW unequal division power

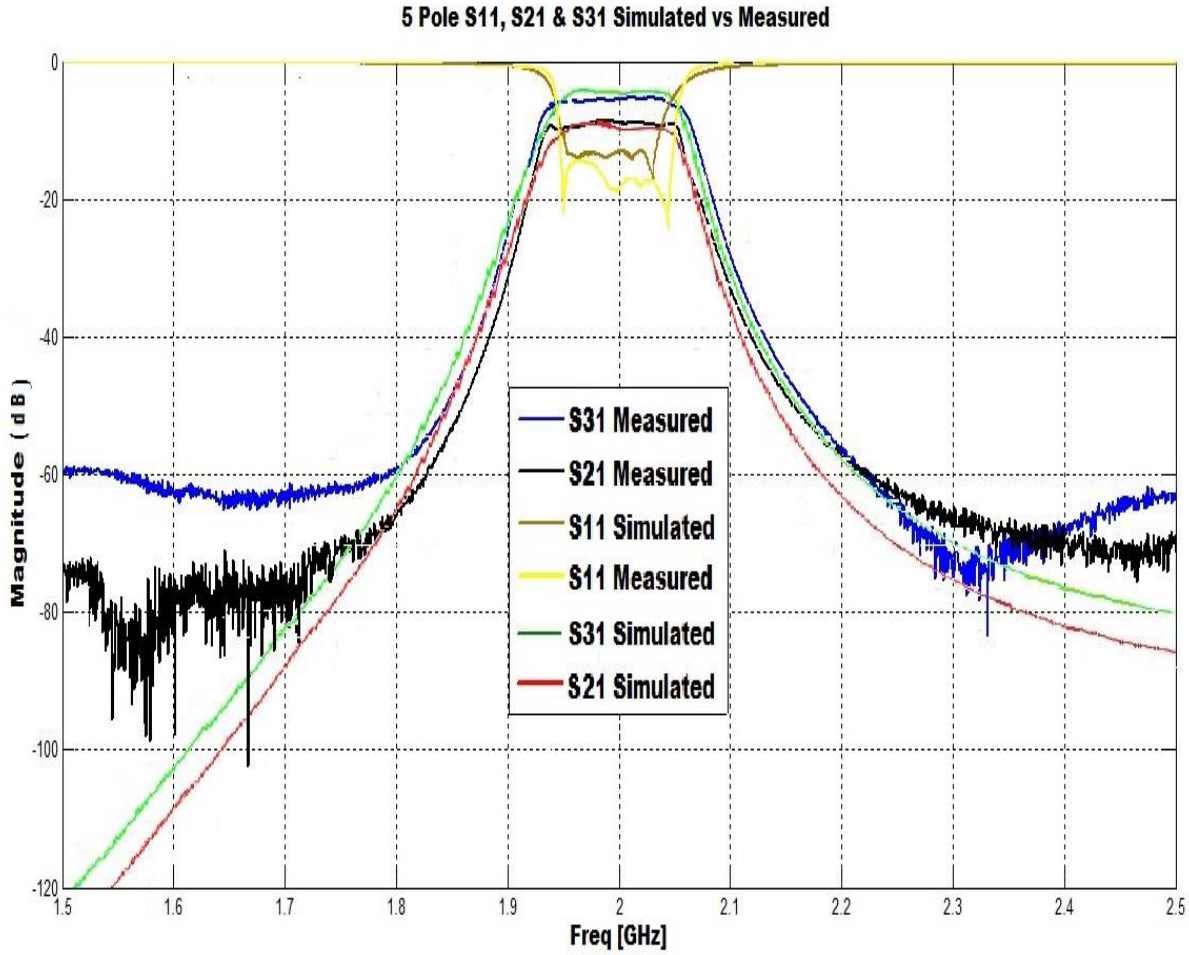

Figure 7.40 Comparison of S_{11}, S_{21} and S_{31} for simulated and fabricated 5-pole unequal division SIW power splitter

The simulated and measured results of the unequal power divider are shown in Figure 7.40. The measured response is in good agreement with the simulated response. The experimental results show that the maximum return loss within the passband is about 16 dB for the simulated and about 17dB for the fabricated component. The minimum insertion loss for $|S_{21}|$ is 7.75dB (7.097% error) and the minimum insertion loss for $|S_{31}|$ is 4.47dB (6.42% error). The percentage errors occur when compared the fabricated component response with the ideal responses at the centre frequency. The measured isolation between the output ports is

16.851 dB in the passband; whilst the simulated isolation is about the same with some ripples and the ideal circuit isolation is 16.532 dB as seen in Figure 7.41.

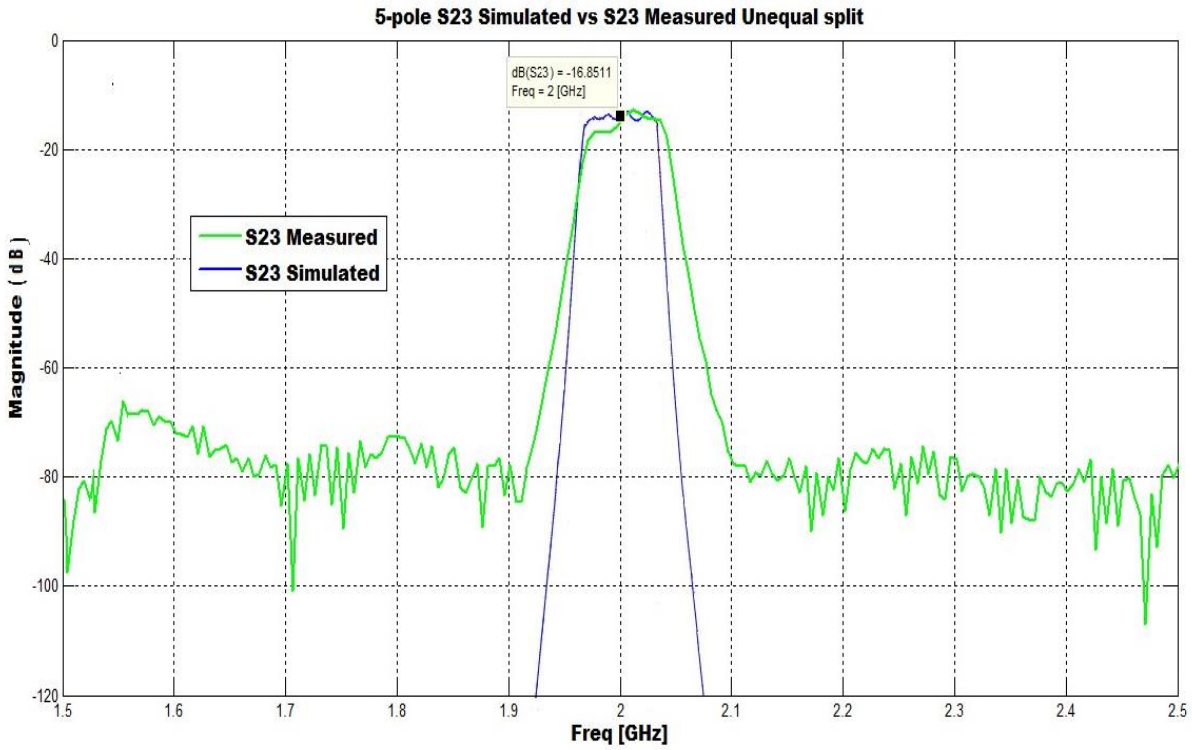

Figure 7.41 3-Pole unequal split Simulated and measured S23

7.16 Summary

This chapter has implemented the filtered powered splitter in SIW. The SIW cavity parameters are initially developed through the conversion of the rectangular cavity to a square resonator cavity and includes extraction of the coupling coefficient and the external quality factor to determine the spacing between resonators and the gaps in the CPW-to-SIW transition. It also gave the SIW filter parameter and the topology that would be adapted to the design and explained the whole process of synthesising the FPS for 3-pole equal and

unequal; and 5-pole equal and unequal. The fabricated components were tuned to give their frequency responses. Then after, the simulated and measured return loss, insertion loss and isolation responses and comparison and analyses were covered for all the design FPS, including the ideal circuit frequency responses. Table 7.7 gives the comparisons of frequency responses for the ideal circuit model, simulated and fabricated for this splitter.

Table 7.7 Comparison of Ideal, simulated and fabricated SIW FPS' frequency responses

Frequency responses	3-Pole Equal division			3-Pole Unequal division		
	Ideal	**Simulated**	**Fabricated**	**Ideal**	**Simulated**	**Fabricated**
S_{11} (dB)	20	14.86	17.1	20	20	22
S_{21} (dB)	3.01	3.57	3.61	4.77	5	5.2
S_{31} (dB)	3.01	3.57	3.61	1.76	1.85	1.88
S_{23} (dB)	6.02	6.79	6.81	6.51	8.7	8.9

Table 7.7 (Continued)

Frequency responses	5-Pole Equal division			5-Pole Unequal division		
	Ideal	**Simulated**	**Fabricated**	**Ideal**	**Simulated**	**Fabricated**
S_{11} (dB)	20	15.58	18.3	20	16	17
S_{21} (dB)	3.03	3.1	3.87	4.77	7.80	7.75
S_{31} (dB)	3.03	3.1	3.87	1.76	4.40	4.47
S_{23} (dB)	14.01	14.63	14.8	16.53	16.85	16.9

CHAPTER 8

CONCLUSION

This PhD describes research into power splitter. This is done using microstrip and SIW approaches. Several SIW filtered power splitters are presented, each of which serves a proof of concept of coupled resonator circuits. It addresses integrating a component capable of performing filtering and power division for current and future communication systems. These power splitters designs seem to be promising candidates for implementation in future phase antenna array systems, and many more applications. The findings from this thesis include designing and fabricating power dividers that has filtering capabilities as well as dividing the power. This has been tested using microwave resonators, SIW resonators with equal and unequal division. The comparison between the microstrip and the SIW 9-resonator and the SIW 5-resonator structure for the equal and unequal split have been given in Table 8.1. The aims and objectives of this research, which is, a comprehensive set of design equations are established and have been deployed to the respective designs. Another contribution to this work is the design of a novel square open loop resonator (SOLR) power splitter have been achieved. The concept to this realisation comes from the basic theory of filter design using coupled resonator approach as has been described by (Hong and Lancaster, 2001) and numerous researchers. Furthermore, another objective and main contribution of designing an equal and unequal split SIW FPS has been established. SIW possesses advantages over techniques like microstrip, stripline, rectangular waveguide etc.; due to its compactness, high power handling low cost of manufacturing and ease of integration with other planar structures. SIW is suitable mostly to millimeter-waves components, although it has

successfully been implemented in microwave (Zhen-Yu and Wu, 2008). However, there has not been much report on the microwave FPS. This has prompted the investigation and implementation of this work. There have been good agreements between the ideal, simulated and measured values except for the 5-pole unequal FPS. This limitation is has prompted further research since it is shown to be very lossy but established an isolation at its outputs.

Table 8.1 Comparison of the Microstrip and SIW bandpass FPS

	5-pole Microstrip	3-pole SIW		5-pole SIW	
		Equal Split	Unequal split	Equal Split	Unequal split
Bandwidth					
S21 (MHz)	120	99	85	140	115
S31 (MHz)	120	99	110	140	142
Fractional bandwidth					
S21 (%)	6	4.74	4.25	7	5.75
S31 (%)	6	4.74	5.5	7	7.1
Insertion loss					
S21(dB)	3.12	3.57	5.2	3.87	7.71
S31 (dB)	3.12	3.57	1.88	3.87	4.47
Return loss (dB)	15	17.1	22	18.3	17
Isolation (dB)	12.6	6.79	8.9	14.79	16.9

From the table, the SIW gained better performance than the microstrip counterpart. It has greater signal flow from the input port to the output ports. Also, it gained bandwidth of about 14% more than the microstrip. However, the microstrip performs better than the 3-pole SIW as seen in the table despite its low return loss. Even though some isolation values are recorded experimentally, it is worthy to note that it is not sufficient enough to lower or stop the amount of signal leakage between the output ports. The table also shows a higher insertion loss from the SIW 5-pole PS as compared with the 5-pole microstrip PD. This is in contrary to the

expected high Q factor as reported by Kumari and Srivastava (2013) where low loss is to be established. There is need for this to be investigated further.

For the unequal division in SIW, as a proof of concept, the minimum insertion loss for S_{21} of the 3rd order FPS is about 4.8% more than when compared to the ideal circuit's return loss of 4.77dB, whilst the minimum insertion loss for S_{31} is about 2.05dB. The maximum return loss for the 5-resonator SIW component has a high value of about 22dB after tuning. Due to the difference in magnitude and phase, the bandwidth is higher in S_{31} than in S_{21}. For the 5-pole UPS, due to its higher number of transmission zeros, it has a wide-bandwidth when compared to its 3-pole counterpart. The minimum insertion loss for S_{21} and S_{31} are 7.75dB and 4.47dB respectively; making a deviation of 7.097% and 6.42% from the ideal circuit. Even though, there is not a perfect matching of all the responses, the minimal errors recorded have proven a good relationship of the concept when compared to the ideal circuit, the simulated and the measured results.

Recommendations and Future Work

As introduced in Chapter one that the power splitter is applied in antenna arrays. These topologies of antenna require more than one antenna as shown in Figure 2.1. However, in this thesis, the division considered is for only two outputs. Therefore, to ensure filtered power to these antennas, they would require multiple power division to split the signals to these antennas. It is then apparent that this design concept be extended to more than two outputs. Secondly, it is observed that there is a low isolation values in all the designs are indications that there is signal flowing between the output ports. As introduced in the Wilkinson power divider (Wilkinson, 1960), there need for proper design technique and fabricate a component that should implement a perfect isolation as well as offering the filtering and power splitting

services. Thirdly, there is need to an improvement of this design because there is a slight increment of Q-factor in the SIW as compared to the microstrip. Lastly, as seen in Chapter 5 and 7, considerations are not made about the matching of the output ports; therefore, it is recommended that future work be done on this.

REFERENCES

Abbosh, A. M. (2007) 'A Compact UWB Three-Way Power Divider', *IEEE Microwave and Wireless Components Letters,* 17(8), pp. 598-600.

Abbosh, A. M. and Bialkowski, M. E. (2007) 'Design of Compact Directional Couplers for UWB Applications', *IEEE Transactions on Microwave Theory and Techniques,* 55(2), pp. 189-194.

Abouzahra, M. D. and Gupta, K. C. (1988) 'Multiport power divider-combiner circuits using circular-sector-shaped planar components', *IEEE Transactions on Microwave Theory and Techniques,* 36(12), pp. 1747-1751.

Alotaibi, S. K. and Hong, J. S. (2008) 'Novel substrate integrated waveguide filter', *Microw. Opt. Technol. Lett,* 50(4), pp. 1111–1114.

Bahl, I. and Bhartia, P. (2003) *Microwave Solid State Circuit Design.* 2nd edn.: Wiley.

Bozzi, M., Pasian, L., Perregrini, L. and Wu, K. (2007) 'On the losses in substrate integrated wavwguides', *Proc. European Microwave Conf.*

Bozzi, M., Perregrini, L. and Wu, K. (2008) 'Modeling of Conductor, Dielectric, and Radiation Losses in Substrate Integrated Waveguide by the Boundary Integral-Resonant Mode Expansion Method', *IEEE Transactions on Microwave Theory and Techniques,* 56(12), pp. 3153-3161.

Bozzi, M., Perregrini, L., Wu, K. and Arcioni, P. (2009) 'Current and future research trend in substrate integrated waveguide technology', *Radio Engineering,* 18, pp. 201-209.

Cameron, R. J. (1999) 'General coupling matrix synthesis methods for Chebyshev filtering functions', *IEEE Transactions on Microwave Theory and Techniques,* 47(4), pp. 433-442.

Cameron, R. J., Kudsia, C. M. and Mansour, R. R. (2007) *Microwave filters for communication systems, fundamentals, design and applications.* 2 edn. New Jersey: John Wiley & Sons.

Cassivi, Y., Perregrini, L., Arcioni, P., Bressen, M., Wu, K. and Conciauro, G. (2002) 'Dispersion characteristics of substrate integrated rectangular waveguide', *IEEE Microwave and Wireless Components Letters,* 12, pp. 333-335.

Chang, K. (2005) 'Encyclopedia of RF and Microwave Engineering', *Encyclopedia of RF and Microwave Engineering*. Hoboken, New Jersey: John Wiley & Sons Inc.

Che, W., Geng, L., Deng, K. and Chow, Y. L. (2008) 'Analysis and Experiments of Compact Folded Substrate-Integrated Waveguide', *IEEE Transactions on Microwave Theory and Techniques,* 56(1), pp. 88-93.

Chen, C. F., Chang, S. F. and Tseng, B. H. (2016) 'Design of Compact Microstrip Sept-Band Bandpass Filter With Flexible Passband Allocation', *IEEE Microwave and Wireless Components Letters,* 26(5), pp. 346-348.

Chen, C. F., Huang, T. Y., Shen, T. M. and Wu, R. B. (2013) 'Design of Miniaturized Filtering Power Dividers for System-in-a-Package', *IEEE Transactions on Components, Packaging and Manufacturing Technology,* 3(10), pp. 1663-1672.

Chen, X. P., Wu, K. and Drolet, D. (2009) 'Substrate Integrated Waveguide Filter With Improved Stopband Performance for Satellite Ground Terminal', *IEEE Transactions on Microwave Theory and Techniques,* 57(3), pp. 674-683.

Chen, X. P., Wu, K. and Li, Z. L. (2007) 'Dual-Band and Triple-Band Substrate Integrated Waveguide Filters With Chebyshev and Quasi-Elliptic Responses', *IEEE Transactions on Microwave Theory and Techniques,* 55(12), pp. 2569-2578.

Cho, Y. and Rebeiz, G. M. (2014) 'Two- and Four-Pole Tunable 0.7–1.1-GHz Bandpass-to-Bandstop Filters With Bandwidth Control', *IEEE Transactions on Microwave Theory and Techniques,* 62(3), pp. 457-463.

Choe, W. and Jeong, J. (2014) 'Compact Modified Wilkinson Power Divider With Physical Output Port Isolation', *IEEE Microwave and Wireless Components Letters,* 24(12), pp. 845-847.

Collin, R. E. (2001) *Foundations for microwave engineering.* John Wiley & Sons.

Dai, Y., Li, B., Ye, Z., Lu, D., Wang, F., Song, Z. and Chen, S. 'A miniaturized LTCC bandpass filter with low insertion loss and high image rejection within 6.5 to 7.1GHz frequency range'. *2009 Asia Pacific Microwave Conference*, 7-10 Dec. 2009, 1307-1309.

Dainkeh, A., Nwajana, A. O. and Yeo, K. S. K. (2016) 'Filtered Power Splitter Using Square Open Loop Resonators', *Progress In Electromagnetics Research C,* 64, pp. 133–140.

Daneshmand, M. and Mansour, R. R. (2005) 'Multiport MEMS-based waveguide and coaxial switches', *IEEE Transactions on Microwave Theory and Techniques,* 53(11), pp. 3531-3537.

Datta, S., Mukherjee, S. and Biswas, A. 'Design of broadband power divider based on Substrate-Integrated Waveguide technology'. *2013 IEEE Applied Electromagnetics Conference (AEMC)*, 18-20 Dec. 2013, 1-2.

Davidson, D. B. (2010) *Computational Electromagnetics for RF and Microwave Engineering.* Cambridge University Press, p. 23-30.

Deslandes, D. and Wu, K. 'Integrated transition of coplanar to rectangular waveguides'. *2001 IEEE MTT-S International Microwave Sympsoium Digest (Cat. No.01CH37157)*, 20-24 May 2001, 619-622 vol.2.

Deslandes, D. and Wu, K. (2006) 'Accurate modeling, wave mechanisms, and design considerations of a substrate integrated waveguide', *Microwave Theory and Techniques, IEEE Transactions on,* 54(6), pp. 2516-2526.

Deslandes, D. and Wu, K. (2001) 'Integrated microstrip and rectangular waveguide in planar form', *IEEE Microwave and Wireless Components Letters,* 11(2), pp. 68-70.

Deslandes, D. and Wu, K. 'Design Consideration and Performance Analysis of Substrate Integrated Waveguide Components'. *Microwave Conference, 2002. 32nd European*, 23-26 Sept. 2002, 1-4.

Deslandes, D. and Wu, K. (2003) 'Single-substrate integration technique of planar circuits and waveguide filters', *IEEE Transactions on Microwave Theory and Techniques,* 51(2), pp. 593-596.

Eccleston, K. W., Sun, Q. C. and Yeo, S. P. (1997) 'Tapered microstrip line power combiners with colinear input ports', *Microwave and Optical Technology Letters,* 15(6), pp. 339-342.

Ehmouda, J. B. A., A. (2009) 'Steered Microstrip Phased Array Antennas', *World Academy of Science, Engineering and Technology,* 49, pp. 319-323.

Fathy, A. E., Lee, S. W. and Kalokitis, D. (2006) 'A simplified design approach for radial power combiners', *IEEE Transactions on Microwave Theory and Techniques,* 54(1), pp. 247-255.

Fenn, A. J., Temme, D. H., William, P. D. and William, E. C. (2000) 'The Development of Phased-Array Radar Technology', *Lincoln Laboratory Journal,* 12(2), pp. 321-340.

Galani, Z. and Temple, S. J. 'A Broadband Planar N-Way Combiner/Divider'. *Microwave Symposium Digest, 1977 IEEE MTT-S International*, 21-23 June 1977, 499-502.

Glubokov, O. and Budimir, D. 'Substrate integrated folded-waveguide cross-coupled filter with negative coupling structure'. *2009 IEEE Antennas and Propagation Society International Symposium*, 1-5 June 2009, 1-4.

Grabherr, W., Huder, W. G. B. and Menzel, W. (1994) 'Microstrip to waveguide transition compatible with MM-wave integrated circuits', *IEEE Transactions on Microwave Theory and Techniques,* 42(9), pp. 1842-1843.

Grebennikov, A. (2011) *RF and microwave transmitter design.* John Wiley & Sons.

Grigoropoulos, N., Sanz-Izquierdo, B. and Young, P. R. (2005) 'Substrate integrated folded waveguides (SIFW) and filters', *IEEE Microwave and Wireless Components Letters,* 15(12), pp. 829-831.

Gunnarsson, S. E., Karnfelt, C., Zirath, H., Kozhuharov, R., Kuylenstierna, D., Alping, A. and Fager, C. (2005) 'Highly integrated 60 GHz transmitter and receiver MMICs in a GaAs pHEMT technology', *IEEE Journal of Solid-State Circuits,* 40(11), pp. 2174-2186.

Gupta, M. S. (1992) 'Degradation of power combining efficiency due to variability among signal sources', *IEEE Transactions on Microwave Theory and Techniques,* 40(5), pp. 1031-1034.

Han, S., Wang, X. L., Fan, Y., Yang, Z. and He, Z. (2007) 'THE GENERALIZED CHEBYSHEV SUBSTRATE INTEGRATED WAVEGUIDE DIPLEXER', *Progress In Electromagnetics Research,* 73, pp. 29-38.

Hee-Ran, A., Kwyro, L. and Noh-Hoon, M. 'General design equations of N-way arbitrary power dividers'. *2004 IEEE MTT-S International Microwave Symposium Digest (IEEE Cat. No.04CH37535)*, 6-11 June 2004, 65-68 Vol.1.

Hill, M. J., Ziolkowski, R. W. and Papapolymerou, J. (2001) 'A high-Q reconfigurable planar EBG cavity resonator', *IEEE Microwave and Wireless Components Letters,* 11(6), pp. 255-257.

Hirokawa, J. and Ando, M. (1998) 'Single-layer feed waveguide consisting of posts for plane TEM wave excitation in parallel plates', *IEEE Transactions on Antennas and Propagation,* 46(5), pp. 625-630.

Hong, J. S. (2000) 'Couplings of asynchronously tuned coupled microwave resonators', *IEE Proceedings - Microwaves, Antennas and Propagation,* 147(5), pp. 354-358.

Hong, J. S. (2006) 'Compact folded-waveguide resonators and filters', *IEE Proceedings - Microwaves, Antennas and Propagation,* 153(4), pp. 325-329.

Hong, J. S. and Lancaster, M. J. (2001) *Microstrip Filters for RF/Microwave Applications.* New York: John Wiley & Sons.

Huang, T. Y., Shen, T. M. and Wu, R. B. (2009) 'Design and modeling of microstrip line to substrateintegrated waveguide transitions', *Passive Microwave Components and Antennas*, pp. 225-246.

Hunter, I. (2006) *Theory and Design of Microwave Filters. IET Electromagneti c Waves* Second edn. London, United Kingdom: The Institution of Engineering and Technology.

Izqueirdo, B. S., Grigoropoulos, N. and Young, P. R. 'Ultra-Wideband Multilayer Substrate Integrated Folded Waveguides'. *2006 IEEE MTT-S International Microwave Symposium Digest*, 11-16 June 2006, 610-612.

Jin, C., Li, R., Alphones, A. and Bao, X. (2013) 'Quarter-Mode Substrate Integrated Waveguide and Its Application to Antennas Design', *IEEE Transactions on Antennas and Propagation,* 61(6), pp. 2921-2928.

Jones, T. R. and Daneshmand, M. (2016) 'Miniaturized Slotted Bandpass Filter Design Using a Ridged Half-Mode Substrate Integrated Waveguide', *IEEE Microwave and Wireless Components Letters,* 26(5), pp. 334-336.

Jung-Hyun, S., Geun-Young, K., Seok-Ho, S., Hyo-Jong, L., Young-Joo, S., Yong-Woo, J., Hyung-Sik, P. and Dal, A. 'Design method of a dual band balun and divider'. *2002 IEEE MTT-S International Microwave Symposium Digest (Cat. No.02CH37278)*, 2-7 June 2002, 1177-1180 vol.2.

Karimabadi, S. S. and Attari, A. R. 'Broadband substrate integrated waveguide four-way power divider'. *6th International Symposium on Telecommunications (IST)*, 6-8 Nov. 2012, 80-83.

Khan, A. A., Mandal, M. K. and Sanyal, S. 'Unloaded quality factor of a substrate integrated waveguide resonator and its variation with the substrate parameters'. *2013 International Conference on Microwave and Photonics (ICMAP)*, 13-15 Dec. 2013, 1-4.

Konishi, Y. (1998) *Microwave Electronic Circuit Technology.* New York: New York: Marcel Dekker Inc, p. 273-292.

Kumari, S. and Srivastava, S. (2013) 'Losses in Waveguide and Substrate Integrated Waveguide (SIW) For Ku Band: A Comparison', *International Journal of Modern Engineering Research (IJMER),* 3(153-57).

Lap Kun, Y. and Ke-Li, W. (2006) 'An LTCC balanced-to-unbalanced extracted-pole bandpass filter with complex load', *IEEE Transactions on Microwave Theory and Techniques,* 54(4), pp. 1512-1518.

Lee, S., Jung, S. and Lee, H. Y. (2008) 'Ultra-Wideband CPW-to-Substrate Integrated Waveguide Transition Using an Elevated-CPW Section', *IEEE Microwave and Wireless Components Letters,* 18(11), pp. 746-748.

Lin, H. H. 'Novel Folded Resonators and Filters'. *2007 IEEE/MTT-S International Microwave Symposium*, 3-8 June 2007, 1277-1280.

Llorente-Romano, S., Garcia-Lamperez, A., Salazar-Palma, M., Daganzo-Eusebio, A. I., Galaz-Villasante, J. S. and Padilla-Cruz, M. J. 'Microstrip filter and power divider with improved out-of-band rejection for a Ku-band input multiplexer'. *2003 33rd European Microwave Conference*, 2-10 Oct. 2003, 315-318.

Lou, Y., Chan, C. H. and Xue, Q. (2008) 'An In-Line Waveguide-to-Microstrip Transition Using Radial-Shaped Probe', *IEEE Microwave and Wireless Components Letters,* 18(5), pp. 311-313.

Ludwig, R. and Bogdanov, G. (2009) *RF circuit design: theory and applications.* Second Edition edn.: Pearson Prentice Hall.

Matthaei, G. L., Young, L. and Jones, E. M. T. (1964) *Microwave filters, impedance matching networks, and coupling structures.* Dedham, MA: Artech House.

Mohammed, A. M. and Wang, Y. 'Four-way waveguide power dividers with integrated filtering function'. *2015 European Microwave Conference (EuMC)*, 7-10 Sept. 2015, 486-489.

Mohottige, N., Glubokov, O., Jankovic, U. and Budimir, D. (2016) 'Ultra Compact Inline E-Plane Waveguide Bandpass Filters Using Cross Coupling', *IEEE Transactions on Microwave Theory and Techniques,* 64(8), pp. 2561-2571.

Montgomery, C. G., Dicke, R. H. and Purcell, E. M. (1948) *Principle of Microwave Circuits.* New York: McGraw-Hill.

Nwajana, A.O., Dainkeh, A., Yeo, K.S.K. (2017) ' Substrate Integrated Waveguide (SIW) Bandpass Filter with Novel Microstrip-CPW-SIW Input Coupling', *Journal of Microwave , Optoelectronics and Electromagnetic Applications.* June 2017, 16(2), 393-402.

Ocket, I., Phommahaxay, A., Tilmans, H. A. C., Mills, J. B. and Nauwelaers, B. 'Millimeter wave micromachined cavity resonators on MCM-D: Oscillator-resonator co-design and packaging considerations'. *2009 IEEE MTT-S International Microwave Symposium Digest*, 7-12 June 2009, 593-596.

Parad, L. I. and Moynihan, R. L. (1965) 'Split-Tee Power Divider', *IEEE Transactions on Microwave Theory and Techniques,* 13(1), pp. 91-95.

Patrovsky, A., Daigle, M. and Ke, W. 'Millimeter-wave wideband transition from CPW to substrate integrated waveguide on electrically thick high-permittivity substrates'. *2007 European Microwave Conference*, 9-12 Oct. 2007, 138-141.

Pengcheng, J., Chen, L. Y., Alexanian, A. and York, R. A. (2003) 'Broad-band high-power amplifier using spatial power-combining technique', *IEEE Transactions on Microwave Theory and Techniques,* 51(12), pp. 2469-2475.

Pozar, D. M. (2011) *Microwave Engineering.* Fourth edn. Hoboken, New Jersey: John Wiley and Sons. Reprint, 4.

Rasmussen, T., Rasmussen, J. K. and Povlsen, J. H. (1995) 'Design and performance evaluation of 1-by-64 multimode interference power splitter for optical communications', *Journal of Lightwave Technology,* 13(10), pp. 2069-2074.

Rayas-Sanchez, J. E. 'An Improved EM-Based Design Procedure for Single-Layer Substrate Integrated Waveguide Interconnects with Microstrip Transitions'. *2009 IEEE MTT-S*

International Microwave Workshop Series on Signal Integrity and High-Speed Interconnects, 19-20 Feb. 2009, 27-30.

Seo, T. Y., Lee, J. W., Cho, C. S. and Lee, T. K. 'Radial guided 4-way unequal power divider using substrate integrated waveguide with center-fed structure'. *2009 Asia Pacific Microwave Conference*, 7-10 Dec. 2009, 2758-2761.

Shelkovnikov, A. and Budimir, D. 'Novel compact EBG waveguide resonators in planar form'. *2005 European Microwave Conference*, 4-6 Oct. 2005, 4 pp.

Shen, T. M., Huang, T. Y. and Wu, R. B. 'A laminated waveguide magic-T in multilayer LTCC'. *2009 IEEE MTT-S International Microwave Symposium Digest*, 7-12 June 2009, 713-716.

Skaik, T. F. (2011) *Synthesis of Coupled Resonator Circuits with Multiple Outputs using Coupling Matrix Optimization.* P.hD Thesis, University of Birmingham, University of Birmingham, UK.

Song, K., Fan, Y. and Zhang, Y. (2008) 'Eight-Way Substrate Integrated Waveguide Power Divider With Low Insertion Loss', *IEEE Transactions on Microwave Theory and Techniques,* 56(6), pp. 1473-1477.

Song, K. and Xue, Q. (2010) 'Novel Ultra-Wideband (UWB) Multilayer Slotline Power Divider With Bandpass Response', *IEEE Microwave and Wireless Components Letters,* 20(1), pp. 13-15.

Suntives, A. and Abhari, R. (2007) 'Design and Characterization of the EBG Waveguide-Based Interconnects', *IEEE Transactions on Advanced Packaging,* 30(2), pp. 163-170.

Tang, X. and Mouthaan, K. (2010) 'Filter integrated Wilkinson power dividers', *Microwave and Optical Technology letters,* 52(12), pp. 830-2833.

Tiwari, R., Mukherjee, S. and Biswas, A. 'Design and characterization of multi-layer Substrate Integrated Waveguide (SIW) slot coupler'. *2015 9th European Conference on Antennas and Propagation (EuCAP)*, 13-17 April 2015, 1-4.

Trantanella, C. J. 'A novel power divider with enhanced physical and electrical port isolation'. *2010 IEEE MTT-S International Microwave Symposium*, 23-28 May 2010, 129-132.

Uchimura, H., Takenoshita, T. and Fujii, M. 'Development of the "laminated waveguide"'. *1998 IEEE MTT-S International Microwave Symposium Digest (Cat. No.98CH36192)*, 7-12 June 1998, 1811-1814 vol.3.

Villegas, F. J., Stones, D. I. and Hung, H. A. (1999) 'A novel waveguide-to-microstrip transition for millimeter-wave module applications', *IEEE Transactions on Microwave Theory and Techniques,* 47(1), pp. 48-55.

Wang, X., Sakagami, I., Mase, A. and Ichimura, M. (2014) 'Wilkinson Power Divider With Complex Isolation Component and Its Miniaturization', *IEEE Transactions on Microwave Theory and Techniques,* 62(3), pp. 422-430.

Wang, Y., Hong, W., Dong, Y., Liu, B., Tang, H. J., Chen, J., Yin, X. and Wu, K. (2007) 'Half Mode Substrate Integrated Waveguide (HMSIW) Bandpass Filter', *IEEE Microwave and Wireless Components Letters,* 17(4), pp. 265-267.

Wilkinson, E. J. (1960) 'An N-Way Hybrid Power Divider', *IRE Transactions on Microwave Theory and Techniques,* 8(1), pp. 116-118.

Wu, K., Deslandes, D. and Cassivi, Y. (2003) 'The substrate integrated circuits-a new concept for high frequency electronics and optoelectronics', *MIcrowave Revolution*, pp. 2-9.

Wu, Y., Liu, Y., Xue, Q., Li, S. and Yu, C. (2010) 'Analytical Design Method of Multiway Dual-Band Planar Power Dividers With Arbitrary Power Division', *IEEE Transactions on Microwave Theory and Techniques,* 58(12), pp. 3832-3841.

Wu, Z., Lee, C. and Chen, H. 'Balun diplexer design in hybrid structure of microstrip line and slot-line'. *2015 Asia-Pacific Microwave Conference (APMC)*, 6-9 Dec. 2015, 1-3.

Xiaoping, C., Wei, H., Cui, T., Jixin, C. and Ke, W. (2005) 'Substrate integrated waveguide (SIW) linear phase filter', *IEEE Microwave and Wireless Components Letters,* 15(11), pp. 787-789.

Xu, F. and Wu, K. (2005) 'Guided-wave and leakage characteristics of substrate integrated waveguide', *IEEE Transactions on Microwave Theory and Techniques,* 53 pp. 66-73.

Yam, Y. O. and Cheung, C. W. (1997) 'High efficiency power amplifier with travelling-wave combiner and divider', *International Journal of Electronics,* 82(2), pp. 203-218.

Yang, S. and Fathy, A. E. 'Synthesis of an Arbitrary Power Split Ratio Divider Using Substrate Integrated Waveguides'. *2007 IEEE/MTT-S International Microwave Symposium*, 3-8 June 2007, 427-430.

Yau, W., Schellenberg, J. M. and Shih, Y. C. 'A New N-Way Broadband Planar Power Combiner/Divider'. *Microwave Symposium Digest, 1986 IEEE MTT-S International*, 2-4 June 1986, 147-149.

Yeo, K. S. K. (2011) *RF and Microwave Engineering Note*.

Yong, H. and Ke-Li, W. (2003) 'A broad-band LTCC integrated transition of laminated waveguide to air-filled waveguide for millimeter-wave applications', *IEEE Transactions on Microwave Theory and Techniques,* 51(5), pp. 1613-1617.

Zakaria, Z., Yik, S. W., Abd Aziz, M. Z. A., Mutalib, M. A. and Haron, N. Z. (2013) 'A Novel Structure of Multilayer SIW Filter and Patch Antenna', *International Journal of Engineering and Technology (IJET),* 5(5), pp. 4400-4411.

Zhang, T. and Che, W. 'A four-way compact unequal power divider with arbitrary power ratio'. *2016 IEEE International Conference on Computational Electromagnetics (ICCEM)*, 23-25 Feb. 2016, 124-126.

Zhang, X., Ma, C. and Wang, F. (2015) 'Design of compact dual-passband LTCC filter exploiting stacked QMSIW and EMSIW', *Electronics Letters,* 51(12), pp. 912-914.

Zhang, X., Wang, Q., Liao, A. and Xiang, Y. 'Millimeter-wave integrated waveguide power dividers for power combiner and phased array applications'. *Microwave and Millimeter Wave Technology (ICMMT), 2010 International Conference on*, 8-11 May 2010, 233-235.

ZhargCheng, H., Wei, H., Hao, L., Hua, Z. and Ke, W. 'Multiway broadband substrate integrated waveguide (SIW) power divider'. *2005 IEEE Antennas and Propagation Society International Symposium*, 3-8 July 2005, 639-642 Vol. 1A.

Zhen-Yu, Z. and Ke, W. 'Broadband half-mode substrate integrated waveguide (HMSIW) Wilkinson power divider'. *2008 IEEE MTT-S International Microwave Symposium Digest*, 15-20 June 2008, 879-882.

Zou, X., Tong, C. and Yu, D. (2011) 'Y-junction power divider based on substrate integrated waveguide', *Electronics Letters,* 47(25), pp. 1375-1376.

APPENDIX A Publications from this work

Progress In Electromagnetics Research C, Vol. 64, 133–140, 2016

Filtered Power Splitter Using Square Open Loop Resonators

Amadu Dainkeh*, Augustine O. Nwajana, and Kenneth S. K. Yeo

Abstract—A microstrip power splitter with band-pass responses is presented in this paper. The design is based on square open loop resonator topology. This filtered power splitter does not require quarter wavelength transformers and will result in a smaller size than a conventional Wilkinson power divider with integrated band-pass filter. It is a two-way equal power splitter with fifth order band-pass filter characteristics. The power splitter is designed to have Chebyshev band-pass response function. A theoretical analytical circuit model will be presented. From the theoretical model, a microstrip filtered power splitter will be designed and simulated. The proposed filtered power splitter is small in size and reduces circuit complexity. The power splitter is simulated and measured, and the results are presented.

1. INTRODUCTION

Recently, the development of telecommunication equipment has shown a tendency to produce components with unique capabilities and specific features such as ability to split signal to other devices and to be distributed. These microwave components can be designed using various approaches. Printed circuit board (PCB) fabrication is most suitable for planar circuit structure due to its low cost, ease of integration and compactness [1]. In most millimeter and microwave communications systems, Wilkinson power divider has played an essential role for splitting or combining power in numerous microwave applications such as mixers, balanced power amplifiers and feeding networks of antenna arrays. But due to band selectivity, which is poor because of band rejection of the conventional Wilkinson power divider, it suffered a major drawback. Recent studies have been shown [2–5] in which efforts have been made to improve the operational frequency of the power splitter passband selectivity. Also, the Wilkinson power divider has a large circuit size since at its desired frequency, it is composed of two quarter wavelength ($\lambda/4$) line sections. Ref. [2] presents an integration of single-stage coupled line band-pass filter and conventional Wilkinson divider. It satisfactorily implemented a power divider with a good filter response. The conventional $\lambda/4$ impedance section of a Wilkinson power divider is replaced by stepped impedance inter-digital coupling element in [3] which gives filtering properties and a good out of band rejection. In [4, 5], in order to achieve a better passband selectivity, the transmission path incorporates fourth-order and second/fourth-order quasi-elliptic filters, respectively.

Like power dividers, another essential component important in both transmitters and receivers is a band-pass filter. A band-pass filter is essential in RF front end to take a signal having a frequency of f_1 to f_2, and rejecting signals outside this range. To realize this, a filter waveguide technology is appropriate when considering low insertion loss. Up to now, there have been some work on the miniaturization of filters [6–12] and also proposals of several resonator types to miniaturize filter size. Among them are the uses of Stepped-Input Resonator [8] which gives a better stopband response and higher spurious resonant frequency with reduced circuit size and microstrip Square Open Loop Resonators (SOLR) [13] in which miniaturization was done using series capacitive loading of the resonators.

Received 20 April 2015, Accepted 16 May 2016, Scheduled 29 May 2016
* Corresponding author: Amadu Dainkeh (u0925309@uel.ac.uk).
The authors are with the Department of Electrical and Electronic Engineering, University of East London, E16 2RD, London, United Kingdom.

A method of integration of power splitter and a band-pass filter into a single unit/component is essential to further reduce circuit size and cost of manufacturing. This gave rise to the proposition of filtering power dividers. In [14], a miniaturised power divider with band-pass characteristics based on coupled-resonator topology was presented, the reduced circuit was due to shrinking of assembled resonator. A filtering microstrip antenna array is presented in [15]. The design's feeding network consists of one power splitter and two baluns utilizing coupled resonator.

In this paper, a filtering power splitter is proposed. It is designed based on coupled resonator concept. It has the advantage of small size and reduction of complex circuitry. The Chebyshev filtered power splitter has been designed by deploying microstrip technology using square open loop resonators. The designed microstrip structure is constructed and tested to verify the proposed concept.

This paper is outlined as follows. Section 1 gives a brief introduction. Section 2 gives the approach used in the design. The microstrip design of the band-pass power splitter is given in Section 3, and Section 4 presents the simulated and measured results.

2. DESIGN OF IDEAL FILTERING POWER SPLITTER

A conventional Wilkinson power splitter is shown in Figure 1. The circuit contains two $\lambda/4$ transformers which results in a larger circuit size. A three-way coupling between adjacent resonators is used in place of the junction of conventional power splitter. The circuit area becomes smaller by implementing a coupled resonator network.

The coupling scheme of the filtered power splitter is shown in Figure 2. The solid lines represent the coupling path, and each of the nodes represents a resonator. At resonance, there is coupling of signal energy from port 1 to port 2 through resonators 1, 2, 3, 4 and 5, and from port 1 to port 3 through resonators 1, B, C, D and E. The circuit is similar to joining two identical 5-pole bandpass Chebyshev

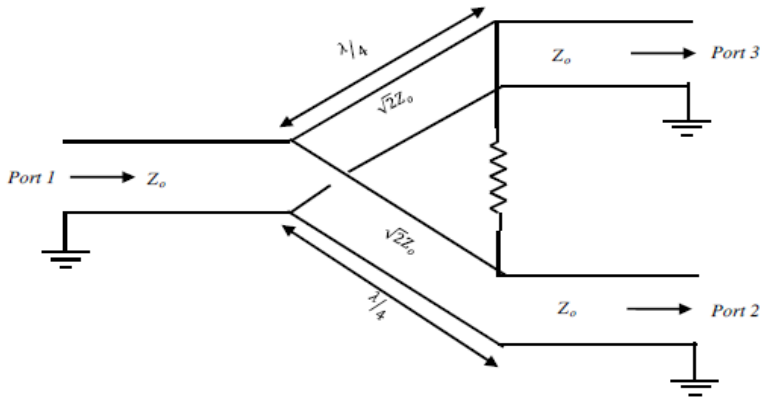

Figure 1. Conventional Wilkinson power splitter , **reproduced courtesy of The Electromagnetics Academy**

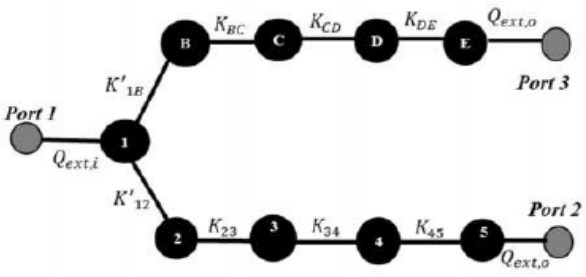

Figure 2. Coupling arrangement of a five-pole Chebyshev band-pass filtered splitter , **reproduced courtesy of The Electromagnetics Academy**

filters at a common resonator 1.

The conventional theory based on coupled resonator bandpass filter knowledge is applicable here. The external quality factor, Q_{ext}, and the coupling coefficient, k_{nm}, can be determined using the usual method used in band-pass filter design as described in [17]. To ensure an equal power split in the two splitting paths, the coupling coefficients are k'_{12} and k'_{1B} and made to equate to $k_{12}/\sqrt{2} = k_{1B}/\sqrt{2}$, where k_{12} and k_{1B} are the coupling coefficients of a standard band-pass filter. This coupling value is based on the theory of establishing equal power splitting, with half power delivering to each branch and having the same return loss performance for each branch [16, 19].

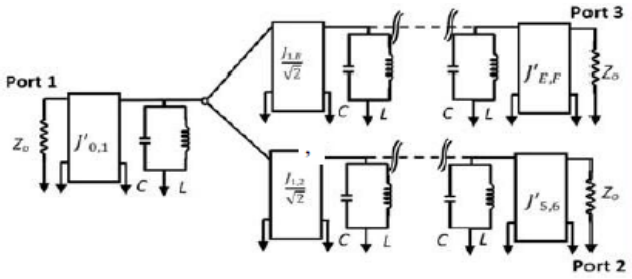

Figure 3. Equivalent circuit of a five-pole Chebyshev bandpass power splitter ,
reproduced courtesy of The Electromagnetics Academy

Figure 3 gives the equivalent circuit of a 5-pole bandpass filter. The admittance J — Inverter method is used to determine the coupling between resonators. g is the normalised low-pass filter value, Z_o the characteristics impedance and $k = 1$ to n, where n is the order of the filter

$$J_{0,1} = J_{5,6} = J_{E,F} = 1$$

$$J'_{0,1} = J'_{5,6} = J'_{E,F} = \frac{1}{Z_o}$$

$$J_{k,k+1} = \sqrt{\frac{g_1^2}{g_k g_{k+1}}} \Big/ Z_o \tag{1}$$

C and L are the self-capacitance and inductance respectively, given by Equation (2), where $\omega_o = 2\pi f_o$, f_o is the fundamental frequency and Δ the fractional bandwidth of the filter.

$$C = \frac{g_1}{\Delta \omega_o Z_o}; \quad L = \frac{1}{\omega_o^2 C} \tag{2}$$

The coupling coefficient, k, and the input/output external quality factor, Q_{ext}, can be determined by [20] as given in Equations (3) and (4).

$$k_{k,k+1} = J_{k,k+1}\sqrt{\frac{L}{C}} \tag{3}$$

$$Q_{ext,i/o} = \omega_o Z_o C \tag{4}$$

The theoretical values of the external quality factor for ports 1, 2 and 3 are all determined as 19.423.

Figure 4 gives the simulated result of the filtered splitter circuit and shows that it has a centre frequency of 2 GHz and a minimum return loss of not greater than 20 dB. This is in conformity with the original design specification. This is in conformity with the original design specification.

3. MICROSTRIP DESIGN OF BANDPASS POWER SPLITTER

3.1. Design Procedure

The proposed filtered Chebyshev power splitter has been designed and implemented using the microstrip technology. The Square Open Loop Resonators (SOLR) topology is deployed. This topology is used

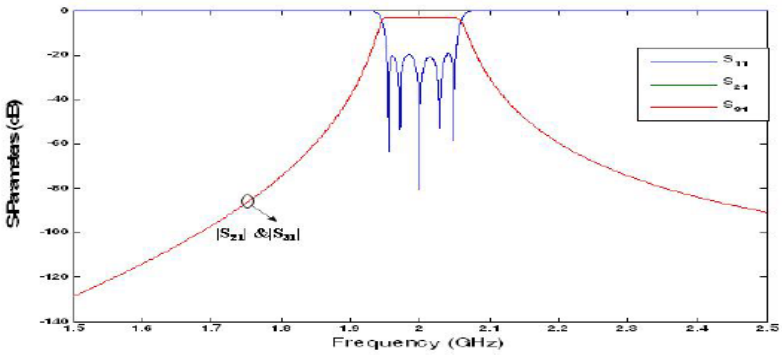

Figure 4. Ideal circuit model responses for proposed five-pole Chebyshev filtered power splitter, **reproduced courtesy of The Electromagnetics Academy**

since it has the advantage of size, weight and cost reduction; also, compared to waveguide cavity cross-coupled filters, it is more flexible to construct a variety of cross-coupled planar filters [18]. The calculated circuit model is simulated using Keysight's Advance Design System (ADS) EM simulator software. Figure 2 shows the resonators and coupling arrangement. These resonators are arranged to realise couplings only between the adjacent resonators.

The following specifications are used in the design of the fifth order Chebyshev band-pass power splitter. The center frequency, f_o, is designed to be 2 GHz. The passband return loss of port 1, R_L, is 20 dB, a fractional bandwidth, Δ of 5% and a characteristics impedance, Z_o of 50 Ω.

The table below gives the normalized Low Pass (LP) parameters of the lumped circuit at a return loss of 20 dB.

Table 1. Lumped element g values, **reproduced courtesy of The Electromagnetics Academy**

g	g_1	g_2	g_3	g_4	g_5	g_6
1	0.9714	1.3721	1.8014	1.3721	0.9714	1

The expressions for coupling coefficient, $k_{n,m}$, and external quality factor, Q_{ext}, have been provided in Eqs. (3) and (4). k'_{12} and k'_{1B} represent the coupling between the common resonator 1 and the next resonator towards Port2 and Port3, respectively. This gives: $k'_{12} = k'_{1B} = 0.0306$, $k_{23} = k_{34} = k_{BC} = k_{CD} = 0.032$, $k_{45} = k_{DE} = 0.043$ and $Q_{ext,i} = Q_{ext,o} = \omega_o Z_o C = 19.428$.

To determine the coupling space between microstrip resonators, two coupled microstrip resonators are simulated, and the two resonance mode frequencies are extracted as f_1 and f_2, where f_1 is the lower resonance mode and f_2 the higher resonance mode. The coupling coefficient can be calculated as

$$k = \frac{f_2^2 - f_1^2}{f_2^2 + f_1^2} \quad \text{where } k \text{ is the coupling coefficient.} \tag{5}$$

Figure 5(a) shows the simulated curve of the coupling coefficients as a function of the coupling space between the microstrip resonators.

To determine the tapping point, t from the input and output resonators, the arrangement as shown in Figure 5(b) (inset) is designed and simulated. The insertion loss curve is used to determine the external quality factor, Q_{ext}, using:

$$Q_{ext} = \frac{f_0}{\delta f @ -3\,\text{dB}} \tag{6}$$

where $\delta f @ -3$ dB is the 3 dB bandwidth of the curve and f_0 the resonant frequency.

Figure 5(b) shows the external quality factor as a function of the tapped location along the microstrip resonator.

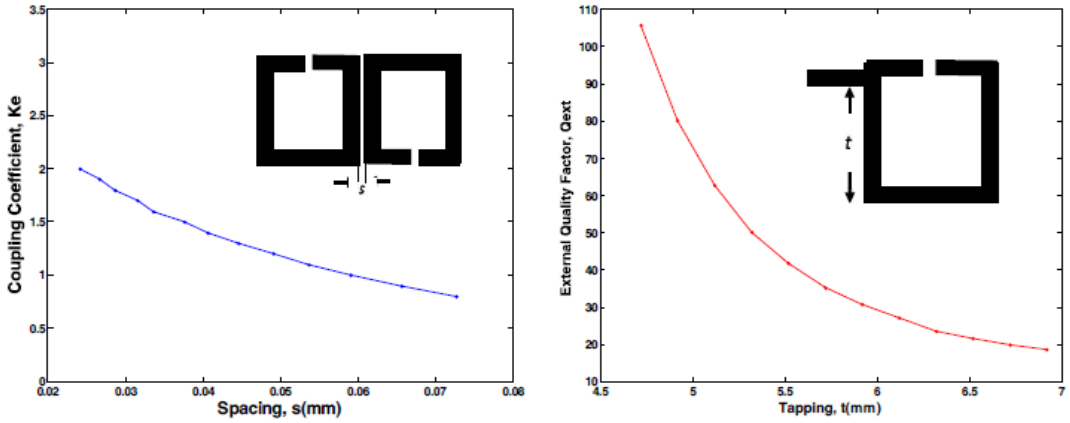

(a) (b)

Figure 5. (a) Coupling Coefficient against spacing. (b) External quality factor against tapping, **reproduced courtesy of The Electromagnetics Academy**

The graphs of Figure 5(a) and Figure 5(b) are used to determine the physical dimensions of the power splitter. From the graphs, the following are obtained: $s_{12} = s_{45} = s_{1B} = s_{DE} = 1.43\,\text{mm}$; $s_{23} = s_{34} = s_{BC} = s_{CD} = 1.77\,\text{mm}$ and $s'_{12} = s'_{1B} = 1.8\,\text{mm}$, $t = 6.88\,\text{mm}$.

3.2. Final Circuit Layout

The microstrip power splitter is achieved by using 9 multi-coupled SOLR as shown in Figure 6. Using Rogers RO3210 substrate with dielectric constant of 10.8 with loss tangent of 0.0023 and thickness of 1.27 mm, the designed circuit is fabricated on this substrate. A copper conductor with conductivity of 5.8×10^7 Siemens/m is used for the top and bottom of the microstrip. The figure also gives the final microstrip schematic layout including its physical dimensions. The effective area is measured $0.97\lambda_g \times 0.90\lambda_g = 0.873\lambda_g^2$, where λ_g is the guided wavelength in mm at 2 GHz. The physical dimensions are given in Table 2.

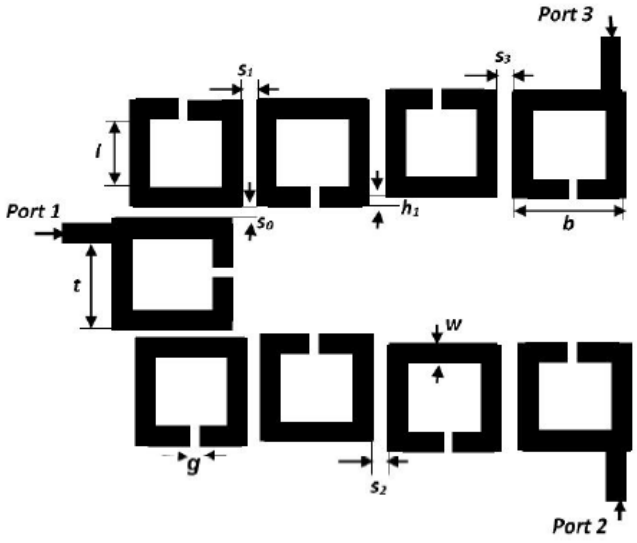

Figure 6. Microstrip schematic layout, **reproduced courtesy of The Electromagnetics Academy**

Table 2. Physical dimensions of the filtering power splitter (mm),
reproduced courtesy of The Electromagnetics Academy

Dimension	Value	Dimension	Value
s	1.28	h_1	0.61
s_1	1.65	g	0.44
s_2	1.39	w	1.12
s_3	1.57	t	6.88
l	7.00	b	8.12

4. SIMULATION AND MEASURED RESULT AND ANALYSIS

The full wave simulation is carried out in Keysight's ADS EM simulation platform. Printed circuit board technology is used to construct the circuit, and the proposed filtering power splitter is measured using Agilent Vector Network Analyser. The proposed splitter is designed to operate at 2 GHz. The values given in Table 2 are employed in realizing the power splitter layout given in Figure 6.

Figure 7 depicts the EM lossy simulation insertion loss of the input to the output ports ($|S_{21}|$ and $|S_{31}|$), and the return loss at input port ($|S_{11}|$). The measured return loss is better than 15 dB, and the

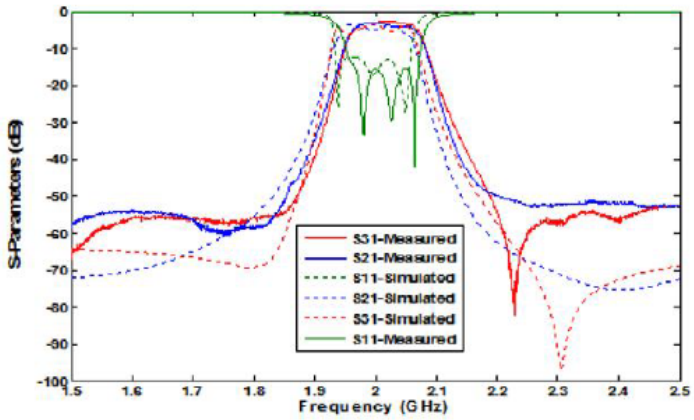

Figure 7. Simulated and measured responses of the fifth order filtering bandpass power filter,
reproduced courtesy of The Electromagnetics Academy

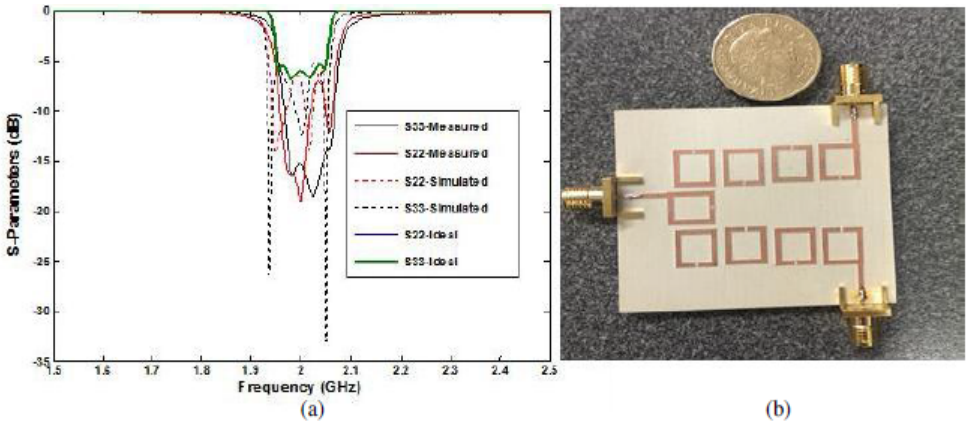

Figure 8. 5-pole filtered power splitter. (a) Output ports return loss results. (b) Pictorial view,
reproduced courtesy of The Electromagnetics Academy

insertion losses of port 2 and port 3 path are 3.12 dB and 2.99 dB ±18% of ripple, respectively. The fractional bandwidth is about 6%. In the EM simulation, the minimum return loss is approximately 20 dB, and the output ports insertion losses are at 3 dB while the fractional bandwidth for this design is 5%. The return loss responses of the output ports 2 and 3 ($|S_{22}|$ and $|S_{33}|$) are given in Figure 8(a), which shows that the ideal return losses on both ports are better than 5.40 dB. The return losses of output ports 2 and 3 are better than 13 dB and 6 dB, respectively for measured power splitter.

5. CONCLUSION

A fifth order Chebyshev Bandpass filtered power splitter is explored. The proposed design has eliminated the need for an additional power splitter when a filtered power splitter is required. The design is simulated and constructed. Measurement is also carried out to verify the design topology, in which there is reasonable good agreement between the simulated and measured results. This design topology validates the concept of the proposed design procedure, i.e., the power splitting can be achieved by merely changing the coupling coefficient of the adjacent resonators at the splitting point. However, there is a drawback in this design which is the isolation of the output ports and the poor matching of the output ports. The good isolation between ports 2 and 3 cannot be easily achieved in the current design. However, this proposed design is still useful for filtered power splitting applications where there is not signal returning from ports 2 and 3.

REFERENCES

1. Singh, P., S. Basu, and Y. H. Wang, "Coupled line power divider with compact size and bandpass response," *IEEE Electronics Letters*, Vol. 45, No. 17, 892–894, 2009.
2. Cheong, P., K. I., Lai, and K. W. Tam, "Compact Wilkinson power divider with simultaneous bandpass response and harmonic suppression," *IEEE MTT-S International. Microwave. Symposium. Digest*, 1588–1591, Anaheim, CA, USA, May 2010.
3. Shao, J. Y., S. C. Huang, and Y.-H. Pang, "Wilkinson power divider incorporating quasi-elliptic filters for improved out-of-band rejection," *IEEE Electronics Letters*, Vol. 47, No. 23, 1288–1289, 2011.
4. Chen, C. F., T. Y. Huang, T. M. Shen, and R. B. Wu, "Design of miniaturized filtering power dividers for system-in-a-package," *IEEE Transaction on Components, Packaging and Manufacturing Technology.*, Vol. 3, No. 10, 1663–1672, 2013.
5. Lee, G. A., M. A. Megahed, and F. D. Flaviis, "Low-cost compact spiral inductor resonator filters for system-in-a-package," *IEEE Transaction on Advanced Packaging*, Vol. 28, No. 4, 761–771, 2005.
6. Ma, K., K. S. Yeo, J. G. Ma, and M. A. Do, "An ultra-compact planar bandpass filter with open-ground spiral for wireless application," *IEEE Transaction on Advanced Packaging*, Vol. 31, No. 2, 285–291, 2008.
7. Cheon, S. J., S. P. Lim, and J. Y. Park, "Ultra-compact WiMAX bandpass filter embedded into a printed circuit board with a SrTiO3 composite layer," *IEEE Transaction on Components, Packaging and Manufacturing Technology*, Vol. 2, No. 3, 375–382, 2012.
8. Kuo, J. T. and E. Shih, "Microstrip stepped-impedance resonator bandpass filter with an extended optimal rejection bandwidth," *IEEE Transaction on Microwave, Theory and Techniques*, Vol. 51, No. 5, 1554–1559, 2003.
9. Chen, C. F., T. Y. Huang, and R. B. Wu, "A miniaturized net-type microstrip bandpass filter using $\lambda/8$ resonators," *IEEE Microwave and Wireless Components Letters*, Vol. 15, No. 7, 481–483, 2005.
10. Chen, C. F., T. Y. Huang, and R. B. Wu, "Novel compact net-type resonators and their applications to microstrip bandpass filters," *IEEE Transaction on Microwave, Theory and Techniques*, Vol. 52, No. 6,1554–1559, 2006.
11. Hong, J. S. and M. J. Lancaster, "Cross-coupled microstrip hairpin-resonator filters," *IEEE Transaction on Microwave, Theory and Techniques*, Vol. 46, No. 1, 118–122, 1998.

12. Lu, H. C., T. W. Chao, Y. L. Chang, T. B. Chan, and Y. T. Chou, "LTCC layer-to-layer misalignment-tolerant coupled inductors and their application to bandpass filter and helical inductors," *IEEE Transaction on Components, Packaging and Manufacturing Technology*, Vol. 1, No. 10,1608–1615, 2011.
13. Ladezma, L. and T. Weller, "Miniaturization of Microstrip Square Open Loop Resonator using surface mount capacitors," *Proceeding 12th Annual Wireless and Microwave Technology Conference*, 1–5, Florida, USA, April 2011.
14. Chen, C. F., T. Y. Huang, T. M. Shen, and R. B. Wu, "Design of miniaturised filtering power dividers for System in a parkage," *IEEE Transaction on Components, Packaging and Manufacturing Technology*, Vol. 3, No. 10, 1663–1672, 2013.
15. Lim, C. K. and S. J. Chung, "A filtering microstrip antenna array," *IEEE Transaction on Microwave, Theory and Techniques*, Vol. 59, No. 11, 2856–2863, 2011.
16. Pozar, D. M., *Microwave Engineering*, 4th Edition, John Wiley and Sons, New York, 2012
17. Hong, J. S., *Microstrip filter for RF/Microwave Applications*, 2nd edition, John Wiley and Sons, New York, 2011.
18. Hong, J. S. and M. J. Lancaster, "Coupling of microstrip square open-loop resonators for cross-coupled planar microwave filters," *IEEE Transaction on Microwave, Theory and Techniques*, Vol. 44, No. 12, 2099–2109, 1996
19. Yeung, L. K. and K. L. Wu, "An LTCC balanced-to-unbalanced extracted-pole bandpass filter with complex load," *IEEE Transaction on Microwave, Theory and Techniques*, Vol. 54, No. 4, 1512–1518, 2006.
20. Yeo, K. S. and M. J. Lancaster, "The design of microstrip six-pole quasi-elliptic filter with linear phase response using extracted-pole technique," *IEEE Transaction on Microwave, Theory and Techniques*, Vol. 49, No. 2, 321–327, 2001.

Journal of Microwaves, Optoelectronics and Electromagnetic Applications, Vol. 16, No. 2, June 2017 393
DOI: http://dx.doi.org/10.1590/2179-10742017v16i2793

Substrate Integrated Waveguide (SIW) Bandpass Filter with Novel Microstrip-CPW-SIW Input Coupling

Augustine O. Nwajana, Amadu Dainkeh, Kenneth S. K. Yeo
Electrical and Electronic Engineering Department, University of East London, London E16 2RD, UK
a.nwajana@ieee.org, a.dainkeh@uel.ac.uk, k.yeo@uel.ac.uk

***Abstract*— A Substrate integrated waveguide bandpass filter is presented with a novel CPW-to-SIW transition at both the input and output ports which also served as the input and output couplings into the filter. The CPW-to-SIW transition structures presented here exploited the step impedance between the 50 ohms input/output feedline and the transition to control the input/output couplings of the filter. The SIW filter is also shown to have very minimum milling or etching requirement which reduces the fabrication error. The proposed SIW filter has been validated experimentally and results presented. The results show that a simulated return loss of 15 dB and an initial measured return loss of 16 dB were achieved. An improved measured return loss of 22 dB was later achieved after some tuining adjustments were performed on the filter input and output couplings. A minimum insertion loss of 1.3 dB was also achieved across the band.**

Index Terms— Bandpass filter, coplanar waveguide (CPW), coupling, substrate integrated waveguide (SIW).

I. INTRODUCTION

Substrate integrated waveguide (SIW) is a new type of transmission line that has evolved since the inception of the twenty-first century. This new technology has become popular in the past decade as it has opened new doors to the design of efficient microwave and millimetre-wave circuits at low cost. This new technology implements a conventional air-filled rectangular waveguide on a piece of printed circuit board (PCB) by replacing the side walls of the waveguide with two rows of metallic posts also known as via holes [1]. The SIW inherits the advantages of the microstrip, i.e. compact size and easy integration, but maintaining some of its waveguide characteristic, i.e. low radiation loss, high unloaded quality factor (Q-factor), as well as the high power handling characteristics. SIW as a transmission line is well established with details equations governing its physical structures, i.e. propagation mode, width of the transmission line and size of the metallic post, reported in [2].

Various authors have reported bandpass filters (BPFs) implemented with different transmission line technologies including: microstrip [3], waveguide [4], and SIW [5]. A BPF is a device that passes frequencies within a single band while rejecting all other frequencies outside the band [6], [7]. BPFs are crucial components in wireless communication systems to reject unwanted spectrum from the communication channels. Some design factors or parameters of filters such as selectivity, cost, size,

Brazilian Microwave and Optoelectronics Society-SBMO *received 16 Sept 2016; for review 22 Sept 2016; accepted 01 Feb 2017*
Brazilian Society of Electromagnetism-SBMag *ISSN 2179-1074*

Journal of Microwaves, Optoelectronics and Electromagnetic Applications, Vol. 16, No. 2, June 2017 394
DOI: http://dx.doi.org/10.1590/2179-10742017v16i2793

sensitivity to environmental effects, power handling capacity, in-band and out-of-band performance metrics, are critical specifications when it comes to the development of radio frequency (RF) and microwave communication front ends. Designers are often required to make compromise between several conflicting requirements as it is rather difficult or even physically and/or electrically impossible to simultaneously achieve all design criteria or specifications. For instance, achieving higher channel selectivity usually requires the use of more resonators, which will result in higher insertion loss along the transmission path [8].

Transition between planar transmission lines and SIW structures are a vital element related to SIW devices [9]. A number of publications have presented SIW research findings with various types of input/output transitions. Microstrip-to-SIW transitions based on a simple taper have been presented in [10], [11]. The tapered section connects a 50 Ohms microstrip line and the SIW. The taper is used for transforming the quasi-TEM mode in the microstrip line into the TE_{10} mode in the SIW. Coplanar waveguide (CPW)-to-SIW transition based on a 90^{o} bend has also been proposed [12]. Another form of transition between a grounded coplanar waveguide (GCPW) and SIW based on a current probe was presented in [13]. The current flowing through the probe generates a magnetic field that matches with the magnetic field inside the SIW structure. Transitions between air-filled waveguide and SIW structure have also been presented [14], [15]. Microstrip-to-SIW transition in a multi-layer substrate have also been investigated and presented in [16]. The work presented in this paper employs a novel Microstirp-CPW-SIW transition as the input/output coupling to the filter's resonator. The proposed transition model makes it easy for RF and microwave designers to achieve controllable external Q-factor for filter design. The transition employs a step impedance from 50 Ohms microstrip to a low impedance GCPW before coupling into the filter using the short low impedance GCPW transmission line. This transition as an input/output coupling for filter is shown to be very efficient as it allows two degrees of freedom in controlling the input/output coupling, i.e. the input/output coupling or the external Q-factor can be varied by either changing the step impedance of the CPW or the length of the short CPW transmission line.

II. SIW DESIGN

Substrate integrated waveguide (SIW) is a planar transmission line with some inherited properties of rectangular waveguide as mentioned in the introduction. The physical structure of an SIW transmission line is shown in Fig. 1. The SIW transmission line itself consist of two metallic plates sandwiched by a dielectric material (dielectric substrate). Two rows of periodic metallic posts run along the length of the substrate to mimic the metallic sidewall of a rectangular waveguide.

Brazilian Microwave and Optoelectronics Society-SBMO *received 16 Sept 2016; for review 22 Sept 2016; accepted 01 Feb 2017*
Brazilian Society of Electromagnetism-SBMag *ISSN 2179-1074*

Journal of Microwaves, Optoelectronics and Electromagnetic Applications, Vol. 16, No. 2, June 2017 395
DOI: http://dx.doi.org/10.1590/2179-10742017v16i2793

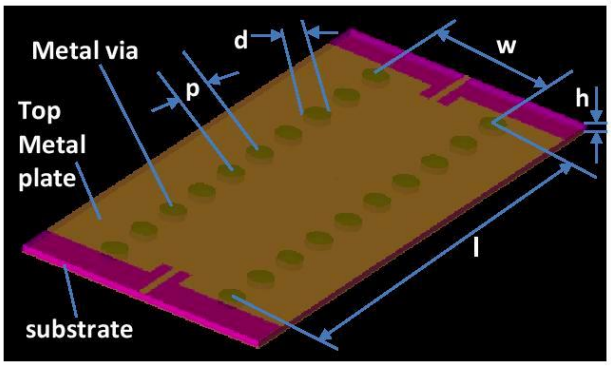

Fig. 1. Substrate integrated waveguide cavity.

To design a SIW transmission line to operate at a given frequency, there are three main design parameters that need to be considered. There are namely; the width of the SIW, w; the diameter of the metallic post, d; and the distance between the metallic posts (also commonly known as the pitch), p. The width of the SIW governs the cut-off frequencies of the propagation mode of the SIW transmission line in the same way as it does with width of the rectangular waveguide. The parameters, d and p, determine how well the SIW transmission line mimics the rectangular waveguide itself. If p is reduced to d/2, the SIW transmission line is effectively reduced to a dielectric filled rectangular waveguide. The larger p becomes the worst it diverges from a rectangular waveguide with electromagnetic energies leaking or radiating out between the metallic posts. According to a study in [17], for an electrically small metallic post, i.e. $d < 0.2\lambda$ where λ is the wavelength of signal propagating in the dielectric material, the radiation loss is negligible when the ratio of d/p is 0.5. For a constant ratio of d/p, the radiation loss decreases as the size of the metallic post get smaller which is conditioned by the fabrication process [18]. It is important to note that the ratio d/p is considered to be more critical than the values for p and d alone.

The size of an SIW cavity, for the fundamental TE_{101} mode, can be determined using the corresponding resonance frequency mode, f_{101} given in (1) [19] where w_{eff} and l_{eff} are the effective width and length of the SIW cavity, μ_r is the relative permeability (which is 1 for non-magnetic substrate) of the substrate, and c_0 is the speed of light in free space. The empirical formulation for w_{eff} and l_{eff} are given in (2) [1].

$$f_{101} = \frac{c_0}{2\pi\sqrt{\mu_r \varepsilon_r}} \sqrt{\left(\frac{\pi}{w_{eff}}\right)^2 + \left(\frac{\pi}{l_{eff}}\right)^2} \tag{1}$$

$$w_{eff} = w - 1.08\frac{d^2}{p} + 0.1\frac{d^2}{w}\ ; \qquad l_{eff} = l - 1.08\frac{d^2}{p} + 0.1\frac{d^2}{l} \tag{2}$$

Brazilian Microwave and Optoelectronics Society-SBMO *received 16 Sept 2016; for review 22 Sept 2016; accepted 01 Feb 2017*
Brazilian Society of Electromagnetism-SBMag *ISSN 2179-1074*

Journal of Microwaves, Optoelectronics and Electromagnetic Applications, Vol. 16, No. 2, June 2017 396
DOI: http://dx.doi.org/10.1590/2179-10742017v16i2793

III. BANDPASS FILTER CIRCUIT MODEL

The test BPF reported in this paper was designed with the following specifications: center frequency f_0, 1684 MHz; fractional bandwidth FBW, 4%; and passband return loss RL, 20 dB. The BPF circuit model was designed based on the technique detailed in [18] and applied in [20]. As explained in [18], [20]; L, C and J are the inductance, capacitance and J-inverter values, respectively. The numerical design parameters for the BPF are shown in Table 1. The lossless circuit model with identical parallel LC resonators and J-inverters is shown in Fig. 2a. The BPF circuit model was simulated using the Agilent Advanced Design System (ADS) circuit simulator. The couplings between resonators were modelled using the method described in [18], i.e. modelling each J-inverter on the circuit model with a pi-network of capacitors. The simulation responses of the test BPF circuit model are shown in Fig. 2b.

TABLE I. 3-POLE CHEBYSHEV BANDPASS FILTER DESIGN PARAMETERS

Filter	f_0 [MHz]	L [nH]	C [pF]	J_{01}	J_{12}
BPF	1684	0.222	40.2424	0.02	0.0176

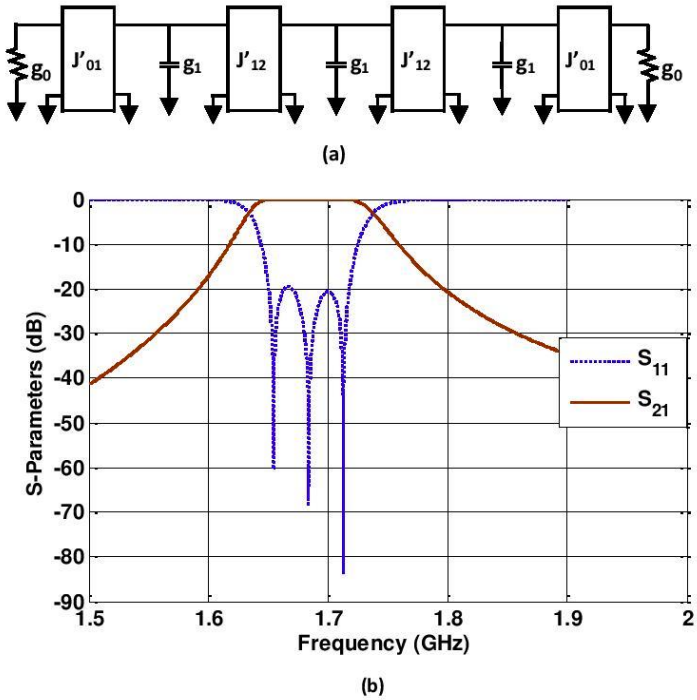

Fig. 2. 3-pole Chebyshev bandpass filter. (a) Circuit model with ideal LC resonators and J-inverters. (b) Simulation responses.

Brazilian Microwave and Optoelectronics Society-SBMO *received 16 Sept 2016; for review 22 Sept 2016; accepted 01 Feb 2017*
Brazilian Society of Electromagnetism-SBMag *ISSN 2179-1074*

Journal of Microwaves, Optoelectronics and Electromagnetic Applications, Vol. 16, No. 2, June 2017 397
DOI: http://dx.doi.org/10.1590/2179-10742017v16i2793

IV. DESIGN AND SIMULATION

The SIW cavity for the test BPF was designed to resonate at the TE_{101} mode resonance frequency, f_0 of 1684 MHz using (1). The filter was designed on a Rogers RT/Duroid 6010LM substrate with ε_r = 10.8, h = 1.27 mm and μ_r = 1. The SIW design parameters were chosen as follows: d = 2 mm, p = 3.725 mm, w = 37.25 mm, and l = 37.25 mm.

All electromagnetic (EM) simulations were carried out using the finite-element method (FEM) of the Keysight electromagnetic professional (EMPro) 3D simulator. A loss tangent, tan δ = 0.0023 was assumed for the substrate, and a conductivity, $\sigma = 5.8 \times 10^7$ S/m for all the metals (copper) with 17 microns (µm) thickness. In order to achieve faster simulation results convergence, each metallized via was implemented as an octadecagon (18 sided polygons).

The theoretical value of the coupling coefficient, k_t, for the filter was determined using (3), where FBW is the filter fractional bandwidth of 4%; J_{12}, L, and C correspond to the values given in Table 1. The simulated value of the coupling coefficient, k, between each pair of SIW cavities were determined using the technique shown in Fig. 3 and using (4), where f_1 and f_2 are the Eigen-modes from simulating a pair of SIW cavities. The value of k that was used to achieve the test filter is k = 0.041 at s = 13.05 mm.

$$k_t = J_{12}\sqrt{\frac{L}{C}} \tag{3}$$

$$k = \frac{f_2^2 - f_1^2}{f_2^2 + f_1^2} \tag{4}$$

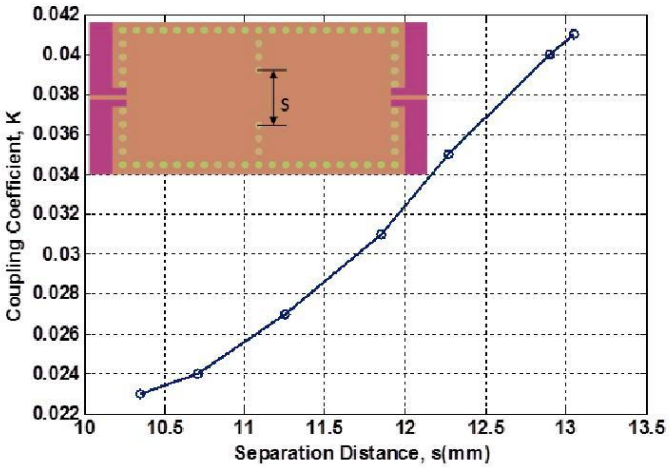

Fig. 3. Coupling coefficient of a pair of substrate integrated waveguide cavities.

Brazilian Microwave and Optoelectronics Society-SBMO *received 16 Sept 2016; for review 22 Sept 2016; accepted 01 Feb 2017*
Brazilian Society of Electromagnetism-SBMag *ISSN 2179-1074*

Journal of Microwaves, Optoelectronics and Electromagnetic Applications, Vol. 16, No. 2, June 2017 398
DOI: http://dx.doi.org/10.1590/2179-10742017v16i2793

The theoretical external quality factor, Q_{ext}, of the filter was extracted using (5), where f_0, J_{01}, and C correspond to the values given in Table 1. Based on (5), the theoretical Q_{ext} value for the test SIW bandpass filter is 21.21. The simulated Q_{ext} value was based on the method shown in Fig. 4. The length corresponding to the 50 Ohms impedance (Z_0) of the microstrip transmission line was determined using the widely known formulations reported in [14]. The impedance (Z_1), at the SIW end of the transition was achieved by adjusting the lengths, a and b, until the required filter Q_{ext} value of 21.21 was achieved. A graph showing the variation of Q_{ext} with a, at constant b (i.e. b = 8.13 mm) is presented in Fig. 5a. Another graph showing the variation of Q_{ext} with b, at constant a (i.e. a = 0.7 mm) is also presented in Fig. 5b. The value of Z_1 that corresponds to the required Q_{ext} value of 21.21 is 24 Ohms. This characteristic impedance value was worked-out by using the length, y_1 (from Fig. 6 and Table 2) and the widely known formulations reported in [18]. It is important to note that an increase in the length, a, would lead to an increase in the characteristic impedance, Z_1, and vice versa.

$$Q_{ext} = \frac{2\pi f_0 C}{J_{01}} \tag{5}$$

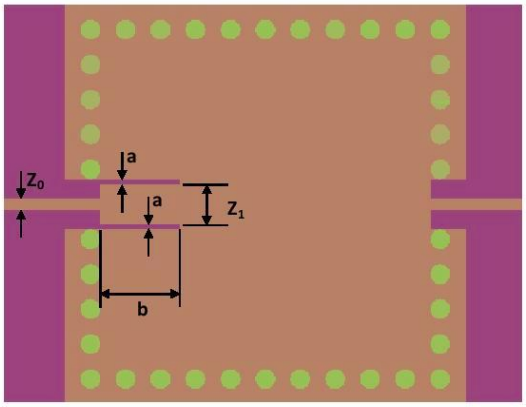

Fig. 4. Microstrip-CPW-SIW input coupling structure for extracting the external Q-factor.

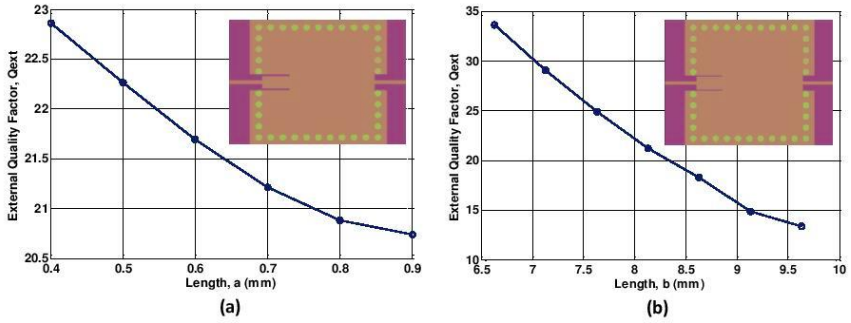

Fig. 5. Graphs for extracting the external Q-factor, Q_{ext}. (a) Variation of Q_{ext}, with length, a, at constant length, b = 8.13 mm. (b) Variation of Q_{ext}, with length, b, at constant length, a = 0.7 mm.

Brazilian Microwave and Optoelectronics Society-SBMO *received 16 Sept 2016; for review 22 Sept 2016; accepted 01 Feb 2017*
Brazilian Society of Electromagnetism-SBMag *ISSN 2179-1074*

Journal of Microwaves, Optoelectronics and Electromagnetic Applications, Vol. 16, No. 2, June 2017 399
DOI: http://dx.doi.org/10.1590/2179-10742017v16i2793

The complete FEM layout of the SIW BPF that was simulated using the Keysight EMPro 3D simulator is shown in Fig. 6, with all the physical dimensions for the filter shown in Table 2. The simulation responses of the proposed filter are presented in Fig. 7. It could be seen from the simulation results that the center frequency of the filter is about 1.68 GHz as designed. A simulated minimum insertion loss (S_{21}) at the passband of 1.3 dB was achieved. The simulated return loss (S_{11}) is better than 14.6 dB across the passband. The filter passband is based on the fractional bandwidth specification and can be controlled by the input/output coupling and the couplings between each pair of SIW cavities. According to [17], [18]; the distance between neighbouring metal vias *p* should be made equal or less than double the diameter of the metal via *d* (i.e. $p \leq 2d$) for best results. The larger the values of p and b, the higher the electromagnetic leakage through the vias. This means higher radiation losses which negatively affect the filter insertion and return losses. The radiation loss becomes negligible at $p = 2d$ as explained in [17].

TABLE II. PHYSICAL DIMENSIONS OF THE SIW BANDPASS FILTER

Dimension	Value [mm]	Dimension	Value [mm]
x_1	8.125	y_1	3.9
x_2	37.25	y_2	0.7
x_3	111.75	y_3	1.1
d	2.0	y_4	37.25
p	3.725	s_1	13.05

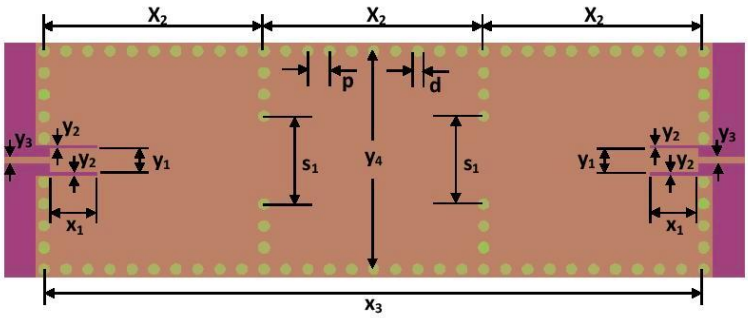

Fig. 6. Substrate integrated waveguide bandpass filter layout with dimensions.

Brazilian Microwave and Optoelectronics Society-SBMO *received 16 Sept 2016; for review 22 Sept 2016; accepted 01 Feb 2017*
Brazilian Society of Electromagnetism-SBMag *ISSN 2179-1074*

Journal of Microwaves, Optoelectronics and Electromagnetic Applications, Vol. 16, No. 2, June 2017 400
DOI: http://dx.doi.org/10.1590/2179-10742017v16i2793

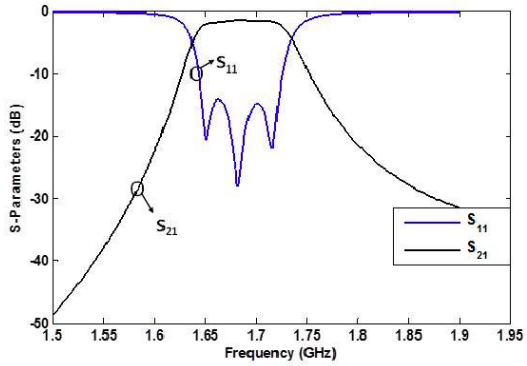

Fig. 7. Simulation responses of the substrate integrated waveguide bandpass filter.

V. FABRICATION AND MEASUREMENT

The SIW bandpass filter was fabricated using the same material employed in the FEM simulation. The fabrication was based on printed circuit board (PCB) micro-milling process using the "Leiterplatten-Kopierfräsen" (LKPF) Protomat C60. The photograph of the fabricated filter is shown in Fig. 8. In order to facilitate measurement of the filter, two SMA (Sub-Miniature version A) connectors were fitted onto the input and output ports as shown. The fabricated filter was measured using the Agilent Vector Network Analyzer. Fig. 9 shows the measured results indicating that a minimum insertion loss (S_{21}) of 1.3 dB was achieved at the passband. The minimum simulated and initial measured return losses (S_{11}) of 15 dB and 16 dB were respectively achieved across the passband. An improved measured return loss of better than 22 dB across the passband was later achieved after some tuning adjustments were made at the input/output couplings. The improved return loss is shown in Fig. 9b. The measurement and simulation results are jointly presented in Fig. 10 for ease of comparison. It is clear from Fig. 10 that the simulation and the initial measurement results are in good agreement. The improved measured return loss of 22 dB shown in Fig. 10 was achieved by tuining the filter input and output couplings, while viewing the responses on a vector network analyzer. The electrical size of the bandpass filter reported in this paper is $0.21\lambda_g$ x $0.63\lambda_g$ which is more compact than the waveguide filter reported in [4], but less compact when compared to the microstrip filter reported in [3]. In general, SIW filters are normally smaller in size when compared to waveguide filters, but are relatively larger in size when compared to microstrip filters. The return loss of the filter reported in this paper is slightly better than that reported in page 2569 of [4] where the measured return loss is about 11 dB, as opposed to the minimum measured return loss of 16 dB achievd here. The roll-off factor and band rejection of our simulated and measured results are very steepy and in good agreement when compared to that of the filter presented in [4].

Brazilian Microwave and Optoelectronics Society-SBMO *received 16 Sept 2016; for review 22 Sept 2016; accepted 01 Feb 2017*
Brazilian Society of Electromagnetism-SBMag *ISSN 2179-1074*

Journal of Microwaves, Optoelectronics and Electromagnetic Applications, Vol. 16, No. 2, June 2017 401
DOI: http://dx.doi.org/10.1590/2179-10742017v16i2793

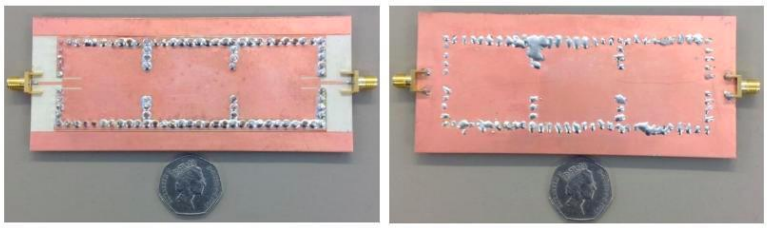

Fig. 8. Fabricated SIW bandpass filter photograph. (a) Top view. (b) Bottom view.

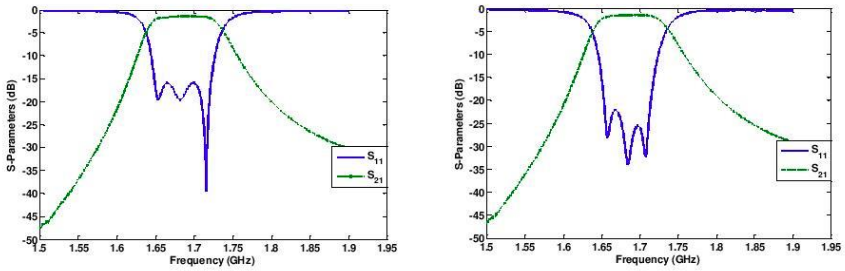

Fig. 9. Measurement results of the SIW bandpass filter. (a) Without tuning. (b) After tuning.

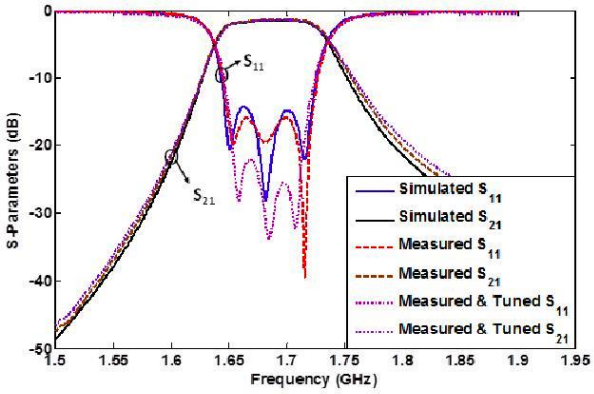

Fig. 10. Comparison of the simulated and measured results of the filter.

VI. CONCLUSION

A substrate integrated waveguide bandpass filter with a new type of Microstrip-CPW- SIW input coupling has been presented. The proposed filter has been designed, simulated, manufactured and

Brazilian Microwave and Optoelectronics Society-SBMO *received 16 Sept 2016; for review 22 Sept 2016; accepted 01 Feb 2017*
Brazilian Society of Electromagnetism-SBMag *ISSN 2179-1074*

Journal of Microwaves, Optoelectronics and Electromagnetic Applications, Vol. 16, No. 2, June 2017 402
DOI: http://dx.doi.org/10.1590/2179-10742017v16i2793

measured. The Microstrip-CPW-SIW transition employed as the input coupling in the design allows two degrees of freedom in controlling the external Q-factor. Stepping the 50 Ohms feedline impedance to a lower impedance at the SIW end of the transition makes it easier to realize the required filter external quality factor, Q_{ext}. Changing the impedance at the SIW end of the transition, changes the Q_{ext}. The experimentally verified results show that a minimum insertion loss of 1.3 dB was achieved across the band. An initial measured minimum return loss of 16 dB was achieved before any tuning was performed on the input/output ports. With some tuning on the filter input and output couplings, a slight improvement of return loss was achieved with a measured minimum of 22 dB. The results presented show that there is a good agreement between the simulated and measured filter responses. Due to the minimum milling/etching of this particular design, a very good agreement between simulation and raw experimental results was achieved.

REFERENCES

[1] S. H. Han, X. L. Wang, Y. Fan, Z. Q. Yang, and Z. N. He, "The generalized Chebyshev substrate integrated waveguide diplexer," *Progress in Electromagnetic Research*, vol. 73, pp. 29–38, 2007.
[2] D. Deslandes, and K. Wu, "Accurate modelling, wave mechanisms, and design considerations of a substrate integrated waveguide"' *IEEE Trans. Microw. Theory and Techn.*, vol. 56, no. 6, pp. 2516–2526, Jun. 2006.
[3] C.-F. Chen, S.-F. Chang, and B.-H. Tseng, "Design of compact microstrip sept-band bandpass filter with flexible passband allocation," *IEEE Microw. Wireless Compon. Lett.*, vol. 26, no. 5, pp. 346-348, May 2016.
[4] N. Mohottige, O. Glubokov, U. Jankovic, and D. Budimir, "Ultra compact inline E-plane waveguide bandpass filter using cross coupling," *IEEE Trans. Microw. Theory and Techn.*, vol. 64, no. 8, pp. 2561–2571, Aug. 2016.
[5] A. Rhbanou, M. Sabbane, and S. Bri, "Design of K-band substrate integrated waveguide band-pass filter with high rejection," *J. of Microw., Optoelectronics and Electromagnetic Applications*, vol. 14, no. 2, pp. 155-169, Dec. 2015.
[6] A. O. Nwajana and K. S. K. Yeo, "Microwave diplexer purely based on direct synchronous and asynchronous coupling," *Radioengineering*, vol. 25, no. 2, pp. 247–252, Jun. 2016.
[7] A. O. Nwajana and K. S. K. Yeo, "Multi-coupled resonator microwave diplexer with high isolation," *in Proc. 46th Eur. Microw. Conf., IEEE*, Oct. 2016, pp. 1167–1170.
[8] X.-P. Chen and K. Wu, "Substrate integrated waveguide filter: basic design rules and fundamental structure features," *IEEE Microw. Mag.*, vol. 15, no. 5, pp. 108–116, Jul. 2014.
[9] M. Bozzi, A. Georgiadis, and K. Wu, "Review of substrate-integrated waveguide circuits and antennas," IET Microw., Antennas & Propagation, vol. 5, no. 8, pp. 909–920, Jun. 2011.
[10] D. Deslandes and K. Wu, "Integrated microstrip and rectangular waveguide in planar form," *IEEE Microw. Wireless Compon. Lett.*, vol. 11, no. 2, pp. 68-70, Feb. 2001.
[11] D. Deslandes, "Design equations for tapered microstrip-to-Substrate Integrated Waveguide transitions," *IEEE MTT-S Int. Microw. Symp. Dig.*, May. 2010, pp. 704–707.
[12] D. Deslandes and K. Wu, "Integrated transition of coplanar to rectangular waveguides," *IEEE MTT-S Int. Microw. Symp. Dig.*, vol. 2, May 2001, pp. 619–622.
[13] D. Deslandes and K. Wu, "Analysis and design of current probe transition from grounded coplanar to substrate integrated rectangular waveguides," *IEEE Trans. Microw. Theory and Techn.*, vol. 53, no. 8, pp. 2487–2494, Aug. 2005.
[14] Y. Huang and K. L. Wu, "A broad-band LTCC integrated transition of laminated waveguide to air-filled waveguide for millimeter-wave applications," *IEEE Trans. Microw. Theory and Techn.*, vol. 51, no. 5, pp. 1613–1617, May 2003.
[15] L. Xia, R. Xu, B. Yan, J. Li, Y. Guo, and J. Wang, "Broadband transition between air-filled waveguide and substrate integrated waveguide," *IET Electron. Lett.*, vol. 42, no. 24, pp. 1403–1405, Nov. 2006.
[16] Y. Ding and K. Wu, "Substrate integrated waveguide-to-microstrip transition in multilayer substrate," *IEEE Trans. Microw. Theory and Techn.*, vol. 55, no. 12, pp. 2839–2844, Dec. 2007.
[17] D. Deslandes and K. Wu, "Single-substrate integration technique of planar circuits and waveguide filters," *IEEE Trans. Microw. Theory and Techn.*, vol. 51, no. 2, pp. 593–596, Feb. 2003.
[18] J.-S. Hong, *Microstrip Filters for RF/Microwave Applications*. New York, NY, USA: 2011.
[19] X. Chen, W. Hong, T. Cui, J. Chen, and K. Wu, "Substrate integrated waveguide (SIW) linear phase filter," *IEEE Microw. Wireless Compon. Lett.*, vol. 15, no. 11, pp. 787-789, Nov. 2005.
[20] K. S. K. Yeo and A. O. Nwajana, "A novel microstrip dual-band bandpass filter using dual-mode square patch resonators," *Progress in Electromagnetic Research C*, vol. 36, pp. 233–247, 2013.

Brazilian Microwave and Optoelectronics Society-SBMO *received 16 Sept 2016; for review 22 Sept 2016; accepted 01 Feb 2017*
Brazilian Society of Electromagnetism-SBMag *ISSN 2179-1074*

APPENDIX B MATLAB Codes

1. Filter/PS design code

```
% MATLAB code developed to generate solution for filter and power
splitter
% design parameters
% Matlab Code
clear all
%calculation for ripple factor(e)%
Rl=20; % return loss in dB used in the specification
e=sqrt(10^(-Rl/10)); % e is ripple factor
%calculate the value of AP, the passband ripple
AP=10*log10(e^2+1);
%calculate the value \beta(b)
b=log(coth(AP/17.37)); % beta is one of the normalised lowpass empirical
variables
% N=5 pole filter, calculate the value of gamma(Y)%
% However, N can be 3,7,9 etc, N=5 because its 5-pole filter
n=5;
% calculating the value \gamma (Y)
Y=sinh(b/(2*n));
%calculate values of a,d and the normalized parameters(g)%
a=zeros(n,1); %This initialises the matrix in 'n' row and one column
d=zeros(n,1); % The results will be in sequence
m = n+1;
g0=1; % As given in the design, this is the first normalised parameter
g(n+1)=1; % this is the last normalised parameter
for k=1:n; % using the "for" loop for k=1, loops till k=n taking steps of
1
    a(k)=sin(pi*(2*k-1)/(2*n));
    d(k)=(Y^2)+(sin((pi*k)/n))^2;
    g=zeros(n,1);
    g(1)=2*a(1)/Y;
    for k=2:n;
    g(k)=(4*a(k)*(a(k-1)))/(d(k-1)*g(k-1));
    end
end
%declare the value of centre frequency (fo)%
Fo=2*10^9; % The centre frequency is 2GHz
Wo=2*pi*Fo;
%fractional bandwidth(fb)%
fb=0.05; % fb was used as 5%
%input and output impedance(R0)
Ro=50;
%Transforming the normalized values to bandpass values
g0=g0*Ro;
g(n+1)=Ro;
C=zeros(n,1);
L=zeros(n,1);
% for k is odd we use thus:
for k=1:2:n;
    C(k)=g(k)/(fb*Wo*Ro);
    L(k)=(fb*Ro)/(g(k)*Wo);
```

```
end
% for k is even we use thus:
for k=2:2:n
    C(k)=(fb)/(g(k)*Wo*Ro);
    L(k)=(g(k)*Ro)/(Wo*fb);
end
%making all g =gl by changing all J inverter(J) values%
m = n+1; % this is because for j inverter, its one term more than g terms
j=zeros(m,1);
% Making all the capacitors equal
j(1)=1; % This represents J0,1
j(m)=1; % This represents Jn,n+1
for t=2:n % since the first term have been defined so the second term
starts
    j(t)=sqrt(g(1)^2/(g(t-1)*g(t)));% shows, J'12,J'23,J'34, etc
end
%frequency and impedance scaling of Lp filter making all g1=C1
jj=zeros(m,1);
C1=g(1)/(Wo*Ro);% this is the capacitor value that is same across in
cascation with J inverters
jj(1)=j(1)/Ro; % where jj(1) means J'0,1
jj(m)=j(m)/Ro; % where jj(m) means J'n,n+1
for t=2:n
    jj(t)=j(t)/Ro; % where jj(2) means J''1,2 and so on
end
%converting the scaled Low pass (LP) to Bandpass (BP)
CC1=C1/fb;% This is the capacitor value that is used in the parallel LC
(Resonator)
L1=1/((Wo^2)*CC1);% This is the Inductor value that is used in the
parallel LC (Resonator)
%
%Question calculate the coupling parameters
% To calculate the Coupling coefficient (Ke)
ke12=jj(2)*sqrt(L1/CC1);%This is Coupling coefficient between resonator
1&2
ke23=jj(3)*sqrt(L1/CC1);%This is Coupling coefficient between resonator
2&3
ke34=jj(4)*sqrt(L1/CC1);%This is Coupling coefficient between resonator
3&4
ke45=jj(5)*sqrt(L1/CC1);%This is Coupling coefficient between resonator
4&5
kke12=((jj(2)/sqrt(2))*sqrt(L1/CC1));
UKKE1B=((jj(2)/sqrt(3))*sqrt(L1/CC1)); %This is Coupling coefficient
between common resonator 1&B to port 1
UKKE12=((jj(2)/sqrt(3/2))*sqrt(L1/CC1)); %This is Coupling coefficient
between common resonator 1&2 to port 2

%To calculate the External quality factor (Qext)
Qext= (Wo*CC1)/jj(1);
CJ01=jj(1)/Wo; % CJ01 is capaitance value when converted from J inverters
CJ12=jj(2)/Wo;
CJ23=jj(3)/Wo;
CJ34=jj(4)/Wo;
CJ45=jj(5)/Wo;
CJ56=jj(m)/Wo;
CJJ12=((jj(2)/sqrt(2))/Wo); % This is the new J value, between the common
resonator and the next one
```

```
UCJJ1B=((jj(2)/sqrt(3))/Wo); % This is the new J value, between the
common resonator and the next one for the port 1
UCJJ12=((jj(2)/sqrt(3/2))/Wo); % This is the new J value, between the
common resonator and the next one for the port 2


% To Determine the band pass filter response
% To analyse the LC bandpass filter using ABCD matrix and S-parameters:
f=[1.5e9:0.1e6:2.5e9]; % taking frequency starting @ 1.5GHz and end @
2.5GHz with step of 1MHz
Zo=50; % characteristics impedance
R1=zeros(2,2,length(f)); % These values are needed for calculating ABCD
matrix (not mentioned in thesis)
R2=zeros(2,2,length(f)); % This will solve the 2x2 matrix, ie
S11,S12,S21,S22 upto the length of frequency
R3=zeros(2,2,length(f));
R4=zeros(2,2,length(f));
R5=zeros(2,2,length(f));
W=zeros(length(f),1); % this is the angular frequency for different value
of f
ABCD=zeros(2,2,length(f)); % This is the ABCD Matrix
S=zeros(2,2,length(f)); % this is the S-Parameters
DEN=zeros(length(f),1); % Denominator in Conversion to S-Parameters
matrix
RL=zeros(length(f),1); % This is the value of the Return loss to analyse
IL=zeros(length(f),1); % This is the value of the Insertion loss to
analyse
for r=1:length(f);
    W(r)=2*pi*f(r);
    R1(:,:,r)=[1,0;(1/(W(r)*L(1)*i)),1]*[1,0;(W(r)*C(1)*i),1];
    R2(:,:,r)=[1,(W(r)*L(2)*i);0,1]*[1,(1/(W(r)*C(2)*i));0,1];
    R3(:,:,r)=[1,0;(1/(W(r)*L(3)*i)),1]*[1,0;(W(r)*C(3)*i),1];
    R4(:,:,r)=[1,(W(r)*L(4)*i);0,1]*[1,(1/(W(r)*C(4)*i));0,1];
    R5(:,:,r)=[1,0;(1/(W(r)*L(5)*i)),1]*[1,0;(W(r)*C(5)*i),1];
    ABCD(:,:,r)=R1(:,:,r)*R2(:,:,r)*R3(:,:,r)*R4(:,:,r)*R5(:,:,r);

DEN(r)=(Zo*ABCD(1,1,r))+ABCD(1,2,r)+((Zo^2)*ABCD(2,1,r))+(Zo*ABCD(2,2,r))
;
    S(:,:,r)=[((Zo*ABCD(1,1,r))+ABCD(1,2,r)-((Zo^2)*ABCD(2,1,r))-
(Zo*ABCD(2,2,r))),((2*Zo)*((ABCD(1,1,r)*ABCD(2,2,r))-
(ABCD(1,2,r)*ABCD(2,1,r))));(2*Zo),(-(Zo*ABCD(1,1,r))+ABCD(1,2,r)-
((Zo^2)*ABCD(2,1,r))+(Zo*ABCD(2,2,r)))]/DEN(r);
    RL(r)=20*log10(abs(S(1,1,r)));  %RL is the return loss curve
    IL(r)=20*log10(abs(S(2,1,r)));  % IL is the insertion loss curve
end
figure(1);
title('Insertion and Return loss graphs');
xlabel('Frequency in Hz');
ylabel('Insertion and Return loss in dB');
plot(f,RL,'-r');% This will plot the Return Loss curve (the red curve)
hold on; % Its the command which make two or more curves in the same
graph
plot(f,IL,'Bl'); % This will plot the Insertion Loss curve (the blue
curve)
grid on; % It will show the lines of the graph

To calculate the resonator parameters
```

```
Zo=50;
er=10.8; % this is the dielectric constant of the substrate material
h=1.27; % thickness
A=(Zo/60*sqrt((er+1)/2)+((er-1)/(er+1)*(0.23+0.11/er)));
B=377*pi/(2*Zo*sqrt(4.4));
M=(8*exp(A)/(exp(2*A)-2));
Co=3*10^11; % velocity of light (mm per second squared)
%if M<=2;
     w=M*h;
   % if M>2;
    %w=((2/pi)*((B-1-log((2*B)-1))+(((er-1)/(2*er))*(log(B-1)+0.39-
(0.61/er))))*h);
    %end
%end
% the SIW calculations
ur=1; % relative permeability
dia=2; % diameter of hole/vias
% p=2*dia; % pitch (distance between vias)
p=2*dia;
% fc101 = fo (cut off frequency of propagation mode 101 is same as
% fundamemental frequency)
Wsiw=Co/(Fo*sqrt(ur*er)); % this is the width of the siw
Weff=Wsiw-(dia^2/(0.95*p)); % this is the effective width of the siw
Leff=(Co*Weff)/sqrt((4*Fo^2*Weff^2*ur*er)-Co^2); % this is the effective
length of the siw
Lsiw=Leff+(dia^2/(0.95*p)); % this is the length of the siw

To find the coupling value at the common resonator of the unequal split
uke12=((jj(2)/sqrt(3))*sqrt(L1/CC1)); % this the k1B of the PS to port 2
uke13=((jj(2)/sqrt(3/2))*sqrt(L1/CC1)); % this is K12 of the PS to port 3
%End of part

To find the new J value used in circuit schematic for the unequal split
uCJ12=((jj(2)/sqrt(3))/Wo); % This is the new capacitance value used in
the schematic in ADS
uCJ13=((jj(2)/sqrt(3/2))/Wo);
%End of part
```

1. Code for realizing Qext and coupling Coefficient values extracted from Microsoft excel

```
% Matlab code for plotting K against s[mm]
y1=[0.013461315, 0.016241103, 0.019024805, 0.023863671, 0.027887945,
0.03329294, 0.043901947, 0.052641937, 0.071627992, 0.083783692];
x=[4.0,3.8,3.7,3.6,3.5,3.4,3.3,3.2,3.1,3.0];
plot(x,y1)
ylabel('Coupling Coefficient')
xlabel('Spacing, s[mm]')
%End

% Matlab code for plotting Qext against t[mm]
x=[3, 3.5, 4, 4.5, 5., 5.5, 6, 6.5, 7, 7.5];
y1=[2.912357581, 3.050805833, 3.236237047, 4.173758865, 5.579196877,
7.066051136, 10.38453555, 14.3125448, 18.16348774, 22.07615894];
plot(x,y1)
```

```
ylabel('External Quality Factor, Qext')
xlabel('D3[mm]')
%End
```

2. Code for reading the result from other platform and be generated in MATLAB

```
% MATLAB code for making comparison as files extracted from ADS/EMPro and
% from the VNA
file = 'S21_5pole_equal.s2p'; % this is the S21 file captured from the
measured result
file2 = 'S31_5pole_equal.s2p'; %this is the S31 file captured from the
measured result
file3 = 'ADS_5pole_equal.s3p'; % this is the file extracted from ADS
file4 = 'S11_5pole_equal.s2p'; %this is the S11 file captured from the
measured result
g = read(rfdata.data,file); % this is just the Matlab syntax used to read
the file
h = read(rfdata.data,file2);
i= read(rfdata.data,file3);
j = read(rfdata.data,file4);
figure
plot(g,'s21','db');
hold on; % hold is the command that allow more than one curve on display
plot(h,'s21','db');
hold on;
plot(i,'s11','db');
hold on;
plot(k,'s11','s21', 's31','db');
%End
```